Towards the Implementation of a Pulse Detonation Combustor into a Gas Turbine

vorgelegt von

M. Sc.

Fabian Enrico Habicht

an der Fakultät V – Verkehrs- und Maschinensysteme
der Technischen Universität Berlin
zur Erlangung des akademischen Grades

Doktor der Ingenieurwissenschaften
– Dr.-Ing. –

genehmigte Dissertation

Promotionsausschuss:

Vorsitzender:	Prof. Dr.-Ing. J. Weiss (Technische Universität Berlin)
Gutachter:	Prof. Dr.-Ing. C. O. Paschereit (Technische Universität Berlin)
	Prof. Dr. sc. P. Stathopoulos (Technische Universität Berlin)
	Prof. M. Bellenoue (Institut P', CNRS-ENSMA-Université de Poitiers)

Tag der wissenschaftlichen Aussprache: 23. September 2021

Berlin 2021

Preface

This thesis would not have been accomplished without the assistance of a number of specific persons. First of all, I want to thank my supervisor Prof. Oliver Paschereit for his support during the entire duration of the project. I appreciate your advice and the objective discussions on many small and large steps along the path of my dissertation. Further, I thank Prof. Panagiotis Stathopoulos for always having an open ear for questions and concerns. Panos, you gave me the opportunity for writing an application for start-up financing for a research project, which unfortunately has not been granted, but somehow brought me to the project, I worked on the last four years. I also want to thank Prof. Marc Bellenoue who immediately agreed to be part of the committee for the evaluation of this thesis.

Many thanks go to numerous colleagues at the Hermann Föttinger Institut and inside the collaborative research center CRC 1029. In the first place, I want to mention Fatma Yücel. Fatos, thanks you for your invaluable support and the countless discussion on technical and less technical issues. Mohammad Rezay Haghdoost and Niclas Garan, I am very happy to work together with you on related research topics. The progress of my project undoubtedly profited from the exchange of knowledge concerning physical aspects and the vicissitude of the test facilities. Special thanks go to Joshua Gray who laid the ground for my work. I really appreciate that you took the time to introduce me to the experimental facilities and never hesitated to help me when needed. Further I want to thank several other colleagues in alphabetical order: Florian Arnold, Eric Bach, Myles Bohon, Richard Bluemner, Neda Djordjevic, Finn Lückoff, Georg Mensah, Allesandro Orchini, Tim Rähse, Thoralf Reichel, Daniel Topalovic, Johann Vinkeloe, and Lisa Zander. You all helped me with your expertise and answers to all kind of questions. I also want to mention Iwo Gotthans, Friederike Großmann, Alexander Jaeschke, Robert Kanisch, Oliver Klement, Viktor Morell, and Adrian Stobbe, who contributed to this work as student research assistants. Thank you for your help on preparing and conducting experiments as well as your assistance in evaluating measurement data.

The experimental research in the scope of this work would not have been possible without the technical supoort from Thorsten Dessin, Andy Göhrs, Robert Bahnweg, Heiko Stolpe, Colin Muxlhanga, Christian Menzel, and Sebastian Schimek. Thank you for the constructive cooperation and your kind advice. Maria Lück, Sandy Meinecke, and Steffi Stehr, thank you for coping with all the bureaucratic formalities associated to this work. Lastly, I want to thank my family for their unconditional support. To my wife Viktoria, I am grateful for your love and for all the memories we share.

Thank you!

Zusammenfassung

Die Deckung des Energiebedarfs durch die Nutzung umweltfreundlicher Ressourcen ist eine der größten Herausforderungen der Gegenwart. Zum Erreichen dieses Ziels ist der verbreitete Einsatz von hocheffizienten Gasturbinen essenziell, da so Zeiträume mit geringer Verfügbarkeit von erneuerbaren Energiequellen überbrückt werden können. Werden hierbei alternative Brennstoffe, wie Wasserstoff, verwendet, kann eine klimaneutrale Bilanz erreicht werden. Um die Verluste auf diesem Weg der Energieerzeugung so gering wie möglich zu halten, ist die Maximierung des thermischen Wirkungsgrades von Gasturbinen über einen breiten Betriebsbereich von großem Interesse. Ein besonders großes Potential bietet der Einsatz eines druckerhöhenden Verbrennungsprozesses, der durch die Integration einer pulsierenden Detonationsbrennkammer (engl. pulse detonation combustor, PDC) realisiert werden kann. Der zugrundeliegende periodische Prozess beruht auf der Verbrennung eines Brennstoff-Luft-Gemisches mittels einer propagierenden Detonationswelle, wodurch ein deutlicher Druckanstieg induziert wird. Neben der möglichen Erhöhung des thermischen Wirkungsgrades, wurden bei vergangen Untersuchungen jedoch auch einige Herausforderungen bei der Integration in eine Gasturbine identifiziert. Zum einen werden durch den periodischen Verbrennungsprozess schwankende Randbedingung an den Schnittstellen zu Turbomaschinenkomponenten hervorgerufen. Zum anderen ist die effiziente Umsetzung der Transition von Deflagration zu Detonation (engl. deflagration-to-detonation transition, DDT) innerhalb einer akzeptablen Distanz herausfordernd. Um den Kenntnisstand bzgl. dieser beiden Aspekte des PDC-Betriebs zu erweitern wurden eine Reihe von experimentellen Untersuchungen im Rahmen dieser Arbeit durchgeführt. Hierfür wurden zwei Versuchsaufbauten (ein Einzelrohr-Prüfstand und ein Multirohr-Prüfstand) am Fachgebiet Experimentelle Strömungsmechanik der TU Berlin errichtet.

An dem Einzelrohr-Prüfstand wurde der Prozess der Detonationsinitiierung mit Hilfe von zwei unterschiedlichen Einbauten untersucht: einer stoßfokussierenden Geometrie und einer Reihe von Blenden, welche jeweils in die PDC integriert wurden. Die experimentellen Ergebnisse zeigten die erfolgreiche Detonationsinitiierung durch Stoßfokussierung unter atmosphärischen Bedingungen, falls gewisse Schwellwerte für den Massenstrom und die Mischungsreaktivität überschritten wurden. Zudem ergaben die durchgeführten Experimente, dass bei dem Betrieb mit der stoßfokussierenden Geometrie ein größeres Volumen des brennbaren Gemisches durch eine Deflagration verbrannt wurde, der Prozess jedoch geringeren stochastischen Schwankungen unterlag als bei der Nutzung einer Reihe von Blenden. Darüber hinaus wurde der Betrieb der PDC unter erhöhten Temperatur- und Druckbedingungen untersucht. Die gewonnenen Daten weisen darauf hin, dass der Einsatz der stoßfokussierenden Geometrie den zuverlässigen Betrieb der PDC unter gasturbinenrelevanten Bedingungen ermöglicht. Des Weiteren wurde die geschichtete Eindüsung des Brennstoffs genutzt um einen stabilen Betrieb mit brenntstoffarmen Gemischen zu erreichen, was für den effizienten Betrieb einer Gasturbine mit geringem Schadstoffausstoß erforderlich ist.

Die Auswirkung des zyklischen PDC-Prozesses auf die Randbedingungen angrenzender Turbomaschinenkomponenten wurde experimentell an dem Multirohr-Prüfstand untersucht. Druckmessungen stromauf und stromab der Brennkammer ermöglichten die Erfassung der Schwankungsamplituden in Abhängigkeit der Betriebsparameter, wie der Feuerungsfrequenz, dem Feuerungsmuster und dem globalen Ã„quivalenzverhältnis. Die aufgezeichneten Druckverläufe in einem annularen Plenum stromab der PDC wurden durch die Anregung von akustischen Eigenschwingungen erklärt. Die Zerlegung der Drucksignale in Bezug auf Modenform und Schwingungsfrequenz ergab, dass die Amplituden und die Anzahl der dominanten Eigenmoden sowohl durch die Wahl der Betriebsparameter als auch durch die akustischen Randbedingungen am Turbineneintritt beeinflusst wurden. Die geeignete Wahl dieser Parameter ermöglichte die Reduktion der Druckschwankungen am Turbineneintritt.

Die im Rahmen dieser Arbeit durchgeführten experimentellen Untersuchungen decken mehrere Aspekte ab, die für die praktische Anwendung einer PDC relevant sind. Dazu zählen die Begutachtung des Potentials zwei verschiedener DDT-Geometrien, die Gewährleistung eines stabilen PDC-Betriebs unter gasturbinenrelvanten Bedingungen sowie die Identifizierung von geeigneten Vorgehensweisen zu Reduktion der Druckfluktuationen an den Schnittstellen zu Turbomaschinenkomponenten. Zudem wurde Wasserstoff bei allen Experimenten als Brennstoff verwendet, wodurch diese Arbeit einen Beitrag zu der fortwährenden Forschung an der Realisierung einer klimaneutralen Energieerzeugung durch hocheffiziente Gasturbinen leistet.

Abstract

Covering the energy demand by using environmentally friendly resources is a major challenge of the present. Gas turbines take a central role in accomplishing this objective, as they allow for bridging periods of a deficit in available renewable energy sources. The application of alternative fuels, such as hydrogen, is particularly desirable to realize an overall climate-neutral energy generation. To minimize the losses on this path, optimizing the thermal efficiency of gas turbines over a broad range of operating conditions is vital. Potentially, this may be achieved by the implementation of a pressure gain combustion process, which can be realized by the integration of a pulse detonation combustor (PDC). The underlaying periodic process is based on the combustion of a fuel–oxidizer mixture by means of a propagating detonation, which induces a considerable pressure increase. However, the cyclic combustion process causes new challenges due to fluctuating boundary conditions for the attached turbomachinery components. Moreover, the efficient realization of deflagration-to-detonation transition (DDT) within a reasonable distance is challenging. To expand the knowledge regarding these two aspects of PDC operation, a number of experimental investigations were conducted in the scope of this thesis. For this, two experimental facilities, i.e. a single-tube PDC and a multi-tube PDC, have been set up at the Chair of Fluid Dynamics at TU Berlin.

The single-tube test rig was used for the experimental investigation of detonation initiation by means of two different DDT geometries: a shock-focusing device and a series of orifice plates. Experimental results revealed successful detonation initiation by shock focusing at atmospheric conditions when certain threshold values for the mass flux and the mixture reactivity were exceeded. In addition, the conducted measurements indicated that the operation with the shock-focusing device required a larger volume of flammable mixture to be consumed by deflagration, but on the other hand implied smaller stochastic variations, when compared to the application of a series of orifice plates. Further, the operation behavior of the single-tube PDC was examined at elevated temperature and pressure conditions. The obtained data suggest that applying the shock-focusing device allows for reliable PDC operation at gas turbine relevant conditions. Furthermore, the stratified injection of fuel was proposed and experimentally confirmed as suitable method for realizing stable PDC operation at globally lean mixture conditions, which is desired to ensure the efficient operation of gas turbines with low pollutant emission.

The effect of the cyclic PDC operation on attached turbomachinery components was examined experimentally on the multi-tube PDC facility. Pressure measurements upstream and downstream of the combustor allowed for capturing the fluctuation amplitudes with respect to various operation parameters, such as the firing frequency, the firing pattern, and the global equivalence ratio. Recorded pressure histories in an annular plenum downstream of the multi-tube PDC are explained by the excitation of natural acoustic oscillations. The decomposition of pressure signals with regard to the mode shape and oscillation frequency revealed that the amplitude and the number of dominant eigenmodes depended on operation parameters as well as the acoustic

boundary conditions. The proper adjustment of these variables allowed for reducing the pressure fluctuations at the turbine inlet.

By examining the potential of two DDT geometries, ensuring stable PDC operation at gas turbine relevant conditions, and identifying strategies for reducing pressure fluctuations at the interfaces to turbomachinery components, the present thesis provides a step towards the practical application of a PDC in a gas turbine. Moreover, all experimental investigations were conducted with hydrogen as fuel. Thus, this work contributes to the ongoing research aiming for climate-neutral energy production by highly efficient gas turbines.

Contents

List of Figures

List of Tables

Nomenclature

Roman Symbols

Symbol	Unit	Name
A	m^2	cross section area
c	m/s	speed of sound
c_p	J/(mol K)	heat capacity at constant pressure
c_v	J/(mol K)	heat capacity at constant volume
D	m	diameter
e	Pa^2	integral energy of pressure oscillations
f	Hz	frequency
g	–	duty cycle
h	J/kg	specific enthalpy
K	–	number of segments
L	m	axial length of the plenum
l	–	axial mode number
M	kg/mol	molar mass
M		Mach number
m	–	azimuthal mode number
$\dot{m}$	kg/s	mass flux
N	–	number of combustion tubes in the multi-tube PDC
n	–	number of simultaneously operated PDC tubes
n	–	radial mode number
p	bar	pressure
q	J/kg	heat addition per unit mass
$\hat{q}$	$bar^2\,s$	cumulated power spectral density
R_s	J/(kg K)	specific gas constant
r	m	radius / radial coordinate
Re		Reynolds number
T	K	temperature
t	s	time
Tu		turbulence intensity
u	m/s	axial velocity
v	m^3/kg	specific volume
X	–	mole fraction
x	m	axial position

Greek Symbols

Symbol	Unit	Name
β		blockage ratio
γ		isentropic exponent
Δ_I	m	induction length
ε_I	–	reduced activation energy
ζ	–	non-dimensional frequency
η	kg/(s m)	dynamic viscosity
η_{th}	–	thermal efficiency
θ	–	azimuthal coordinate
λ	m	detonation cell width
ν	m^2/s	kinematic viscosity
Π		pressure ratio
ρ	kg/m^3	density
$\dot{\sigma}$	1/s	thermicity
τ	s	ignition delay time
φ		equivalence ratio
χ	–	non-dimensional stability parameter
Ψ	bar	acoustic eigenmode
ω	1/s	angular frequency

Subscripts and Acronyms

Index	Meaning
0	initial state
a	acoustic
amb	ambient conditions
b	blockage
CJ	Chapman-Jouguet
c	compressor
cf	combustion front
CVC	constant volume combustion
D	detonation front
DDT	deflagration-to-detonation transition
det	detonation (section)
DME	dimethyl ether
eff	effective
FT	Fourier transform
glob	global
I	ionization probe
i	inner

inj	injection
is	ignition spark
L	leading shock
max	maximum
meas	measurement
mix	mixture
o	outer
ox	oxidizer
P	pressure sensor
PDC	pulse detonation combustor
PGC	pressure gain combustion
PID	proportional–integral–derivative
pre	pre-detonation chamber
PSD	power spectral density
R	retonation wave
RDC	rotating detonation combustor
ref	reference case
RMS	root–mean–square
RPC	resonant pulse combustor
s	sampling
SEC	shockless explosion combustion
sf	shock-focusing device
st	stoichiometric conditions
sup	superposition
SWACER	shock wave amplification by coherent energy release
T	thermocouple
TDLAS	tunable diode laser absorption spectroscopy
tof	time-of-flight
TPI	transient plasma ignition
vN	von Neumann

Superscripts

Index	**Meaning**
$\bar{x}$	mean value
$\dot{x}$	time derivative
x'	fluctuation

Chapter 1

Introduction

Considering the increasing worldwide energy demand along with the threats of progressive global warming, the sufficient generation of electric energy with minimal environmental impact is a key challenge of the present. Conventional electricity generation by combustion of fossil fuels emits enormous amounts of greenhouse gases, e.g. carbon dioxide (CO_2), as well as nitrogen oxides (NO_x). In particular, NO and NO_2 cause acid rain, negatively affect the ozone concentration in the stratosphere [1], and harm the human health due to their toxic nature [2]. Beside the ongoing effort for improving the efficiency and minimizing pollutant emission of existing concepts for power generation utilizing fossil fuels, such as coal or natural gas, renewable energy sources have shifted into the scope of research as an environmentally friendly alternative. Despite the plurality and the advanced state of development of concepts, e.g. solar and wind, the high energy demand cannot be exclusively covered by renewables. This is caused by fluctuations in both energy demand (throughout the day, week, and year) and the availability of renewable energy resources, which depends on weather conditions, and thus, is unpredictable to some extent. Therefore, fast responding technologies are needed in order to bridge periods, where the energy consumption exceeds the generation from renewable resources.

Gas turbines are an attractive choice for this purpose due to their relatively fast ramp up and flexibility in the operational load. They are therefore expected to play a significant role in covering the demand of electricity over the next decades [3]. Tremendous efforts have been invested in the past in order to further improve the cycle efficiency and reduce the emission of CO_2 and other pollutants [4]. Great progress was achieved by the implementation of lean pre-mixed combustion leading to a significant reduction of NO_x. Besides, extending the range of applicable fuels for gas turbines is a current research topic. Thereby, one major target is to utilize hydrogen as a fuel or additive in gas turbine applications [5]. Hydrogen is regarded as a sustainable alternative to fossil fuels since it can be derived from numerous sources including carbon neutral ones like biofuels, wind and solar energy. In addition, hydrogen is applicable in multiple concepts for power generation or mobility, e.g. internal combustion engines and fuel cells [6]. Although a part of the available hydrogen is produced from fossil fuels, gasification and electrolysis offer efficient and environmentally friendly concepts for hydrogen generation from any renewable energy source [7, 8]. Thus, excess energy during periods of high availability of

renewable resources and low energy demand can be stored in the form of hydrogen. Using the produced hydrogen for electricity generation, e.g. in a gas turbine, depicts a path for the storage of renewable energy with zero emission of CO_2 and CO. If not burnt directly, hydrogen can be fed into the natural gas supply system, which facilitates its distribution. The hydrogen amount in the natural gas pipeline infrastructure is however limited to approximately 15 % volume fraction. Beyond that, safety issues may occur in some pipelines and end-use applications due to the increased reactivity of the fuel [9, 10]. Alternatively, hydrogen can be used for the generation of methane through the process of methanation. Here, H_2 is combined with CO_2 in order to produce CH_4, which can subsequently be fed into the natural gas supply system without any restriction. However, as the feeding of hydrogen into the natural gas supply system is limited and the process of methanation requires considerable additional effort, the direct usage of hydrogen is desirable to achieve a maximum efficiency.

The substitution of conventional fuels by hydrogen in gas turbines poses a number of technical challenges. Firstly, using hydrogen as fuel increases the flame speed significantly [11]. This raises the risk of flash back, which can seriously harm the structure of the combustor. Secondly, the flame temperature for a given fuel–oxidizer ratio increases, which induces elevated demands on material resistance and cooling technologies. Simultaneously, this high temperature promotes the formation of NO_x [12]. In order to reduce NO_x emission, premixed combustion is desired, which is however challenging when using hydrogen as fuel due to the high mixture reactivity and the induced risk of flash back. Therefore, the development of alternative concepts for reduction of pollutant emission is necessary [13]. Lastly, in comparison to hydrocarbon fuels, hydrogen has a low volumetric energy density. Hence large storage reservoirs and supply lines are needed. Furthermore, the compression of hydrogen requires additional energy and special safety regulations have to be considered for pipeline transportation [14]. Thus, long transportation routes should be avoided and decentralized application, as small scale onshore facilities, should be preferred. Despite the mentioned challenges, the advantages of hydrogen as easily producible and environmentally friendly fuel justifies the enormous effort that is put into research and development of electricity generation from hydrogen combustion.

In order to minimize losses during the conversion from chemical to electric energy, the optimization of gas turbines is a key challenge. However, a stagnation in the development of the thermal efficiency was observed during the past decades. This can be explained by the extensive efforts that have been invested in the optimization of turbine and compressor, which caused the efficiency of these components to converge towards the physical limits. In comparison, the optimization of the combustion process has gained less attention, since modifying the process of heat addition affects the operation characteristics of all gas turbine components. Due to this, improving the combustion process holds a large potential for achieving a significant increase in thermal efficiency of gas turbines [15, 16].

1.1 Pressure Gain Combustion

Traditionally, gas turbine combustors are operated with a stationary turbulent flame, which ideally adds heat to the working fluid at constant pressure. In real applications, however, a slight decrease in stagnation pressure across the combustion chamber is observed. This pressure

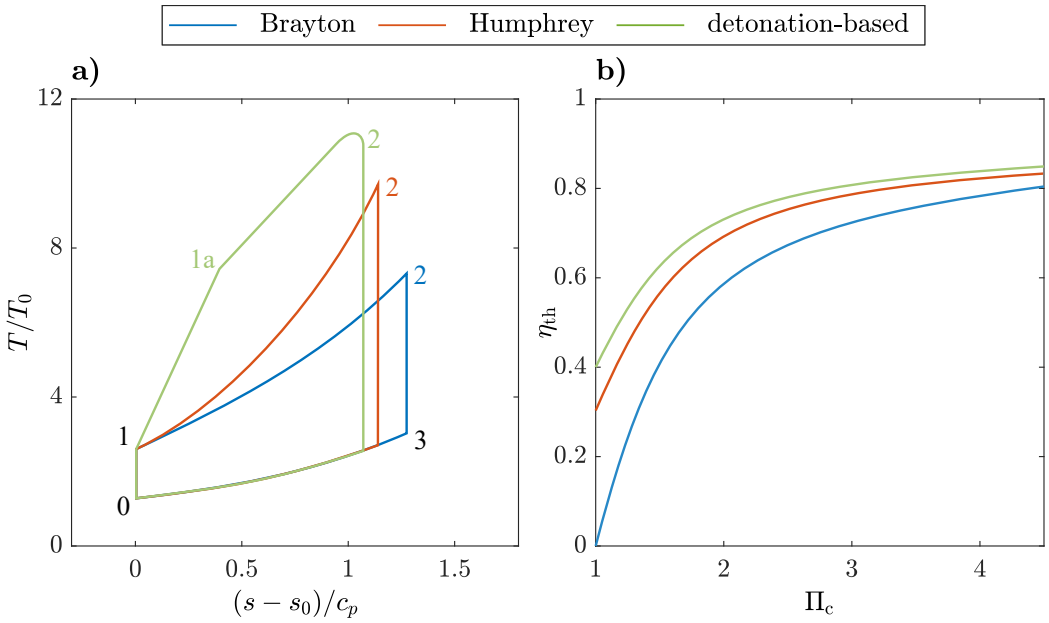

Figure 1.1: Comparison of the conventional Brayton cycle with the Humphrey cycle and a detonation-based cycle (adapted from [18]): (a) T–s diagram and (b) ideal thermal efficiency η_{th} as a function of the compressor pressure ratio Π_c

drop is required to ensure a good mixing of fuel and oxidizer and to allow for effective cooling of the combustor walls [17]. Heiser and Pratt [18] demonstrated that operating a gas turbine with the Humphrey instead of the conventionally applied Brayton cycle potentially leads to a significant increase in thermal efficiency. As shown in Fig. 1.1 a, the involved exchange of the heat addition ($1 \rightarrow 2$) at constant pressure by a constant volume combustion (CVC) leads to a higher turbine inlet temperature T_2 and less entropy production. This eventually results in an increased thermal efficiency η_{th} for all compressor pressure ratios Π_c, as visualized in Fig. 1.1 b. A third cycle based on the considerations of Jacobs [19] was introduced by Fickett and Davis [20]. The so-called Fickett–Jacobs cycle contains heat addition by a propagating detonation wave. Here, the flammable gas is compressed by a shock wave ($1 \rightarrow 1a$) before heat release due to chemical reactions lead to a further increase in temperature ($1a \rightarrow 2$). This approach follows the one-dimensional ZND structure of a detonation wave (named after Zel'dovich, von Neumann, and Döring), which is discussed in Sec. 1.2.1. Compared to the Humphrey cycle, a further increase in thermal efficiency is achieved. The largest improvement in η_{th} with respect to the Brayton cycle is found for small compressor pressure ratios Π_c. Thus, the substitution of constant pressure combustion by CVC or a detonation-based concept suggest a considerable gain in efficiency for the ideal gas turbine cycle. Gray et al. [21] confirmed these findings for non-ideal conditions by evaluating the cycle performance with a polytropic compressor efficiency of 90 % and the usage of suitable turbine operational maps.

Both CVC and detonation-based combustion, induce an increase in pressure simultaneous to the heat release in the combustor. These concepts are therefore known as pressure gain combustion (PGC). In order to realize PGC, various concepts have been developed during the last decades, e.g. resonant pulse combustor (RPC), pulse detonation combustor (PDC), rotating

detonation combustor (RDC), and shockless explosion combustor (SEC). To facilitate the inflow of the working fluid against the positive pressure gradient across the combustor, these concepts are all based on a periodic combustion process. This results in non-stationary flow variables inside the combustor itself, but also at the interfaces to the attached components. As compressor and turbine of a conventional gas turbine are designed for steady-state conditions, the integration of PGC into such a device evokes new requirements on the turbomachinery components in order to assure a stable and efficient operation [22, 23]. In the following, the mentioned PGC concepts are introduced and for each, the current state of research and development is briefly discussed.

1.1.1 Resonant Pulse Combustor

Resonant pulse combustion was one of the earliest proposed concepts to realize PGC in a gas turbine [24]. The process is based on the deflagration of a fuel–oxidizer mixture in a confined geometry. This confinement limits the expansion of the burnt gases and thus leads to an increase in pressure and temperature in the combustion chamber (Fig. 1.2 a). Due to the increased pressure, the inlet valve, commonly a passive flutter valve [25], is closed, which prevents the backflow of combustion products into the supply lines. The expansion of the burnt gases force a high-momentum flow through the exhaust (Fig. 1.2 b), which results in a pressure drop in the combustion chamber below the supply pressure. The inlet valve opens and the combustor is filled with fresh mixture (Fig. 1.2 c). Simultaneously, the burnt gases in the exhaust are partly sucked back into the combustion chamber, where they mix with the fresh mixture. Local contact burning initiates a deflagration front (Fig. 1.2 d) and a new combustion cycle begins.

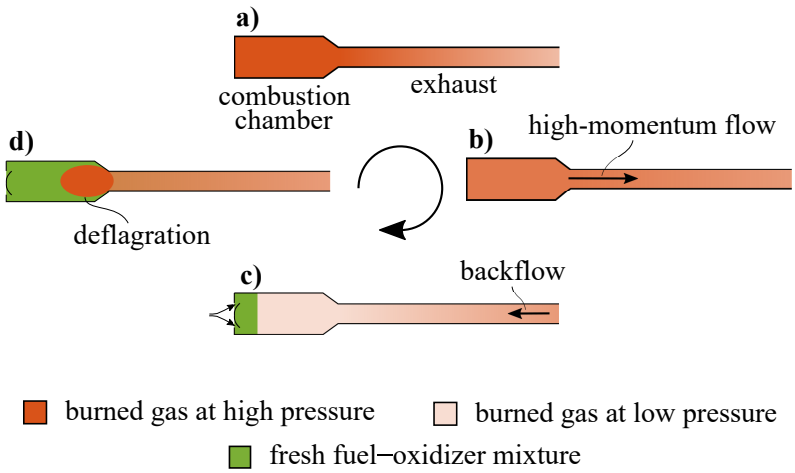

Figure 1.2: Periodic combustion process in an RPC

RPCs profit from their robust and simple design with only one moving part (inlet valve) and can be operated with several fuel types. As first PGC concept, Paxson and Dougherty [25] demonstrated an overall pressure rise of approximately 3.5 % by using an ejector attached to an RPC. However, the operational range of these devices is limited, since characteristic chemical and mixing time scales have to be adjusted considering the acoustic resonance frequency [26] in order to maximize the specific thrust of the combustor. In addition, the achievable pressure gain is restricted, since the concept is based on a confined volume combustion rather than CVC.

Therefore, Litke et al. [27] found that the PDC cycle is more efficient than the RPC cycle at comparable operating conditions and should therefore be preferred for gas turbine application.

1.1.2 Pulse Detonation Combustor

Pulse detonation combustion aims for realizing PGC by means of a propagating detonation wave. This extremely fast reaction front, e.g. $u_{\mathrm{det}} \approx 2000\,\mathrm{m/s}$ for stoichiometric hydrogen–air mixtures at atmospheric conditions, burns the flammable mixture quasi-instantaneously, leaving the gas almost no time expand. The combustion process is realized periodically by filling the combustor with a mixture of fuel and oxidizer (Fig. 1.3 a). Subsequently, the combustion process is triggered by an externally controlled ignition source, e.g. an ignition spark (Fig. 1.3 b). Direct detonation initiation is very energy consuming and is therefore not a practical technique in PDCs. Instead, a detonation is commonly initiated through deflagration-to-detonation transition (DDT). For this, several concepts have been proposed, such as the integration of obstacles, plasma-induced flame acceleration, and shock focusing. Since the flame has to undergo DDT in each cycle, a proper design of this process is essential for achieving efficient PDC operation. A more detailed discussion on the DDT process and the available literature on this topic is given in Sec. 1.3.1. After the successful initiation of a detonation wave, the supersonic reaction front propagates downstream the PDC (Fig. 1.3 c), resulting in combustion products at high temperature and pressure conditions. Expansion of the burnt gases then leads to a blowdown through the combustor outlet. Subsequently, the cycle starts over by filling the PDC with a fresh fuel–oxidizer mixture that is separated from the combustion products by a buffer of pure oxidizer in order to prevent premature ignition (Fig. 1.3 d).

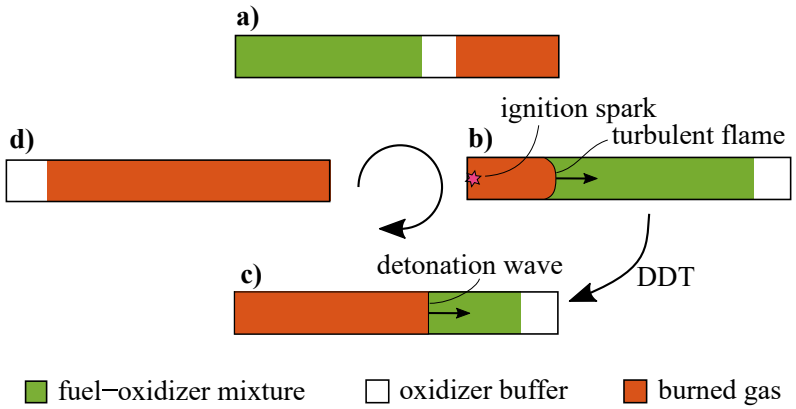

Figure 1.3: Periodic combustion process in a PDC

Several investigations attest the PDC to hold the potential for significantly increasing the efficiency of a gas turbine [21, 27]. However, the implementation of this concept still faces numerous challenges. On the one hand, the large pressure rise in the combustor poses high demands on the design of the combustor inlet in order to prevent backflow of hot exhaust gases. On the other hand, a proper designed DDT enhancing geometry should be integrated in the combustor in order to achieve reliable detonation initiation within a reasonable distance. Further, PDC operation results in considerable pressure fluctuations upstream and downstream of the combustor, which affect the performance of attached turbomachinery components and cause

additional mechanical stress on the engine structure. These fluctuations can be reduced by a certain degree by combining multiple PDC tubes. A larger number of combustors allows for an increase in the frequency of pressure fluctuations, and thus, getting closer to quasi-stationary flow conditions at the turbine inlet. A detailed discussion on available literature considering the integration of a PDC into a gas turbine is given in Sec. 1.3.2.

1.1.3 Rotating Detonation Combustor

Recently, the RDC has gained increasing attention in the research on PGC devices. Its attractiveness is based on the very high power density, a simple design, and a high operation frequency resulting in quasi-stationary flow conditions in the exhaust. The combustion chamber consists of a annular duct, as visualized in Fig. 1.4 a. Fuel and oxidizer are injected at the combustor inlet. The mixture subsequently convects downstream until it is consumed by a detonation wave propagating in azimuthal direction. The visualization of the periodic combustion process (Fig. 1.4 b) only shows the main features of the complex flow field, which has been studied in detail by Naples et al. [28] and others. Due to the increase in pressure behind the detonation front, a backflow of combustion products into the supply is observed for a certain period, which is followed by the injection of fresh fuel–oxidizer mixture after the recovery of the supply pressure.

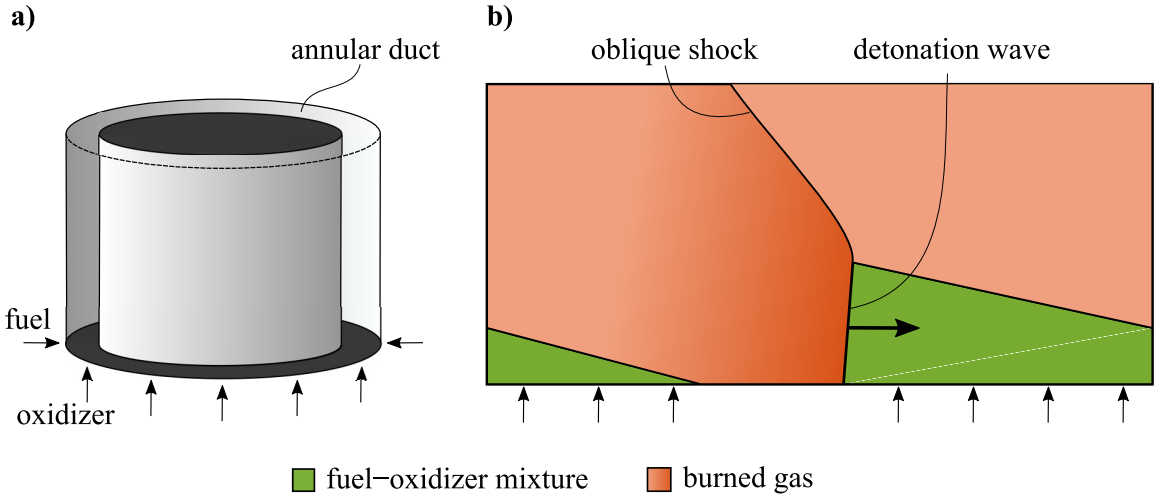

Figure 1.4: (a) Fundamental design and (b) visualization of the main aspects of the combustion cycle of an RDC

Resulting from the high propagation velocity of the combustion front in azimuthal direction (usually around 80 % of the theoretical value of a stable, planar propagating detonation wave [29]), fluctuations in the the exhaust flow are observed in the order of 1 kHz. Compared to PDC applications, these fluctuations at the combustor outlet of RDCs are characterized by smaller amplitudes and higher frequencies [30], which is favorable for the integration into a gas turbine. Together with the compact and simple design, this extremely high operation frequency is a major advantage of RDCs over other PGC concepts.

Nevertheless, numerous throwbacks have been faced during the research on RDCs. Firstly, a significant pressure loss at the inlet of the combustor is required in order to hinder the backflow of exhaust gases into the reactant supply. Considerably decreasing this pressure drop was

found to result in unstable operation [31]. Secondly, the high power density of RDCs induces a significantly elevated heat flux compared to conventional combustion chambers. Although several cooling techniques have been proposed and tested [32, 33], their influence on the combustion process is still not fully understood. Furthermore, various operation modes have been reported, depending on the types of fuel and oxidizer, the geometry of the combustor, the reactant mixing and the boundary conditions [34]. Beside the conventional RDC operation with a single rotating detonation wave [31], multiple co-rotating detonation waves [35], as well as counter-rotating combustion fronts [36] were observed. In addition, longitudinal pulsed operation was experimentally found for certain conditions [37]. Despite the effort in understanding the different phenomena and the respective stimulating mechanisms, the prediction of the combustion modes is still the object of ongoing research.

1.1.4 Shockless Explosion Combustor

Achieving approximate CVC by quasi-homogeneous autoignition is the aim in an SEC. The concept was proposed by Bobusch et al. [38] and consists of a periodic combustion process, sketched in Fig. 1.5. At the beginning of each cycle, fuel is added to the oxidizer flow at the combustor inlet. The mixture then convects downstream (Fig. 1.5 a) until the residence time of the fuel–oxidizer package exceeds the ignition delay time and autoignition occurs. A spatial stratification of the fuel concentration is applied to compensate for the gradient in residence time, and thus, achieve quasi-homogeneous autoignition across the entire fuel–oxidizer mixture. The heat release in the aerodynamically confined volume results in a pressure rise in the burnt gas, which generates a pressure wave at the contact surface to the previously injected oxidizer buffer (Fig. 1.5 b). At the acoustically open combustor outlet, this pressure wave is reflected as a suction wave that travels upstream (Fig. 1.5 c). When the suction wave reaches the combustor inlet, the pressure falls below the oxidizer supply pressure, which promotes the injection of an oxidizer buffer followed by a stratified fuel–oxidizer mixture, which marks the start of the next cycle (Fig. 1.5 d).

To realize this resonant operation, which is characterized by the cycle duration matching the acoustic time scales of the combustor in order to synchronize mixture injection and the occurrence

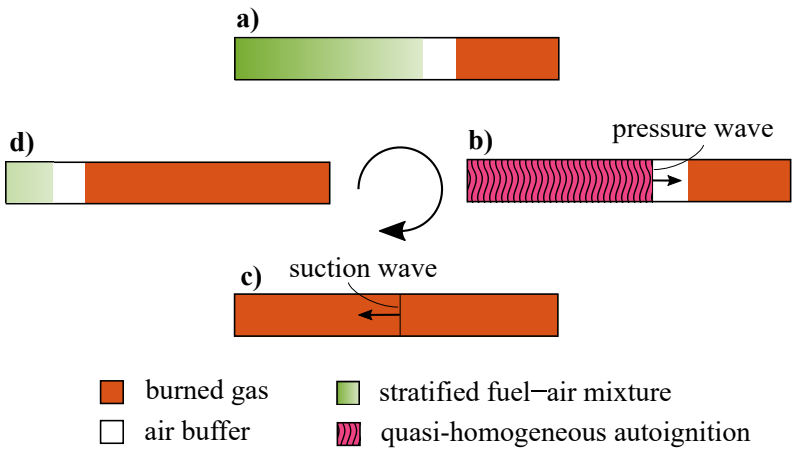

Figure 1.5: Periodic combustion process in an SEC (adapted from [39])

of the suction wave, extremely short ignition delay times are required. For most fuels, this demands elevated temperature and pressure conditions. Therefore, resonant SEC operation has not been realized experimentally yet. Nevertheless, experimental investigations of the autoignition process at atmospheric pressure conditions with a preheated air flow and dimethyl ether (DME) as fuel were conducted. Since the flammable mixture is exposed to turbulent mixing [40] and heat convection when being convected downstream, the optimum control trajectory for fuel injection cannot be easily derived theoretically. Reichel et al. [41] achieved an increased homogeneity of the autoignition event in a DME–air mixture by applying an iterative learning controller to adjust the fuel injection. Yücel et al. [39] demonstrated that an increase in ignition homogeneity induces a larger pressure amplitude in the combustor. Although the results showed that the cycle-averaged operation characteristics of the SEC could be influenced by adjusting the fuel injection trajectory, a significant cycle-to-cycle variation was observed due to the high sensitivity of the combustion process on perturbations in mixture composition and temperature.

Conceptually, shockless explosion combustion offers several advantages over other PGC concepts. Firstly, approximate CVC is obtained without geometric confinement or the use of a propagating detonation wave, which reduces entropy generation and therefore potentially increases the combustion efficiency. Secondly, due to the absence of a detonation wave, pressure fluctuations at the combustor inlet and outlet are much smaller than for PDCs and RDCs, which is beneficial for the operation of attached turbomachinery components. However, resonant operation has not been demonstrated experimentally so far. Hence, further research and development is needed in order to allow for integrating an SEC into a gas turbine.

1.1.5 Positioning of this Thesis in the Context of Ongoing PGC Research

All concepts, that were presented in the previous sections, hold the potential of significantly increasing the thermal efficiency of gas turbines. However, PDCs are particular attractive since they allow for the implementation of the Fickett–Jacobs cycle, which induces an additional gain in efficiency compared to the Humphrey cycle, as depicted in Fig. 1.1. Thanks to the enormous effort that has been invested in the examination of PDC devices, the underlaying mechanisms of the combustion cycle are mostly well understood. Furthermore, the individual processes are partly independent of each other, e.g. the characteristics of the propagating detonation are mostly unaffected by the applied DDT enhancing concept. This allows for the targeted evaluation of single aspects by applying variations in the combustor geometry or changing the operating conditions. Therefore, findings from PDC investigations are often not only relevant for this particular device, but also for fundamental detonation research or other detonation-based concepts, e.g. the RDC. In the scope of this thesis, both the geometry and the operating conditions of a PDC were selectively modified to expand the knowledge on specific aspects, e.g. the detonation initiation by means of two different concepts, the operation at gas turbine relevant conditions, and the interaction with attached turbomachinery components.

1.2 Theoretical Considerations

Since the detonation-based combustion process in a PDC was investigated experimentally in the scope of this thesis, an introduction to the theory of propagating detonations is given in

this section. First, the one-dimensional structure is derived from fluid mechanical conservation equations, following the considerations by Lee [42] and Williams [43]. The deduced equations allow for the determination of the propagation velocity based on the composition and the thermodynamic state of the flammable mixture, which was used to verify successful detonation initiation in the experimental investigations in the scope of this thesis. Further, the axial structure of the combustion front is discussed. Subsequently, the inherent multi-dimensional nature of propagating detonations is introduced, which is closely linked to the reactivity of the fuel–oxidizer mixture. Then, the influence of elevated initial temperature and pressure conditions of the flammable mixture on the detonation characteristics is examined. These predictions help to interpret the results from measurements at these conditions, which are presented in Ch. 4. Lastly, a brief introduction to acoustic modes in annular ducts is given, which is included here to support the evaluation of measured pressure oscillations in an annular plenum downstream of a multi-tube PDC in Ch. 5.

1.2.1 One-dimensional Detonation Theory

For the following considerations we assume a combustion front propagating at the velocity u_{cf} through a gas with the initial thermodynamic state $[p_0, \rho_0, T_0]$, defined by the pressure p, the density ρ, and the temperature T. We then chose the reference frame so that the combustion front does not move, but rather the gas moves towards the combustion front with the opposite velocity $u_0 = -u_{\mathrm{cf}}$. Across the combustion front, the velocity of the gas changes to u_1 and the thermodynamic state of the burnt mixture is given by $[p_1, \rho_1, T_1]$. Figure 1.6 illustrates the velocities and the thermodynamic states of the gas upstream and downstream the combustion front.

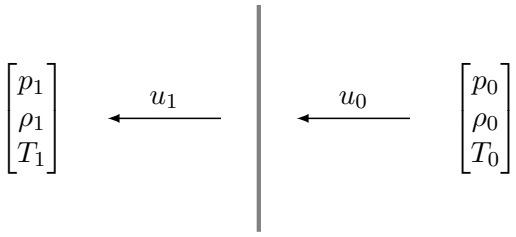

Figure 1.6: Illustration of the velocities and thermodynamic states on both sides of a combustion front, propagating at the velocity $u_{\mathrm{cf}} = -u_0$

For the given conditions the fluid mechanical conservation equations for mass, momentum, and energy are given by

$$\rho_0 u_0 = \rho_1 u_1, \tag{1.1}$$

$$p_0 + \rho_0 u_0^2 = p_1 + \rho_1 u_1^2, \tag{1.2}$$

$$h_0 + q + \frac{u_0^2}{2} = h_1 + \frac{u_1^2}{2} \tag{1.3}$$

with the specific enthalpy h and the heat addition per unit mass at the combustion front q. Introducing the mass flux $\dot{m} = \rho u$ and the specific volume $v = 1/\rho$, equations 1.1 and 1.2 can be

combined to

$$p_1 = p_0 + \dot{m}^2 \left(v_0 - v_1\right). \tag{1.4}$$

This equation denotes the Rayleigh line and can be illustrated by a straight line in a p–v diagram with the slope $\dot{m}^2$. Replacing the velocities in Eq. 1.3 by using Eq. 1.4 leads to the formulation of the Hugoniot curve

$$h_1 - (h_0 + q) = \frac{1}{2}\left(p_1 - p_0\right)\left(v_0 + v_1\right). \tag{1.5}$$

Assuming the validity of the ideal gas equation

$$p = \rho R_\mathrm{s} T \tag{1.6}$$

with the specific gas constant R_s and introducing the isentropic coefficient $\gamma = c_p/c_v$ as the ratio of the heat capacities at constant pressure and constant volume, respectively, the caloric equation

$$h = \frac{\gamma}{\gamma - 1} pv, \tag{1.7}$$

can be derived. When substituting the enthalpy in Eq. 1.5 by the expression from Eq. 1.7, the Hugoniot curve can be written as a function of p and v exclusively. The resulting hyperbolic function is plotted in Fig. 1.7 together with possible solutions for the Rayleigh line.

Since Eq. 1.4 and Eq. 1.5 are derived from the conservation equations of fluid mechanics, they both have to be fulfilled. Therefore, possible solutions can be found at the intersections of the two curves in the p–v diagram. In particular, two regimes that contain potential solutions can

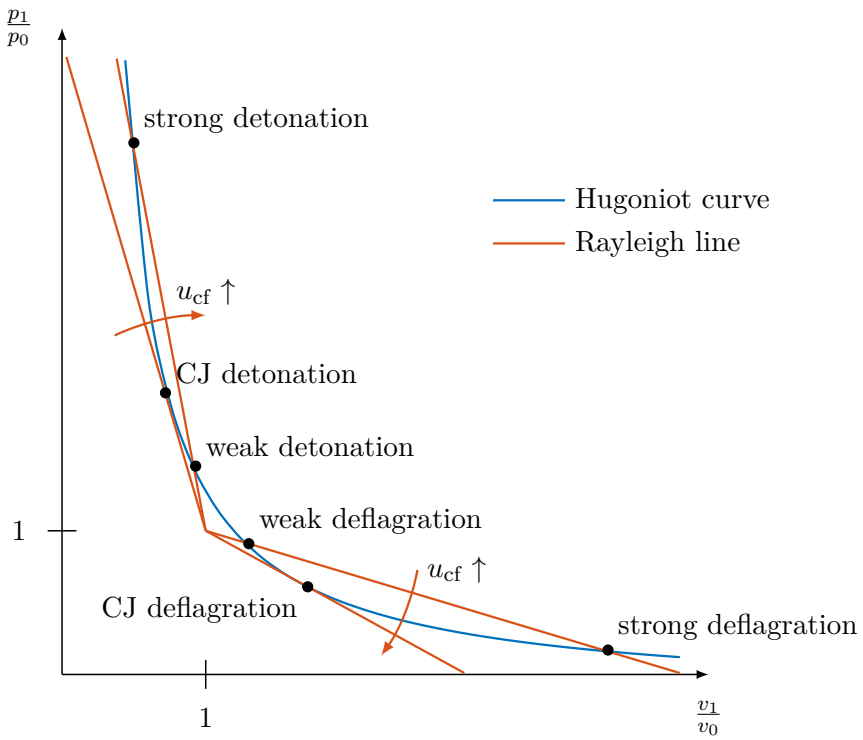

Figure 1.7: Normalized p–v diagram with possible Rayleigh lines and the Hugoniot curve for the initial state $[p_0, v_0]$

be distinguished: detonation with $\frac{p_1}{p_0} > 1$ and $\frac{v_1}{v_0} < 1$ and deflagration with $\frac{p_1}{p_0} < 1$ and $\frac{v_1}{v_0} > 1$. Generally, two solutions can be found in each regime, referred to as strong and weak detonation and strong and weak deflagration, respectively. However, only one single detonation velocity was found in experiments. Chapman [44] postulated that this velocity belongs to the minimum propagation velocity of the combustion front u_{cf}, which results in a single common point of the Releigh line and the Hugoniot curve. Jouguet [45] postulated the same velocity resulting from the assumption of the burnt gas to propagate at the speed of sound relative to the combustion front. In fact, both criteria are equivalent and result in the Rayleigh line to be tangential to the Hugoniot curve, which leads to a single solution for the propagation of a detonation. The corresponding thermodynamic state $[p_1, \rho_1, T_1]$ is therefore named the Chapman–Jouguet (CJ) state and the associated propagation velocity of the detonation front is called the CJ velocity u_{CJ}.

A more detailed theory on the one-dimensional structure of a detonation front, known as ZND theory, was independently developed by Zel'dovich [46], von Neuman [47], and Döring [48]. They postulated, that the combustion front can be split into a shock wave that compresses the unburnt gas and a following reaction zone that involves heat release. Figure 1.8 displays the induced changes in the thermodynamic state. The adiabatic compression across the shock wave can be described by the Hugoniot curve without heat release, as visualized in Fig. 1.8 a. The propagation velocity u_{CJ}, and therefore, the slope of the Rayleigh line is given by the CJ theory. The intersection of the deduced Rayleigh line with the Hugoniot curve for $q = 0$ leads to a well-defined thermodynamic state behind the shock front known as von Neumann point. The compression by the shock wave leads to an increase in pressure and temperature as shown in the distribution of these parameters across the detonation front in Fig. 1.8 b. Due to the high temperature and pressure conditions in the induction zone, the rates of chain branching reactions

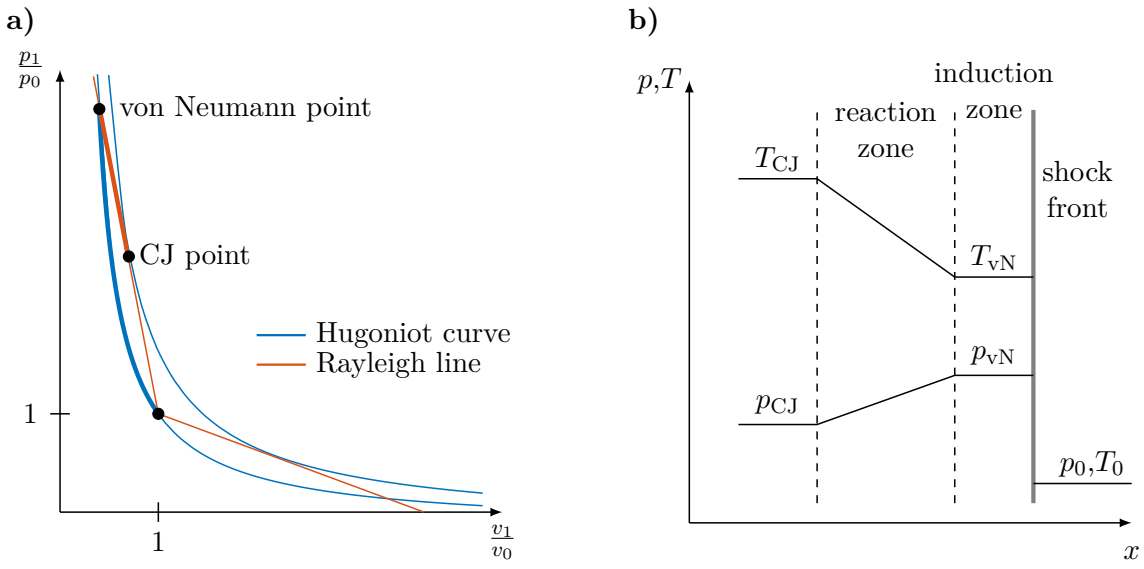

Figure 1.8: Illustration of the changes in thermodynamic state according to the ZND theory: (a) Rayleigh line and Hugoniot curves with and without heat release and (b) evolution of the pressure p and the temperature T across the detonation front

are increased, leading to the accumulation of reactive species. After a characteristic time span, i.e. the ignition delay time τ_{vN}, a sharp increase in heat release is observed, representing the autoignition of the mixture. The induction length Δ_I can be determined as the product of the ignition delay time at the von Neumann state τ_{vN} and the particle velocity u_{vN} behind the shock wave:

$$\Delta_I = \tau_{\mathrm{vN}} u_{\mathrm{vN}}. \tag{1.8}$$

Across the reaction zone, the thermodynamic state of the gas follows the Rayleigh line to the CJ point, as illustrated in Fig. 1.8 a. Due to heat release, the temperature increases further while the pressure decreases due to expansion until the CJ state is reached.

Calculations of CJ parameters and the von Neumann state play an important role in the experimental investigation of a PDC. On the one hand, they allow for predicting the propagation velocity of the detonation front, which can be used to verify, whether successful detonation initiation was achieved. On the other hand, the maximum pressure and temperature amplitudes can be deduced, which helps to accurately design the combustor to ensure safe operation. In order to estimate, the performance of a PDC, however, further considerations are required for two main reasons. Firstly, the gas behind the detonation front moves with the velocity $u_{\mathrm{CJ}} - u_1$ with respect to the combustor, which does not suffice the boundary conditions at the closed combustor inlet. Therefore, the propagating detonation is followed by a so-called Taylor expansion wave, which causes the combustion products to come to a rest [49]. Secondly, the detonation is commonly initiated with a certain axial distance to the combustor head by means of DDT, resulting in a complex pressure evolution inside the PDC. As these two processes impact the thermodynamic state of the exhaust gases, they have to be considered in the performance analysis of PDCs. This was implemented by Gray et al. [21], who used one-dimensional simulations to evaluate the power output of a PDC-driven gas turbine. In addition, Joshi and Lu [50], Kasahara et al. [51], and others performed direct thrust measurements to examine the performance of PDC rocket engines. Undoubtedly, these methods are relevant for optimizing PDCs and are therefore mentioned here. However, they were not applied in the scope of this thesis as it focuses on achieving reliable DDT and minimizing pressure fluctuations at the interfaces to turbomachinery components.

1.2.2 Multi-dimensional Structures in Detonations

Further investigations on the structure of detonation waves revealed that the interaction of the shock wave and the following reaction zone is very sensitive to perturbations. Fluctuations, e.g. in heat release rate in the reaction zone, lead to local pressure variations propagating to the shock front and causing a variation of the associated pressure ratio. Eventually, the induction time and length change, resulting in a discontinuous propagation of the reaction zone leading again to pressure fluctuations. This feedback loop results in a periodic change in the propagation velocity of the detonation wave. Since, pressure fluctuations simultaneously propagate in transverse direction, spatial instabilities occur. Optical visualizations by White [52] and soot foil experiments by Denisov and Troshin [53] revealed that propagating detonation waves contain inherent instabilities, which they described as cellular structure. Voitsekhovskii et al. [54], Soloukhin [55], Strehlow and Crooker [56], Takai et al. [57], and others conducted further investigations on the structure of detonation fronts and found that the interaction of the

incident shock with transverse shock waves lead to a Mach reflection pattern. The intersection of the two shock waves and the resulting Mach stem is referred to as triple point. As the detonation propagates in axial direction, the traces of these triple points form a cellular structure on a two-dimensional plane, as shown in Fig. 1.9.

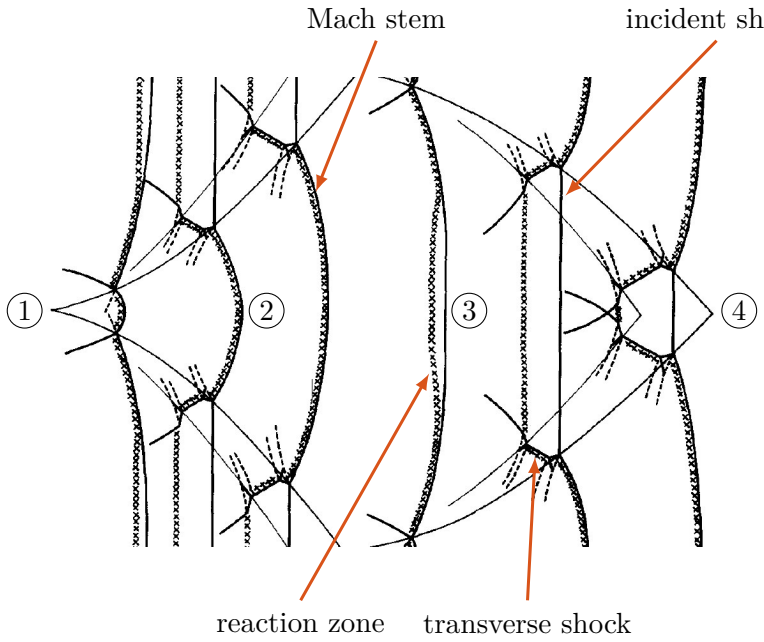

Figure 1.9: Detailed structure of a detonation cell (adapted from [56]). The detonation front propagates from left to right.

A new cell originates from two intersecting transverse waves (1). As they propagate away from each other, a Mach stem can be observed in between that induces a stronger increase in pressure and temperature than the incident shock wave (2). Therefore, the induction length is reduced resulting in a higher propagation velocity. As the area of the Mach stem increases it flattens and transforms to an incident shock (3). Simultaneously, the induction length increases and the propagation velocity decreases. The intersection of two other transverse shock waves finally marks the end of the detonation cell (4). The periodic fluctuation in the propagation velocity of a detonation was first reported by Strehlow and Crooker [56]. However, they found that the average velocity matches well the CJ velocity, which can be determined from thermodynamic considerations as discussed in Sec. 1.2.1. Pintgen et al. [58] used direct visualization techniques to monitor the reaction front in a propagating detonation wave and confirmed the findings from Strehlow and Crooker that the induction length increases along the axial dimension of a detonation cell.

The width of the detonation cells λ was found to be a good measure for various properties of propagating detonation waves, e.g. λ defines the detonability of a mixture as well as detonation limits. In particular, Mitrofanov and Soloukhin [59] found the $13\,\lambda$ criterion for the critical tube diameter that describes the minimum tube dimension from which a spherical detonation can transmit into a unconfined space. In addition, the minimum energy deposition to allow for the onset of a stable detonation was correlated to the cell size by Lee [60]. Furthermore, the minimum tube diameter in which a detonation wave can be established was found by Lee [61] to

be in the range of the cell width λ.

For conditions close to the detonation limits, spinning detonations, as described by Campbell and Woodhead [62], can be observed in a straight tube. For this detonation mode, the propagation is characterized by a front moving along a helical structure while the pitch angle to the wall is related to the tube diameter. The axial propagation velocity is generally lower than the CJ value due to the deviation of the actual propagation direction of the detonation front and the tube axes. For larger tubes, however, these two converge resulting in a propagation velocity close to u_{CJ}. In addition, spinning detonations were found to be linked to significant fluctuations in propagation velocity and pressure of the burnt gas. Mooradian and Gordon [63] measured large fluctuations in static pressure behind the detonation front. Fay [64] proposed spinning detonations to be a self exciting vibratory phenomenon based on the interaction between pressure fluctuations and variations in heat release. Duff [65] confirmed this theory experimentally and stated that multiple modes of fluctuations may coexist. Schott [66] combined optical techniques and sooted foil measurements for detailed investigations on the structure of spinning detonations in acetylene–oxygen mixtures highly diluted with argon. He found the primary shock front to be non-planar. In addition, only part of the fuel–air mixture was consumed by the reaction front attached to the primary shock. The rest of the gas was observed to react in a wave that propagated in circumferential direction. Due to the lower axial propagation velocity of spinning detonations, giving the gas time to expand, the initiation of a stable planar detonation wave propagating at the CJ velocity is desired for PDC operation, which should be considered when dimensioning the combustor. Thus, the determination of the cell width λ for the used fuel–oxidizer mixture at the envisaged temperature and pressure conditions is an important step towards the design of a reliably operating PDC.

Numerous research groups have worked on reliably determining the detonation cell width for a variety of mixture compositions and thermodynamic conditions. The experimental determination of λ, however, is challenging due to irregularities in the cellular pattern, which result in a distributed value of the observed detonation cell-width. Shepherd et al. [67] analyzed the effect of argon dilution on the regularity of the cellular structure and the detonation cell width for various fuels, i.e. acetylene, hydrogen and ethane. For all fuels, dilution with argon increased the regularity of the pattern recorded on sooted foils resulting in less broad distribution of the size of detonation cells. Simultaneously, a decrease in the average width of the recorded cells was observed. Lee et al. [68] developed a digital image processing using the two-dimensional autocorrelation function for determination of the dominant cell size in oxygen–acetylene mixtures. Besides the dominant cell width, the algorithm provides information on the regularity of the cellular structure. Analogous to the results from Shepherd et al., an increasing argon dilution led to a more regular pattern, which resulted in larger and more distinct maxima in the autocorrelation function. Kaneshige and Shepherd [69] collected experimental data from cell size measurements for hydrogen and hydrocarbon fuels over a broad range of parameters. For hydrogen–air mixtures with varying equivalence ratio, the data reveal a minimum cell size for stoichiometric conditions. When applying elevated initial pressure conditions, a decrease in λ was observed, whereas dilution with an inert gas resulted in an increased measured cell width.

To allow for the determination of the detonation cell width for any arbitrary gas composition and initial conditions, semi-empirical models have been developed. Ng et al. [70] postulated the

detonation cell width to be linked to the induction length Δ_I by

$$\lambda = A(\chi)\,\Delta_I, \tag{1.9}$$

where $A(\chi)$ represents a rational function of the non-dimensional stability parameter χ with fixed coefficients, which are specified in [70]. The value of χ can be calculated from

$$\chi = \varepsilon_I\,\Delta_I\,\frac{\dot{\sigma}_{\max}}{u_1}, \tag{1.10}$$

where ε_I, $\dot{\sigma}_{\max}$, and u_1 denote the reduced activation energy, the maximum thermicity, and the particle velocity behind the detonation relative to the shock front, respectively. All these parameters can be extracted from calculations of the ZND profile, by using a series of zero-dimensional chemical reactors [71]. This approach allows for the prediction of the detonation cell width for a stable detonation propagating through an arbitrary fuel–oxidizer mixture at given conditions. However, due to the high sensitivity of the model parameters on changes in temperature and pressure, a validation by experimental results is required.

1.2.3 Detonation Characteristics at Elevated Temperature and Pressure Conditions

When integrating a PDC into a gas turbine, it has to operate at elevated initial temperature and pressure conditions. As discussed in Sec. 1.1, the application of a PDC is especially promising for micro gas turbines, as they hold the largest potential increase in thermal efficiency by modifying the thermodynamic cycle. For these devices, 400 K and 3 bar are typical operating conditions at the combustor inlet. As the previously introduced characteristics of a detonation front are sensitive to the initial mixture conditions, operation at gas turbine relevant conditions affects the initiation and propagation of a stable detonation wave in a PDC. Hence, profound knowledge about the induced variations in characteristic detonation parameters is required to ensure stable PDC operation at these conditions. Some of these parameters can be easily derived from CJ calculations, while others must be determined experimentally as they are either inherently linked to the combustor design or their dependence on the initial conditions is not yet fully understood. As instances of the latter category, measurements of the detonation cell width and the identification of an operating regime to ensure reliable detonation initiation were conducted in the scope of this thesis, which are presented in Ch. 4. In the following, two relevant parameters from the first category are evaluated based on CJ calculations: the CJ velocity u_{CJ} and the pressure ratio across the detonation front Π_{CJ}. The computation results for stoichiometric hydrogen–air mixtures are shown in Fig. 1.10 with respect to the initial temperature T_0 and the initial pressure p_0, respectively.

When increasing the initial temperature T_0 at atmospheric pressure conditions, a decrease in both parameters u_{CJ} and Π_{CJ} is observed, as shown in Fig. 1.10 a This can be explained by a reduced mixture density at elevated temperature conditions. Simultaneously, the speed of sound increases. As the absolute value of the heat release remains constant, the induced temperature increase relative to the initial mixture temperature T_{CJ}/T_0 is reduced. This eventually results in a smaller Mach number of the propagating detonation. Thus, the pressure ratio Π_{CJ} is reduced, as it is directly linked to the Mach number of the shock front. Further, the decreasing Mach

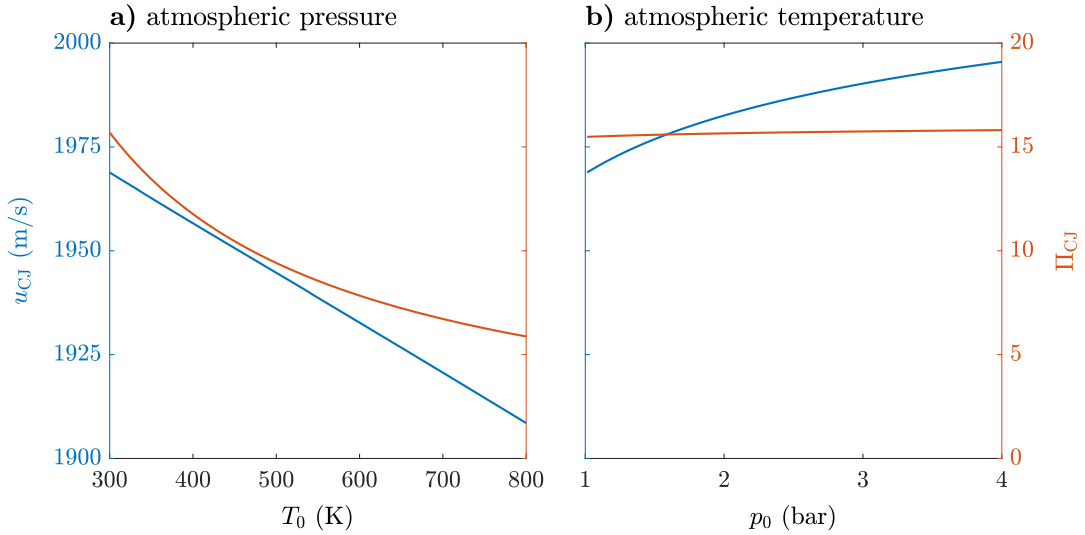

Figure 1.10: CJ velocity u_{CJ} and pressure ratio across the detonation front Π_{CJ} (a) for a variation in the initial temperature T_0 and (b) for elevated initial pressures p_0

number and the increasing speed of sound result in an overall decrease of the CJ velocity.

Increasing the initial pressure p_0 while maintaining ambient temperature conditions, as presented in Fig. 1.10 b, causes a slight increase in the pressure ratio Π_{CJ} and a simultaneous rise in u_{CJ}. Analogous to the considerations for elevated temperature conditions, the pressure ratio Π_{CJ} is closely correlated to the temperature ratio T_{CJ}/T_0. Due to a gradual decrease in the heat capacity c_p of the burnt gas with increasing initial pressure and the constant initial temperature, increasing values of T_{CJ}/T_0 and Π_L are obtained. As the speed of sound is not affected by the change in p_0, the increasing Mach number causes a gradual increase in the CJ velocity u_{CJ} for elevated initial pressure conditions.

The influence of the initial temperature T_0 on the cellular structure of a detonation wave in hydrogen–air mixtures has been rarely studied in the past. Besides, the few published investigations on this topic draw partially contradicting results. Ciccarelli et al. [72] experimentally found that increasing the initial temperature of a stoichiometric hydrogen–air mixture from 300 to 650 K results in a decrease in the cell width from $\lambda \approx 9$ mm to $\lambda \approx 5$ mm. In contrast to that, a zero-dimensional numerical study conducted by Djordjevic et al. [13] suggests an increasing cell width for an increasing mixture temperature. This disagreement can be attributed to two competing effects that are caused by a variation in the mixture temperature. On the one hand, an increase in T_0 leads to a rise in the von Neumann temperature and a drop in the von Neumann pressure [13]. While a larger temperature generally induces a smaller ignition delay time τ_{ign}, the simultaneous decrease in pressure leads to a non-linear dependency on the initial temperature. On the other hand, the increased value of T_{vN} results in a larger speed of sound behind the shock wave, and thus, in an elevated particle velocity u_{vN}. Furthermore, the stability parameter χ is very sensitive to variations in the chemical properties, such as the reduced activation energy and the maximum thermicity in the induction zone. As the available kinetic models have not been validated for the von Neumann state, the numerical model suffers from inaccuracies that may affect the predicted detonation cell width. In order to complement the available experimental data

on the detonation cell width for increased initial mixture temperatures, a systematic examination of the cellular pattern on sooted foils was conducted in the scope of this thesis. The results are presented in Sec. 4.1 and allow for predicting operation characteristics of the used PDC at elevated temperature conditions. Moreover, they offer the possibility to validate numerical models and improve their accuracy at these conditions.

The influence of the initial pressure on the detonation cell size has been investigated by Stamps and Tieszen [73] for hydrogen–air mixtures. They reported a small decrease in λ for experiments with elevated initial pressure of 3 bar compared to measurements at atmospheric conditions. These findings agree well with the numerical results from Djordjevic et al. [13]. These consistent outcomes indicate an increase in the reactivity of the flammable mixture for elevated pressure conditions, which is expected to facilitate the initiation of a stable detonation at elevated pressure conditions. This presumption was verified by an experimental study in the scope of this work. The results of this examination are presented in Sec. 4.2.

1.2.4 Acoustic Pressure Oscillations in Annular Ducts

As already mentioned in Sec. 1.1, the fluctuating pressure conditions at the intersections of PGC devices to turbomachinery components is a major drawback on the way towards the integration into a gas turbine. This is especially true for the outlet of PDCs, were large pressure amplitudes are caused by the detonations that periodically propagate through the combustor. Therefore, the mitigation of these pressure fluctuations is crucial for ensuring the save and efficient operation of a hybrid PDC–turbine system. The integration of an annular plenum downstream of the PDC outlet was proposed by Rezay Haghdoost et al. [74]. Their experimental results revealed a substantial reduction of the maximum pressure amplitude along the plenum axis. In the scope of this thesis, however, the evaluation of recorded pressure histories in the annular plenum downstream of a multi-tube PDC revealed considerable pressure oscillations during the entire operation time. As the occurrence of these oscillations counteract the purpose of the annular plenum, an experimental study was conducted, aiming for understanding the underlaying mechanisms and identifying dependencies between the observed oscillation amplitudes and the operation parameters. As acoustic eigenfrequencies of the annular plenum were found to play a major role, a short introduction to the physical background of acoustic pressure oscillations in an annular duct is given in the following.

Assuming small fluctuations in pressure, density, and velocity $(p', \rho', \vec{u}')$ with respect to the time-averaged conditions $(p_0, \rho_0, \vec{u}_0)$ and negligible influence of sheer stress and gravity, the inhomogeneous wave equation

$$\nabla \left(\frac{1}{\rho_0} \vec{\nabla} p' \right) - \frac{1}{\gamma p_0} \frac{\partial^2 p'}{\partial t^2} = - \frac{\gamma - 1}{\gamma} \frac{\partial \dot{q}'}{\partial t} \tag{1.11}$$

can be derived from the fluid mechanical conservation equations with the isentropic coefficient γ. The quantity $\dot{q}'$ determines the fluctuation in local heat release rate. Considering the speed of sound c_0 with $c_0^2 = \gamma \frac{p_0}{\rho_0}$ and the homogeneous ansatz functions $p'(\vec{x}, t) = \hat{p}(\vec{x})\, e^{i\omega t}$ and $\dot{q}'(\vec{x}, t) = \hat{\dot{q}}(\vec{x})\, e^{i\omega t}$, the wave equation can be written in the frequency domain as

$$c_0^2 \nabla^2 \hat{p} + \omega^2 \hat{p} = -i\omega (\gamma - 1)\, \hat{\dot{q}} \tag{1.12}$$

with the angular frequency $\omega = 2\pi f$. Since heat release due to chemical reaction of fuel and oxidizer takes place in the PDC tubes, $q = 0$ holds for the entire plenum and Eq. 1.12 can be reduced to the homogeneous Helmholtz equation given by

$$c_0^2 \nabla^2 \hat{p} + \omega^2 \hat{p} = 0. \tag{1.13}$$

This homogeneous wave equation describes a linear eigenvalue problem

$$\mathcal{L}(\omega)\hat{p} = 0 \tag{1.14}$$

with the eigenvalues ω^* and the eigenvectors $\hat{p}^*$. Any solution of Eq. 1.13 can be written as a superposition of the eigenvectors, which will be referred to as eigenmodes Ψ in the following. In annular ducts, Rienstra and Hirschberg [75] found that the eigenmodes are composed of one dimensional harmonic functions in axial, azimuthal, and radial direction, respectively. The mode numbers l, m, and n define the number of pressure maxima in the corresponding direction. Each eigenmode $\Psi_{l,m,n}$ is linked to a fixed eigenfrequency $f_{l,m,n}$, which can be calculated by solving the eigenvalue problem in Eq. 1.14.

For simple geometries, e.g., for annular ducts with homogeneous inlet and outlet boundary conditions, the Helmholtz equation can be solved analytically. Moeck et al. [76] used this approach to predict azimuthal thermoacoustic instabilities in an annular Rijke tube. Comparison to experiments revealed good performance of the analytical approach. For more complex configurations like multiple combustion chambers connected to an annular duct, eigenmodes can be found by the application of a network model based on the analytical solution on a one-dimensional domain [77, 78]. Acoustic modes in an arbitrary geometry can be determined by numerical solution of the eigenvalue problem by a finite element solver, as proposed by Walz et al. [79]. Camporeale et al. [80] adopted this method for the numerical solution of the inhomogeneous thermoacoustic Helmholtz equation. The computational costs for solving the eigenvalue problem in annular combustion chambers with a certain degree of symmetry can be decreased by the application of Bloch wave theory, as demonstrated by Mensah et al. [81]. This approach allows for the calculation of azimuthal mode shapes by solving the numeric problem only for a wedge of the annular geometry. As the annular plenum downstream of the PDC, which was investigated in the scope of this thesis, is axissymmetric, this method was used to numerically predict its acoustic eigenmodes and eigenfrequencies. More information of the conducted calculations and the applied boundary conditions are given in Sec. 2.4.

1.3 Previous Investigations on Pulse Detonation Combustion

PDCs have been studied intensively in the past decades. This section gives an overview on the conducted investigations, which are relevant in the context of this thesis. The focus of this literature review is put on two topics: the process of DDT and the flow conditions at the inlet and outlet of the combustor that define the boundary conditions for attached turbomachinery components. These two aspects of PDC research are vital for realizing a stable and efficient operation, as well as the integration in a gas turbine. Furthermore, the discussed investigations form the basis for the experimental research conducted in the scope of this thesis.

1.3.1 Detonation Initiation and Propagation

The detonation initiation is a crucial aspect of PDC operation, as it must be realized in each individual combustion cycle. Moreover, achieving reliable detonation initiation while minimizing fluid dynamical and thermal losses in order to maximize the combustor efficiency is a challenging task. For this reason, several concepts for PDC application have been proposed and investigated in the past, of which the most prominent will be discussed in the following. The local deposition of sufficiently high energy can lead to local explosion, and thus, allows for direct detonation initiation. However, conventional ignition sources are not capable of providing such high energy deposition [82]. Moreover, the required energy deposition drastically reduces the net power output of the device. Therefore, the application of direct detonation initiation in a PDC is not feasible. In order to initiate a detonation wave by the application of a reasonably small energy deposition, DDT has turned out as convenient process for detonation initiation in PDCs. Here, a conventional ignition source, e.g. a spark plug, is used to initiate a deflagration, typically close to the inlet of the combustor. The flame front is accelerated on its way downstream the combustor due to two mechanisms [60]. Firstly, the expansion of the burnt gases directly accelerates the reaction front. Secondly, turbulent velocity fluctuations at the flame front lead to an increase in the flame surface due to flame folding, resulting in a further acceleration of the combustion front. Moreover, fluctuations in the local heat release rate lead to the generation of additional pressure waves. These pressure waves further increase the flow velocity of the unburnt gas ahead of the flame front, and thus, the turbulent fluctuations, which closes a positive feedback loop. This flame accelerating mechanism can either be achieved by a sufficiently high flow rate during the injection of the flammable mixture or due to the acceleration of the unburnt gases due to the expansion of the exhaust gases. Regardless of the formation mechanism, the pressure waves eventually accumulate ahead of the flame forming a leading shock [83, 84], which compresses the unburnt mixture before the reaction front arrives. The acceleration of the deflagrative flame typically finishes when the propagation velocity reaches the speed of sound of the burnt gas. This state was described as high-speed turbulent deflagration or choked flame by Lee et al. [85]. More recent investigations by Chao and Lee [86] suggest that this flame propagation regime is however mainly driven by an autoignition front following the leading shock. When the flame is accelerated to this state, it likely transforms into a detonation within a distance in the order of one meter in a straight tube [60].

In order to allow for the targeted promotion of DDT, the underlaying mechanisms were studied intensively in the past. Over the years, a number of different mechanisms were found to be responsible for detonation initiation depending on the individual experimental setup. The mechanisms, which are relevant in for this thesis, are discussed in the following. According to Oppenheim et al. [87], the highly turbulent flow characteristics ahead of the flame front can lead to pockets of unburnt mixture passing through the reaction zone. These volumes are subsequently burned by deflagrative implosion, leading to locally occurring high pressure conditions. If the resulting pressure is sufficiently high, a local explosion is generated that potentially triggers the onset of a propagating detonation. This postulate was confirmed by experimental investigations by Urtiew and Oppenheim [88]. A second mechanism for the onset of a detonation was proposed by Zel'dovich [89], who introduced combustion regimes for the propagation of autoignition

fronts in a non-uniform mixture. These spatial inhomogeneities in autoignition delay time may arise from temperature or mixture fluctuations caused by turbulence. If the spatial gradient in autoignition delay time τ is in the order of $1/c$, where c denotes the speed of sound, heat release and pressure wave couple and amplify each other, eventually resulting in the onset of a detonation. Finally, a combination of the two mechanisms mentioned above was proposed by Lee et al. [90], known as shock wave amplification by coherent energy release (SWACER). This approach postulates local explosions being amplified by the coupling of a pressure wave and a reaction front.

Before the initiation of the detonation, the combustion process in a PDC is predominated by deflagration, which limits the potential of the PDC in increasing the thermal efficiency of the gas turbine cycle when being compared with the conventional Brayton cycle. Hence, the realization of a short DDT run-up distance is vital for ensuring efficient PDC operation. Numerous concepts to promote the process of DDT have been developed in the past of which relevant instances for PDC application are presented in the following. Shchelkin [91] found that the repetitive blockage of the combustion tube decreases the DDT run-up distance significantly. His analysis resulted in the design of the Shchelkin spiral, a helical structure close to the tube wall. This device increases the amplitude of turbulent fluctuations, which leads to increased flame acceleration and promotes the process of DDT. The effect of the blockage ratio of Shchelkin spirals on the DDT run-up distance was further investigated experimentally by New et al. [92]. They found that low DDT run-up distances could only be achieved by the use of reasonably large blockage ratios. Similar results were obtained for a series of equidistant orifice plates by Lee et al. [85] and Silvestrini et al. [93]. A blockage ratio of 0.43 of each orifice plate has been reported consistently as adequate constriction of the tube cross section area for fast flame acceleration and promotion of DDT in several investigations [94, 95, 96]. Numerical studies by Ma et al. [97] revealed two mechanisms of detonation initiation inside an obstacle filled tube: a local explosion subsequent to the collision of the leading shock with an obstacle and the previously discussed process of SWACER.

A series of orifice plates was used for several experimental studies in the scope of this thesis for two main reasons. On the one hand, the results represent a valid benchmark for the evaluation of alternative DDT concepts. On the other hand, this concept was applied when other aspects of the PDC operation were examined and the mechanism of DDT played a secondary role. For these experiments, a series of orifice plates were chosen as DDT geometry due to the reliable detonation initiation, even for mixtures with reduced detonability. However, the integration of orifice plates or a Shchelkin spiral causes a substantial loss in total pressure and an increase in heat transfer. Therefore, the application of orifices with high blockage ratios decreases the specific impulse of the PDC [98]. Additionally, the formation of recirculation areas near the obstacles hinder the purging of the detonation tube before it is filled with a fresh fuel–oxidizer mixture for the subsequent cycle. Insufficient purging of the hot exhaust gases leads to uncontrolled premature combustion of the injected fuel–oxidizer mixture by contact burning, which prevents reliable high-frequency operation. For these reasons, alternative concepts for DDT promotion have been investigated in recent years.

Cathey et al. [99] demonstrated that the application of transient plasma ignition (TPI) can significantly decrease the delay times to detonation initiation. Further experimental investigations

by Starikovskiy et al. [100] revealed two mechanisms that promote DDT when TPI was applied. Firstly, the spatially distributed discharge caused simultaneous ignition across the entire volume. At the end of this volume, a shock and and a reaction front are initialized that likely turn into a detonation after a reasonable short run-up distance. Secondly, non-uniformly excitation of the mixture was successfully applied promoting the amplification of the resulting autoignition front by a suitable gradient in the autoignition delay time as supposed by Zel'dovich [89]. Numerical simulations by Zhou et al. [101] confirmed the potential decrease in DDT run-up distance by the application of plasma assisted ignition. Gray and Lacoste [102] demonstrated the ability of nanosecond repetitively pulsed plasma discharges to enhance flame acceleration. Based on their observations, the authors propose this technique to replace DDT promotion by obstacles like orifice plates or a Shchelkin spiral. However, the additional system complexity is a clear drawback for the practical application of plasma discharges in a PDC. Furthermore, the underlaying mechanisms on flame acceleration and detonation initiation are not fully understood, which hinders the transfer of the reported results to other PDC devices or different operating conditions.

An alternative concept was introduced by Murray et al. [103], who used a pre-detonator to operate a PDC with commercial fuels that are typically difficult to detonate. In their experiments, a small tube, referred to as pre-detonator, was filled with a highly reactive acetylene–oxygen mixture enabling fast DDT. Due to the high detonation velocity inside the pre-detonator, successful transmission into the detonation tube filled with an acetylene–air mixture was observed for diameters of the pre-detonator down to 3.37 times smaller than the critical tube diameter. Although this approach allows for the application of less reactive fuels for PDC operation, the additional complexity of the system and the necessity of providing a supply of pure oxygen are significant disadvantages compared to conventional methods to promote DDT.

Frolov et al. proposed a concept for detonation initiation through a single obstacle. In their experiments with propane–air mixtures [104] and natural gas–air mixtures [105], a shock wave was generated via a bursting diaphragm. A nozzle shaped obstacle was applied in order to focus the shock wave in the center of the combustion tube, which resulted in extremely high temperature and pressure conditions at the focal point, sufficient for detonation initiation. Semenov et al. [106] showed that proper adjustment of the shape of the shock-focusing device, e.g. sinusoidal shaping of the conic diverging part, can promote detonation initiation. However, this concept was not feasible for cyclic PDC operation due to the usage of a bursting diaphragm. This drawback can be overcome when the shock wave is generated only by means of the flame, which was successfully demonstrated for a hydrogen–oxygen–air mixture by Gray et al. [107]. In their experiments, a deflagration was initialized by a spark discharge. The leading shock, generated by the accelerating combustion front, was then focused at the converging geometry of a single obstacle, which resulted in successful detonation initiation. The conducted experiments were reproduced in numerical simulations by Bengoechea et al. [108], which confirmed the onset of the detonation at the focal point of the shock-focusing device. Further calculations by Bengoechea et al. [109] revealed two mechanisms being responsible for detonation initiation, depending on the pressure ratio across the leading shock. If the leading shock is strong enough, the extremely high pressure and temperature conditions at the focal point result in direct initiation of a propagating detonation. If the pressure ratio across the leading shock is slightly lower, the released energy is not sufficient for initiating a detonation but rather triggers autoignition. As the reflected

shock propagates further two collapsing points along the center are observed traveling away from the focal point. If the propagation speed of this pressure wave couples with the triggered autoignition, a detonation is initiated by means of SWACER. In experiments, however, the two different mechanisms leading to successful detonation initiation cannot be separated. Rather the lower limit of the latter process can be examined to identify the required operating conditions for reliable PDC operation, which has been performed in the scope of this thesis for atmospheric and elevated pressure conditions, respectively.

1.3.2 Interaction with Turbomachinery Components

In recent years, several experimental investigations were conducted in order to demonstrate the work extracting from the PDC exhaust by means of a turbine. Glaser et al. [110, 111] examined the performance of an axial turbine downstream of a multi-tube PDC. They conclude that the efficiency of a PDC-driven turbine and a turbine driven by a conventional steady-state combustor were comparable. Rasheed et al. [112] even demonstrated a potential increase in thermal efficiency of the gas turbine cycle by the application of pulse detonation combustion. The experiments were conducted at a hybrid PDC–turbine facility with eight combustion tubes arranged in a can-annular configuration. The measured turbine efficiency was comparable with the value for isobaric combustion although the experimental setup was not optimized for the operation with a PDC. Accounting for improvements in the reactant injection, the authors predict a potential of 25 % improvement in thermal efficiency of the hybrid system compared to conventional steady-state combustion. Comparable results were reported by Rouser et al. [113, 114], who operated a radial turbine by a hydrogen-fueled PDC. They observed the produced power with an effective turbine efficiency of 40 % to be equivalent to the power obtained from operation with steady-state combustion with 60 % turbine efficiency. However, detailed analyses of the flow characteristics in the turbine revealed large potential for optimization. In particular, Schauer et al. [115] reported high losses through the turbine stage expansion for stable operation of a single-tube PDC with a downstream attached radial turbine. Furthermore, pressure measurements at the turbine inlet and exit indicated that the amplitude of the shocks exiting the PDC were significantly attenuated by the turbine stage. Hence, the unsteadiness of the flow conditions at the inlet of potentially following turbine stages is drastically decreased. Similar results were found by Dean et al. [116] who evaluated the operation behavior of a two-stage axial turbine attached to a PDC. They found that the application of the turbine reduces the noise emission of the PDC by 28 dB. Complementary numerical simulations revealed significant shock reflections in the turbine that were found to be dependent on the turbine design. Rasheed et al. [117], who achieved stable operation of an axial turbine driven by eight circumferentially arranged PDCs, reported 20 dB peak pressure attenuation and 10 dB reduction of broad band noise by a single turbine stage.

The mentioned studies consistently report a drastic attenuation of pressure fluctuations by the first turbine stage, so that downstream stages are only marginally affected by the periodic combustion in the PDC. Nevertheless, the first turbine stage is exposed to considerable pressure amplitudes, which reduces the turbine efficiency [114] and causes additional mechanical stress [118] for the turbine components. These findings were supported by results from time-resolved measurements of pressure, temperature, and velocity at the inlet and exit of a radial turbine, which was attached downstream of a PDC [119]. The authors reported secondary unsteady flow

features with amplitudes as high as the absolute value of the mean flow. Therefore, several studies addressed the targeted decrease of the amplitude of pressure fluctuations at the PDC outlet by adjusting the operation parameters. Two concepts for the attenuation of the shock waves exiting a PDC were proposed: adjusting the chronological succession of firing combustion tubes in a multi-tube PDC and the integration of a plenum between the combustor outlet and the turbine inlet.

Caldwell et al. [120] found that the simultaneous firing of two parallel arranged PDC tubes led to a large shock amplitude entering the turbine. In contrast, a small time delay induced a considerable decrease in the amplitude of the second shock due to the blow down in the first PDC tube. Rasheed et al. [121] found that the proper adjustment of the firing pattern allows for a reduction of the peak pressure measured at the turbine inlet. They reported the lowest amplitudes for sequential firing of the eight circumferentially arranged PDC tubes, while highest peak values were observed for simultaneous operation. Similar results were found by Qiu et al. [122], who investigated the effect of the applied firing pattern of a combustor with two PDC tubes on the performance of a turbocharger turbine. Asynchronous firing resulted in smaller pressure amplitudes and a higher rotary speed of the turbine when compared to synchronous operation of both PDC tubes. An alternative concept was proposed by Rezay Haghdoost et al. [123, 74], who integrated an annular plenum downstream of a multi-tube PDC with six tubes in order to achieve an attenuation of the shocks exiting the combustor. The measured shock amplitude was found to monotonically decrease along the axis of the plenum. Compared to the firing of a single PDC tube, the application of a sequential firing pattern resulted in a additional reduction of the shock amplitude at the plenum outlet. In conclusion, the combination of the proper adjustment of operation parameters, e.g. firing pattern and firing frequency, and the integration of a suitable plenum downstream of the PDC, allows for a significant reduction of the pressure amplitude at the turbine inlet. As mentioned in Sec. 1.2.4, the integration of an annular plenum downstream of a multi-tube PDC was found to cause a second type of pressure fluctuations downstream of the combustor, which were coupled to the acoustic eigenmodes of the plenum. In the scope of this thesis, the introduced methods for reducing pressure fluctuations were applied and their effect on the acoustic pressure oscillations was analyzed.

Up to now, only few publications focus on the interaction of PDCs with upstream attached compressors. Hoke et al. [124] demonstrated the feasibility of a turbine-driven centrifugal compressor to provide an adequate air flow into a PDC. Lu et al. [125] conducted an experimental study on the operation of a four-tube PDC with an upstream attached centrifugal compressor. Their results revealed pressure fluctuations of 80 to 130 % at the compressor outlet due to the periodic combustion process. The induced temporal blockage of single compressor passages resulted in a decreased air mass flow rate in the compressor. These results suggest that the proper design of the combustor inlet is vital to ensure safe, stable and efficient operation of the compressor. Ideally, the combustor inlet design should fulfill the following requirements. Firstly, the combustor inlet should reduce the amplitude of upstream propagating pressure waves as they prevent the continuous flow of oxidizer, and thus, impede the purging of exhaust gases. Moreover, they can harm the operation and structure of a compressor attached upstream. Secondly, the pressure loss of the flow during the injection of flammable mixture is desired to be low to increase the specific thrust of the PDC. Thirdly, the design of the PDC inlet should

promote flame acceleration by ensuring a large flow resistance in upstream direction. Lastly, the injection control for fuel and oxidizer should be independent when operating a multi-tube PDC to allow for adjusting the firing pattern. Due to the diverse requirements, several designs for the PDC inlet have been realized in previous studies. Rouser et al. [114] used valve heads from an automotive piston engine driven by a cam shaft to block the combustor inlet during the combustion process. A similar effect was achieved by a rotary valve designed by Matsuoka et al. [126]. Both designs allowed for reliable and stable operation but the cycle timings, e.g. the ratio of the injection duration and the cycle period, were fixed, which prevented the flexible adjustment of operation parameters and therefore restricted the operating range. This flexibility was ensured by a valveless design of the inlet geometry, realized by Wang et al. [127]. However, considerable backflow of the exhaust gases was observed, which prevented the operation of the PDC with a well-controlled composition of the fuel–oxidizer mixture due to inherent exhaust gas recirculation. The PDC facilities, which have been examined in the scope of this thesis, were chosen to contain a valveless oxidizer supply. This was essential to allow for evaluating the effect of independent variations in the firing frequency and the firing pattern during the operation of the multi-tube PDC.

1.4 Scope of the Thesis

The present thesis contributes to the ongoing research on the implementation of pulse detonation combustion into a gas turbine. As highlighted in the previous section, the two major challenges on this path are to achieve highly reliable detonation initiation with reasonably small additional loss in total pressure and reducing pressure fluctuations at the interfaces to attached turbomachinery components. In this work, three specific aspects of current PDC research are addressed by means of experimental investigations on PDC test facilities. First, the concept of shock-focusing for achieving detonation initiation is compared against a series of orifice plates, which represents a conventional concept for DDT promotion. Second, the reliability of DDT at gas turbine relevant conditions is investigated. Lastly, pressure fluctuations upstream and downstream of a PDC are examined for a variety of operation parameters, which allows to draw conclusions on favorable conditions for achieving small pressure amplitudes. In order to provide a systematic presentation of the conducted experimental investigations and the deduced results, the thesis is structured as follows:

Chapter 2 presents the experimental facilities. First, the single-tube PDC is introduced, which was used to investigate the effect of varying boundary conditions on the PDC operation. Subsequently, the setup of the multi-tube PDC is discussed, which allows for the evaluation of the interaction of six combustion tubes, as well as the measurement of pressure fluctuations upstream and downstream of the combustor. The introduction of operation parameters, such as firing frequency, equivalence ratio, oxygen concentration in the oxidizer, and firing pattern, is followed by a discussion on the used measurement techniques and signal processing methods. In particular, the experimental methodologies for the determination of reactant mass flow rates and initial mixture conditions are presented. Furthermore, details on the applied techniques for the evaluation of the combustion process, fuel concentration measurements, and the determination

of the detonation cell width are given. Lastly, a numerical method for the prediction of acoustic eigenmodes and eigenfrequencies of the annular plenum downstream of the multi-tube PDC is presented.

Chaper 3 discusses the operation characteristics of the single-tube PDC equipped with two different DDT geometries: a shock-focusing device and a series of orifice plates. First, the successful onset of a propagating detonation at the focal point is validated by high-speed imaging and pressure histories. Second, the influence of the applied operation parameters, e.g. Reynolds number of the flow and reactivity of the flammable mixture, on the success rate of detonation initiation is analyzed, which allows for identifying required conditions for reliable operation. Furthermore, the detonation initiation by shock focusing is compared with DDT promotion by a series of orifice plates. The necessary operation parameters for both setups are examined on the basis of experimental investigations with invariable mixture composition. Additionally, cycle-to-cycle variations and the pressure evolution at the combustor inlet are evaluated, which allows for comparing the feasibility of these DDT geometries for PDC application.

Chapter 4 examines the process of detonation initiation in the single-tube PDC at gas turbine relevant conditions. For this, the detonation cell width is evaluated for increased mixture temperatures based on the imprints on sooted foils. These measurements allow for assessing the detonability of the fuel–oxidizer mixture, which is a key challenge in predicting the reliability of DDT at elevated temperature conditions. Subsequently, the formation of the leading shock and the detonation initiation by shock focusing is investigated for elevated initial pressure conditions. Lastly, the reliable operation of the single-tube PDC with shock-focusing device at globally lean fuel–oxidizer mixtures was achieved by means of fuel stratification. The results of these experimental studies allow for predicting the required operating conditions for achieving reliable detonation initiation under gas turbine relevant conditions.

Chapter 5 evaluates pressure fluctuations upstream and downstream of the multi-tube PDC test rig. Small pressure amplitudes upstream and downstream of the combustor are desired to ensure save and efficient operation of attached turbomachinery components. In order to find optimum operation parameters for the investigated setup for minimizing the pressure fluctuations upstream of the combustor, the air supply pressure is analyzed for variations in the geometric confinement of the oxidizer supply, the firing pattern and the equivalence ratio. In addition, pressure measurements in the annular plenum downstream of the multi-tube PDC revealed considerable acoustic pressure oscillations during the entire operation duration. To examine the excitation mechanisms of these acoustic oscillations, recorded signals of an array of circumferentially distributed pressure sensors are analyzed by azimuthal and frequency decomposition. Further, the conducted investigations allow for determining the impact of various operating conditions, i.e. the firing frequency, the firing pattern, and the acoustic boundary condition at the outlet of the plenum. Moreover, a recommendation for setting the operation parameters to minimize pressure fluctuations is deduced based on a quantitative comparison of the integral energy of acoustic pressure oscillations and the number of excited modes.

Chapter 6 summarizes the findings of the presented experimental studies in the scope of this thesis and evaluates the results in the context of current PDC research. In addition, future perspectives for further research topics are highlighted.

Chapter 2

Experimental Facilities and Measurement Techniques

The test facilities, which were used for experimental investigations in the scope of this thesis, are presented in this chapter. Subsequently, the operation procedures of the test rigs are described and characteristic parameters are introduced. In addition, the applied measurement techniques and signal processing methods are discussed. In the last section of this chapter, the applied methodology for predicting acoustic eigenmodes and eigenfrequencies of the annular plenum is described.

2.1 Single-tube PDC Test Rig

A single-tube PDC test facility has been set up at the Chair of Fluid Dynamics at TU Berlin by Gray [71], which allowed for the investigation of the DDT and the propagating detonation wave at atmospheric pressure and temperature conditions in low-frequency operation. In the scope of this thesis, the test rig design was further improved to allow for reliable multi-cycle operation at elevated firing frequencies up to 33 Hz. In addition, the process of flame acceleration and detonation initiation was investigated under elevated temperature and pressure conditions, respectively. The single-tube PDC test rig was situated in a combustion laboratory with individually controlled supply lines for air, oxygen, and fuel. A schematic of the test facility including the gas supply and the installed instrumentation is presented in Fig. 2.1. All instruments were operated by a LabVIEW interface, which was separated from the control of the test rig.

Compressed air was provided by a reservoir that is pressurized to 12 bar. For all measurements, a continuous air flow was applied, which was maintained by a proportional–integral–derivative (PID) controller. For this, the air mass flow rate, measured by a Coriolis mass flow meter (Endress+Hauser Promass 80A), was evaluated. The control error was then used to define the position of an electric proportional valve (Bürkert 2712). In order to increase the reactivity of the flammable mixture, oxygen enriched air was used in some investigations in the scope of this thesis. Oxygen was taken from a bundle of gas cylinders with a maximum pressure of 300 bar. A

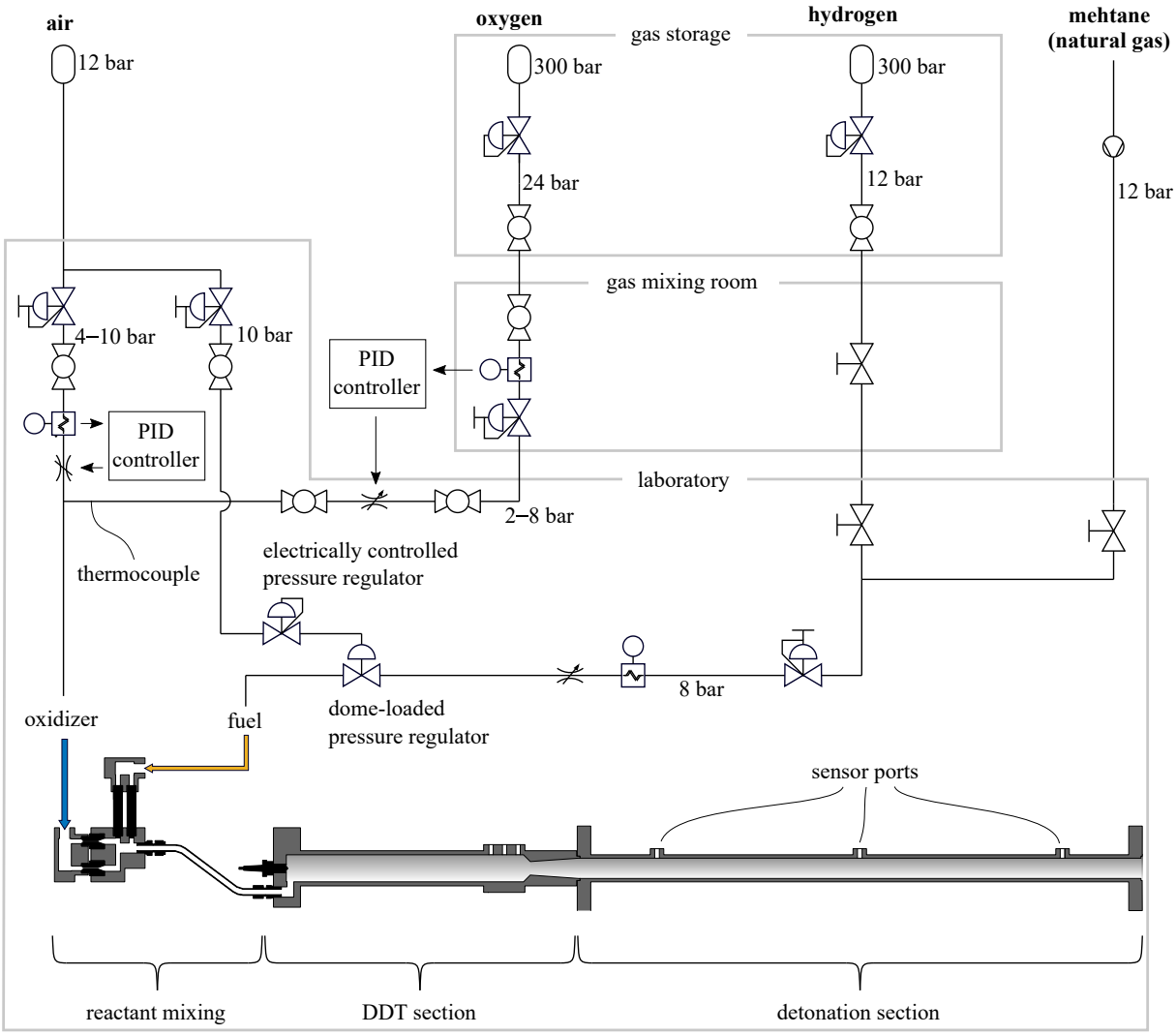

Figure 2.1: Schematic of the gas supply lines and the relevant instrumentation for the single-tube PDC test rig

pressure regulator was installed to reduce the pressure to a constant value of 24 bar. Analogous to the air supply, a Coriolis mass flow meter (Endress+Hauser Promass 83F) and a proportional valve (Bürkert 2712) were used to setup a PID controller. The controller settings for the oxygen line were adjusted to prevent rapid changes in the valve position to ensure save operation. As reported in [128], fast changes in the valve position may lead to pressure waves, which can result in ignition in the oxygen line. To increase the operating range of the mass flow controller, a manual pressure regulator was installed to reduce the line pressure to a value in the range of 2 to 8 bar.

Hydrogen was used as fuel for all combustion experiments conducted in the scope of this thesis. It was provided by a bundle of gas cylinders equipped with a pressure regulator, which reduced the pressure to 12 bar. An additional manual pressure regulator in the laboratory allowed for a further reduction of the supply pressure to 8 bar. Unlike the oxidizer gases, the fuel was injected periodically, which prohibits the establishment of a steady-state flow rate. Therefore, the amount of injected fuel was not controlled by a PID controller but rather by the supply

pressure upstream of the injection valves. Fore this, a dome-loaded pressure regulator was applied to allow for the accurate adjustment of the fuel supply pressure upstream of the solenoid injection valves. Without this pressure regulator, the supply pressure drops when the valves are opened, resulting in a gradual decrease of the injected fuel mass flow over time. By the installation of the dome-loaded pressure regulator, this pressure drop was significantly reduced and the time until a steady-state value in the supply pressure was reached was decreased to the order of milliseconds. This procedure allowed for the injection of a nearly constant mass flow rate throughout the entire injection period. To investigate the fuel distribution inside the PDC, tunable diode laser absorption spectroscopy (TDLAS) was applied, which provided a time-resolved line-of-sight measurement of the fuel concentration. For these measurements, natural gas was used as tracer fuel, since the absorption feature of methane at 1,653.7 nm matches the wavelength of the available diode laser. The gas was taken from an access to the natural gas distribution system of Berlin, which ensured methane to be the predominant species in the used tracer fuel. After being compressed to 12 bar, the gas was guided to the fuel supply line upstream of the manual pressure regulator.

Besides the gas supply, the laboratory was equipped with a high-speed data processing module (National Instruments MXI). This system allowed the control of actuators and data acquisition for 20 channels at 1 MHz. A separate LabVIEW program has been developed at the Chair of Fluid Dynamics to allow for the cyclic operation of the PDC. The PDC test rig itself was designed modularly and consists of three main sections: reactant mixing, a DDT section, and a detonation section. For the latter, a straight tube with a circular cross section area was used for all measurements. At several axial positions, ports were mounted to allow for the application of sensors. Measurement procedures and signal processing methods, which have been applied in the scope of this thesis, are presented in Sec. 2.3. In the following, relevant operation parameters of the single-tube PDC are introduced. Subsequently, geometric details of the reactant mixing and DDT section are presented. Lastly, the control and monitoring of the fuel injection is discussed.

2.1.1 Operating Parameters

The PDC cycle is defined by three parameters:

t_{cycle}	cycle duration
t_{inj}	injection duration
t_{ign}	time of ignition with respect to the beginning of the cycle

The cycle duration t_{cycle} defines the length of each cycle during the periodic operation of the PDC. This parameter is directly related to the firing frequency

$$f_{\mathrm{tube}} = \frac{1}{t_{\mathrm{cycle}}}. \tag{2.1}$$

An illustration of the introduced parameters and other deduced timings is given in Fig. 2.2. The PDC cycle starts with the injection of fuel, which is realized by opening the solenoid fuel valves (1). The injection duration t_{inj} denotes the period, in which fuel is added to the oxidizer

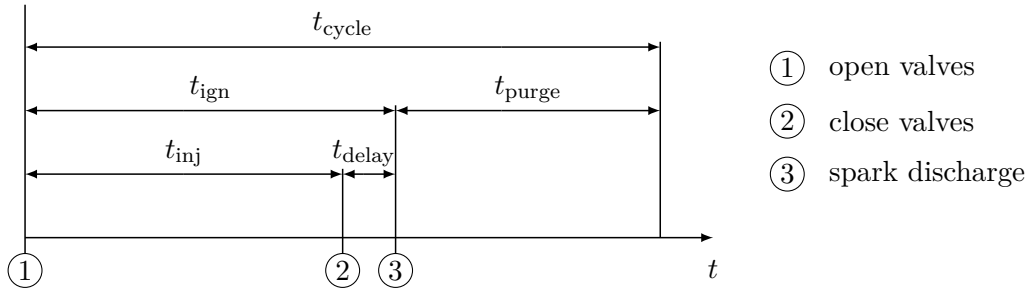

Figure 2.2: Illustration of the cycle timings for the periodic operation of the PDC

flow. The duty cycle of the fuel injection is defined as

$$g_{\mathrm{inj}} = \frac{t_{\mathrm{inj}}}{t_{\mathrm{cycle}}}. \tag{2.2}$$

After the injection of the reactive mixture is finished by closing the fuel valves (2), the ignition is triggered by spark discharge after t_{ign} elapses (3). A time delay $t_{\mathrm{delay}} = t_{\mathrm{ign}} - t_{\mathrm{inj}}$, usually in the order of some milliseconds, between the closing of the fuel valves and the triggering of the ignition spark is applied to allow for purging the mixing section with pure oxidizer. This procedure minimizes the fuel concentration upstream of the PDC inlet, and thus hinders the initiated reaction front from propagating upstream into the supply line, where it would cause undesired thermal and mechanical stress. Simultaneously, this time delay should be reasonably small to ensure a high reactivity of the mixture around the ignition spark. Otherwise, the reactive mixture is purged from the combustor inlet, which results in ignition failure. Subsequent to the combustion event, the PDC tube is purged with pure oxidizer for the remaining cycle duration t_{purge} to separate the hot exhaust gases from the fresh mixture that is injected in the subsequent cycle.

2.1.2 Combustor Inlet Design

The combustor inlet affects multiple aspects of PDC operation, e.g. the mixing of reactants during the injection period, the propagation of the reaction front subsequent to the ignition by a spark plug, and the back flow of hot exhaust gases as a result of a pressure increase in the combustor. An ideal inlet geometry would assure the injection of perfectly mixed reactants, while preventing pressure waves or combustion products from traveling upstream. In addition, the inlet geometry should be designed to minimize the loss of total pressure during the injection. As discussed in Sec. 1.3.2, these requirements are partly contrary. Thus, all geometries, that have been proposed in the available literature, suffer from missing at least one objective.

In the scope of previous studies at TU Berlin, Gray [71] designed a hemispherical combustor head to promote the formation of a strong leading shock in front of the propagating flame due to the reflection of upstream propagating pressure waves. A cross section of the geometry is sketched in Fig. 2.3. The continuous flow of the oxidizer is guided through an annular duct, in which fuel is added during the injection period. The flow direction of the mixture is then changed by 180 degrees before the mixture is injected into the PDC through an annular gap. The ignition spark is located in the center of the hemispherical wave reflector. This setup was

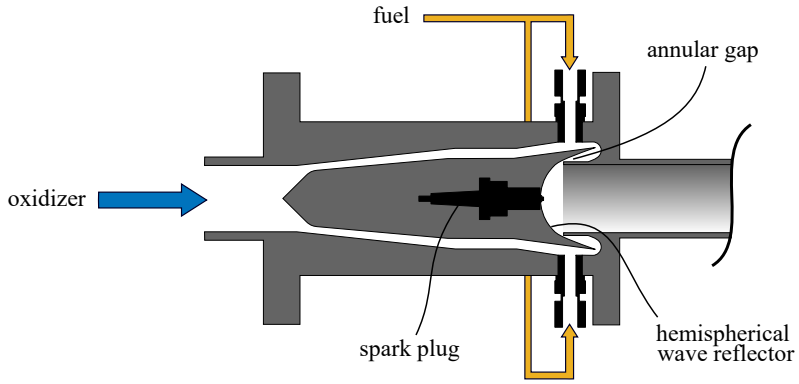

Figure 2.3: Cross section of the PDC inlet with hemispherical wave reflector

successfully used for reliable detonation initiation by shock focusing in hydrogen–oxygen–air mixtures [71, 107]. In the scope of the present thesis, the hemispherical wave reflector was applied for experimental investigations of the detonation cell width in stoichiometric hydrogen–air mixtures at elevated temperature conditions, as presented in Sec. 4.1. The compact design of the inlet geometry resulted in low heat loss, which allowed for experiments over a broad range of mixture temperatures. However, when applying the hemispherical wave reflector, the firing frequency was limited to a maximum of 5 Hz due to the occurrence of contact burning at low purging times. This was found to be caused by a low flow resistance in upstream direction, which allowed for expansion of exhaust gases into the oxidizer supply subsequent to the combustion event. This backflow of hot gases caused the inlet geometry to be exposed to enormous thermal and mechanical stress. In addition, a long purging time was required before a fresh fuel–oxidizer mixture could be injected without the risk of contact burning. The need to avoid this contact burning required a sufficiently long purging duration, which imposed a restriction on the firing frequency. Therefore, the inlet geometry including the hemispherical wave reflector is not suitable for multi-cycle operation.

In order to allow for the investigation of PDC operation at elevated firing frequencies, the inlet geometry was modified. In the new configuration, shown in Fig. 2.4, the air flow is guided through six parallel arranged nozzles, of which only two are visualized. The fuel is injected downstream of the choked nozzles through parallel arranged solenoid valves (Bosch 0280158827). The mixture is then fed to the PDC through three circumferentially distributed injection ports close to the planar combustor head. The mixing station is connected to these radial injection ports by three mixing tubes. In Fig. 2.4, only one out of three parallel arranged mixing lines is shown for simplicity.

Two different nozzle designs, which differ in the diameter of the cross section area, were applied in the scope of this thesis. The respective diameters of 2 and 2.8 mm result in total cross section areas of the air supply of 75 and 148 mm^2. The integration of this obstruction causes choked flow conditions inside the nozzles. Hence, the oxidizer supply pressure p_{ox} recorded by the thin-film metal pressure sensor P_{ox} (Festo SPTW) is a measure for the oxidizer mass flow rate. Analogous to the oxidizer flow, the fuel flow was choked during the injection period allowing for assessing the fuel mass flow from the fuel supply pressure p_{fuel}, which was recorded by the static pressure transducer $\mathrm{P}_{\mathrm{fuel}}$. A detailed description of the procedure for monitoring the reactant flow rates

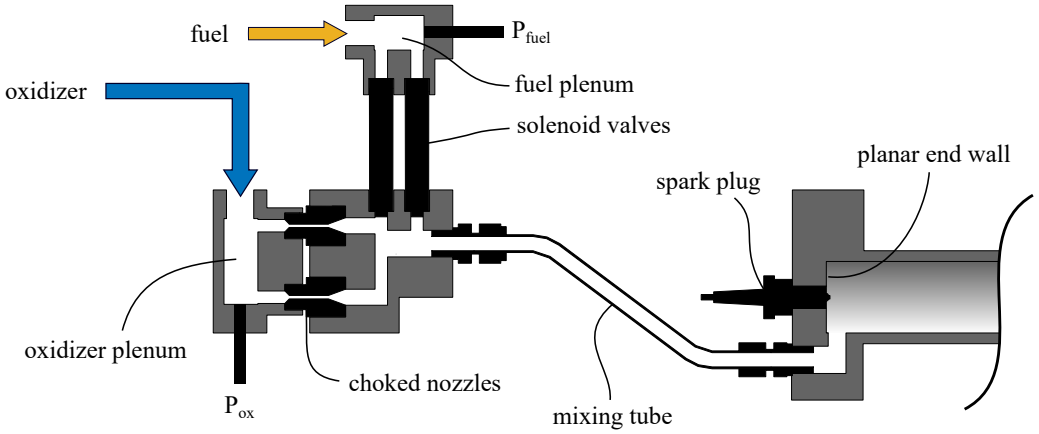

Figure 2.4: Cross section of the PDC inlet configuration with planar end wall of the combustion tube and choked nozzles in the oxidizer supply

is given in Sec. 2.1.4. Upstream propagating pressure waves, that were generated by combustion in the PDC tube, were found to be damped significantly by the integrated oxidizer plenum. Therefore, no large fluctuations in pressure or mass flow rate were observed in the oxygen supply line. Thus, the design allowed for the safe operation with oxygen-enriched air as oxidizer.

2.1.3 DDT Section

As discussed in Sec. 1.3.1, several concepts have been proposed in the past in order to promote the initiation of a detonation and reduce the DDT run-up distance. Two concepts were investigated in the scope of this thesis: a series of orifice plates and a shock-focusing device. In Ch. 3, the performance of both concepts are elaborated for varying operating conditions and their suitability for PDC application is compared. The first considered DDT geometry consisted of a series of orifice plates, equally spaced at a distance of 85 mm in a tube with an inner diameter of 30 mm. The configuration is sketched in Fig. 2.5 a. Each orifice plate had a thickness of 2 mm and a blockage ratio of 0.43, which has been reported as adequate parameters for fast flame acceleration and promotion of DDT in previous studies [94, 95, 96]. The number of orifice plates was varied from 1 to a maximum of 6. The tube segments between two consecutive obstacles were bolted together through muffs. These connections and the dimensions of the tube wall were designed to allow for PDC operation at elevated pressure conditions up to an initial pressure of 3 bar. The described DDT enhancing geometry was used in the scope of this thesis for investigations at elevated temperature conditions (Sec. 4.1). Furthermore, it was integrated into the multi-tube test rig, which is presented in Sec. 2.2.

The second DDT geometry was designed to realize detonation initiation by shock focusing as proposed by Gray et al. [107] based on considerations by Frolov and Aksenov [104]. The applied geometry contained a pre-detonation chamber and a single obstacle consisting of a converging and a diverging part, as sketched in Fig. 2.5 b. The converging part consisted of an axisymmetric constriction of the cross section area with a wall angle of 45° with respect to the tube axis. By this, the tube diameter was decreased from 40 mm to 20 mm. In the diverging part, the tube diameter was increased again to 30 mm with an angle of 4° of the conic wall with respect to the tube axis in order to avoid flow separation. In Ch. 3, the detonation initiation by shock focusing

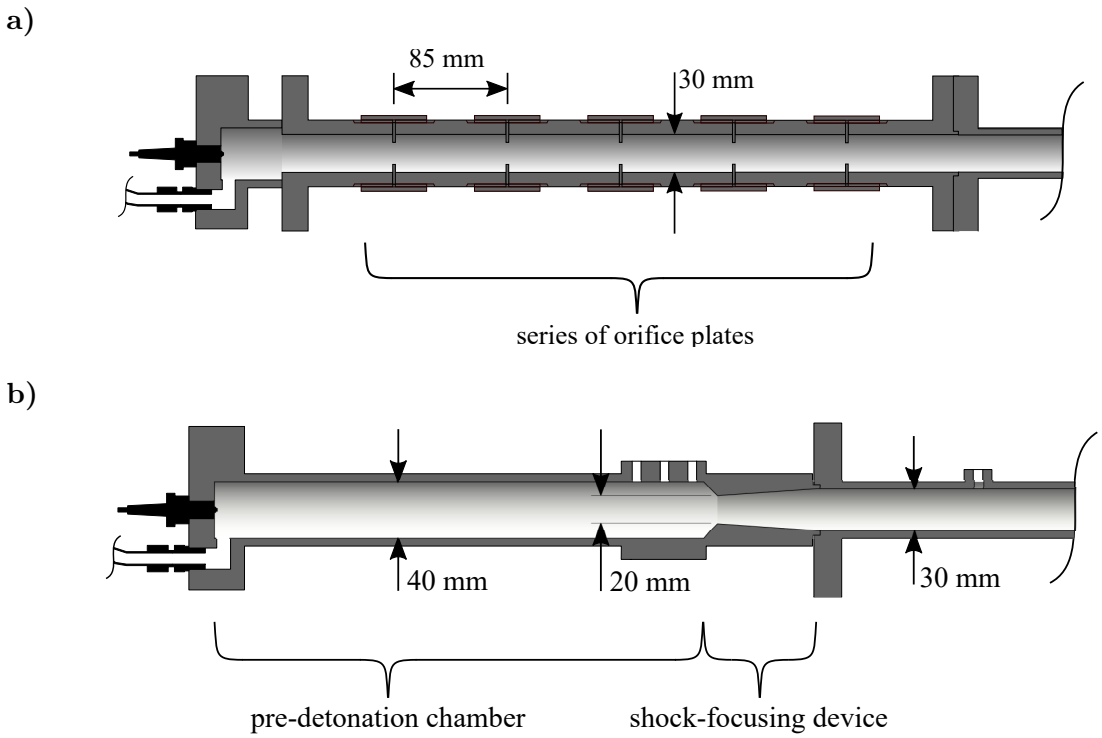

Figure 2.5: Cross sections of the two investigated DDT geometries: (a) a series of orifice plates and (b) a shock-focusing device

is examined at atmospheric temperature and pressure conditions and the results are compared to the PDC operation with a series of orifice plates. In addition, the operation of the single-tube PDC, equipped with the shock-focusing device, was examined at elevated pressure conditions (Sec. 4.2) and under globally lean mixture conditions (Sec. 4.3).

2.1.4 Control and Monitoring of the Fuel Injection

The accurate injection of the fuel and the subsequent mixing with the oxidizer during the filling of the PDC is vital for achieving a well-controlled fuel–oxidizer mixture across the combustor. For steady-state pressure conditions downstream of the fuel valves, which was assured by applying a continuous oxidizer flow rate, the fuel mass flow rate solely depended on the static pressure upstream of the valves. Hence, the precise control of the static pressure during the entire injection period was required to achieve the desired fuel concentration throughout the combustor. In this section, the need of integrating a dome-loaded pressure regulator into the fuel supply line is highlighted. Further, a method for evaluating the fuel mass flow rate during the injection period of a multi-cycle operation is presented.

Due to inertia of the fuel supply lines, opening the fuel valves resulted in an instant drop in the supply pressure p_{fuel}, that was measured by a thin-film metal sensor (Festo SPTW). The underlaying principle and the sensor functionality will be discussed in Sec. 2.3.2. Without the integration of the dome-loaded pressure regulator, a gradual decrease in pressure was observed subsequently. Hence, an injection duration of several seconds was required for investigations of the DDT process under controllable mixture composition and spatially constant fuel concentration.

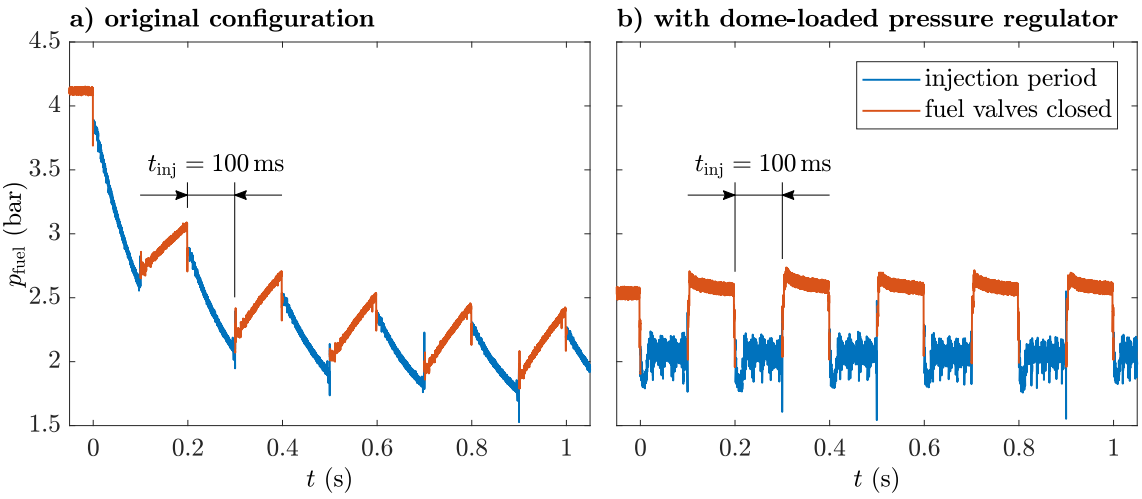

Figure 2.6: Fuel supply pressure in multi-cycle operation (a) before and (b) after the integration of a dome-loaded pressure regulator for a firing frequency of 5 Hz and an injection duration of 100 ms

In addition, no repeatable multi-cycle operation was possible, illustrated by the cycle-to-cycle deviation of the fuel supply pressure in Fig. 2.6 a. The integration of a dome-loaded pressure regulator drastically decreased the inertia of the supply line, which resulted in a nearly constant supply pressure already after approximately 2 ms subsequent to the start of the injection period (Fig. 2.6 b). Thus, this procedure allowed for the accurate and repeatable injection of a nearly homogeneous mixture in multi-cycle operation with reasonably short injection periods.

As mentioned above, Coriolis mass flow meters were installed in each supply line of air, oxygen, and fuel, which are suited for the direct and non-intrusive measurement of the mass flow rate of any gas. However, due to inertia of the supply lines and the relatively low sampling rate of the Coriolis mass flow meters, this procedure only allowed for the reliable measurement of the flow rates for steady-state flow conditions, which were achieved for oxygen and air but not for the periodically injected fuel. Nevertheless, the fuel mass flow rate during the injection period could be determined from a linear calibration curve that matched the fuel supply pressure to $\dot{m}_{fuel}$. The applied procedure for deducing this calibration curve is presented in the following. To obtain a continuous flow of fuel, long injection times with $t_{inj} > 4\,s$ were required. By this, a constant fuel mass flow rate was obtained from the output signal of the Coriolis mass flow meter, as shown in Fig. 2.7 a. The recorded signal slowly rises after the fuel valves are opened at $t = 0\,s$ and converges to $\dot{m}_{fuel} = 4.4\,kg/h$ after roughly 4 s. As shown by the graph in Fig. 2.7 c, the fuel supply pressure measured in the fuel plenum, reaches a steady-state value of $p_{fuel} = 3.7\,bar$ almost instantaneously, which indicates stationary flow conditions upstream of the fuel valves, and thus, a constant injected fuel mass flow rate of 4.4 kg/h throughout the entire injection period.

When conducting multi-cycle operation, the fuel is injected periodically resulting in a fluctuating mass flow rate. As expected, the Coriolis mass flow meter is not capable of resolving this periodic fluctuation (Fig.2.7 b). However, the evaluation of the fuel supply pressure (Fig. 2.7 d) during the injection period allows for an alternative way for the determination of the injected fuel mass

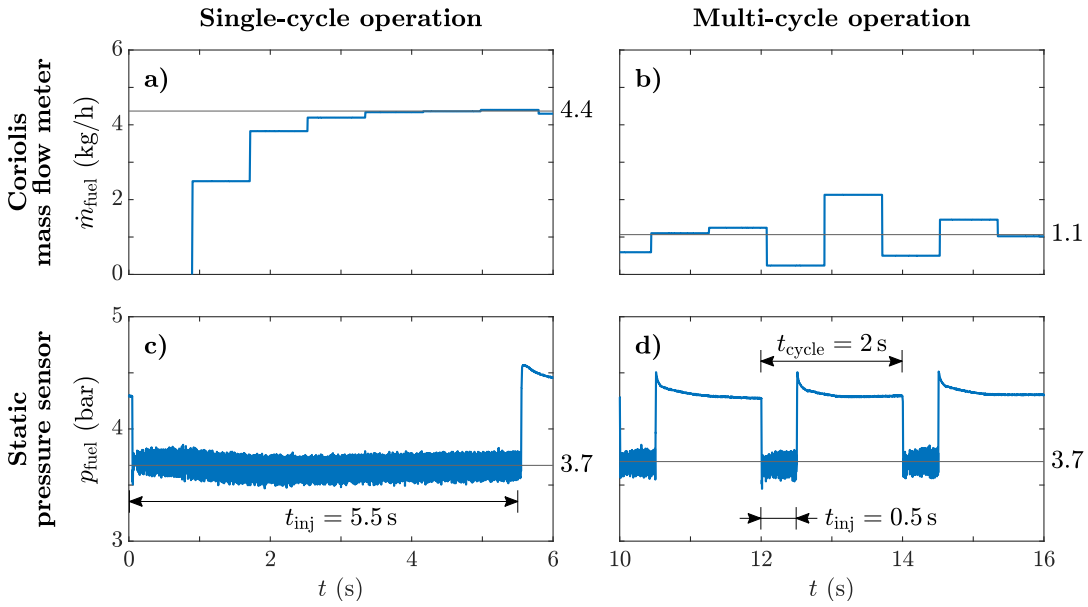

Figure 2.7: Fuel mass flow rate and supply pressure for single-cycle operation with an injection duration of $t_{\mathrm{inj}} = 5.5\,\mathrm{s}$ and for multi-cycle operation with $t_{\mathrm{inj}} = 0.5\,\mathrm{s}$

flow rate. The measured value of p_{fuel} in multi-cycle operation is equal to the supply pressure during a single long injection. When the fuel valves are closed, the supply pressure recovers quickly to roughly 4.3 bar, which ensures repeatable conditions for all conducted cycles. By using the correlation between the directly measured fuel mass flow rate and p_{fuel} for steady-state flow conditions, the fuel mass flow rate of 4.4 kg/h can be deduced from the measured fuel supply pressure during the injection period of $t_{\mathrm{inj}} = 0.5\,\mathrm{s}$.

Measurements of the fuel mass flow rate and the corresponding supply pressure for steady-state flow conditions at various flow rates resulted in a linear calibration curve for $\dot{m}_{\mathrm{fuel}}$ as a function of p_{fuel}. The measured data and the resulting linear fit are shown in Fig. 2.8 for a continuous

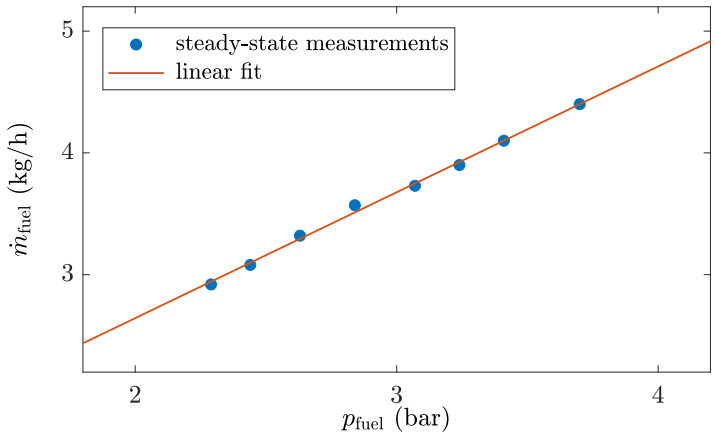

Figure 2.8: Measured fuel mass flow rate $\dot{m}_{\mathrm{fuel}}$ as a function of the fuel supply pressure p_{fuel} for a continuous air flow of 150 kg/h. The measured data are complemented by a linear fit, which is used for calibration.

air mass flow rate of 150 kg/h. This procedure allowed for determining the injected fuel mass flow rate for an arbitrary fuel supply pressure for injection durations far below 4 s. In order to account for geometry modifications as well as variations in the flow rate and the compositions of the oxidizer, this linear correlation curve was recorded before each individual measurement campaign, which is presented in this thesis.

The evaluation of the mass flow rates of fuel, air, and oxygen allows for the determination of the mixture composition, which is defined by two characteristic parameters, i.e. the equivalence ratio and the oxygen concentration in the oxidizer. The equivalence ratio φ, can be deduced from the fuel–oxidizer ratio according to

$$\varphi = \frac{\frac{\dot{m}_{\mathrm{fuel}}}{\dot{m}_{\mathrm{ox}}}}{\left(\frac{\dot{m}_{\mathrm{fuel}}}{\dot{m}_{\mathrm{ox}}}\right)_{\mathrm{st}}}, \tag{2.3}$$

with the mass flow rates of fuel $\dot{m}_{\mathrm{fuel}}$ and oxidizer $\dot{m}_{\mathrm{ox}}$, respectively, compared to stoichiometric conditions. The mole fraction of oxygen in the oxidizer $X_{\mathrm{O_2,ox}}$ is used as a measure for the oxygen enrichment. Its value is deduced from the measured mass flow rates for air and oxygen by

$$X_{\mathrm{O_2,ox}} = \frac{\frac{\dot{m}_{\mathrm{O_2}}}{M_{\mathrm{O_2}}} + 0.21\frac{\dot{m}_{\mathrm{air}}}{M_{\mathrm{air}}}}{\frac{\dot{m}_{\mathrm{O_2}}}{M_{\mathrm{O_2}}} + \frac{\dot{m}_{\mathrm{air}}}{M_{\mathrm{air}}}}, \tag{2.4}$$

where $M_{\mathrm{O_2}}$ and M_{air} denote the molar mass of oxygen and air, respectively.

2.2 Multi-tube PDC Test Rig

When considering a PDC for replacing the conventional isobaric combustion chamber in a gas turbine, a multi-tube configuration is favorable, as it allows for the increase of the effective firing frequency, and thus, a reduction of fluctuations in the flow parameters at the turbine inlet as discussed in Sec. 1.3.2. Based on the design of the single-tube test rig that was introduced in Sec. 2.1, a multi-tube PDC facility was designed to allow for the investigation of interaction mechanisms between the combustion tubes, as well as pressure fluctuations upstream of the combustor and inside an annular plenum attached to the combustor outlet. A cross section of the mutli-tube facility is sketched in Fig. 2.9.

For all conducted experiments on the multi-tube PDC, the inlet section with planar combustor head and choked air flow (Fig. 2.4) was integrated to allow for multi-cycle operation at elevated firing frequencies. The DDT section consisted of a series of five orifice plates, as sketched in Fig. 2.5 a. Analogous to the single-tube facility, the continuous oxidizer flow rate was controlled by an electro-pneumatic proportional valve adjusted by a PID controller based on the output signal of a Coriolis mass flow meter. The flow rate of hydrogen during the injection period, which was used as fuel, was controlled by the set pressure of a dome-loaded pressure regulator upstream of the solenoid valves. The data acquisition system allowed for parallel recording of 23 measurement signals with a sampling rate of 1 MHz. Additional 9 channels could be recorded at 10 kHz, which was sufficient for the recording of output signals of thermocouples, as well as monitoring the static pressure in the plena of oxidizer and fuel, respectively. Sensors can be

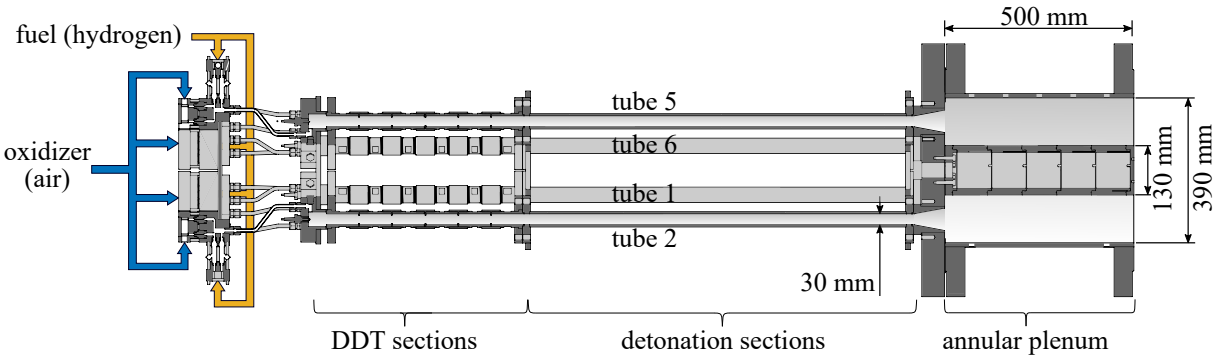

Figure 2.9: Cross section of the multi-tube test facility consisting of six PDC tubes and a downstream attached plenum arranged in a can-annular configuration. The six fuel and air plena are fed by common supply lines of fuel and oxidizer, respectively.

applied to each PDC tube at three axial positions in the detonation section, equally spaced by 300 mm.

Downstream of the PDC outlet, a generic annular plenum was attached in a can–annular configuration, as sketched in Fig. 2.9. The tube outlets were equipped with a conically diverging nozzle, increasing the cross section area by a factor of 2.25 to allow for a smoother transition of the propagating shock wave into the plenum. In particular, the divergent geometry at the combustor outlet is expected to result in a reduced pressure loss compared to a straight design due to smoother diffraction of the shock wave exiting the PDC as well as smaller recirculation zones at the plenum inlet. The annular gap of the plenum was scaled to match the distance of two neighboring PDC tubes of 130 mm. The same measure was chosen for the diameter of the center body, leading to a diameter of the outer wall of 390 mm. The length of the plenum was 500 mm. For some experiments, the outlet of the plenum was partially blocked by an orifice plate. The blockage ratio β was then given by the ratio of the blocked area and the total cross section area of the annular gap and can be calculated according to

$$\beta = \frac{r_\mathrm{o}^2 - r_\mathrm{b}^2}{r_\mathrm{o}^2 - r_\mathrm{i}^2} \tag{2.5}$$

with r_i and r_o denoting the radii of the plenum inner and outer wall, respectively. The inner radius of the blockage plate is represented by r_b.

2.2.1 Firing Patterns

When operating the multi-tube PDC, the chronological order of ignition events in the PDC tubes is an additional degree of freedom compared to the operation of the single-tube test rig. In the measurements, which are presented in this thesis, six different firing patterns were applied, which are illustrated in Fig. 2.10 b next to a sketch of the rear view of the multi-tube PDC with attached annular plenum downstream of the combustor outlet (Fig. 2.10 a). Below, the relative time delays between the start of the combustion cycle in the six PDC tubes are given with respect to the cycle duration (Fig. 2.10 c). The naming convention of the firing patterns is related to the number of simultaneously firing tubes and the rotation direction of the sequence.

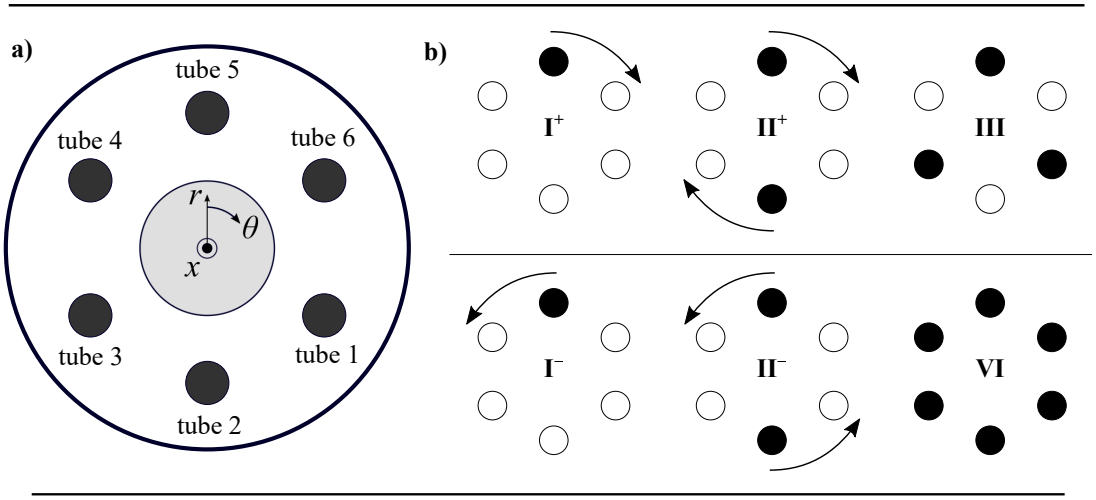

c)

	$(t_{\mathrm{ign,tube}} - t_{\mathrm{ign,1}})\,/t_{\mathrm{cycle}}$					
firing pattern	tube 1	tube 2	tube 3	tube 4	tube 5	tube 6
I^{+}	0	1/6	2/6	3/6	4/6	5/6
I^{-}	0	5/6	4/6	3/6	2/6	1/6
II^{+}	0	2/6	4/6	0	2/6	4/6
II^{-}	0	4/6	2/6	0	4/6	2/6
III	0	3/6	0	3/6	0	3/6
VI	0	0	0	0	0	0

Figure 2.10: Illustration of the firing patterns for the operation of the multi-tube PDC. (a) The arrangement of the tubes is sketched in the rear view of the test rig. (b) The naming convention of the firing patterns is based on the number of simultaneously firing tubes and the rotation direction with respect to the azimuthal coordinate θ. (c) The time delay for the firing of each tube normalized by the cycle duration is given with respect to the various firing patterns.

Pattern **I** denotes a sequential firing of the tubes. The time delay between two consecutively firing tubes is $t_{\mathrm{cycle}}/6$. While a positive rotation direction with respect to the azimuthal coordinate θ is applied for pattern **I**$^{+}$, operation with pattern **I**$^{-}$ results in opposite rotation direction. The rotation directions of patterns **II**$^{+}$ and **II**$^{-}$ are defined in the same way, while two opposed tubes are operated simultaneously with a respective delay of $t_{\mathrm{cycle}}/3$. Firing pattern **III** denotes the alternate firing of three simultaneously operated tubes with a delay of $t_{\mathrm{cycle}}/2$. All six PDC tubes are operated simultaneously when applying firing pattern **VI**.

The introduced firing patterns affect the frequency, at which the combustion events take place. Based on the firing frequency of a single PDC tube f_{tube} (Eq. 2.1), the effective firing frequency is defined by

$$f_{\mathrm{eff}} = \frac{N}{n}\, f_{\mathrm{tube}}. \tag{2.6}$$

Here, N denotes the total number of PDC tubes and n represents the number of tube that are operated simultaneously. While $N = 6$ holds for all conducted measurements in the scope of this thesis, the value of n depends on the applied firing pattern.

2.2.2 Fuel Injection

When operating the multi-tube PDC, the evolution of the fuel supply pressure does not only depend on the firing frequency and the injection duration, but also on the applied firing pattern. To examine the effect of the firing pattern on the fuel injection, all six introduced patterns were applied for a constant firing frequency of $f_{\mathrm{tube}} = 16.7\,\mathrm{Hz}$ and an injection duration of 30 ms, which implies a duty cycle of $g_{\mathrm{inj}} = 0.5$. These operation parameters resulted in a varying number of PDC tubes that were simultaneously filled, as illustrated in the top row of Fig. 2.11. For sequential firing (pattern **I**) and for the alternate firing of three simultaneously operated tubes (pattern **III**), a constant number of three PDC tubes was filled with a fuel–oxidizer mixture during the entire operation period. When applying pattern **II**, the number of simultaneously filled tubes alternated between 2 and 4. The largest variation was obtained for the operation with pattern **VI**, where all six tubes were filled simultaneously for $t_{\mathrm{inj}} = 30\,\mathrm{ms}$. As mentioned in Sec. 2.1.4, the fuel mass flow rate during the injection period is a function of the static pressure upstream of the fuel valves. Thus, the evaluation of p_{fuel}, measured by a piezoresistive pressure transducer (Kulite EWCTV-312), allows for assessing the injected fuel mass flow rate throughout the injection duration. More information on the applied sensor is given in Sec. 2.3.2. The cycle-averaged pressure histories in the fuel plenum of PDC tube 1 are shown in the bottom row of Fig. 2.11. For all configurations, the fuel injection of tube 1 starts at $t = 0\,\mathrm{ms}$.

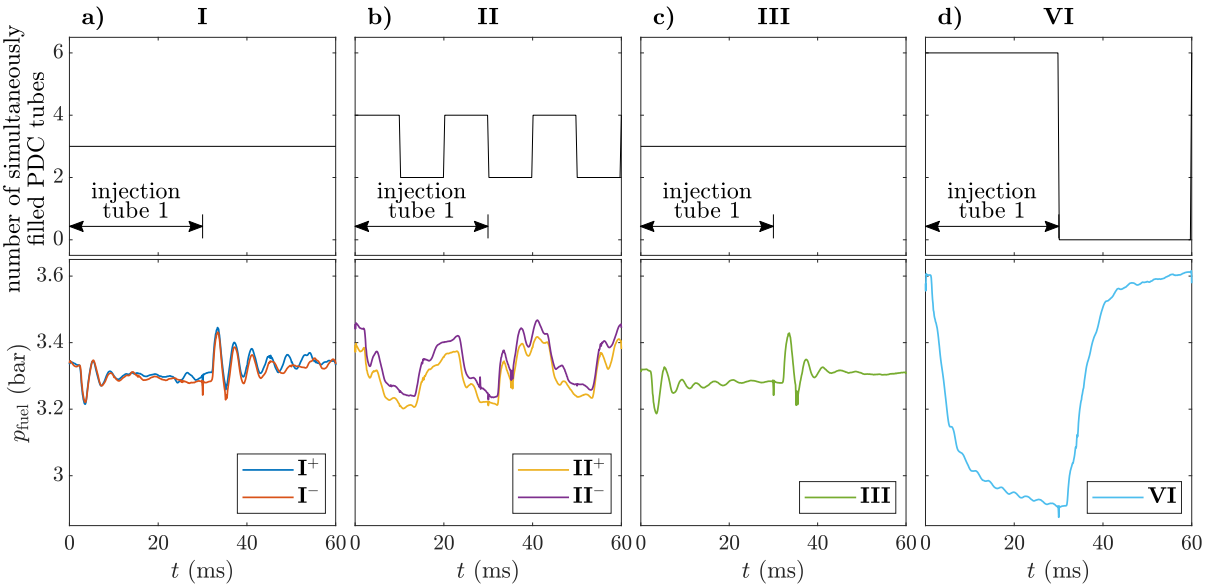

Figure 2.11: (top row) Number of simultaneously filled PDC tubes and (bottom row) cycle-averaged fuel supply pressure in the fuel plenum of PDC tube 1 for all applied firing patterns

For sequential firing (patterns $\mathbf{I}^+$ and $\mathbf{I}^-$), the pressure decreases by roughly 0.1 bar subsequent to the valve opening (Fig. 2.11 a). This pressure drop is followed by an oscillation with decaying amplitude that can be accounted to acoustic pressure fluctuations in the fuel plenum of the PDC tube 1. At $t = 30\,\mathrm{ms}$, the fuel valves of tube 1 close, resulting in a pressure rise followed again by an acoustic oscillation. Beside these acoustic pressure oscillations, a nearly constant fuel supply pressure is obtained, which corresponds in the invariant number of simultaneously filled

PDC tubes. Since the combustion event is initiated after closing the solenoid fuel valves, the resulting pressure increase in the combustor does not affect the pressure in the fuel plenum. The pressure history for the simultaneous firing of two opposite tubes (patterns **II**$^+$ and **II**$^-$), as shown in Fig. 2.11 b, is predominated by an oscillation with an amplitude of 0.2 bar and a cycle duration of 20 ms. This can be explained by the changing number of simultaneously filled tubes throughout the injection period of tube 1. For both patterns, **I** and **II**, the rotation direction has no effect on the fuel supply pressure as the number of simultaneously filled PDC tubes does not change. The pressure signal for firing pattern **III** (Fig. 2.11 c) is very similar to the data for sequential firing, which results from the constant number of tubes that are filled simultaneously. As expected, the largest variation in p_{fuel} is obtained when applying pattern **VI**, as shown in Fig. 2.11 d. The opening of the fuel valves of all PDC tubes at $t = 0$ ms results in a decrease in the supply pressure by roughly 0.7 bar. After the end of the injection duration, the fuel supply pressure recovers before the beginning of the subsequent cycle.

Due to inertia of the fuel flow, high-frequency fluctuations in the fuel supply are expected to have negligible influence on the fuel mass flow rate. In addition, diffusion due to turbulent mixing results in the attenuation of small spatial gradients in fuel concentration. Thus, a nearly constant fuel concentration throughout the entire PDC tube is expected when applying patterns **I** and **III**. Fluctuations in the fuel supply line of larger amplitude, as observed for the pattern **II**, may result in a non-homogeneous distribution of the fuel concentration along the combustor. For this configuration, an increased fuel mass flow rate in the early phase of the injection period causes an increased fuel concentration at the downstream end of the injected fuel–oxidizer package. As the applied injection period of 30 ms results in a just completely filled tube, this position matches the outlet of the combustor. Additionally, an increased fuel concentration is expected for $0.2 < x/L_{\mathrm{tube}} < 0.5$ due to the elevated value of p_{fuel} for 15 ms $< t <$ 24 ms. The axial positions are deduced from comparing the deduced times with the injection period of 30 ms. For the other applied firing patterns, a nearly constant equivalence ratio along the entire combustion tube is achieved. For pattern **VI**, the mean fuel supply pressure during the injection period is considerably reduced, which leads to a decreased fuel mass flow rate, and thus to a smaller global equivalence ratio when compared to the other firing patterns. Nevertheless, a large gradient in fuel concentration is only expected during the early phase of the injection period, which just affects the axial distribution of fuel concentration close to the combustor outlet. Therefore, a nearly constant equivalence ratio prior to the ignition is assumed throughout the DDT section and most of the detonation section for simultaneous operation of all PDC tubes.

As the combustion process (especially the DDT) is sensitive to the mixture reactivity, the findings presented above propose that the operation parameters, i.e. the duty cycle of the fuel injection and the firing pattern, do have a considerable influence on the combustion performance of the multi-tube PDC. This correlation is examined in Ch. 5 based on the frequency of occurrence of successful detonation initiation as a function of the global equivalence ratio.

2.3 Measurement Techniques and Signal Processing

Parameters defining the initial mixture conditions are introduced in this section. Moreover, an overview on the applied measurement techniques is given and signal processing methods that are

used throughout this thesis are discussed.

2.3.1 Initial Mixture Conditions

In addition to the mixture composition that can be deduced from the mass flow rates of air, oxygen, and fuel, the initial conditions for the combustion process in a PDC tube are defined by the thermodynamic state of the gas, i.e. the temperature T_0 and the pressure p_0. The temperature of the oxidizer T_{ox}, which was preheated for some experiments, was measured upstream of the mixing geometry by means of a sheathed thermocouple (type K). The fuel was always injected at ambient temperature conditions. The mixture temperature can thus be calculated from the mass-averaged enthalpy according to

$$T_0 = \frac{\dot{m}_{\mathrm{ox}} c_{p,\mathrm{ox}} T_{\mathrm{ox}} + \dot{m}_{\mathrm{fuel}} c_{p,\mathrm{fuel}} T_{\mathrm{fuel}}}{\dot{m}_{\mathrm{ox}} c_{p,\mathrm{ox}} + \dot{m}_{\mathrm{fuel}} c_{p,\mathrm{fuel}}}. \tag{2.7}$$

The static pressure p_0 prior to the ignition is measured directly by a thin-film metal pressure transducer (Festo SPTW) inside the PDC tube. Combining the known mixture composition with the thermodynamic state properties T_0 and p_0 allows for calculating the main features of a stable propagating detonation wave, as discussed in Sec. 1.2.1. However, further information on the flow properties are required to allow for the accurate evaluation of measurement data. In particular, the mean flow velocity has to be quantified to allow for comparing the propagation velocity of the detonation wave, measured within the laboratory frame, with the calculated CJ velocity. Further discussion on this issue is given in Sec. 2.3.2. The mean flow velocity $\bar{u}_{\mathrm{flow}}$ is determined from

$$\bar{u}_{\mathrm{flow}} = \frac{T_0}{p_0 A_{\mathrm{tube}}} \left(\dot{m}_{\mathrm{air}} R_{s,\mathrm{air}} + \dot{m}_{\mathrm{O_2}} R_{s,\mathrm{O_2}} + \dot{m}_{\mathrm{H_2}} R_{s,\mathrm{H_2}} \right). \tag{2.8}$$

Here, A_{tube} represents the cross section area of the PDC tube and R_s the specific gas constant of air, oxygen, and hydrogen, respectively. Further, the amplitude of turbulent fluctuations of the flow velocity u'_{flow} plays an important role in the acceleration of the deflagration and the process of DDT, as highlighted in Sec. 1.3.1. Although, u'_{flow} is not explicitly quantified in the scope of this thesis, a qualitative assessment of the fluctuation amplitude with respect to the mean flow velocity and the Reynolds number is derived in the following. The turbulence intensity Tu, which is defined as

$$\mathrm{Tu} = \frac{\sqrt{\overline{u'^2_{\mathrm{flow}}}}}{\bar{u}_{\mathrm{flow}}}, \tag{2.9}$$

can be expressed as a function of the Reynolds number. For the conducted measurements in the scope of this thesis, the Reynolds number was calculated from

$$\mathrm{Re} = \frac{\bar{u}_{\mathrm{flow}} D_{\mathrm{tube}}}{\nu_{\mathrm{mix}}} \tag{2.10}$$

with the tube diameter D_{tube} and the kinematic viscosity of the fuel–oxidizer mixture ν_{mix}. Depending on the applied mass flow rates and the mixture composition, the Reynolds number was varied in the range from $2.7 \cdot 10^4$ to $7.5 \cdot 10^4$. Following the findings from Russo and Basse [129], the turbulence intensity for turbulent pipe flows gradually decreases for an increasing

Reynolds number. Nevertheless, due to the proportional increase in $\bar{u}_{\text{flow}}$, the amplitude of velocity fluctuations increases with increasing Re. Hence, operating the PDC at an increased Reynolds number, while ensuring a constant ν_{mix}, results in larger turbulent velocity fluctuations, which potentially promotes the DDT process. In this work, multiple experimental investigations are presented over a range of Reynolds numbers to examine its effect on the flame acceleration and the detonation initiation.

2.3.2 Pressure Sensors

Two different sensor types were used in the scope of this thesis for measuring the static pressure: thin-film and piezoresistive transducers. Thin-film metal pressure transducers (Festo SPTW) were applied to determine the static pressure in the supply lines as well as in the combustion tube during the injection period. These sensors contain a Wheatstone bridge, consisting of four strain gauges that are arranged on a thin-film diaphragm attached to a metallic base element. The applied pressure results in a deformation of the membrane, which causes a variation in the resistance of the strain gauges. The resulting deviation in the output voltage is therefore a measure for the applied static pressure. The used sensors are designed to accurately measure the relative pressure with respect to ambient conditions with a sampling rate of of roughly 650 Hz. This rate was sufficient to resolve the pressure fluctuations due to the operation of the solenoid valves, as discussed in Sec. 2.1.4. Piezoresistive sensors were used for recording pressure fluctuations in the supply lines of the multi-tube PDC. These pressure transducers utilize a semiconductor diaphragm. Due to the piezoresistive effect, a deformation of the material causes a variation in the electrical resistance, which is again quantified by means of a Wheatstone bridge. The sensors, which were used in this work (Kulite EWCTV-312), allowed for the measurement of a fluctuating static pressure with a frequency up to 5 kHz.

Piezoelectric pressure transducers were applied in the scope of this thesis to measure high-frequency pressure fluctuations in the combustion tubes as well as in the annular plenum downstream of the multi-tube PDC. Two different sensor types were applied: PCB 112A05 and PCB 113B03, which were both suitable for the conducted investigations. All piezoelectric sensors were recorded with a sampling rate of 1 MHz. The application of a force on a piezoelectric material evokes a measurable difference in electric charge across the object. This voltage is proportional to the applied force and can thus be used as a measure for the difference in static pressure across the material. Due to their fast response to a change in static pressure and their robust design, piezoelectric pressure transducer are widely used for the investigation of DDT and propagating detonation waves [85, 104, 130, 131]. However, the increase in temperature that is associated to a detonation, results in a so-called thermal drift of the sensor signal, which is caused by a thermal expansion of the housing, implying a decrease in pressure on the piezo crystal. Thus, the resulting drop in the output voltage, which is commonly observed subsequent to the detection of a detonation wave, suggests a non-physical decrease in pressure. An example pressure signal recorded during multi-cycle operation of the single-tube PDC is shown in Fig. 2.12. The sensor was located 46 mm upstream of the shock-focusing device, which was installed as DDT geometry.

In each of the ten conducted cycles, the focusing of the leading shock led to the initiation of a detonation wave, which subsequently propagated downstream the detonation section of

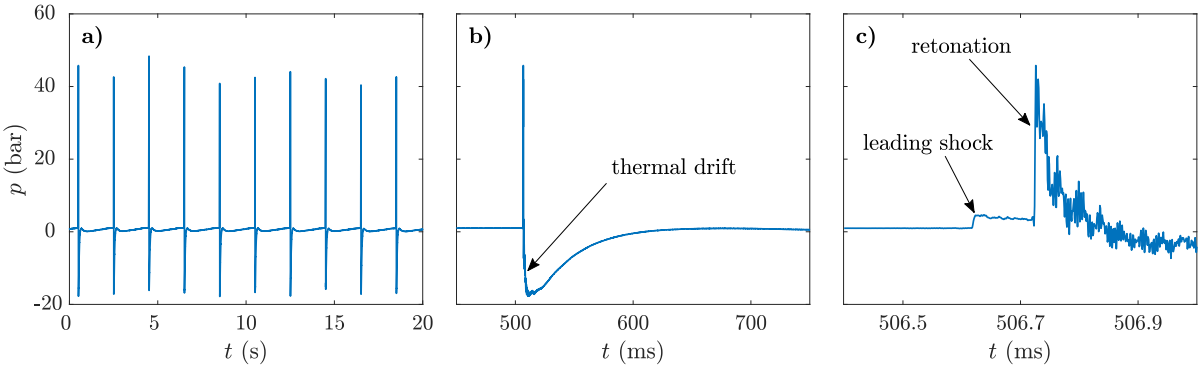

Figure 2.12: Signal of a piezoelectric pressure sensor in multi-cycle operation

the PDC. In addition, a so-called retonation wave was initiated that propagated in upstream direction. When this retonation passed the sensor position, a pressure amplitude of roughly 40 bar was recorded (Fig. 2.12 a). Subsequent to these peaks, local minima of approximately −15 bar are visible in the pressure history due to thermal drift. The pressure signal, shown in Fig. 2.12 b, presents a closer view to the first cycle. The thermal drift occurs subsequent to the pressure peak and the signal recovers within approximately 100 ms as a result of the decrease in temperature in the PDC tube. Due to the mentioned thermal drift, piezoelectric pressure sensors cannot be used to yield reliable quantitative information on the pressure history after the detection of the detonation. However, the recorded pressure histories inside the PDC allow for the accurate tracing of shock fronts. A detailed look at the recorded pressure trace of the first cycle (Fig. 2.12 c) reveals a step increase in pressure caused by the leading shock, which is followed by a sharp pressure increase due to the retonation.

In order to spatially track the generated shock waves in the PDC, the test rig was equipped with multiple piezoelectric pressure transducers at different axial positions. An example set of pressure signals is given in Fig. 2.13 for a successful detonation initiation by shock focusing. Here, sensors P_1 and P_2 were installed upstream of the shock-focusing device, while sensors P_3, P_4, and P_5 were mounted at different axial positions in the detonation section with a distance of 300 mm between two consecutive sensors. The presented pressure histories are characteristic for the operation with the shock-focusing device. The main features, which can be extracted from the recorded signals, are introduced in the following.

The propagating leading shock initially causes a step increase in the sensors upstream of the shock-focusing device. For each of the two sensors, the time when the shock arrives at the respective axial position as well as the pressure amplitude across the leading shock can be extracted, which can be used to quantify the shock strength. Shortly after the onset of a detonation inside the shock-focusing device, an upstream propagating detonation front, referred to as retonation, is visible by a sudden increase in pressure at the positions of sensors P_1 and P_2. Additionally, a detonation wave propagates downstream through the flammable mixture and is detected by sensors P_3 to P_5. Determining the propagation velocity of the combustion front in the detonation section u_{det} allows for the reliable detection of the success of detonation initiation by comparing it to the CJ velocity. Considering Δt to be the time-of-flight between the detection of the shock front by two pressure sensor separated by the axial distance Δx, the

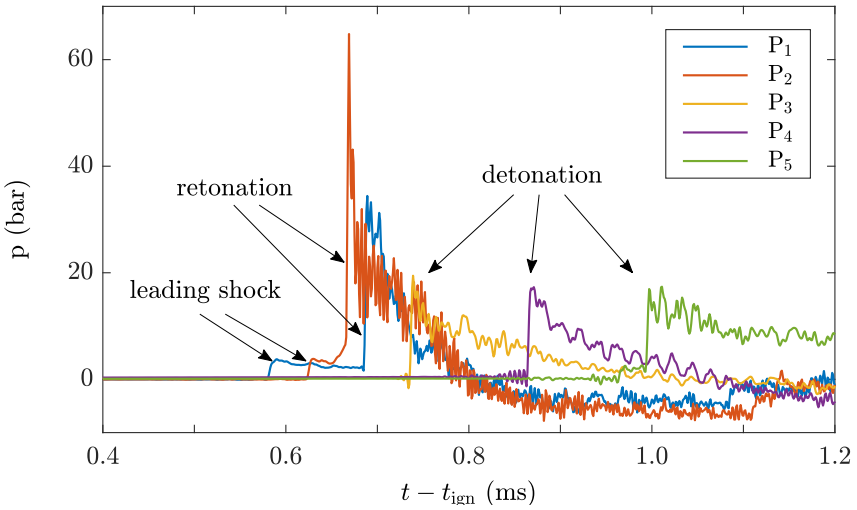

Figure 2.13: Signals of multiple pressure transducers installed at various axial positions along the combustion tube for the operation with the shock-focusing device

propagation velocity of the detonation front with respect to the gas can be calculated from

$$u_{\mathrm{det}} = \frac{\Delta x}{\Delta t} - \bar{u}_{\mathrm{flow}}. \tag{2.11}$$

A successful detonation initiation is considered, when the deduced propagation velocity matches the predicted CJ velocity. As all the piezoelectric pressure sensors were recorded with a sampling rate of 1 MHz, the time when the detonation passes a specific sensor can be determined with an accuracy of $\pm 1\,\mu$s. Assuming $\Delta x = 0.3$ m and a CJ velocity in the order of 2000 m/s, which represents a typical value for a propagation velocity of a planar detonation wave in a hydrogen–air mixture, u_{det} is determined with an uncertainty of ± 27 m/s.

2.3.3 Ionization Probes

The used piezoelectric pressure transducers can be applied for initial mixture temperatures up to 580 K. Thus, for investigations at elevated temperature conditions, ionization probes were installed to detect the detonation front. These provide a robust alternative method to the pressure sensors and have already been used in numerous studies [71, 126, 132]. The measurement principle of this sensor type is based on a current between two electrodes with differing electric potential, induced by ions that are generated in the reaction zone of the detonation front. The induced current results in a drop of the measured voltage at one side of a voltage divider, which allows for spatially tracking of the combustion front.

The output signals of four ionization probes installed at different axial locations in the single-tube PDC are shown in Fig. 2.14 for an example cycle. Sensors I_1 and I_2 were located close to the combustor head in the DDT section, while sensors I_3 and I_4 were installed in the detonation section with an axial distance of 0.4 m. For $t = t_{\mathrm{ign}}$, the spark discharge is visible in the output signals of all ionization probes. After roughly 0.5 ms, an increase in ion concentration leads to a voltage drop for I_1, and subsequently for I_2. As expected at the axial position of these sensors, the gradual increase at each of the two sensors indicates a deflagration. A much steeper

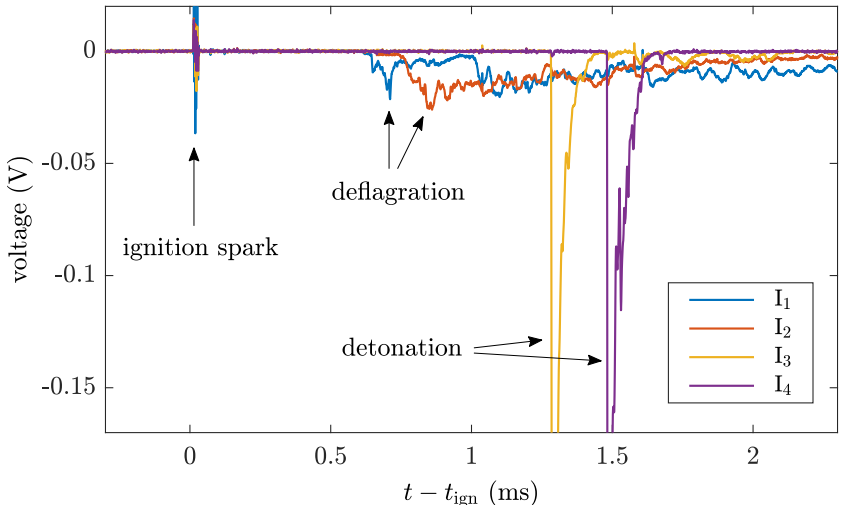

Figure 2.14: Signals of multiple ionization probes installed at various axial positions along the combustion tube for operation with a series of orifice plates.

drop in the output voltage is observed for I_3 and I_4, indicating the detection of a propagating detonation wave. Evaluating the time-of-flight allows for determining the propagation velocity of the detonation front from Eq. 2.11.

2.3.4 Fuel Concentration Measurements

Optical non-reactive fuel concentration measurements were conducted in order to verify the capability of injecting a well-defined fuel profile. This was especially relevant when aiming for a spatial gradients in the fuel concentration along the PDC tube prior to ignition, as realized in the measurements presented in Sec. 4.3. Tunable diode laser absorption spectroscopy (TDLAS) was applied as a time-resolved line-of-sight technique. This method has already been applied to several setups for the purpose of fuel concentration measurements [39, 133, 134] and has proven to be an accurate and inexpensive technique. The required optical access to the single-tube PDC was realized by integrating a quartz glass tube into the combustor. A sketch of the applied setup is given in Fig. 2.15.

A near-infrared diode laser was operated at a default wavelength of 1,653.7 nm and modulated with a frequency of 10 kHz and an amplitude of 0.04 nm. A collimator guided the laser light through the combustion tube, where the concentration of fuel along the laser path determined the attenuation of the intensity due to absorption. The remaining light intensity was detected and the signal was fed into a lock-in amplifier, which calculated the first and second harmonics (R_1 and R_2, respectively) of the detected signal with respect to the modulation signal. The ratio of these two harmonics R_1 and R_2 is a measure of the fuel concentration X_{fuel} in the combustor:

$$X_{\text{fuel}} \propto \frac{R_2}{R_1}. \tag{2.12}$$

This application of wavelength modulation spectroscopy (WMS) provides an elevated measurement accuracy and lower sensitivity to noise when compared to conventional absorption spectroscopy.

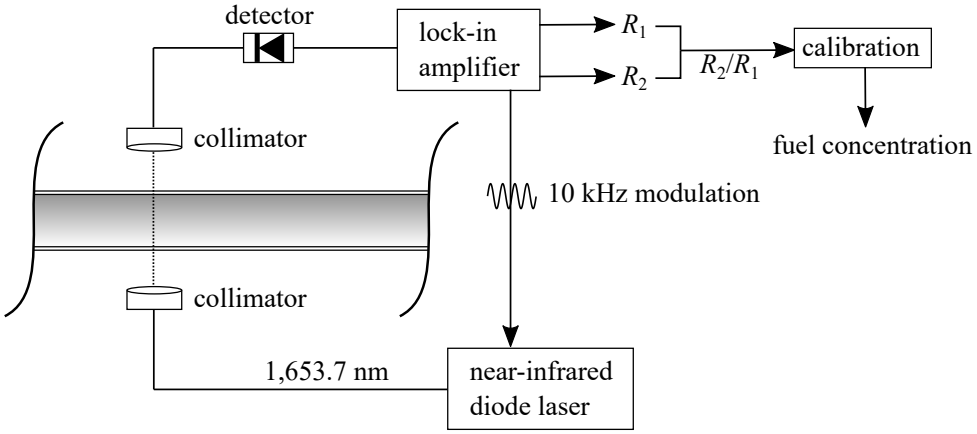

Figure 2.15: Setup for fuel concentration measurements by TDLAS

Quantitative measurements of the fuel concentration were achieved by using a linear calibration curve obtained from preliminary experiments. The calibration measurements were conducted in steady-state flow conditions for both the oxidizer and the fuel, which allowed for correlating the time-averaged measurement signal from TDLAS to the fuel mass flow rate recorded by the Coriolis mass flow meter in the supply line.

Methane was used as tracer fuel to benefit from its absorption feature that matches the wavelength of the available laser. The change of fuel from hydrogen, which was used for reactive measurements, to methane resulted in a variation of the molecular diffusion coefficient of the fuel. However, due to the large Reynolds number of the flow ($\mathrm{Re} > 1.8 \cdot 10^4$) and the highly turbulent flow, molecular diffusion is assumed to play only a minor role in comparison to the turbulent mixing of fuel and oxidizer. To ensure comparable flow conditions and mole fractions for measurements with both non-reactive measurements with methane and reactive measurements with hydrogen, the fuel supply pressure p_{fuel} was held constant. By this, similar volumetric flow rates, and thus, comparable convection velocities were achieved.

2.3.5 Cell Size Measurements

As discussed in Sec. 1.2.2, the detonation cell width λ is a characteristic parameter of propagating detonation waves, which can be used to assess the mixture reactivity and detonation limits. Soot foils have been extensively used for the experimental investigation of detonation cells in the past. It is agreed that the imprinted cellular structure on sooted foils corresponds to the trajectories of the triple points, as demonstrated by Pintgen and Shepherd [135] who performed soot foil measurements and simultaneously recorded the emitted light from planar laser-induced fluorescence, which allowed for the detection of the reaction zone. However, the mechanism that is responsible for soot transport is not fully understood. High pressure, vorticity, and soot combustion have been proposed [136]. Numerical simulations performed by Inaba et al. [137] suppose the variation in sheer stress parallel to the shock front to be responsible for soot gathering inside the Mach stem along the shear layer.

As reported by other researchers, the cellular pattern for hydrogen–air mixtures contains irregularities, which makes it hard to determine a single representative value of the detonation cell

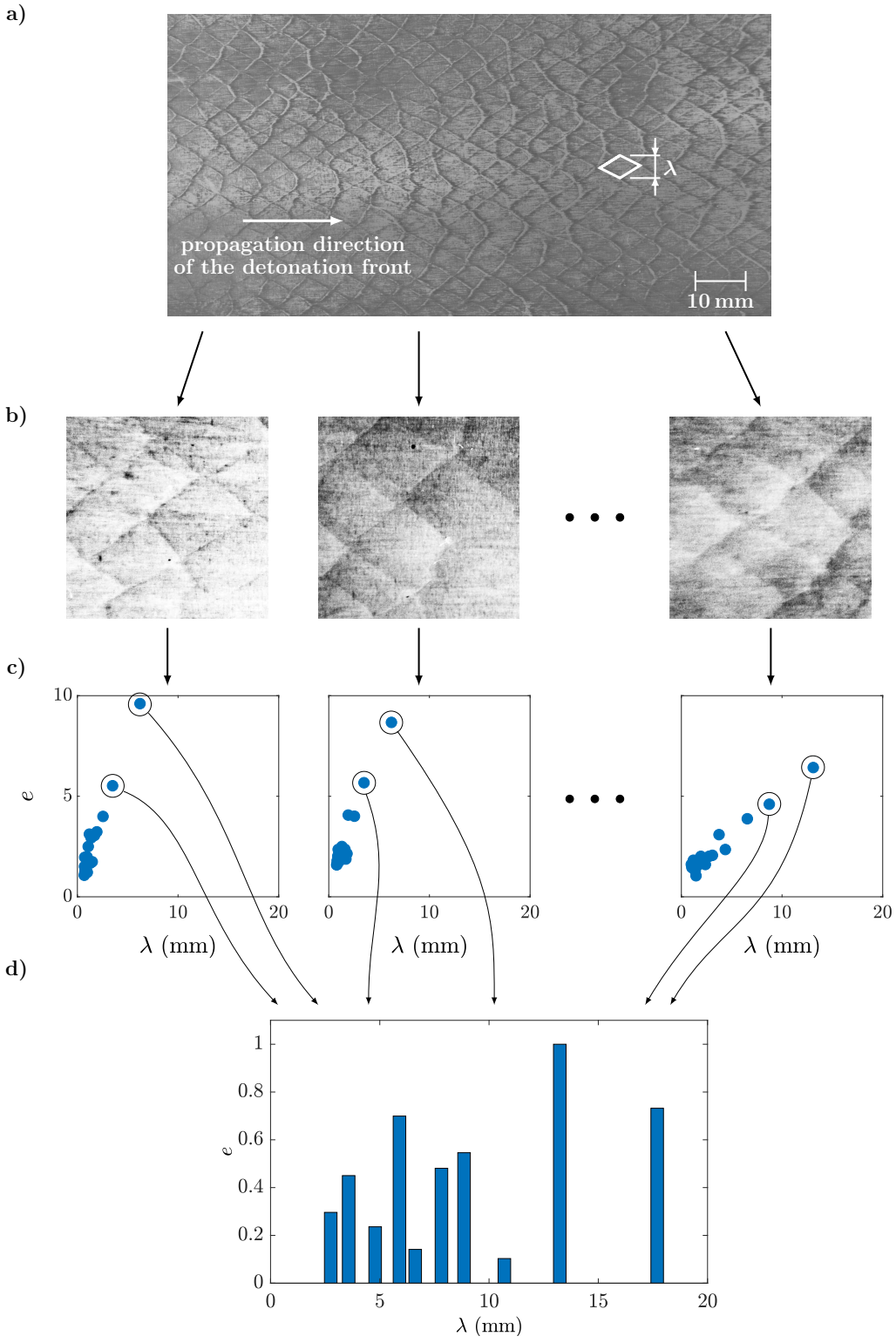

Figure 2.16: Schematic of the used methodology for the evaluation of detonation cells on sooted foils for an example measurement with a stoichiometric hydrogen–air mixture at $T_0 = 768\,\mathrm{K}$. (a) The original photograph is separated into (b) multiple image sections. (c) For each segment, the dominant cell structures are identified. (d) Lastly, the cumulative energy is determined for cell width between 2 and 20 mm.

width [136, 72]. Hébral and Shepherd [138] developed a semi-automated approach for determining the most pronounced detonation cell sizes and their respective energy in the visible pattern. In this approach, the application of the two-dimensional autocorrelation function allows for the detection of the displacement perpendicular to the propagation direction that results in a maximum congruence of the original and the moved picture. By this, the dominant cell widths λ_i and their corresponding energy e_i can be extracted from the measurement data in a reproducible and repeatable way. This methodology was adapted in the scope of this thesis to evaluate the detonation cells in hydrogen–air mixtures over a range of initial mixture temperatures. A detailed description of the applied processing procedure is given in the following.

Rectangular pieces (100 mm × 600 mm) of precision spring steel with a thickness of 0.1 mm were sooted by a fuel-rich diffusion flame of acetylene in air. The sooted foil was then rolled up and inserted in the rear part of the detonation section of the single-tube PDC. After a single detonation event, the foil was removed from the test rig and the imprinted cellular pattern was digitized by a camera. A photograph of an example foil is shown in Fig. 2.16 a. Several quadratic sections of the recorded image of the cellular pattern imprinted on the sooted foil (Fig. 2.16 b) were examined individually. This was necessary to compensate gradients in the brightness of the photographs due to undulation of the foil and reflections from the illumination. Image processing, including adjustments in brightness, contrast, and gamma, was then applied to each segment to improve the visibility of the recorded structures. By applying the tool from Hébral and Shepherd [138], the dominant cell widths and the respective energy values were determined, as visualized in Fig. 2.16 c. Subsequently, the two most pronounced cell widths of each image are used to compute a cumulative distribution of the energy with respect to λ, shown in Fig. 2.16 d. This number was chosen, since most examined distributions contained two cell widths with a substantially larger energy than the rest of the data points. In particular, points for very small values of λ are most likely linked to uncleanliness of the imprinted cellular pattern onto the sooted foil and were therefore neglected for further examination. To calculate the distribution of the energy over the cell width, as shown in Fig. 2.16 d, the range of $2\,\text{mm} < \lambda < 20\,\text{mm}$ was discretized into 25 segments. For each segment, the sum of e for all considered values of λ in the respective range was calculated. The values were then normalized by the maximum value of the cumulative energy. By this, the dominant detonation cell widths across the entire sooted foils were determined. Further, the respective relative energies were quantified, providing a measure for the regularity of the recorded cellular pattern.

2.3.6 High-speed Imaging

Taking high-speed images of the combustion event allows to gain detailed insights into the ongoing physical processes. In the scope of this thesis, a high-speed camera (Photron Fastcam SA-Z) with a frame rate of 210,000 fps was used to capture the light emission during the detonation initiation by shock focusing. For this, two setups were realized, which are illustrated in Fig. 2.17. Firstly, a transparent shock-focusing device was manufactured out of acrylic glass and integrated into the single-tube PDC in order to allow for a view perpendicular to the tube axis. Secondly, a planar mirror was installed 0.5 m downstream of the PDC outlet, providing a rear view of the combustion tube. The images were recorded without the usage of an optical filter. Hence, the detected light is mainly linked to the emission from hot water vapor. The captured images,

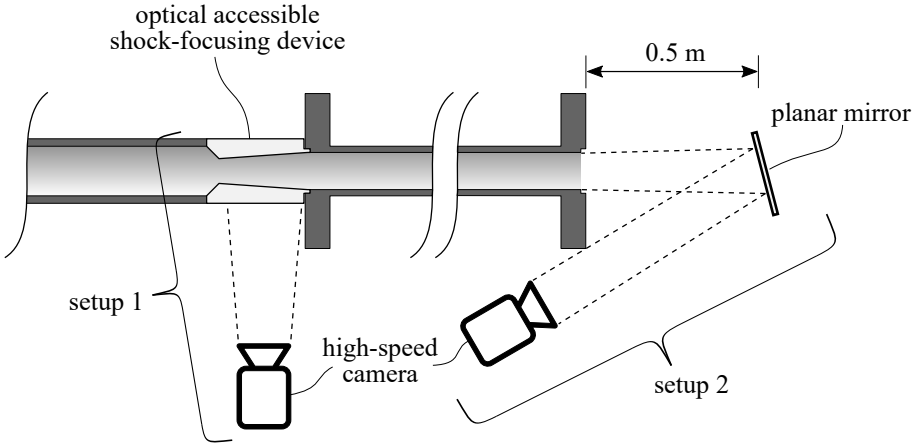

Figure 2.17: Sketch of the two applied experimental setups for high-speed imaging

presented in Sec. 3.1, therefore allow for the detection of the propagating combustion front during the detonation initiation by a local explosion inside the shock-focusing device.

2.4 Prediction of Acoustic Modes in the Annular Plenum

To support the evaluation of measured pressure oscillations in the annular plenum downstream of the multi-tube PDC, its acoustic eigenmodes were estimated. This prediction was implemented by using the finite element solver PyHoltz, which has been developed at TU Berlin by Mensah and Moeck [139]. For this purpose, an unstructured mesh representing the geometry of the annular plenum was set up with a characteristic length of 15 mm, as shown in Fig. 2.18. All solid walls (upstream wall, outer wall, center body, and blocked plenum outlet) were modeled by the application of sound hard boundary conditions, where the velocity fluctuation normal to the wall was set to zero. The open outlet area was considered by a sound soft boundary condition with $p' = 0$.

The speed of sound c_0 was determined based on an isentropic coefficient of $\gamma = 1.4$, a specific gas constant of $R_s = 287\,\mathrm{J/(kg\,K)}$, and a temperature of $T_0 = 550\,\mathrm{K}$ according to

$$c_0 = \sqrt{\gamma R_s T_0}. \tag{2.13}$$

The value of T_0 was set to the measured cycle-averaged gas temperature near the outlet of a PDC tube for quasi-steady-state operating conditions of the multi-tube PDC with a firing frequency of $f_{\mathrm{tube}} = 16.7\,\mathrm{Hz}$. These conditions were achieved by operating the PDC tubes for 200 cycles, each, which led to a quasi-constant measured temperature. The acoustic eigenmodes were calculated with the assumption of constant gas properties of pure air in space and time, which does not replicate the exact conditions in the experimental investigations. There, the cyclic combustion process rather resulted in periodic fluctuations of the gas properties and the mixture composition due to the emitted shock waves and the blowdown of exhaust gases. However, calculations assuming perfect mixing and thermodynamic equilibrium revealed that accounting for the exhaust gas resulted in a maximum deviation in the predicted eigenfrequencies of 3 %. In addition, relatively small pressure fluctuations were observed for most time instances

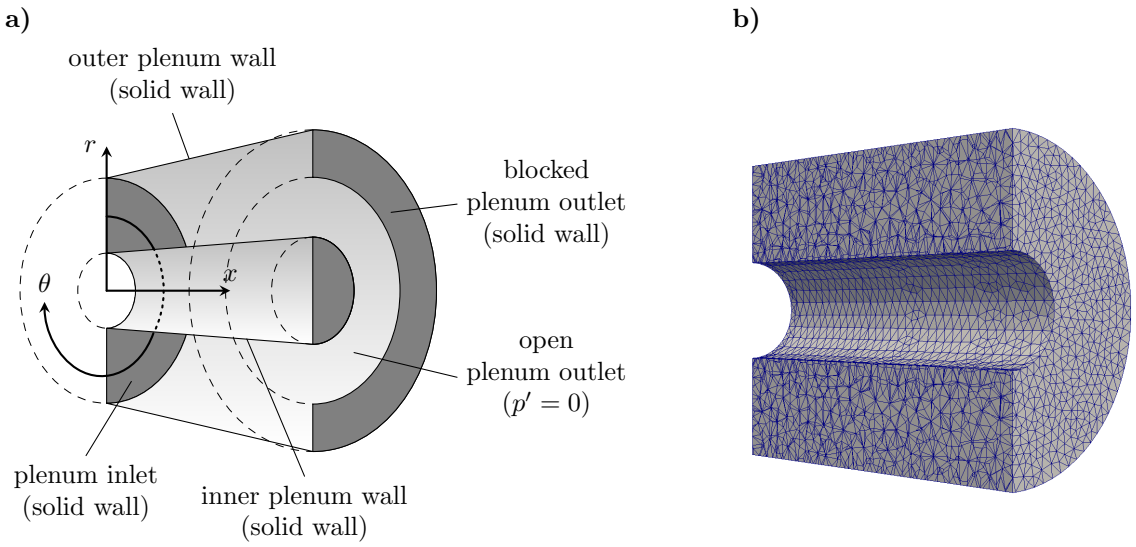

Figure 2.18: Geometry of the plenum used for the prediction of the acoustic eigenmodes with (a) applied boundary conditions and (b) the used unstructured grid.

($p' < 0.1\,\mathrm{bar}$ for 86 % of recorded data points), which justifies the made assumption.

For the experimental setup used in the scope of this thesis, eigenmodes with radial mode numbers of $n > 0$ were found to be associated to eigenfrequencies of $f_{l,m,n} > 4\,\mathrm{kHz}$. However, measured pressure signals at the outer wall of the plenum revealed that only negligible pressure oscillations at these frequencies were observed in the plenum downstream of the multi-tube PDC. Therefore, acoustic eigenmodes in the annular plenum are distinguished in the following exclusively by their axial and azimuthal mode numbers, l and m. Due to the periodic nature of the azimuthal dimension, the eigenmodes can be written as

$$\Psi_{l,m}\left(x,\theta,r\right) = \Phi_{l,m}\left(x,r\right) e^{im\theta} \tag{2.14}$$

with the axial, azimuthal, and radial coordinates x, θ, and r, respectively. The predicted acoustic eigenmodes and the corresponding eigenfrequencies of the annular plenum are presented in Ch. 5, where the results are used to support the evaluation of measured acoustic pressure oscillations during the operation of the multi-tube PDC.

Chapter 3

Evaluation of Detonation Initation by Shock Focusing

Realizing the reliable and repeatable detonation initiation is vital for achieving an efficient PDC operation. In addition to this essential requirement, however, several aspects of the process of DDT contribute to the overall combustor efficiency. An important aspect of an efficient PDC process is a short DDT run-up distance in order to minimize the volume of flammable mixture that is burnt by a deflagration rather than by a detonation. By minimizing this volume, the pressure gain resulting from the combustion process is maximized. Furthermore, the pressure loss due to the integration of a DDT enhancing geometry should be reasonably small. As discussed in Sec. 1.3.1, these two partly contradicting aspects resulted in various designs of DDT geometry, which differ in geometry and system complexity. In numerous studies, a series of orifice plates with an individual blockage ratio of 0.43 emerged as a reliable concept for achieving repeatable detonation initiation within a reasonably small DDT run-up distance [85, 93]. Therefore, this geometry was considered as benchmark in the scope of this work. Nevertheless, several disadvantages are associated to the repetitive blockage of the combustor, e.g. a substantial pressure loss and the establishment of recirculation areas, which hinders the effective purging of hot exhaust gases. As a consequence, several alternative concepts to achieve DDT in a reliable and efficient way have been proposed. One promising technique is the integration of a shock-focusing device. The concept was proposed by Frolov et al. [104, 105] and first adapted to a PDC by Gray et al. [107].

In this chapter, both concepts, i.e. the shock-focusing device and a series of orifice plates, are evaluated and compared with regards to their suitability for PDC application. First, a detailed experimental analysis of the process of detonation initiation in the shock-focusing device is conducted by means of high-speed images and pressure signals. Second, a methodology for the reliable detection of the success of DDT by shock focusing is deduced. Then, required operating conditions for reliable DDT in hydrogen–oxygen–air mixtures are elaborated by systematically varying the mixture reactivity as well as the flow rate. For this, measurements at atmospheric temperature and pressure conditions were conducted on the single-tube PDC with both DDT geometries, presented in Sec. 2.1.3. Further, the cycle-to-cycle variations of the DDT and the

pressure histories at the combustor inlet are evaluated for both setups.

3.1 Verification of Detonation Initiation by Shock Focusing

By means of numerical simulations, Bengoechea et al. [108] found a local explosion at the focal point to be responsible for the detonation initiation in a stoichiometric hydrogen–oxygen–air mixture with $X_{O_2,ox} = 0.4$. Moreover, a comparison of measured pressure histories with numerical results by Gray et al. [107] suggested a local explosion at the focal point to mark the onset of a stable propagating detonation. However, the successful detonation initiation at the focal point was first proven experimentally in the scope of this thesis. For this, high-speed imaging, as presented in Sec. 2.3.6, was applied to record the light emission from the combustion process. In order to ensure comparability to the simulations, the measurements were conducted for stoichiometric hydrogen–oxygen–air mixture with $X_{O_2,ox} = 0.4$ at ambient pressure and temperature conditions. The cross section of the single-tube PDC test rig, shown in Fig. 3.1, illustrates the used configuration, including a pre-detonation chamber with a length of 364 mm and the optical accessible shock-focusing device. A planar mirror, which was placed 0.5 m downstream of the combustor outlet, provided a rear view of the PDC. To allow for further evaluation of the combustion process, five piezoelectric pressure transducers were installed at different axial position to detect propagating pressure waves during the combustion process. The pressure history at the combustor inlet was recorded by sensor P_0. Two sensors (P_1 and P_2) were located in the pre-detonation chamber 53 and 13 mm upstream of the shock-focusing device, respectively. Additional two sensors (P_3 and P_4) allowed for the detection of the combustion front in the detonation section.

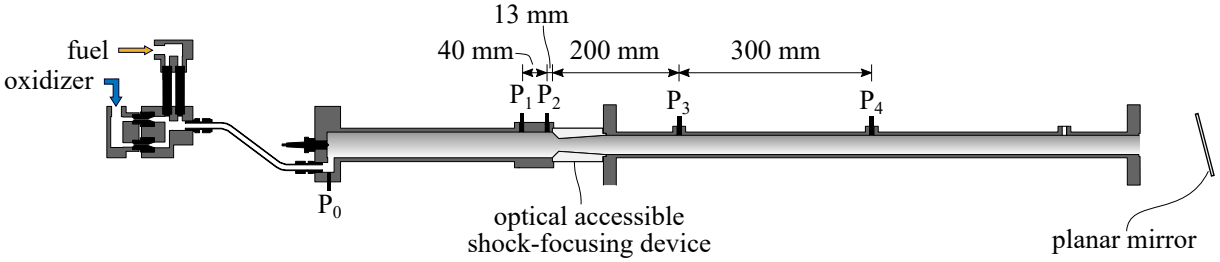

Figure 3.1: Sketch of the single-tube PDC test rig with planar end wall and a shock-focusing device as DDT geometry

The recorded images, shown in Fig. 3.2, illustrate the propagation of the reaction front in the diverging part of the shock-focusing device. The two columns visualize the light emission from hot water vapor for both applied measurement setups, which were introduced in Sec. 2.3.6. On the left, the camera was oriented perpendicular to the tube axis. The integration of a transparent shock-focusing device out of acrylic glass allowed for monitoring the reaction zone by the means of light emission from hot water vapor. In the right column of Fig. 3.2, the process was observed through the mirror downstream of the combustor outlet. Since only one camera was available, the two cycles were recorded separately. The evaluation of multiple combustion cycles, however, revealed a very repeatable process, which allows for the comparison of the recorded high-speed images from both setups. The images were inverted resulting in dark areas representing regions

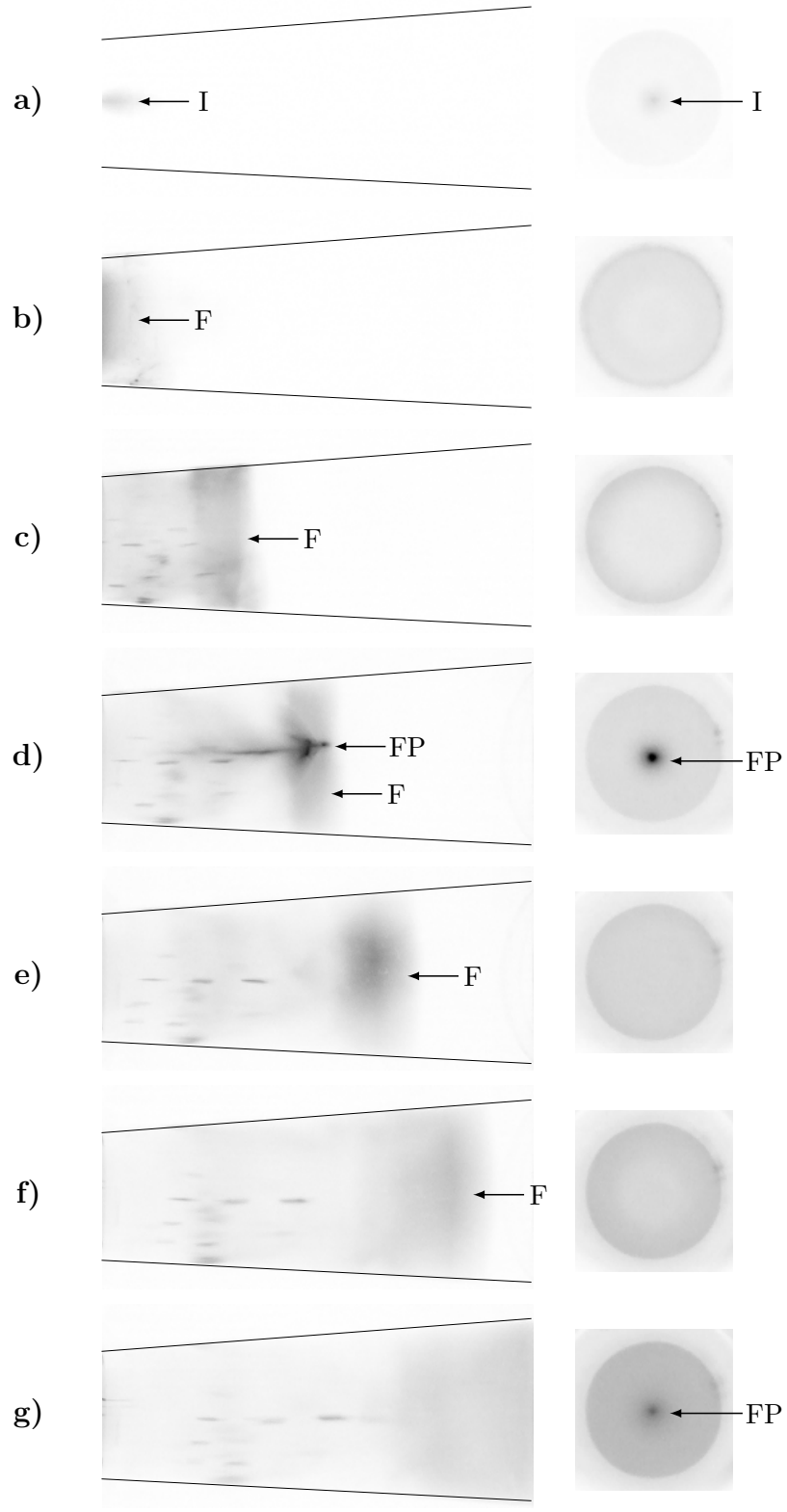

I: detonation initiation, F: flame front, FP: focal point

Figure 3.2: High-speed images of the reaction front during detonation initiation by shock focusing (adapted from [131]). (left) View perpendicular to the flow direction. (right) View from the rear end of the PDC through a planar mirror.

of high light emission, whereas regions without chemical reaction appear white.

In Fig. 3.2 a, a distinct dark spot (I) is visible at the tube axis close to the axial position of the smallest cross section area. The confined radial dimension suggests the initiation of a combustion event rather than an already existing reaction front propagating through the shock-focusing device. This presumption is supported by the fact, that only very low light emission could be observed through the planar mirror before this time instance. In the following images, the initiated flame front (F) travels along the tube axis. For Figs. 3.2 c to h, a nearly constant propagation velocity of approximately 2500 m/s was derived from tracking the axial position of the reaction zone. Comparing this value to the CJ velocity of $u_{\mathrm{CJ}} = 2250\,\mathrm{m/s}$ for the given initial conditions, i.e. stoichiometric hydrogen–oxygen–air mixture with $X_{\mathrm{O_2,ox}} = 0.4$ at atmospheric temperature and pressure conditions, confirms the existence of a propagating detonation. Shortly after the initiation (Figs. 3.2 a to c), a slightly larger axial propagation velocity is deduced. This observation indicates an overdriven detonation, which has been observed in other studies during the early phase of a propagating detonation [96, 140, 141].

The images, taken through the planar mirror downstream of the combustor outlet, reveal an axisymmetric appearance of the combustion event. In addition to the first image, circular dark spots are visible in Figs. 3.2 d and g, which reveals a periodic nature of the process with a period of 14 μs. During this time, the region of highest light emission travels from the tube axis in radial direction towards the tube wall, where it is reflected and condensed to a focal point (FP) in the center of the tube. The radial velocity of this structure can by calculated from the known tube diameter as $u_{\mathrm{rad}} = 1570\,\mathrm{m/s}$. The ratio of this velocity and the CJ value is similar to the fraction of width and length of detonation cells in a stable propagating detonation front, which was deduced from the cellular pattern on sooted foils. An example of the recorded structure is shown in Fig. 2.16 a. As the ratio of radial and axial propagation velocities is similar to the aspect ratio of detonation cells, the observed periodic structure is most likely caused by a shock structure propagating perpendicular to the tube axis as a result of the initially spherical detonation front. In conclusion, the presented evaluation of the high-speed images clearly confirms the successful detonation initiation by shock focusing through a local explosion at the focal point.

To systematically evaluate the PDC operation with the shock-focusing device at various operating conditions a method for the reliable determination of the success of detonation initiation by shock focusing is essential. For this, the previously discussed examination of high-speed images is not suitable due to the enormous required effort regarding the measurement setup, the amount of generated data, and the post processing. Thus, a trustworthy method exclusively based on recorded pressure signals is introduced in the following. The procedure is exemplarily presented for a set of measurements with stoichiometric hydrogen–oxygen–air mixtures with $X_{\mathrm{O_2,ox}} = 0.4$, which matches the operating conditions for the high-speed images. Fig. 3.3 illustrates the pressure histories of example shots for (a) successful detonation initiation and (b) for unsuccessful DDT. The pressure histories are shifted vertically by the axial position of the sensors with respect to the upstream end of the shock-focusing device. Symbols indicate the time when a shock wave is detected. The vertical position of each symbol corresponds to the axial position of the sensors. This allows to draw trajectories for the leading shock (L), the detonation wave (D), and the retonation wave (R) that propagates in upstream direction.

As discussed in Sec. 2.3.2, comparing the propagation velocity of the combustion front derived

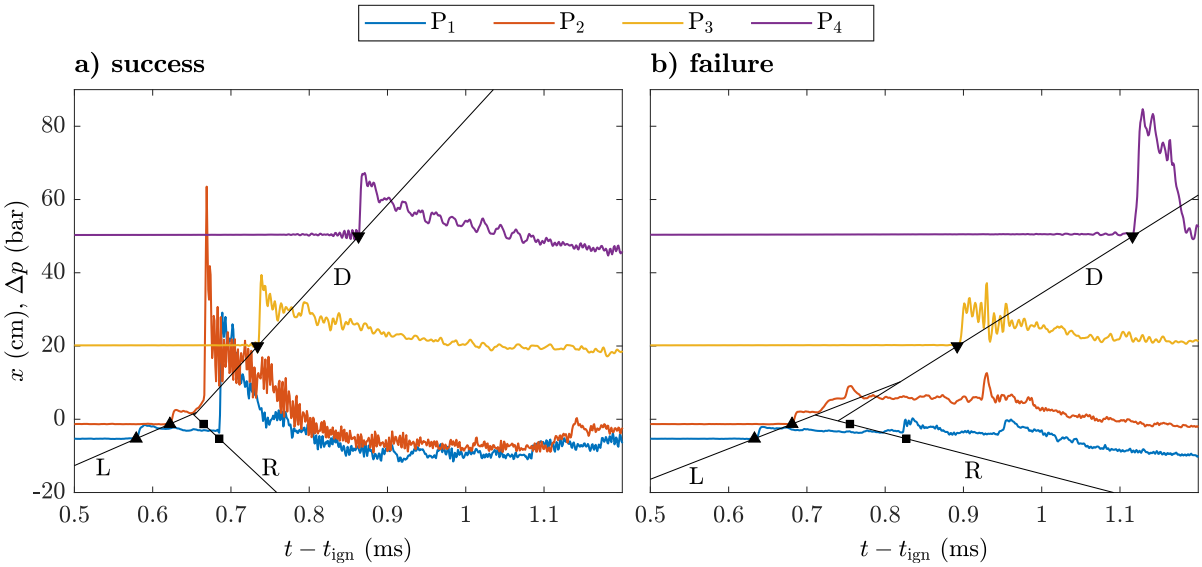

Figure 3.3: Pressure histories at four different axial positions for (a) successful detonation initiation by shock focusing and (b) failure. The sensor signals are shifted in vertical direction by their respective axial distance to the upstream end of the shock-focusing device.

from the time-of-flight (Eq. 2.11) with the CJ velocity allows for determining whether a detonation was initiated successfully or not. When using the shock-focusing device, however, this single criterion is not sufficient to determine if the detonation was successfully initialized by shock focusing. In particular, for certain operating conditions, spontaneous DDT was observed downstream of the shock-focusing device if no successful detonation initiation was achieved at the focal point. Although this mechanism results in a stable detonation, it adversely affects the deterministic nature of DDT by shock focusing. Therefore, an additional criterion is presented in the following to reliably distinguish these events. When the focusing of the leading shock results in successful detonation initiation, the intersections of all three trajectories collapse to a single point, representing the point of detonation initiation inside the shock-focusing device. Otherwise, the intersections of the trajectories are found at different positions. In the example shot, shown in Fig. 3.3 b, the leading shock is weaker than in the successful case, shown in Fig. 3.3 a, indicated by the smaller slope of the trajectory L in the x–t diagram. Thus, the amplitude in temperature and pressure at the focal point is not sufficiently high to initiate a detonation. Rather, the partially reflected leading shock is detected at sensor P_2 and subsequently P_1 (R). The slope of trajectory D, which represents the propagating combustion front in the detonation section, is smaller than for a CJ detonation. In addition, the intersection of trajectories L and D is located downstream of the shock-focusing device. Both findings indicate a failure in detonation initiation by shock focusing for this case. Processing of pressure data from numerous cycles revealed the axial position x_{LD} of the intersection of the leading shock (L) and the detonation wave (D) in combination with the propagation velocity of the combustion front in the detonation section u_{det} to provide a reliable indicator for the success of detonation initiation by shock focusing.

The obtained values for u_{det} normalized by the CJ velocity and x_{LD} are illustrated in Fig. 3.4 a and Fig. 3.4 b, respectively, for measurements with stoichiometric hydrogen–oxygen–air mixtures

with $X_{O_2,ox} = 0.4$. The measurements were conducted for various mass flow rates, which are linked to a range of Reynolds numbers (Eq. 2.10). As discussed in Sec. 2.3.1, the Reynolds number is correlated to the turbulent velocity fluctuations and was therefore chosen for the evaluation of the PDC behavior at various operating conditions.

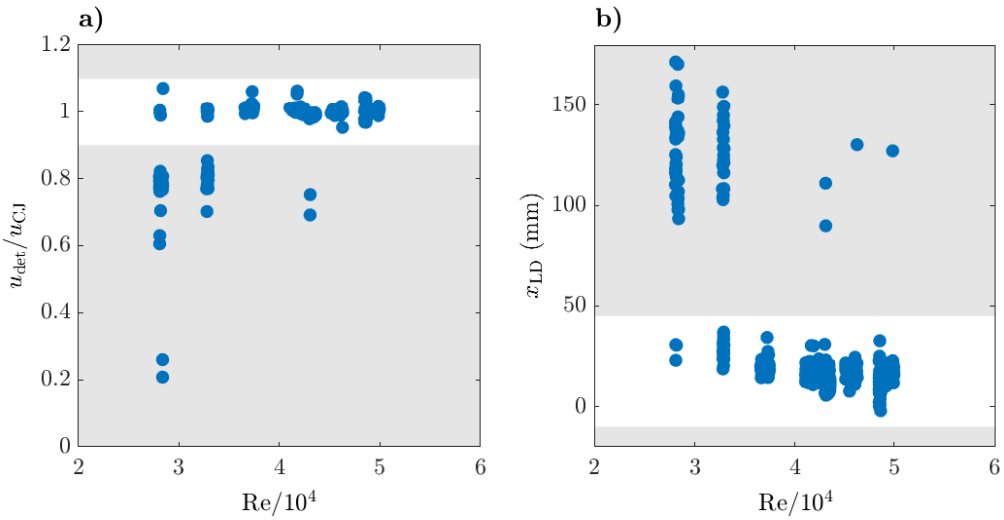

Figure 3.4: (a) Propagation velocity of the shock front in the detonation section relative to the CJ velocity and (b) axial position of the interaction of the trajectories for the leading shock and the detonation wave with respect to the Reynolds number for stoichiometric hydrogen–oxygen–air mixtures with $X_{O_2,ox} = 0.4$

A stable propagating detonation is assumed if the velocity u_{det} matches the CJ velocity. In order to account for measurement uncertainties, values between 90 % and 110 % of the CJ value are tolerated, indicated by the white area in Fig. 3.4 a. In case of successful DDT, x_{LD} is located inside the shock-focusing device, illustrated by the white area for $-10 < x_{LD} < 45$ in Fig. 3.4 b. When both criteria are fulfilled, the detonation initiation by shock focusing was considered as successful. It should be noted, that although the presented methodology ensures the reliable detection of successful detonation initiation by shock focusing, it is not suitable to precisely determine the axial position of the onset of the detonation wave. By assuming constant propagation velocities of all trajectories, the effect of an overdriven detonation directly after the initiation, as observed in Fig. 3.2, is neglected. The evaluation of the high-speed images revealed that the propagation velocity of the detonation front in the initial phase is larger than the CJ velocity. Accounting for this effect would result in a smaller gradient of trajectory D in the x–t diagram in Fig. 3.3 a close to the point of detonation initiation. This eventually causes the actual axial position of DDT to be further upstream than indicated by the data shown in Fig. 3.2 b. Thus, the results from pressure measurements and the findings from the high-speed imaging consistently indicate the position of detonation initiation by shock focusing to be close to the position of the smallest cross section area of the converging–diverging obstacle ($x = 0$ mm).

3.2 Conditions for Reliable Operation

In order to evaluate the potential of shock focusing for the application in a PDC operated with hydrogen as fuel, the two most relevant aspects of the DDT process in this geometry are analyzed in this section. First, the formation of the leading shock is evaluated, which strongly influences the temperature and pressure conditions at the focal point. Subsequently, the success of detonation initiation is determined with respect to the operating conditions. In addition to the reference case with $X_{O_2,ox} = 0.4$, the investigations were performed for a reduced oxygen enrichment, resulting in $X_{O_2,ox} = 0.35$. All measurements, which are presented in this section, were conducted with a pre-detonation chamber with a length of 364 mm.

3.2.1 Formation of the Leading Shock

The increase in static pressure across the leading shock can be derived from the recorded pressure history upstream of the shock-focusing device. Combining the measured shock amplitude Δp_L with the known initial pressure p_0 allows for determining the pressure ratio across the leading shock Π_L by

$$\Pi_L = \frac{\Delta p_L + p_0}{p_0}. \tag{3.1}$$

As a result of measurement uncertainties due to noise and a non-perfect stepwise increase in the recorded pressure signal, the obtained value of Π_L may deviate from the actual value by a maximum of ± 0.5. The obtained values for Π_L are visualized in Fig. 3.5 for measurements with two different oxygen concentrations in the oxidizer as a function of the Reynolds number. Each data point represents the average value for 50 combustion cycles, respectively. The bars illustrate the cycle-to-cycle standard deviation.

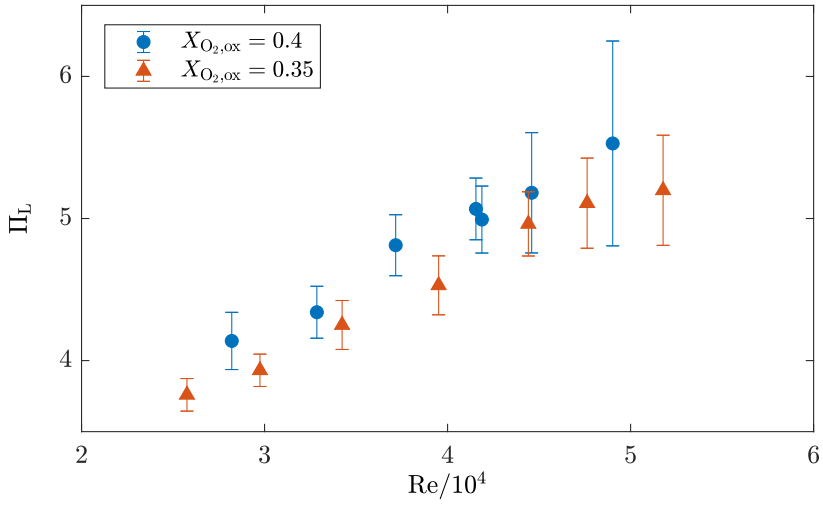

Figure 3.5: Pressure ratio across the leading shock as a function of the Reynolds number

The examined data indicate an almost linear increase in the pressure ratio across the leading shock for an increasing Reynolds number. This increase in Π_L can be explained by the effect of elevated turbulent fluctuations, as discussed in Sec. 2.3.1. According to the findings of Lee [60], an increase in the amplitude of turbulent velocity fluctuations results in larger pressure waves

being generated due to the interaction of heat release fluctuations in the flame front with the turbulent flow. As the leading shock is formed by the accumulation of these pressure waves, the associated pressure ratio Π_L is positively correlated to the Reynolds number of the flow. When decreasing the oxygen enrichment of the oxidizer, the reactivity of the flammable mixture is reduced. This results in a slower turbulent flame, which eventually causes a reduced pressure ratio across the leading shock.

3.2.2 Success of Detonation Initiation at the Focal Point

Evaluating the success rate of detonation initiation by shock focusing for all the conducted measurements allows for identifying the required conditions for reliable DDT. The success rate represents the frequency of occurrence of successful detonation initiation and is calculated from the ratio between the number of cycles with successful detonation initiation and the total number of examined combustion cycles. In Fig. 3.6 a, the success rate is shown as a function of the pressure ratio across the leading shock. For this, all conducted combustion events were grouped to a previously defined number of clusters with regard to the measured value of Π_L, while the data points represent the mean values of each cluster. This representation of the measurement data allows for examining the required shock strength to achieve reliable detonation initiation by shock focusing. Since the formation of the leading shock is completely disregarded in this consideration, the obtained results describe the operation behavior of the shock-focusing device independent of the combustor inlet. In Fig. 3.6 b, the success rate is plotted as a function of the Reynolds number to evaluate the overall PDC operation. Here the two mechanisms, i.e. the formation of the leading shock and the detonation initiation at the focal point, are examined together. As a consequence, the results are dependent on the used PDC setup but also allow for determining the required mass flow rate of the injected fuel–oxidizer mixture to ensure reliable PDC operation.

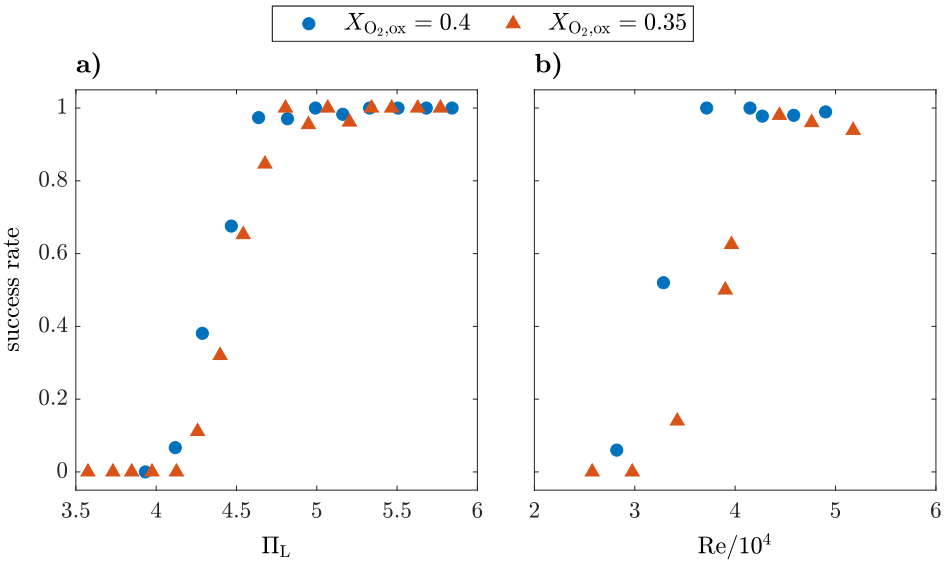

Figure 3.6: Success rate of detonation initiation by shock focusing with respect to (a) the pressure ratio across the leading shock Π_L and (b) the Reynolds number

The data, shown in Fig. 3.6 a, reveal that reliable detonation initiation was achieved, when the pressure ratio across the leading shock exceeded a certain threshold, which depends on the mixture reactivity. For $X_{O_2,ox} = 0.4$, repeatable DDT is observed for $\Pi_L > 4.6$. For a reduced oxygen enrichment ($X_{O_2,ox} = 0.35$), a slightly stronger shock is required with $\Pi_L > 4.8$. This effect can be explained by a reduced reactivity of the flammable mixture at the focal point for smaller oxygen concentration in the oxidizer. However, the pressure ratio across the leading shock can only be adjusted indirectly by modifying the operating conditions of the PDC, as shown in Fig. 3.6 b. Thus, the evaluation of the correlation between the success rate of detonation initiation and the Reynolds number of the flow is essential to identify suitable operating conditions to achieve reliable detonation initiation by shock focusing. For $X_{O_2,ox} = 0.4$, reliable operation was observed for $Re > 3.7 \cdot 10^4$. When the oxygen concentration in the oxidizer is reduced to 0.35, the required Reynolds number increased to $4.4 \cdot 10^4$.

Independent of the mixture reactivity, the presented results indicate a clear dependence between the pressure ratio across the leading shock and the success rate of detonation initiation by shock focusing. When the value of Π_L is small, almost no successful DDT was observed. When the shock strength exceeds a certain threshold, repeatable detonation initiation ($> 95\,\%$) is obtained. Between these two regimes, the success rate increases monotonically with increasing pressure ratio. The width of this increase with regard to Π_L can well be explained by the measurement uncertainty in the shock strength. Thus, the experimental results support the observations from Bengoechea et al. [109], who postulated a deterministic correlation between the shock strength and the success of detonation initiation by shock focusing. However, during the periodic operation of the PDC at a given Reynolds number, a considerable cycle-to-cycle variation of Π_L was observed, as illustrated by the bars in Fig. 4.6, which cannot be explained exclusively by the measurement uncertainties but are rather coupled to the stochastic nature of the process of flame acceleration. Hence, a regime of monotonically increasing success rate with increasing Reynolds number is revealed in Fig. 3.6 b. In order to ensure repeatable DDT during the periodic operation of the PDC, it is therefore recommended to set the Reynolds number above a value, where the generated leading shocks in all cycles exceed the respective threshold value. As expected, the required value of Re depends on the reactivity of the mixture, which was varied here by changing the oxygen concentration in the oxidizer.

3.3 Comparison to a Series of Orifice Plates

In this section, the operation behavior of the single-tube PDC is evaluated for both DDT geometries, i.e. the shock-focusing device and a series of orifice plates. The results for the two setups are compared on the basis of three features. First, the required operation parameters with respect to mixture reactivity and Reynolds number of the flow are evaluated, followed by the examination of the cycle-to-cycle variations. Subsequently, the pressure evolution at the combustor inlet is discussed as it gives information on pressure wave propagating into the air supply and on the expected backflow of hot exhaust gases.

3.3.1 Required Operation Parameters

In order to compare the feasibility of the shock-focusing and a series of orifice plates device to enhance DDT, experiments with oxygen enriched air as oxidizer were conducted for both configurations. The results from investigations on detonation initiation by shock focusing were presented in the previous section. In this section, results from measurements with a series of orifice plates are discussed. In the conducted measurements, the number of orifice plates was varied from a single obstacle to a maximum number of five plates. For this, the length of the DDT section, as presented in Fig. 2.5 a, was adjusted by removing the unused orifice plates together with the same number of tube segments, each with a length of 85 mm. For each configuration, the PDC was operated for 100 cycles at a firing frequency of 5 Hz. This procedure resulted in the exhaust gases being completely purged out of the combustor before the start of the fuel injection for the subsequent cycle. Analogous to the measurements with the shock-focusing device, mixtures with two different oxygen concentrations in the oxidizer were examined: $X_{O_2,ox} = 0.35$ and 0.4. The data in Fig. 3.7 visualize the success rate of DDT in a PDC equipped with (a) one or (b) two orifice plates, respectively, as a function of the Reynolds number. As discussed in Sec. 1.3.1, the onset of the detonation in a tube filled with a series of orifices is coupled to the interaction of the combustion front and the obstacles. Therefore, the leading shock and the retonation wave are no characteristic features of the DDT process in this configuration and the success of detonation initiation was determined exclusively by comparing the propagation velocity of the combustion front in the detonation section to the CJ velocity. When integrating three or more orifice plates (not shown here for brevity), a success rate of 1 was observed for all applied parameters.

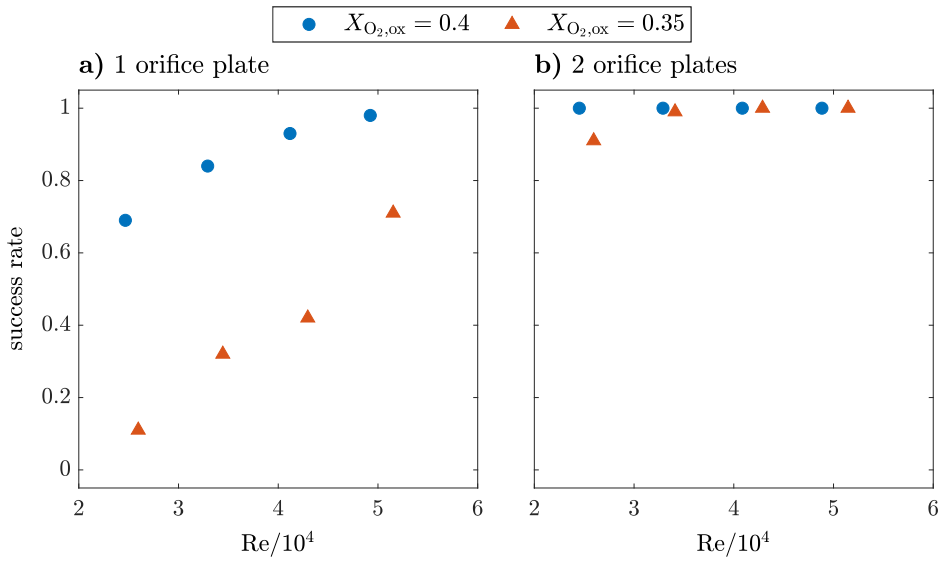

Figure 3.7: Success rate of detonation initiation by means of a series of orifice plates as a function of the Reynolds number when integrating (a) one or (b) two orifice plates

For measurements with a single orifice plate (Fig. 3.7 a), a monotonic increase in the success rate with increasing Reynolds number is observed for both investigated oxygen enrichments. In addition, the oxygen concentration in the oxidizer largely influences the probability of a successful detonation initiation. For $X_{O_2,ox} = 0.4$ and $\mathrm{Re} \approx 4.9 \cdot 10^4$, reliable detonation is observed. When

decreasing the Reynolds number, the success rate is reduced simultaneously. When increasing the number of orifice plates to two (Fig. 3.7 b), the success rate for given operation parameters increases. Repeatable DDT for mixtures with $X_{O_2,ox} = 0.4$ is observed for all applied Reynolds numbers. Few cycles with unsuccessful detonation initiation are observed for the smallest flow rate ($Re \approx 2.6 \cdot 10^4$) when applying an oxygen concentration in the oxidizer of $X_{O_2,ox} = 0.35$.

The volume of fuel–oxidizer mixture that is required to achieve DDT is a vital parameter for the comparison of different methods for DDT enhancement. When installing the shock-focusing device, the pre-detonation chamber had a length of 364 mm and an inner diameter of 40 mm, and thus, a volume of 457 cm^3. Here, reliable detonation initiation was observed for $Re \geq 3.7 \cdot 10^4$ and $Re \geq 4.4 \cdot 10^4$ for mixtures with $X_{O_2,ox} = 0.4$ and $X_{O_2,ox} = 0.35$, respectively. When replacing the shock-focusing device by a series of two orifice plates, reliable DTT was achieved for similar operating conditions and mixture compositions. For this configuration, the DDT section is composed of a section with an inner diameter of 40 mm and a length of 47 mm at the combustor head and two tube segments with an inner diameter of 30 mm and an individual length of 85, which results in a volume of 179 cm^3. Thus, compared to a series of two orifice plates with an axial distance of 85 mm, the required volume for reliable DDT is increased by roughly 150 %. These results suggest that using the shock-focusing device for detonation initiation implies an increased volume of the DDT section for reliable PDC operation at atmospheric temperature and pressure conditions.

3.3.2 Induced Pressure Loss

Beside the ability to achieve DDT within a short distance, the pressure loss of the flow through the PDC should be minimized to ensure a maximum overall combustor efficiency. Conceptually, the shock-focusing device was designed to reduce the pressure loss across the DDT section Δp_{DDT} compared to a series of orifice plates, which was verified experimentally in the scope of this thesis. For this, the static pressure was measured at the combustor inlet and in the detonation section close to the outlet of the DDT-section by two piezoresistive pressure sensors (Kulite EWCTV-312) for a steady-state air flow. The measured difference in static pressure is shown in Fig. 3.8 as a function of the air mass flow rate. Varying the length of the pre-detonation chamber did not affect the measured pressure loss. Therefore, only one configuration for using the shock-focusing device is illustrated. Alongside, five configurations for applying orifice plates are shown, differing in the number of installed obstacles.

As expected, the pressure loss decreases when reducing the number of orifice plates in the DDT section. Furthermore, the measurements reveal that installing the shock-focusing device allows for further reduction of the pressure loss. Compared to two orifice plates, which was found to result in similar success rates for detonation initiation in Sec. 3.3.1, a reduction of roughly 13 % was achieved when applying shock focusing for detonation initiation. These results indicate that replacing the conventionally used DDT enhancing geometry consisting of a series of orifice plates by the shock-focusing device allows for a substantial reduction in pressure loss across the DDT enhancing geometry.

It should be noted that the design of the combustor inlet is expected to result in a considerable pressure loss due to the collision of three impinging jets, which enter the combustor through the circumferentially distributed injection ports. Future improvements on the inlet geometry

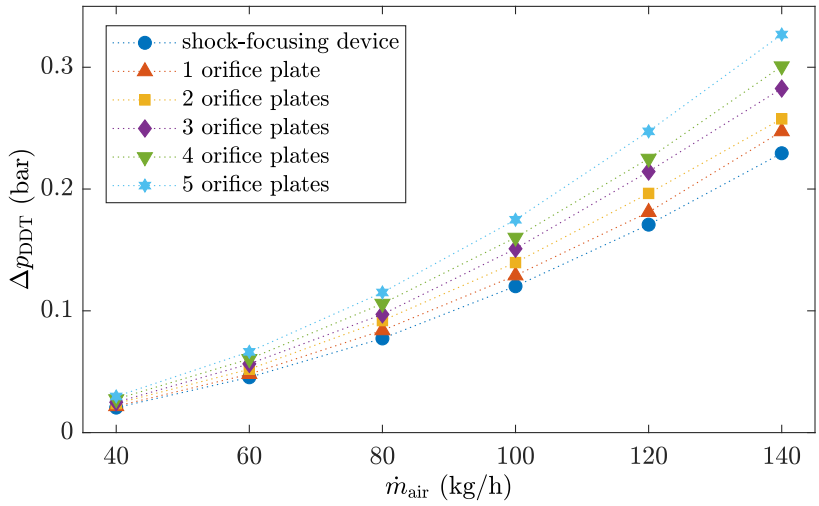

Figure 3.8: Static pressure loss across the PDC inlet and the DDT section as a function of the air mass flow rate

are expected to allow for reducing the overall pressure loss across the combustor, which would emphasize the importance of a small pressure loss induced by the DDT section.

3.3.3 Cycle-to-cycle Variations

The gradual increase in success rate with increasing Reynolds number for the integration of orifice plates depicts a significant stochasticity in the process of DDT. For the operation with the shock-focusing device, a steeper increase of the success rate with increasing Reynolds number was observed, which indicates a more deterministic behavior. In order to further examine the cycle-to-cycle variations in the DDT for both investigated configurations, the time delay between spark discharge at the combustor head and the detection of the detonation front at the axial position of sensor P_4 is evaluated in the following. This time delay is relevant when integrating the PDC into a gas turbine as it determines the succession of shock waves exiting the combustor. A constant value results in a periodic occurrence of shock waves while a large cycle-to-cycle fluctuation indicates a significantly varying time difference between two consecutive shock waves. In particular, a constant time delay between the ignition and the shock wave exiting the combustor is aspired when applying well-defined firing patterns in a multi-tube configuration, as investigated in Ch. 5. A number of three orifice plates is chosen for this evaluation to ensure a nearly constant length of the DDT section for both setups. The deduced time delays for cycles with successful detonation initiation are plotted in Fig. 3.9 as a function of the Reynolds number. The cycle-averaged values are complemented by bars representing the cycle-to-cycle standard deviation.

For both setups, an overall decrease in the time delay with increasing Reynolds number is observed. Independent of the applied DDT geometry, this correlation can be explained by two effects. First, the mean flow velocity is increased due to the larger flow rate of the injected fuel–oxidizer mixture. Second, the increased turbulent fluctuations promote flame acceleration, and thus, cause earlier DDT due to an elevated propagation velocity of the deflagration. Both

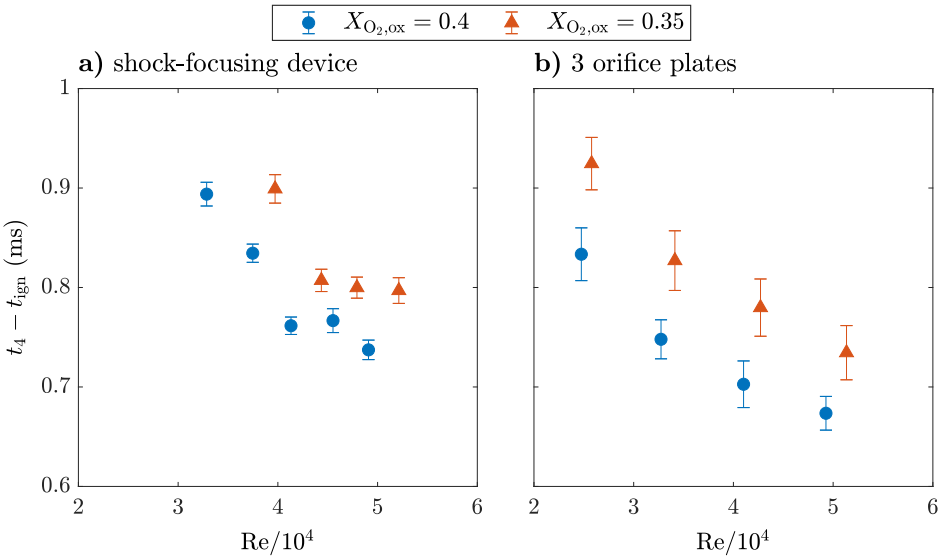

Figure 3.9: Time delay between the spark discharge and the detection of the detonation front at sensor P_4 as a function of the Reynolds number for measurements with (a) the shock-focusing device and (b) 3 orifice plates

mechanisms eventually result in an earlier arrival of the detonation front at the position of sensor P_4. Due to the similar distance between the combustor inlet and the pressure transducer for both setups, the cycle-averaged time delays for the shock-focusing device and three orifice plates are similar. However, a significantly larger cycle-to-cycle variation is observed when using a series of orifice plates. As discussed in Sec. 1.3.1, detonation initiation in obstacle filled tubes may occur due to SWACER [90] or a local explosion subsequent to a collision of the leading shock with an orifice plate [97]. Both mechanisms are closely linked to axial positions of the orifice plates. In contrast to the shock-focusing device, detonation initiation is not restricted to a single axial position, but can rather be achieved at each orifice plate with a specific probability. As a result, the axial position of detonation initiation in the conducted experiments is not constant for all combustion cycles, but rather varies by the order of 85 mm, which is the axial difference between two consecutive orifice plates. As the propagation velocity of the deflagration is significantly smaller than the CJ velocity, the axial position of the detonation initiation largely affects the time delay $t_4 - t_{ign}$. In particular, an early DDT results in a small time delay, while a larger value is obtained, when the transition occurs further downstream. This eventually results in the large cycle-to-cycle variation in the time when the detonation front passes the axial position of sensor P_4, as illustrated in Fig. 3.9 b. When using the shock-focusing device, the axial position of the detonation initiation is fixed to the focal point. Thus, a considerably smaller cycle-to-cycle variation in the arrival time of the shock wave at the position of sensor P_4 is obtained for this configuration.

3.3.4 Pressure Evolution at the Combustor Inlet

As a result of the pressure increase induced by the combustion event, pressure waves are generated, which propagate upstream into the oxidizer supply due to the valveless design of the considered PDC. When integrating the combustor into a gas turbine, these pressure waves affect the outlet

conditions of the attached compressor. This is affects the operation stability [142] and result in a reduced compressor efficiency [22]. Additionally, the supply of fresh oxidizer is interrupted and a backflow of hot exhaust gases is induced when the pressure in the combustor exceeds the oxidizer supply pressure. These high-temperature gases need to be purged from the supply lines before starting the injection of fuel at the beginning of the subsequent cycle in order to avoid premature ignition. Therefore, large pressure amplitudes at the PDC inlet are undesirable. Furthermore, the pressure evolution at the combustor inlet throughout the combustion event is meaningful for the maximum operation frequency of the PDC. Ideally, only a small amount of exhaust gases travel upstream of the combustor inlet, which allows for the operation with small purge durations and thus high firing frequencies. In the following, the pressure histories at the combustor inlet are examined for both investigated DDT geometries in two consecutive steps. First, recorded pressure peaks are qualitatively described and explained in combination with pressure signals at various axial positions along the combustion tube. Second, a quantitative evaluation of the amplitudes and the integral value of the pressure signals is conducted and the results for both setups are compared.

In Fig. 3.10, two sets of pressure signals are shown for representative example cycles with successful detonation initiation (a) by shock focusing and (b) by means of a series of orifice plates, respectively. Although a considerable amount of stochasticity in the DDT was reported in the previous sections, the pressure signals at the combustor inlet were found to be qualitatively similar for all conducted cycles. Both presented measurements were conducted with $\mathrm{Re} \approx 4.1 \cdot 10^4$ and $X_{\mathrm{O_2,ox}} = 0.4$. Similar to Fig. 3.3, the sensor signals are shifted vertically by their respective axial positions, which allows for drawing trajectories of the leading shock (L), the retonation (R), and the detonation (D). When applying a series of orifice plates, only sensors $\mathrm{P_0}$, $\mathrm{P_3}$, and $\mathrm{P_4}$ were installed. Thus, the leading shock and the retonation wave cannot be detected and trajectory D is the only one that can be drawn. The lower limit of the figures represent the combustor head, while the scale of the y-axis is consistent. For both figures $x = 0$ represents the downstream end of the DDT section.

As expected, the slopes of the detonation front in the x–t diagrams are similar for both configurations as a result of the constant propagation velocity of the detonation, which matches the CJ velocity. When comparing the pressure signals of $\mathrm{P_0}$ for the two investigated DDT geometries, the amplitude of approximately 13.5 bar as well as the shape of the first pressure peak at $t - t_{\mathrm{ign}} \approx 0.3\,\mathrm{ms}$ is similar for both setups. This can be explained by the fact that this pressure peak originates from the ignition event at the spark plug. However, as the subsequent combustion process is fundamentally different for the two investigated setups, the pressure signal of $\mathrm{P_0}$ highly depends on the installed DDT geometry for $t - t_{\mathrm{ign}} > 0.4\,\mathrm{ms}$. When operating the PDC with the shock-focusing device (Fig. 3.10 a), multiple distinct pressure peaks are visible. Subsequent to each local maximum, the pressure recovers to a relatively low value of $\Delta p \approx 2\,\mathrm{bar}$. In particular, the largest pressure amplitude of 17 bar is visible for the second peak at $t - t_{\mathrm{ign}} \approx 0.7\,\mathrm{ms}$. As indicated by the trajectory R, this pressure peak results from the arrival of the retonation at the combustor inlet. At the flat end wall of the combustion tube, the associated shock wave is reflected and subsequently propagates downstream where it is detected by sensors $\mathrm{P_1}$ and $\mathrm{P_2}$ approximately 0.9 ms after the spark discharge. At the converging part of the shock-focusing device, the pressure wave is partly reflected and causes a third pressure

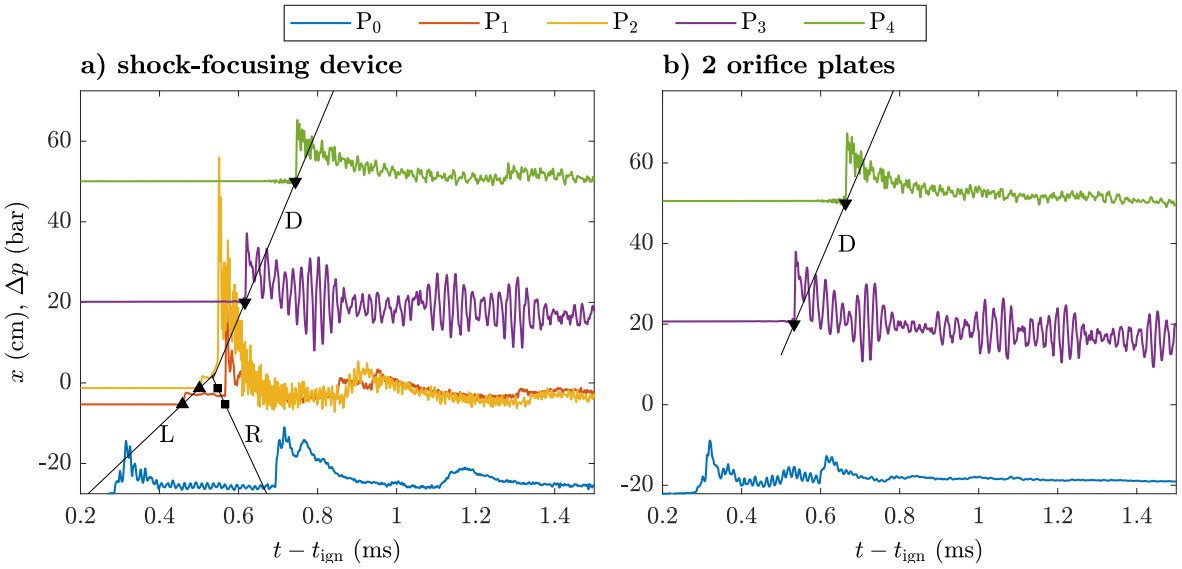

Figure 3.10: Pressure histories for successful detonation initiation by means of (a) the shock-focusing device and (b) a series of two orifice plates. The sensor signals are shifted in vertical direction by their respective axial distance to the downstream end of the DDT section.

pulse at the combustor inlet at $t - t_{\mathrm{ign}} \approx 1.1\,\mathrm{ms}$. In conclusion, the pressure fluctuations at the combustor inlet subsequent to the ignition are mainly driven by pressure waves propagating inside the pre-detonation chamber. For measurements with two orifice plates (Fig. 3.10 b), the pressure history at sensor P_0 reveals considerable pressure fluctuations only for the first 0.8 ms after the spark discharge. In this period, however, several local pressure maxima are visible in the recorded data, which most likely emanate from reflections of the leading shock at the orifice plates. Subsequently a nearly constant pressure value is observed at the combustor inlet, which however lies well above the initial pressure.

A more detailed examination of the recorded pressure histories at P_0 is shown in Fig. 3.11 a. The illustrated time period of $0.2\,\mathrm{ms} < t - t_{\mathrm{ign}} < 2.5\,\mathrm{ms}$ is chosen based on the observation of a gradually decreasing pressure for $t - t_{\mathrm{ign}} > 2.4\,\mathrm{ms}$, which is associated to the expansion of the burnt gas during the blowdown. In addition, the integral pressure values during periods of potential backflow of hot exhaust gases into the oxidizer supply are given in Fig. 3.11 b. These periods are characterized by the pressure in the combustion chamber exceeding the oxidizer supply pressure. The integral pressure value I is calculated by

$$I = \int_{0.2\,\mathrm{ms}}^{2.5\,\mathrm{ms}} \Big(p_0 \left(p_0 > p_{\mathrm{ox}}\right) - p_{\mathrm{ox}} \Big) \mathrm{d}t. \tag{3.2}$$

I represents a valuable parameter for the characterization of the conditions at the combustor inlet, since it scales with the backflow of hot exhaust gases. As the oxidizer supply pressure might vary due to a change in the oxidizer mass flow rate or in the design of the inlet geometry, the integral pressure I is plotted in Fig. 3.11 b as a function of the oxidizer supply pressure p_{ox}. The visualized variation in p_{ox} was not applied in the experiments, where a value of $p_{\mathrm{ox}} = 2.2\,\mathrm{bar}$

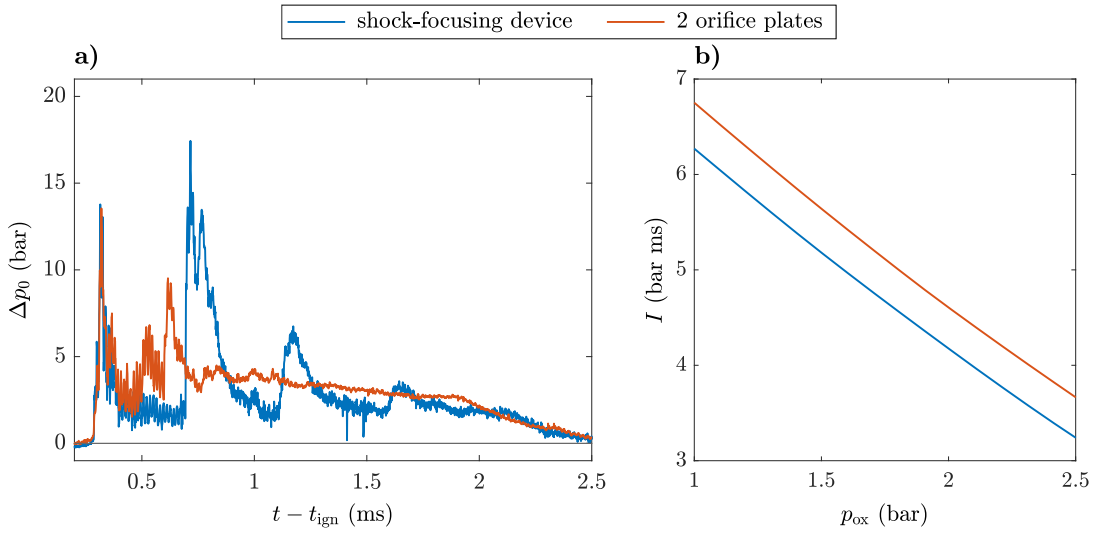

Figure 3.11: (a) Pressure evolution at the combustor inlet for successful DDT and (b) integral pressure during periods of potential backflow

was set. However, calculating I for a range of oxidizer supply pressures, allows for assessing the backflow of exhaust gases for other PDC inlet designs, which induce a smaller pressure drop.

It should be noted that the integral pressure value of the recorded signal from a piezoelectric pressure transducer should be carefully interpreted since the value might be affected by charge leakage and thermal drift. The discharge time constant of the applied pressure sensor was specified by the manufacturer as DTC = 12 s, which indicates a decrease of the output signal by 63 % when applying a constant pressure during this period. In the evaluated time period of 2.5 ms, the charge leakage can be calculated to 0.02 %, which allows for neglecting the effect on the calculated integral pressure. As highlighted in Sec. 2.3.2, a considerable thermal drift is visible in pressure signals inside the PDC tube. However, the sensor P_0 at the combustor inlet is less exposed to high-temperature gases since the applied ignition delay results in minimizing the fuel concentration upstream of the combustor inlet prior to the spark discharge, resulting in a buffer of pure oxidizer between the hot exhaust gases and the sensor P_0. Thus, the thermal drift is expected to be significantly reduced in comparison to sensors that are flush mounted to the wall of the detonation tube. Furthermore, similar conditions at the combustor inlet are given for the conducted measurements of both DDT geometries. Hence, it is reasonable to expect the thermal drift to have a comparable effect on both pressure histories, which allows for the qualitative comparison of the two integral pressure values.

Comparing the recorded pressure signals at the combustor inlet, shown in Fig. 3.11 a for both investigated DDT geometries, a larger peak amplitude of 17 bar is observed when using the shock-focusing device. When installing a series of orifice plates, the largest pressure amplitude of 14 bar is a direct result of the ignition event. Hence, slightly larger pressure waves travel upstream when applying the shock-focusing device. However, earlier arrival times of reflected shock structures when a series of orifice plates is installed prevent the pressure to recover in the meantime, resulting in a larger integral pressure value. As illustrated in Fig. 3.11 b, this difference in I for the two investigated DDT geometries is nearly constant for all considered oxidizer supply pressures. Therefore, the presented examination of the pressure signal at the combustor inlet

reveals that the backflow of hot exhaust gases into the oxidizer supply is expected to be smaller when the shock-focusing device is installed instead of a series of two orifice plates.

3.4 Concluding Remarks

By applying high-speed imaging of the reaction front, the detonation initiation inside the shock-focusing device was experimentally confirmed to occurred due to a local explosion close to the axial position of the smallest cross section area of the converging–diverging geometry. Since this procedure required huge experimental effort, a trustworthy method for the detection of successful detonation initiation by shock focusing was elaborated on the basis of four pressure signals from transducers, mounted to the combustor wall at various axial positions. Measurements with two different oxygen concentration in the oxidizer revealed that repeatable successful detonation initiation by shock focusing was achieved above a certain threshold of the Reynolds number of the flow. This was explained by the continuous growth in the pressure ratio across the leading shock when increasing the Reynolds number. Above a certain shock strength, the generated pressure and temperature conditions at the focal point allowed for the onset of a detonation. The required Reynolds number was determined in this section to be specific to the experimental setup as well as the mixture composition. However, the described correlation between the pressure ratio across the leading shock and the success rate of detonation initiation by shock focusing only depends on the geometry of the shock-focusing device, but is invariant for variations in all other design parameters, e.g. the combustor inlet geometry.

The comparison to the PDC operation with a series of orifice plates demonstrated that the required volume of hydrogen–oxygen–air mixtures at ambient temperature and pressure conditions to achieve reliable detonation initiation was larger when using the shock-focusing device. However, the detonation initiation by shock focusing largely depended on the formation of a strong leading shock. In the conducted experiments, this shock was generated in a straight tube. The integration of shock enhancing features, e.g. turbulence generators, may increase the pressure ratio across the leading shock, and thus, promote detonation initiation at the focal point. Furthermore, the targeted stratification of fuel concentration throughout the PDC emerged as efficient method for generating a strong leading shock in the scope of this work. The conducted experimental investigations on this aspect are presented in Sec. 4.3.3. Moreover, the process of DDT is dominated by deterministic mechanisms when applying shock focusing. When using a series of orifice plates, the cycle-to-cycle variations of the time delay between the ignition and the detonation wave reaching the combustor outlet increases, which is undesired when integrating the PDC into a gas turbine. In addition, a smaller integral pressure increase at the combustor inlet was observed when using the shock-focusing device, which indicates less backflow of hot exhaust gases and a smaller required purge time to prevent unintended contact burning at the start of the fuel injection. Thus, the shock-focusing device is a promising concept to promote the detonation initiation inside a practicable PDC. Nevertheless, a clear drawback is the large required mixture reactivity at atmospheric conditions. To assess the feasibility of shock focusing and the PDC operation behavior at gas turbine relevant conditions, experimental investigations at increased temperatures and at elevated pressure conditions are examined in the following chapter.

Chapter 4

PDC Operation at Gas Turbine Relevant Conditions

The cyclic process in a PDC involves numerous mechanisms, e.g. turbulent mixing of fuel and oxidizer, ignition by spark discharge, flame acceleration, DDT, and the propagation of the initiated detonation wave. All these processes are sensitive to flow features, mixture properties, and boundary conditions. Thus, results from experiments at atmospheric conditions cannot be used without restrictions to predict the PDC operation at gas turbine relevant operating conditions. Therefore, characteristic properties of propagating detonations and the process of DDT were studied in the scope of this thesis under variable boundary conditions in order to assess the operational range of pulse detonation combustion at gas turbine application. In particular, the conducted experiments were tailored to examine PDC characteristics at typical operating conditions of a micro gas turbine (3 bar and 400 K). For this engine type, the integration of a PGC device holds a large potential for a significant gain in thermal efficiency, as discussed in Sec. 1.1. Furthermore, hydrogen fueled micro gas turbines are well-suited for the decentralized generation of electricity in periods with a shortage of available renewable resources.

In this chapter, characteristic parameters of the PDC operation are examined at elevated temperature and pressure conditions, respectively. First, the size of the detonation cells are evaluated for increased initial mixture temperatures to extend the partly contradicting results from previous studies that were discussed in Sec. 1.2.3. Second, PDC operation characteristics are investigated at increased initial pressures. As the available experimental and numerical data for these conditions consistently predict a decrease in the detonation cell width, the measurements conducted in the scope of this thesis focused on other relevant parameters, i.e. the formation of the leading shock and the detonation initiation by shock focusing. The results from the conducted experimental studies allow for assessing the operation behavior of a PDC at elevated temperature and pressure conditions, and thus, contribute to the development of a PDC, which can potentially be integrated into a micro gas turbine.

In addition, lean combustion is desired in gas turbine applications due to its potential in increasing the cycle efficiency while decreasing the emission of pollutants, such as NO_x. Since

low equivalence ratios induce a significantly reduced mixture reactivity, the reliable operation of a PDC at these conditions is extremely challenging. Fuel stratification is proposed in this thesis as a suitable concept to realize repeatable detonation initiation at globally lean mixture conditions, which was verified by a systematic experimental study that is presented in the third section of this chapter.

4.1 Increased Mixture Temperature

As discussed in Sec. 1.2.2, the size of detonation cells is highly correlated to the reactivity of the mixture and can thus be used as a measure to describe detonation limits. Since elevated oxidizer temperatures are present at the combustor inlet when integrating the PDC into a gas turbine, knowing the dependence of these limits on the initial temperature of the injected fuel–oxidizer mixture is crucial for predicting the operation behavior of the PDC at gas turbine relevant conditions. However, the influence of elevated temperature conditions on the detonation cell width λ of a hydrogen–air mixture is not yet fully understood. While experimental results from Ciccarelli et al. [72] suppose a decrease in λ for a temperature variation from 400 to 650 K, a numerical model from Djordjevic et al. [13] predicts an increase in the cell width. The authors state that this discrepancy emerges from two competing effects, i.e. an increasing post-shock temperature and a simultaneous decrease in the Mach number of the detonation front due to the elevated speed of sound. The effects of these parameters on the induction length, and thus, on the detonation cell width is still subject of ongoing research. In the scope of this theses, the detonation cell width is measured experimentally for a variety of mixture temperatures using sooted foils. By this, the change in detonability of a hydrogen–air mixture when increasing the initial mixture temperature T_0 from ambient to gas turbine relevant conditions is assessed. The findings of this study have been partly published in 2018 [143].

4.1.1 Measurement Procedure

The measurements were conducted on the single-tube PDC test facility, sketched in Fig. 4.1. An electric heater was attached upstream of the PDC to allow for increasing the temperature of the continuous air flow with $\dot{m}_{\mathrm{air}} = 80\,\mathrm{kg/h}$ up to 1100 K. The fuel was injected through four solenoid valves without the usages of a dome-loaded pressure regulator. The hemispherical wave reflector was chosen as inlet geometry for the combustor because of its robust design and low heat loss. The fact that this geometry limits the firing frequency was not of importance here, since the usage of sooted foils demanded for single-cycle operation anyway. A series of six orifice plates with a distance of 85 mm between two consequent obstacles was applied to promote DDT. Detonation initiation by shock focusing was not feasible, since the experiments could only be conducted with pure air as oxidizer. The used heater did not allow for elevated oxygen concentrations and the injection of oxygen in a preheated air flow was not suitable for two reasons. Firstly, the injection of cold oxygen would have reduced the temperature of the oxidizer, and thus limited the range of achievable mixture temperatures. Secondly, the high temperature at the injection position of oxygen would have evoked the risk of ignition in the oxygen supply line [128]. Downstream of the DDT section with a length of 1.2 m, a detonation

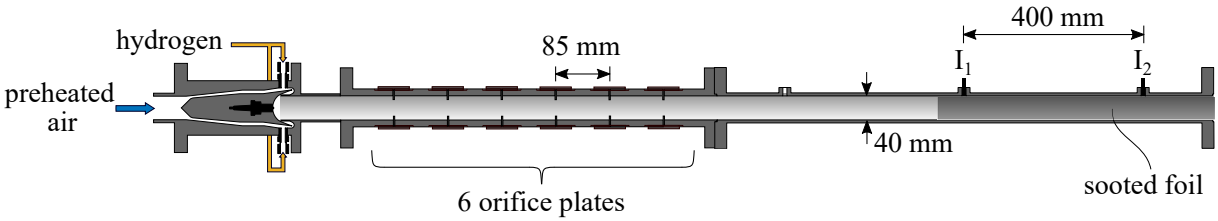

Figure 4.1: Sketch of the single-tube PDC with hemispherical wave reflector and a series of six orifice plates used for investigations at elevated pressure conditions. A sooted foil was inserted at the rear end of the measurement section to record the detonation cells.

section of 1 m length was attached for investigations on the propagating detonation wave. All sections of the combustion tube had an inner diameter of 40 mm.

The air mass flow was set to 80 kg/h with an accuracy of ±5 kg/h measured by a Coriolis mass flow meter. The fuel mass flow was controlled by setting the supply pressure in order to achieve a stoichiometric mixture. The stationary fuel mass flow rate with continuously open valves was measured as 2.34 ± 0.05 kg/h. In combination with the uncertainty in the oxidizer flow rate, an equivalence ratio of $0.91 \leq \varphi \leq 1.09$ was obtained. According to experimental observations by Guirao et al. [144], this variation in the equivalence ratio causes a deviation of the measured cell size by approximately +5%, while only positive deviations occur as the minimum value of λ is obtained for stoichiometric conditions. The temperature of the oxidizer was measured by a sheathed thermocouple (type K), which allowed for calculating the temperature of the injected hydrogen–air mixture according to Eq. 2.7. The initial mixture temperature was varied from ambient conditions (300 K) up to a maximum value of $T_0 = 770$ K. A summary of the applied settings is given in Tab. 4.1.

Configuration	
test facility	single-tube PDC
injection geometry	hemispherical wave reflector
DDT geometry	orifice plates
number of orifice plates	6
Constant parameters	
firing frequency	single-cycle operation
injection duration	$t_{\mathrm{inj}} = 2$ s
initial pressure	$p_0 = 1$ bar
oxidizer	air ($X_{\mathrm{O_2,ox}} = 0.21$)
equivalence ratio	$\varphi \approx 1$
Variable parameters	
initial temperature	$295\,\mathrm{K} \leq T_0 \leq 770\,\mathrm{K}$

Table 4.1: Parameters for investigations on PDC operation at elevated temperature conditions

4.1.2 Detonation Velocities

Two ionization probes were installed in the detonation section, allowing the calculation of the propagation velocity of the combustion front across the sooted foil according to Eq. 2.11. The output signal of the ionization probes were recorded with a sampling rate of 1 MHz, which resulted in an accuracy of $\pm 1\,\mu$s for the determination of the times t_3 and t_4, representing the instances when the combustion front passes the sensors. This eventually leads to an uncertainty of $\pm 1\,\%$ for the measured detonation velocity. The deduced velocities u_{det} are shown in Fig. 4.2 a as a function of the initial temperature T_0 of the flammable mixture. The cycle-averaged values are complemented by bars, representing the cycle-to-cycle standard deviation.

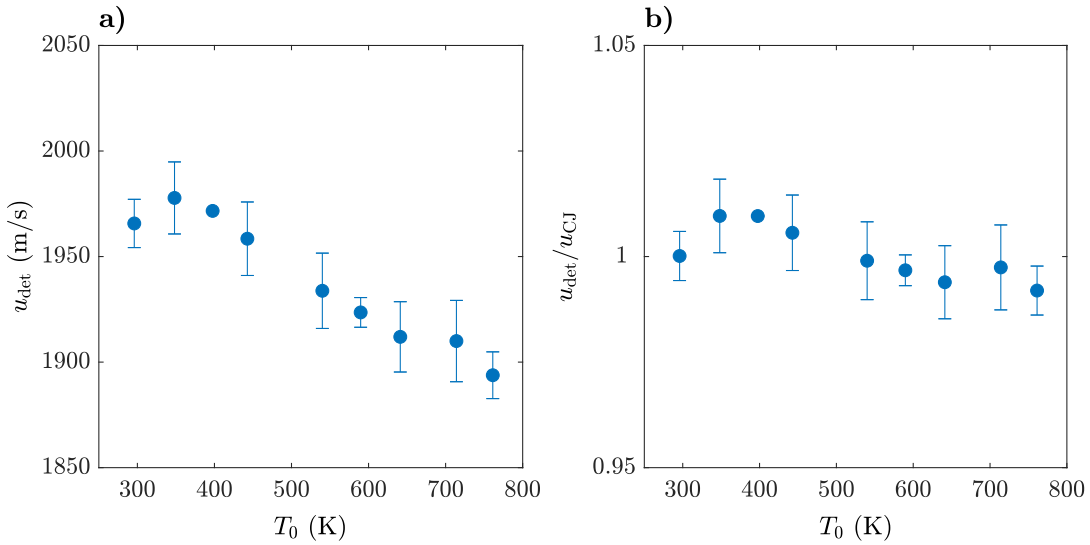

Figure 4.2: Measured propagation velocities u_{det} with respect to the mixture temperature from ambient conditions to $T_0 = 770\,\mathrm{K}$. Both (a) absolute values and (b) normalized values by the CJ velocity are plotted as cycle-averaged values with bars representing the cycle-to-cycle standard deviation.

The measurement values show a gradual decrease of the detonation velocity with increasing initial mixture temperature T_0. This dependence was expected, as the CJ velocity of a detonation propagating through a stoichiometric hydrogen–air mixture decreases with increasing initial temperature, as discussed in Sec. 1.2.3. A comparison of the measured detonation velocity and the value of u_{CJ} is shown in Fig. 4.2 b. The plotted data reveal that the measured velocities match well with the theoretical values within the range of measurement accuracy. The propagating combustion front inside the measurement section therefore represent a stable CJ detonation.

4.1.3 Measurements of the Detonation Cell Width

Sooted foils were inserted at the rear end of the combustion tube prior to a single combustion event. After removing the foils from the PDC tube, the imprinted cellular pattern was digitized by a camera. The obtained images were processed by using a tool adapted from Hébral and Shepherd [138] including two-dimensional autocorrelation. More details on the applied processing method is given in Sec. 2.3.5. For each applied temperature condition, a histogram, representing

the energy distribution over the predominant cell widths, was deduced. An example plot of such a histogram is shown in Fig. 4.3 a for the lowest investigated initial mixture temperature of $T_0 = 295\,\mathrm{K}$. The energy e is normalized by the maximum value, which was obtained in this case for a cell width of $\lambda = 13.2\,\mathrm{mm}$. The five cell widths λ_i with the largest associated energy are plotted in Fig. 4.3 b for all applied temperature conditions. The size of the data points represents the respective energy e_i normalized by the cumulative energy of the five considered cell widths. Additionally, the mean cell width λ_{avg} is calculated as the weighted average according to

$$\lambda_{\mathrm{avg}} = \frac{\sum_{i=1}^{5} e_i \lambda_i}{\sum_{i=1}^{5} e_i}. \tag{4.1}$$

The measurement results are accomplished by results form Ciccarelli and Dorofeev [83], who experimentally determined the predominant detonation cell width in stoichiometric hydrogen–air mixtures for 300 and 650 K, respectively.

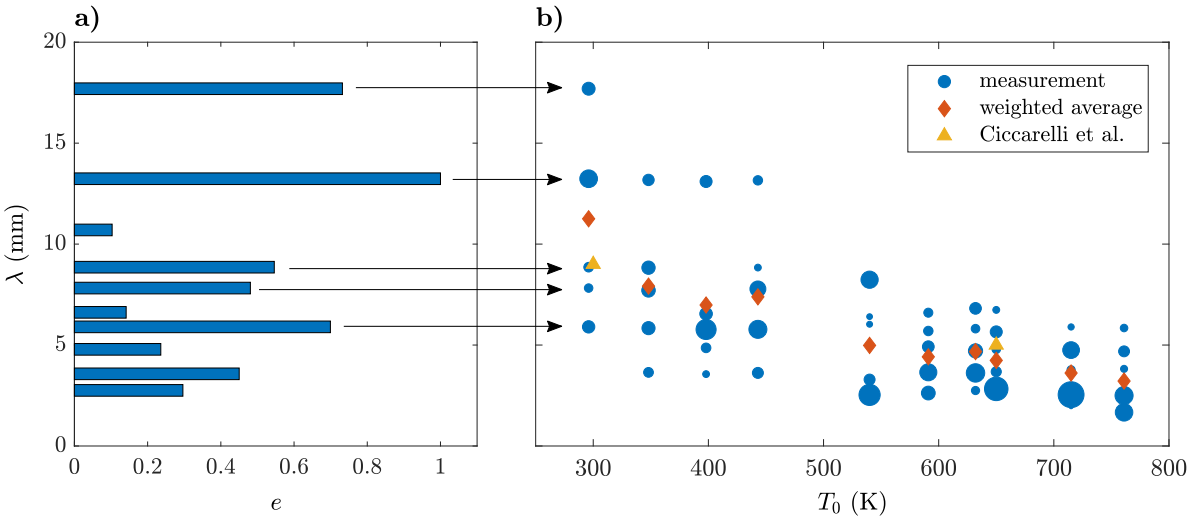

Figure 4.3: (a) Distribution of energy over a range of detonation cell widths at ambient temperature conditions and (b) dominant detonation cell widths with respect to the mixture temperature from ambient conditions to $T_0 = 770\,\mathrm{K}$. The results are complemented by experimental results from Ciccarelli et al. [72].

The data reveal a significant distribution of the detonation cell width λ for a given initial mixture temperature T_0. However, a considerable decrease in the determined cell widths is visible for an increasing initial temperature. This observation is supported by an almost monotonic decrease in λ_{avg} with increasing T_0. In particular, for $T \approx 300\,\mathrm{K}$ and $T \approx 650$ the results agree fairly well with the findings from Ciccarelli et al. [72] who found cell width of 9 mm and 5 mm, respectively. Nevertheless, the results reveal that the determination of a single representative cell width is not sufficient to describe the instabilities that cause the generation of the observed irregular cellular pattern, as shown in Fig. 1.9. Rather, the recorded structure can be explained by the interaction of variously sized detonation cells.

In conclusion, the results plotted in Fig. 4.3 b reveal an overall decrease in the detonation cell

widths with increasing combustor inlet temperature, which indicates an increased detonability of the mixture. In addition, Dorofeev et al. [145] experimentally showed that the DDT run-up distance in an obstructed channel is closely linked to the detonation cell width. According to these findings, the process of DDT in a PDC equipped with a series of orifice plates is expected to be facilitated at elevated temperature conditions. Furthermore, the increased detonability for elevated temperature conditions is assumed to allow for the reliable detonation initiation by shock focusing with a reduced oxygen enrichment compared to the required operating conditions for ambient mixture temperatures, which were examined in Sec. 3.2.

4.2 Operation at Elevated Pressure Conditions

In contrast to the effect of elevated temperature conditions, the influence of an increase in the initial pressure on the detonation cell width is consistently reported to result in a decrease in λ [73, 13]. Following the discussion in the previous section, this decrease in λ is expected to facilitate the detonation initiation when operating a PDC at gas turbine relevant conditions. However, detonation initiation by shock focusing under elevated pressure conditions has not been investigated experimentally before. Therefore, a systematic study of the PDC operation at these conditions was conducted in the scope of this thesis. In particular, the formation of the leading shock and the detonation initiation inside the shock-focusing device was investigated experimentally at various initial pressure conditions and Reynolds numbers. The obtained results have been partly published in [131].

4.2.1 Measurement Procedure

The influence of the initial pressure on the PDC operation was examined on the single-tube PDC test rig, which allowed for the operation at increased pressure conditions up to an absolute value of 3 bar. The test rig, sketched in Fig. 4.4, consisted of a mixing geometry with injection tubes attached, a pre-detonation chamber, the shock-focusing device, and a detonation section. A detailed description of the components of the test facility is given in Sec. 2.1. The application of an outlet blockage allowed for an additional pressure loss at the combustor outlet, resulting in an elevated pressure in the PDC tube.

Oxygen enriched air was used as oxidizer to increase the reactivity of the mixture. Analogous to the experimental study at atmospheric pressure conditions, which is presented in Sec. 3.2, the mole fraction of oxygen in the oxidizer $X_{O_2,ox}$ was varied between 0.35 and 0.4. The firing frequency was set to 0.5 Hz, which implies a cycle duration of 2 s. This frequency was chosen to allow for independent combustion cycles, since pressure fluctuations in the combustion tube as

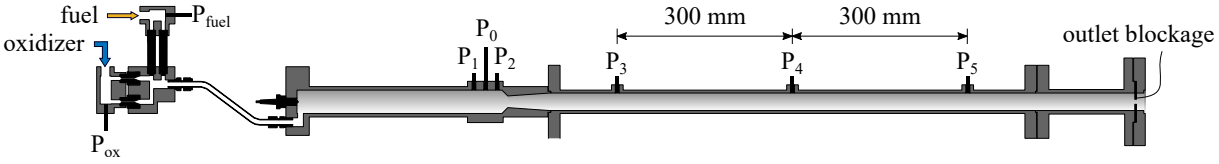

Figure 4.4: Cross section of the single-tube PDC with planar end wall and the shock-focusing device used for investigations at elevated pressure conditions.

well as in the oxidizer and fuel supplies were found to decay within 500 ms. The injection duration was set to $t_{\mathrm{inj}} = 500\,\mathrm{ms}$ in all conducted measurements. Taking the maximum duration for filling the entire tube of 100 ms into account, the applied injection time resulted in an overfilled combustion tube with a constant equivalence ratio throughout the entire combustor for all applied mass flow rates. The purge time t_{purge} exceeded the required time to fill the entire PDC tube by a factor of 15. In addition, no premature ignition of the injected fuel–oxidizer mixture due to the contact with hot exhaust gases from the previous combustion cycle was observed. Thus, exhaust gases were successfully removed from the combustor before the start of the subsequent injection period, which allowed for experiments at well-controlled mixture conditions.

The intended increase in static pressure prior to the combustion event was achieved by installing a blockage plate at the combustor outlet, which generated an additional pressure loss depending on the applied flow rate. Four different blockage ratios β were applied to the PDC outlet: 0, 0.75, 0.85, and 0.9. For an oxygen mole fraction in the oxidizer of 0.4, all four blockage ratios were applied. For $X_{\mathrm{O_2,ox}} = 0.35$, only the minimum and the maximum blockage ratios were applied. For each configuration, the mass flow rates of oxidizer and fuel were varied while maintaining a nearly constant equivalence ratio of $\varphi = 1 \pm 0.1$. This procedure allowed for a variation of the Reynolds number (Eq. 2.10) of the injected mixture between $2.4 \cdot 10^4$ and $5.7 \cdot 10^4$. The configuration of the test rig and the applied operation parameters are summarized in Tab. 4.2.

The installed blockage at the PDC outlet induced a pressure loss that depended on the flow rate of the injected mixture. Hence, the measured initial pressure p_0 in the pre-detonation chamber increased with an increasing Reynolds number when an outlet blockage was applied, as shown in Fig. 4.5 a for an oxygen mole fraction in the oxidizer of 0.35 and in Fig. 4.5 b for $X_{\mathrm{O_2,ox}} = 0.4$. Each data point represents the average measured value of at least 50 combustion cycles. When the outlet blockage was absent ($\beta = 0$), only a small pressure increase was measured

Configuration	
test facility	single-tube PDC
injection geometry	choked nozzles in air supply and mixing tubes
DDT geometry	shock-focusing device
DDT run-up distance	$l_{\mathrm{DDT}} = 346\,\mathrm{mm}$
Constant parameters	
firing frequency	$f_{\mathrm{tube}} = 0.5\,\mathrm{Hz}$ (quasi single-cycle operation)
injection duration	$t_{\mathrm{inj}} = 500\,\mathrm{ms}$
initial temperature	$T_0 \approx 300\,\mathrm{K}$ (ambient conditions)
equivalence ratio	$\varphi = 1$
Variable parameters	
oxidizer	oxygen enriched air ($0.21 \leq X_{\mathrm{O_2,ox}} \leq 0.4$)
outlet blockage ratio	$\beta = [0, 0.75, 0.85, 0.9]$
Reynolds number	$2.4 \cdot 10^4 < \mathrm{Re} < 5.7 \cdot 10^4$

Table 4.2: Parameters for investigations on PDC operation at elevated pressure conditions

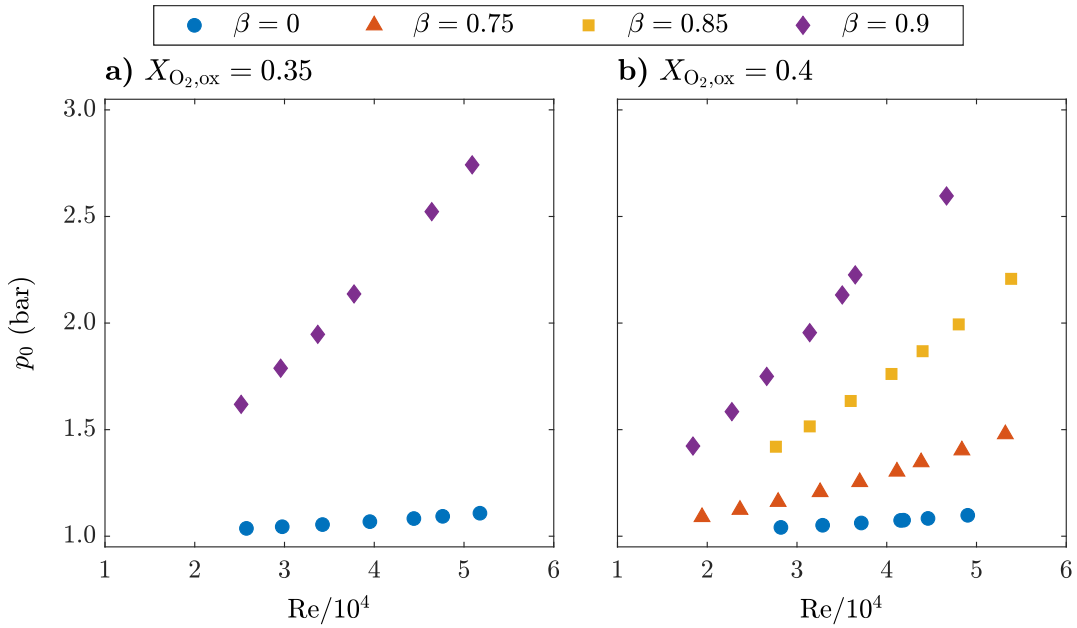

Figure 4.5: Initial pressure p_0 as a function of the Reynolds number Re for (a) 35 % and (b) 40 % oxygen in the oxidizer, respectively.

indicating nearly ambient pressure conditions ($p_0 = 1\,\text{bar}$) in the DDT section prior to ignition. As discussed in Sec. 3.3.2, this gradual increase in the static pressure with increasing flow rate was generated by the shock-focusing device. When an outlet blockage was applied, the measured static pressure in the pre-detonation chamber is a function of both pressure losses. However, the data clearly indicate, that the DDT geometry only played a secondary role, as the initial pressure p_0 is mainly influenced by the Reynolds number and the blockage ratio β. For all applied parameter settings, a cycle-to-cycle variation in p_0 with a relative standard deviation of less than 1 % was observed, which indicates repeatable initial conditions during the periodic PDC operation. Furthermore, the presented data reveal that the experimental setup allowed for investigations on the detonation initiation by shock focusing for initial pressures in the range from ambient conditions to a maximum value of $p_0 \approx 2.75\,\text{bar}$. It should be considered that an increase in the initial pressure for a fixed blockage ratio at the combustor outlet could only be achieved by a variation in the Reynolds number of the flow. The application of various blockage plates, however, allowed for the examination of the effect of p_0 on the formation of the leading shock and the onset a detonation at the focal point for a fixed Reynolds number.

4.2.2 Formation of the Leading Shock

The evaluation of the detonation initiation by shock focusing at atmospheric pressure conditions in Sec. 3.2 revealed that the success of detonation initiation at the focal point highly depends on the pressure ratio across the leading shock. The obtained values of Π_L for measurements with the application of an outlet blockage are plotted in Fig. 4.6 as a function of the Reynold number for two different mole fractions of oxygen in the oxidizer (0.35 and 0.4). The bars indicate the standard deviation of the cycle-to-cycle variation in the obtained pressure ratio. For all applied outlet blockages the pressure ratio increases with an increasing Reynolds number. Further,

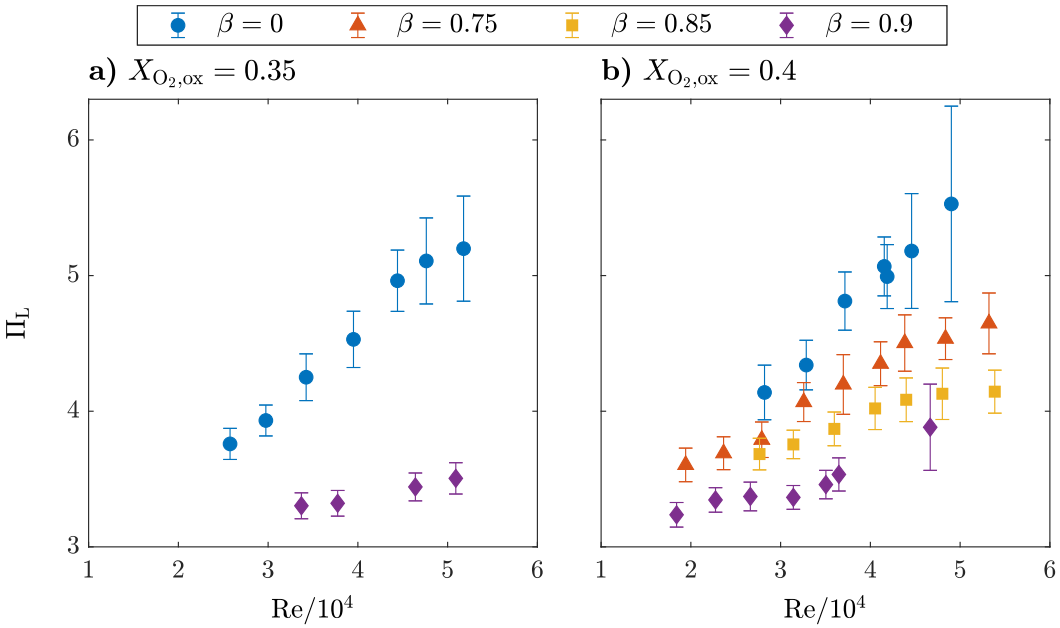

Figure 4.6: Pressure Ratio across the leading shock Π_L with respect to the Reynolds number for various blockage ratios and two oxygen concentrations in the oxidizer

the slope of this nearly linear growth decreases for higher blockage ratios. Therefore, weaker shocks are obtained when increasing the initial pressure for a constant Reynolds number. This observation can be explained by two phenomena. On the one hand, the laminar flame speed for elevated pressure conditions is reduced [146, 147, 148], which is expected to result in the generation of weaker pressure waves that eventually prevents the formation of a strong leading shock. On the other hand, turbulent fluctuations in the flow velocity decrease with increasing value of p_0. Assuming the validity of the ideal gas equation (Eq. 1.6), the Reynolds number (Eq. 2.10) can be expressed by

$$\mathrm{Re} = \frac{D_{\mathrm{tube}}}{\eta R_{\mathrm{s}} T_0}\, p_0\, \bar{u}_{\mathrm{flow}}, \tag{4.2}$$

with η denoting the dynamic viscosity. Both η and R_{s} are constant for a given mixture. Thus, an increase in the initial pressure p_0 for a given Reynolds number results in a decrease in the mean flow velocity. As the turbulence intensity (Eq. 2.9) is a function of the Reynolds number, a constant value of Tu and thus a reduction in turbulent velocity fluctuations are obtained for elevated initial pressure conditions. As discussed in Sec. 1.3.1, these velocity fluctuations play a central role in the acceleration of the combustion front, and thus, in the formation of the leading shock. Therefore, the application of a higher blockage ratio at the PDC outlet results in a reduced pressure ratio across the leading shock when a constant Reynolds number is maintained.

4.2.3 Detonation Initiation via Shock Focusing

The experimental investigations at atmospheric pressure conditions, presented in Sec. 3.2.2, revealed that reliable detonation initiation by shock focusing is achieved when the pressure ratio across the leading shock exceeds a certain threshold. In particular, $\Pi_L > 4.6$ was required for an oxygen concentration in the oxidizer of $X_{O_2,ox} = 0.4$. In this section the correlation between the

strength of the leading shock and the success rate is examined at elevated pressure conditions up to $p_0 \approx 2.7\,\text{bar}$. The obtained success rate of detonation initiation is shown in Fig. 4.7 with respect to the initial pressure and Π_L. For this, the measurement results from all the conducted combustion cycles over a range of Reynolds numbers and four different blockage ratios were clustered with respect to the values of p_0 and Π_L. For each data point, the respective marker size illustrate the number of cycles that contribute to the presented cycle-averaged value. The color of the data points represent the value of the success rate from 0 (blue) to 1 (orange).

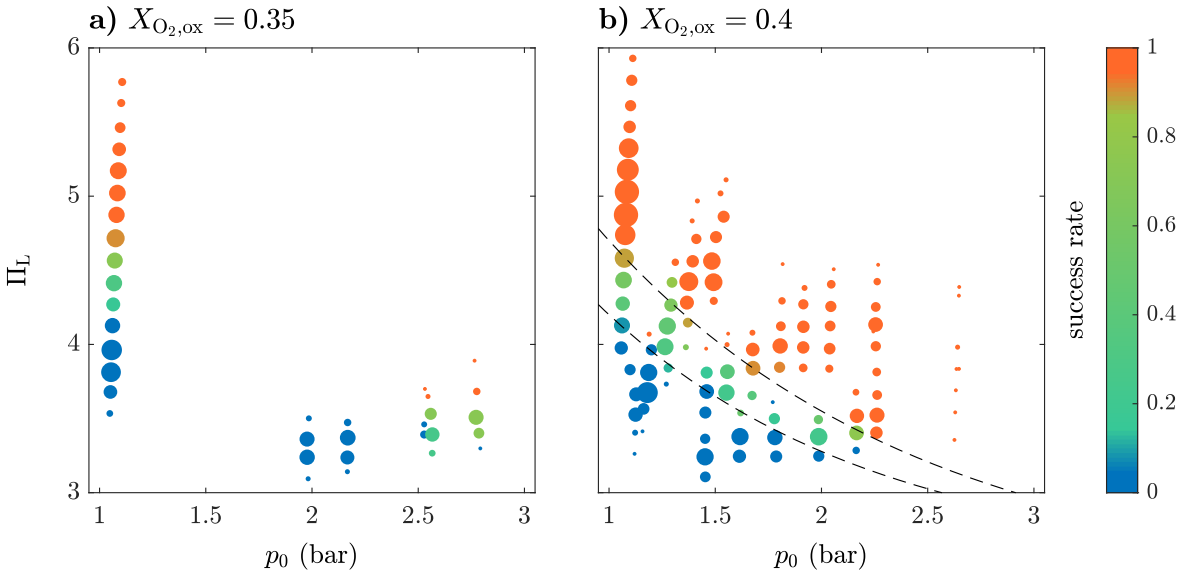

Figure 4.7: Success rate of detonation initiation by shock focusing with respect to the pressure ratio across the leading shock Π_L and the initial pressure p_0

The data points at ambient pressure conditions represent the results, which have already been examined in Fig. 3.6. Here, reliable DDT was achieved for $\Pi_\text{L} > 4.6$ when operating with a hydrogen–oxygen–air mixture with $X_{O_2,ox} = 0.4$ and $\Pi_\text{L} > 4.8$ for $X_{O_2,ox} = 0.35$, respectively. The additional results, which are plotted in Fig. 4.7, allow for determining this threshold value for initial pressure values above atmospheric conditions. As the measurements for $X_{O_2,ox} = 0.35$ were only conducted for $\beta = 0$ and 0.9, no data points could be plotted for large areas in Fig. 4.7 a. However, the plotted data for $p_0 \approx 2.8\,\text{bar}$ indicate, that the required shock strength to achieve successful detonation initiation by shock focusing at these initial pressure conditions is reduced by 1.1 to $\Pi_\text{L} > 3.7$. The large number of recorded data for $X_{O_2,ox} = 0.4$ allows for separating the results, shown in Fig. 4.7, in two regimes. No successful onset of detonation was observed for small values of p_0 and Π_L. In contrast, large values of these parameters result in reliable detonation initiation by the focusing of the leading shock, indicated by a success rate of 1. The boundary between these two regimes is represented by data points with a success rate between 0 and 1. Considering the measurement uncertainty for Π_L of $\pm 0.5\,\text{bar}$, the observed stochastic behavior can be explained by measurement errors in the shock amplitude, as discussed in Sec. 3.2.1. Despite the resulting uncertainty in the exact value of the required shock strength, a significant reduction of the threshold value with increasing initial pressure is evident. In particular, a

reduction by 1.3 bar is observed for $X_{O_2,ox} = 0.4$ when the initial pressure is increased from ambient conditions to 2.6 bar. When comparing the results for the two different investigated mixtures, two statements can be derived from the presented examination. Firstly, an increase in the oxygen concentration in the oxidizer results in a reduction of the threshold value for the strength of the leading shock, which has to be exceeded to achieve repeatable DDT in the shock-focusing device. Generally, the decrease in the required value of Π_L for elevated pressure conditions can be explained by an increase in the reactivity of the mixture, which was reported by Stamps and Tieszen [73]. Their experimental investigations revealed that the detonation cell width for hydrogen–air mixtures decreases with an increase in pressure for a given equivalence ratio, which indicates an increased mixture reactivity. Secondly, the gradient of the observed decrease in the required shock strength was found to be steeper for a larger value of $X_{O_2,ox}$. Presumingly, this effect is caused by a decrease in the concentration of inert nitrogen in the flammable mixture for elevated oxygen concentration in the oxidizer.

Considering the entire DDT process in the investigated single-tube PDC, the application of elevated pressure conditions has two opposing effects. On the one hand, the formation of the leading shock is hindered, as discussed in Sec. 4.2.2, which is undesired due to a smaller resulting pressure amplitude at the focal point. On the other hand, the initiation of a detonation is supported due to an increased mixture reactivity, as observed in the data shown in Fig. 4.7. When operating a PDC, these two processes interact and determine if reliable DDT can be achieved. The success rate of detonation initiation by shock focusing with respect to the operating conditions, represented by the Reynolds number, the outlet blockage, and the oxygen concentration in the oxidizer, is shown in Fig. 4.8. For $X_{O_2,ox} = 0.4$ (Fig. 4.8 b), the obtained detonation success rate is almost independent of the applied blockage ratio. As shown in Fig. 4.6 b, the increase in the blockage ratio leads to smaller pressure ratios across the leading shock for a given Reynolds

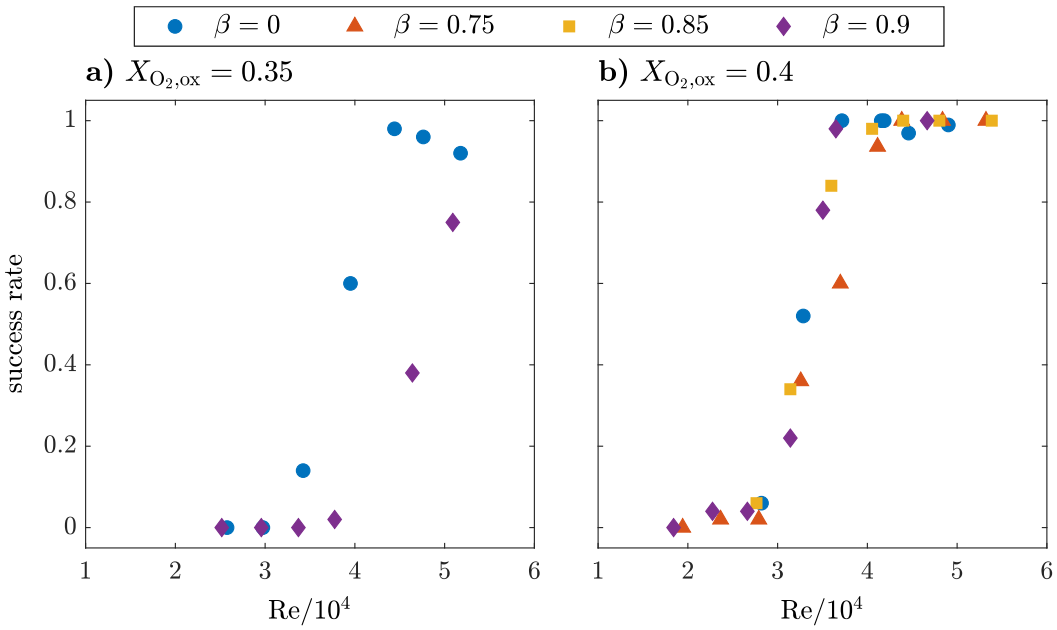

Figure 4.8: Success rate of detonation initiation by shock focusing with respect to the Reynolds number

number. This effect, however, is compensated by the simultaneous decrease in the required pressure ratio Π_L, as shown in Fig. 4.7 b. Due to this, the success of detonation initiation by shock focusing for a hydrogen–oxidizer–air mixture with $X_{O_2,ox} = 0.4$ is a function of the Reynolds number only. For $Re < 3 \cdot 10^4$, almost no successful detonation initiation was observed. As discussed above, an increase in the Reynolds number of the flow results in an elevated initial pressure and simultaneously to a stronger leading shock. Both effects support the initiation of a detonation inside the shock-focusing geometry, and therefore lead to an increase in the success rate shown in Fig. 4.8. For $Re > 4 \cdot 10^4$, reliable DDT was achieved. A reduction of the oxygen concentration in the oxidizer results in a decrease in reactivity, which hinders the successful onset of a detonation. For ambient pressure conditions ($\beta = 0$), this results in the formation of a weaker leading shock and an increase in the required value of Π_L. This causes an increase in the minimum Reynolds number, which is necessary for reliable DDT to $Re \approx 4.5 \cdot 10^4$. For the maximum applied blockage ratio of 0.9, this effect is even more pronounced. This can be explained by the fact, that the difference in the required strength of the leading shock for a given value of p_0 is larger at elevated pressure conditions. The slight decrease in the pressure ratio across the leading shock due to the decrease in reactivity has therefore a greater effect on the overall success rate of DDT.

In conclusion, three statements regarding the detonation initiation by shock focusing under elevated pressure conditions can be derived from the conducted experimental study. Firstly, when assuring a constant Reynolds number, an increase in initial pressure leads to a decrease in the pressure ratio across the leading shock due to a smaller turbulent fluctuations and a decrease in density. Secondly, increasing the initial pressure promotes the onset of a detonation inside the shock-focusing device causing a decrease in the critical pressure ratio for reliable detonation initiation. Lastly, these two opposed effects can cancel out each other, as observed in the presented experimental study for hydrogen–oxygen–air mixtures with $X_{O_2,ox} = 0.4$, where comparable DDT success rates were observed for a constant Reynolds number and a varying blockage ratio. For smaller oxygen concentrations in the oxidizer, however, the effect of the weaker leading shock was more pronounced. Thus, the increase of the blockage ratio led to an increase in the minimum required Reynolds number to achieve reliable detonation initiation.

4.3 Lean Operation by Fuel Stratification

In addition to the realization of a reliable DDT in each combustion cycle, maximizing the combustor efficiency and minimizing pollutant emission are the central demands on a PDC. Previous studies revealed that operating at lean mixture conditions allows for the specific impulse of the combustor to be increased [149] and pollutant emission to be decreased [13, 150, 151, 152] simultaneously and is therefore desirable for efficient and clean PDC operation. However, achieving reliable DDT at lean conditions is very challenging due to a considerable reduction in mixture reactivity when compared to stoichiometric mixture conditions. This effect introduces significant limitations on the operating range of a PDC when injecting a spatially homogeneous fuel–oxidizer mixture. In the scope of this work, fuel stratification is proposed to enable reliable detonation initiation in globally lean hydrogen–oxygen–air mixtures. Results of this study were partly published in [153].

4.3.1 Measurement Procedure

Experimental investigations on detonation initiation under globally lean mixture conditions were conducted on the single-tube PDC test rig, which was introduced in Sec. 2.1. The facility was equipped with a choked air supply and the shock-focusing device downstream of a pre-detonation chamber with a length of 364 mm. Similar to the previously presented study, oxygen enriched air was used as oxidizer with $X_{O_2,ox} = 0.4$. The oxidizer flow was composed of continuous flows of air and pure oxygen, individually controlled to 60 kg/h and 21 kg/h, respectively. A 300 mm long tube section containing a pitot-shaped probe was attached to the combustor to allow for exhaust gas sampling. The probe was connected to a gas analyzer by a heated line at 190 °C to prevent condensation. The NO_x concentration was measured on a wet basis in a chemiluminescence detector (KNESTEL CLD dual BASIC) with a maximum measurement of 0–300 ppm. In parallel, a dry gas sample was used to evaluate the content of oxygen and hydrogen by a paramagnetic sensor (ABB Magnos 106) and a thermal conductivity sensor (ABB Caldos 27), respectively.

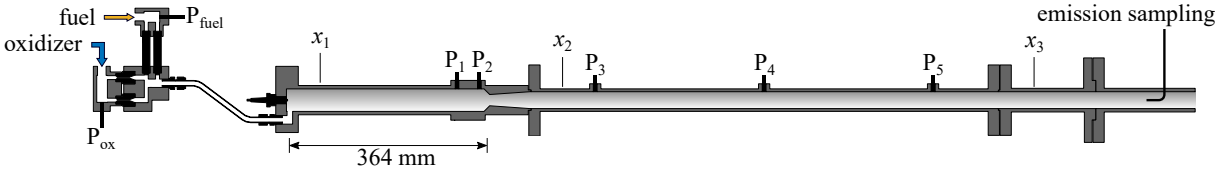

Figure 4.9: Cross section of the single-tube PDC with planar end wall and the shock-focusing device used for investigations at globally lean mixture conditions

During the PDC operation, a continuous oxidizer flow rate was guided through six choked nozzles with an individual cross section area of 3.14 mm^2. Six individually controlled solenoid valves were installed for the injection of fuel with $t_{inj} = 50$ ms. The variation of the number of open valves throughout the injection period allowed for introducing a spatial stratification of the fuel concentration across the combustor prior to the ignition event. The global equivalence ratio φ_{glob} was defined by the average equivalence ratio across the combustor and is derived from the average fuel mass flow rate throughout the entire injection period. In order to facilitate the discussion, five equivalence ratios are introduced:

φ_{is}	local equivalence ratio at the ignition source
φ_{sf}	local equivalence ratio at the shock-focusing device
φ_{pre}	average equivalence ratio in the pre-detonation chamber
φ_{det}	constant equivalence ratio in the detonation section
φ_{glob}	global equivalence ratio

As described in Sec. 2.1.4, the mass flow rates of fuel and oxidizer were monitored by two thin-film metal pressure transducers P_{fuel} and P_{ox}, respectively. Two piezoelectric pressure transducers (P_1 to P_2) were installed upstream of the shock-focusing device, allowing for the detection of the leading shock ahead of the reaction front in the pre-detonation chamber. Three additional sensor (P_3 to P_5) were located in the detonation section with a distance of 300 mm between two sensors. Similar to the previously discussed investigations at elevated pressure conditions (Sec. 4.2), this instrumentation allowed for the quantification of the pressure ratio across the leading shock Π_L, as well as the success of detonation initiation by shock focusing. Five control

trajectories, illustrated in Fig. 4.10 a, were applied to achieve various stratification profiles. The resulting idealized spatial distributions of the equivalence ratio prior to the ignition are plotted in Fig. 4.10 b.

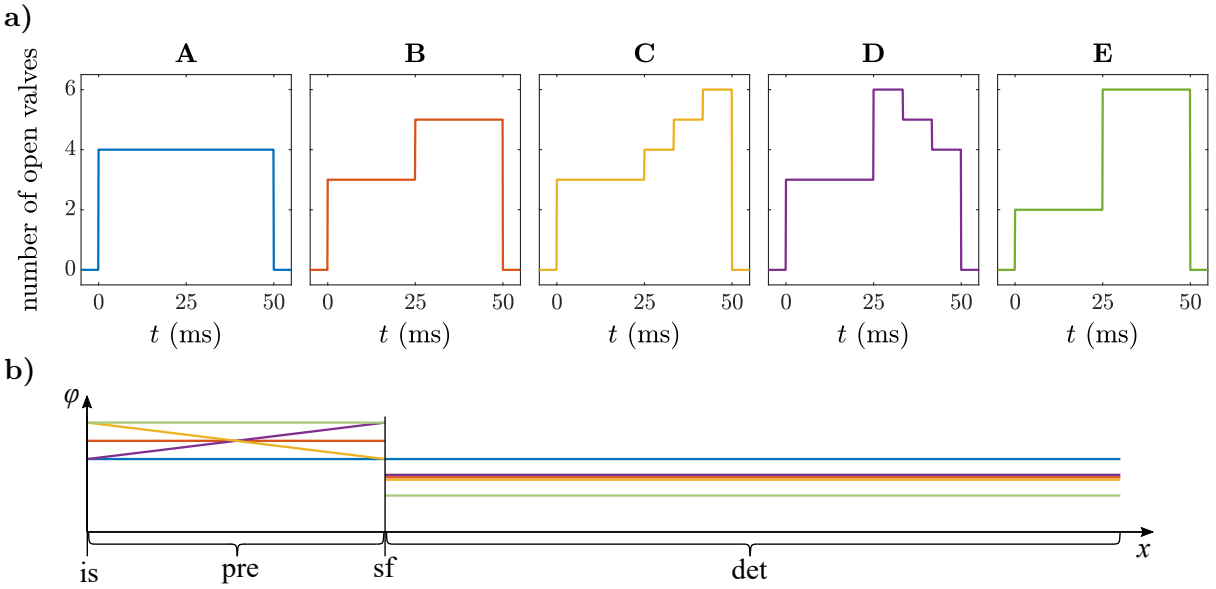

Figure 4.10: (a) Control trajectories for fuel injection and (b) the idealized spatial distribution of the equivalence ratio across the PDC

When applying trajectory **A**, four valves were opened during the entire injection period, resulting in a constant fuel concentration across the PDC tube. As this trajectory was applied in the previously presented investigations, it was considered as the reference case for this study. Although the shape of the applied control trajectories significantly differed, the averaged number of open fuel valves was equal for all cases to ensure comparable global equivalence ratios. During the first 25 ms of the injection period, the number of open fuel valves was held constant for all five control trajectories, which resulted in a spatially constant fuel concentration throughout the detonation section downstream of the shock-focusing device. The applied variations in the number of open valves during the second half of the injection period resulted in either constant or gradual fuel profiles along the pre-detonation chamber. In conclusion, the five introduced trajectories allowed for the investigation of two effects on the PDC operation. On the one hand, the difference in fuel concentration between the pre-detonation chamber and the detonation section was varied for trajectories **A**, **B**, and **E**. On the other hand, the spatial gradient of fuel concentration in the pre-detonation chamber was modified for trajectories **B**, **C**, and **D**. In particular, the equivalence ratio in the detonation tube φ_{det} and the mean fuel concentration in the DDT section were equal for trajectories **B**, **C**, and **D**. For trajectory **B**, the number of open valves was increased to five in the second half of the injection period, leading to an increased equivalence ratio in the DDT section when compared to trajectory **A**. For trajectory **C**, a negative spatial gradient in φ from the ignition source to the shock-focusing device was applied. Control trajectory **D** resulted in a positive spatial gradient in the DDT section with a maximum fuel concentration at the shock-focusing device. Similar to trajectory **B**, control trajectory **E** resulted in a constant equivalence ratio across both the detonation tube and the DDT section,

Configuration	
test facility	single-tube PDC
injection geometry	choked nozzles in air supply and mixing tubes
DDT geometry	shock-focusing device
DDT run-up distance	$l_{\mathrm{DDT}} = 346\,\mathrm{mm}$
Constant parameters	
firing frequency	$f_{\mathrm{tube}} = 5\,\mathrm{Hz}$
injection duration	$t_{\mathrm{inj}} = 50\,\mathrm{ms}$
initial temperature	$T_0 = 300\,\mathrm{K}$
initial pressure	$p_0 = 1\,\mathrm{bar}$
oxidizer	oxygen enriched air ($X_{\mathrm{O_2,ox}} = 0.4$)
Variable parameters	
global equivalence ratio	$0.2 \leq \varphi_{\mathrm{glob}} \leq 1$
control trajectory for fuel injection	**A**, **B**, **C**, **D**, **E**

Table 4.4: Parameters for investigations on PDC operation at lean mixture conditions

respectively. However, compared to **B**, trajectory **E** resulted in a further reduced φ_{det} while the value of φ_{pre} was increased. Thus, the application of trajectory **E** led to the largest amount of fuel stratification, characterized by the greatest difference in fuel concentration between the pre-detonation chamber and the detonation section.

By adjusting the set pressure of the dome-loaded pressure regulator in the fuel supply line between 2 and 4.2 bar, the global equivalence ratio was modified in the range of $0.2 \leq \varphi_{\mathrm{glob}} \leq 1$. For each combination of global equivalence ratio and injection trajectory, four consecutive runs with 100 cycles were conducted at a firing frequency of 5 Hz. This operation duration allowed for qualitatively comparing the NO_x concentration in the exhaust for various operating conditions based on a steady-state measurement signal. Pressure signals of sensors P_1 to P_5 were recorded for the last 28 cycles of each run. Thus, the derived values of Π_{L} and the success rate are based on the evaluation of 112 cycles for each parameter setting. The applied operating conditions are summarized in Tab. 4.4.

4.3.2 Fuel Concentration Measurements

In order to assess the actual spatial distribution of fuel concentration prior to the ignition event, time-resolved fuel concentration measurements by TDLAS were conducted. For this, a quartz tube was inserted successively at three different axial positions x_i, visualized in Fig. 4.9. As discussed in Sec. 2.3.4, methane was used as tracer fuel for these measurements, which induced a variation in the molecular diffusion coefficient compared to the combustion experiments with hydrogen as fuel. However, the evolution of the fuel concentration profile during the filling is expected to be mainly driven by turbulent mixing due to the large Reynolds number of the flow. Therefore, the results allow for a qualitative assessment of the spatial distribution of fuel concentration along the combustion tube prior to the ignition in the combustion experiments.

Preliminary measurements at various steady-state fuel flow rates were used to deduce a linear calibration curve that maps the measurement signal to the mole fraction of the fuel X_{fuel} in the combustor. The obtained cycle-averaged fuel concentration profiles at the first measurement position x_1 for the five applied control trajectories are shown in Fig. 4.11 as a function of time. The results generally show good agreement with the control trajectories, indicating that the applied injection strategy is suitable to achieve the desired distribution of fuel concentration along the PDC tube.

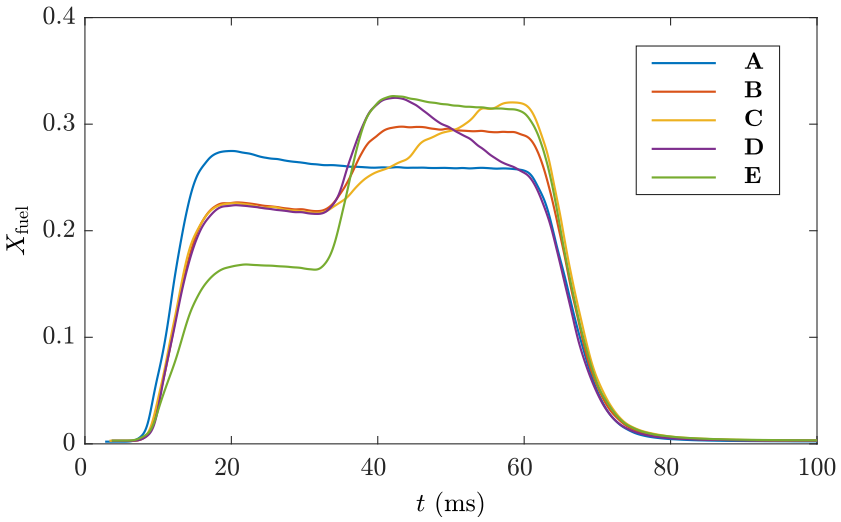

Figure 4.11: Measured fuel concentration over time for all injection trajectories measured at x_1

For all trajectories, the first injected fuel is detected roughly 10 ms after the beginning of the injection period. This time delay can be attributed to the distance between the solenoid valves and the measurement position x_1. The end of the injected fuel package is detected at $t \approx 70$ ms for all trajectories. Hence, the local variation in the volumetric flow rate resulting from the choice of the fuel trajectory does not affect the overall convection velocity of the mixture. Therefore, the position of the fuel–oxidizer package at the time of ignition is expected to be equal for all measurements. On the one hand, the congruent signals for trajectories **B**, **C**, and **D** for $t < 35$ ms indicate good repeatability. On the other hand, the visible variation in the measured fuel concentration in this time span when applying trajectories **A** or **E** reveals an adequate sensitivity of the injected fuel flow rate on the number of open valves. The constant number of open valves, which is applied during the first half of the injection period, results in nearly constant fuel concentration at x_1 for $15\,\mathrm{ms} < t < 35\,\mathrm{ms}$. In addition, the measurement signals for $40\,\mathrm{ms} < t < 60\,\mathrm{ms}$ illustrate that the desired distributions along the tube axis in the pre-detonation chamber are achieved. Almost constant values are obtained for trajectories **A**, **B**, and **E**. As intended, applying trajectories **C** and **D** results in a distinct gradient in fuel concentration over time.

As the injected fuel–oxidizer mixture is convected downstream by the mean flow, it is exposed to turbulent mixing resulting in dispersion effects on the spatial distribution of fuel concentration. This process explains the smoothing effects, which are visible in all profiles shown in Fig. 4.11. The largest smoothing is obtained at the positions of steep gradients in fuel concentration, i.e. at the beginning and end of the fuel package, as well as for $t \approx 40$ ms. However, the measured fuel

profiles agree fairly well with the ideal fuel stratifications, which are illustrated in Fig. 4.10 b. Nevertheless, the obtained profiles of fuel concentration cannot simply be converted to spatial fuel stratifications along the combustor at the time of ignition. This is caused by the fact that the first injected fuel is convected to the combustor exit while the latest injected fuel is only convected to the combustor inlet before being consumed by the reaction front. Therefore, a monotonic rise in convection time from the combustor inlet to the exit is obtained. In order to examine the effect on the spatial fuel concentration, the fuel concentration profiles measured by TDLAS at three different axial position along the combustor are compared in Fig. 4.12 for injection trajectories **A** and **B**, respectively.

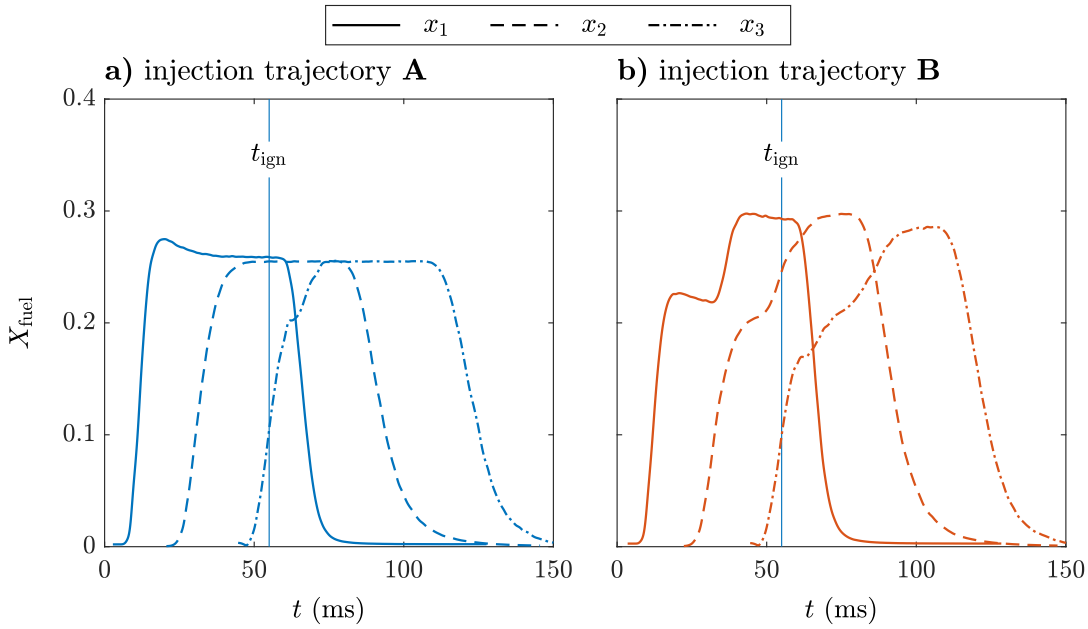

Figure 4.12: Measured fuel concentration over time at various measurement positions for injection trajectories (a) **A** and (b) **B**

As expected, the largest diffusion effects are observed for measurement position x_3, which is located the furthest downstream. For injection trajectory **A** (Fig. 4.12 a), this effect is best visible at the beginning of the fuel package. At x_1, an overshoot is observed before a constant fuel concentration is measured. This signal results from the drop in fuel supply pressure subsequent to the opening of the solenoid valves. Due to turbulent mixing, however, this overshoot is not visible in the signals for measurement positions x_2 and x_3. Furthermore, the steepness of the gradients at the start and the end of the injection period decreases with increasing convection distance. However, the fuel concentration in the middle of the injection duration is not affected significantly. When the fuel injection is stratified, as shown in Fig. 4.12 b for control trajectory **B**, the fuel concentration varies within the injection duration resulting in additional gradients. According to the findings from Fig. 4.12 a, the steepness of these gradients decreases during the convection downstream the PDC tube resulting in decreasing length of regions with constant equivalence ratio. The measurement results indicate significant smoothing of the intended gradients in fuel concentration during the convection of the fuel–oxidizer package. However, these findings are partially irrelevant for PDC operation since ignition is triggered at $t_{ign} = 55\,ms$. At this

time, the earliest injected fuel particle reaches the PDC outlet indicated by the first rise in fuel concentration at x_3. Hence, the chosen value of t_{ign} results in a just completely filled combustor. In Fig. 4.12 b, the second increase in X_{fuel} at $t = 55\,\mathrm{ms}$ for the measurement at x_2 confirms that the fuel injected in the first half of the injection period, is convected to the detonation tube and the applied control trajectories are well suited for achieving the desired distribution of fuel concentration throughout the PDC.

4.3.3 Formation of the Leading Shock and Detonation Initiation

In this section, the effect of the applied injection trajectories on the formation of the leading shock and the DDT are investigated. As discussed earlier, the detonation initiation by shock focusing mainly depends on two parameters: the reactivity of the mixture at the focal point and the induced increase in both temperature and pressure. The mixture reactivity can be influenced by adjusting the equivalence ratio φ_{sf}, which depends on the global equivalence ratio and the applied injection trajectory. The value of φ_{sf} can be assessed by multiplying the global equivalence ratio by the fraction of the number of valves that are open for $33.3\,\mathrm{ms} < t < 41.7\,\mathrm{ms}$ and the averaged number of open valves, which is four for all trajectories. The parameters are listed in Tab. 4.5 for all five applied injection trajectories.

control trajectory	**A**	**B**	**C**	**D**	**E**
average number of open valves	4	4	4	4	4
number of open valves for $33.3\,\mathrm{ms} < t < 41.7\,\mathrm{ms}$	4	5	4	6	6
$\varphi_{\mathrm{sf}}/\varphi_{\mathrm{glob}}$	1	1.2	1	1.33	1.33

Table 4.5: Dependence of the local equivalence ratio at the focal point φ_{sf} on the global equivalence ratio φ_{glob} for the applied control trajectories

The induced temperature and pressure conditions at the focal point are strongly correlated to the strength of the leading shock, which was therefore identified in the previously presented investigations (Sec. 3.2.2 and Sec. 4.2.3) as an important parameter to predict the success rate of detonation initiation by shock focusing. The obtained pressure ratio Π_{L}, measured directly upstream of the shock-focusing device, is plotted in Fig. 4.13 for all investigated injection trajectories as a function of the global equivalence ratio. The bars represent the standard deviation of the cycle-to-cycle variation. As expected, the measurement results for the reference trajectory **A** indicate a clear correlation between the global equivalence ratio and Π_{L}. In particular, a gradual increase in the shock strength is observed when increasing φ_{glob} in the combustor, which in this case is equal to the equivalence ratio in the pre-detonation chamber. Close to stoichiometric conditions, however, this gradient flattens. The observed dependence can be explained by an increase in the heat release rate in the combustion front when increasing the fuel concentration. When comparing the data from all investigated injection trajectories, the graphs clearly show that fuel stratification is a suitable tool to increase the strength of the leading shock compared to the reference case **A**. Two aspects of the influence of the fuel profile on the strength of the leading shock are analyzed separately in the following. First, the dependence of Π_{L} on φ_{pre} is examined for trajectories with a constant number of open valves during the

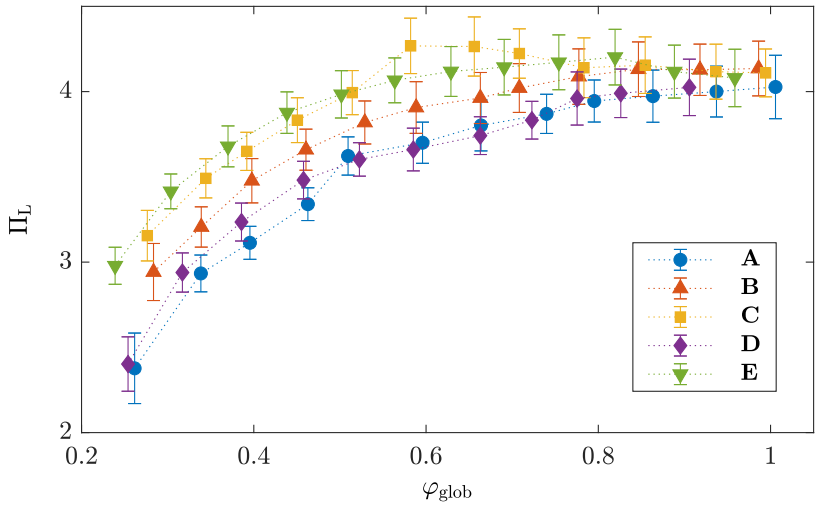

Figure 4.13: Pressure ratio across the leading shock Π_L as a function of the global equivalence ratio φ_{glob}

second half of the injection period (trajectories **A**, **B**, and **E**). Second, the effect of the spatial gradient in fuel concentration throughout the combustor is evaluated by comparing the strength of the leading shock for trajectories **B**, **C**, and **D**.

For measurements with trajectory **A** and $\varphi_{glob} = 1$, a pressure ratio of $\Pi_L = 4$ is achieved. Due to the constant fuel distribution for this trajectory, stoichiometric conditions are induced in the pre-detonation chamber. Equal conditions in the pre-detonation chamber are achieved for $\varphi_{glob} = 0.8$ when applying trajectory **B** and $\varphi_{glob} = 0.67$ for trajectory **E**, respectively. Hence, similar pressure ratios are obtained for these settings. A maximum pressure ratio for constant fuel concentration along the pre-detonation chamber is observed for $\varphi_{glob} = 0.8$ and trajectory **E** ($\varphi_{pre} = 1.2$). In conclusion, applying fuel stratification while maintaining a spatially constant equivalence ratio throughout the pre-detonation chamber results in an increased φ_{pre}. Thus, the obtained pressure ratio across the leading shock as a function of the global equivalence ratio is shifted towards lower values of φ_{glob} when increasing the amount of fuel stratification. Hence, fuel stratification allows for the generation of a strong leading shock even for the operation at globally lean conditions.

When considering a varying gradient of X_{fuel} from the ignition source towards the shock-focusing device (trajectories **B**, **C**, and **D**), the data shown in Fig. 4.13 reveal that a negative spatial gradient in the fuel concentration with a maximum equivalence ratio near the ignition source, promotes the formation of a strong leading shock. For $\varphi_{glob} = 0.6$ and trajectory **C**, the largest value of Π_L is found. These settings imply nearly stoichiometric conditions at the combustor inlet ($\varphi_{sf} \approx 1$) with decreasing fuel concentration in flow direction. The obtained value of Π_L even exceeds the pressure ratio for $\varphi_{pre} = 1.2$ with a constant fuel concentration along the pre-detonation chamber. However, when applying fuel-rich conditions at the ignition source ($\varphi_{glob} > 0.6$), this positive effect of the negative spatial gradient in fuel concentration on the pressure ratio across the leading shock diminishes. As a result, similar values of Π_L are observed for trajectories **C** and **E** for $\varphi_{glob} > 0.75$. In contrast to this, the operation at fuel lean mixture conditions at the ignition source ($\varphi_{glob} < 0.6$) results in a weaker leading shock when

applying a negative spatial gradient in fuel concentration.

In conclusion, the fuel concentration at the ignition source has the largest effect on the pressure ratio of the leading shock. In addition, it was found that a negative spatial gradient of X_{fuel} along the pre-detonation chamber can be used to achieve a strong leading shock for operation with $\varphi_{\mathrm{is}} \approx 1$. This shock is then focused due to the converging shape of the installed obstacle which potentially leads to detonation initiation. The success rate, which denotes the number of successful detonation initiations divided by the number of conducted combustion cycles, is shown in Fig. 4.14 for the five control trajectories with respect to the global equivalence ratio. Analogous to the previously presented studies, the success of detonation initiation was evaluated on the basis of the propagation velocity of the combustion front in the detonation section and the intersection of the trajectories of the leading shock and the detonation wave. More details on this procedure are given in Sec. 3.1.

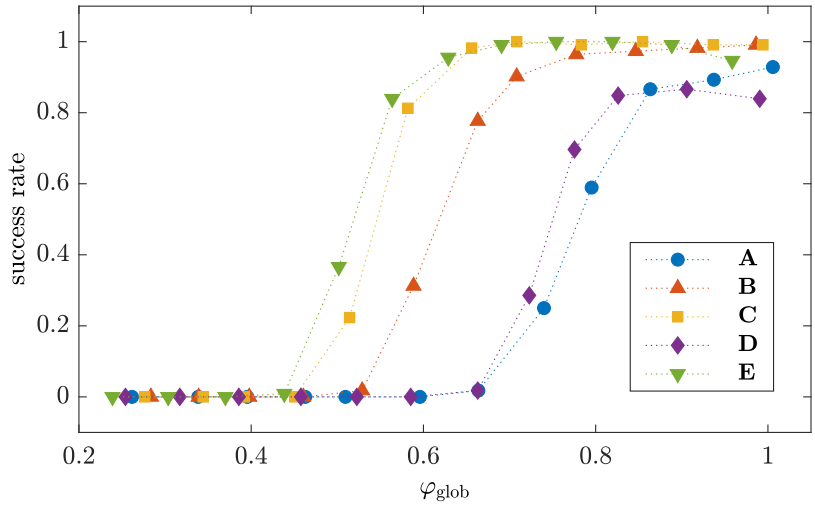

Figure 4.14: Success rate of detonation initiation by shock focusing as a function of the global equivalence ratio φ_{glob}

Without fuel stratification (trajectory **A**), almost no successful DDT is observed for $\varphi_{\mathrm{glob}} < 0.7$. When increasing the fuel concentration, the success rate increases until reliable detonation initiation is ensured for $\varphi_{\mathrm{glob}} > 0.85$. When increasing φ_{pre} while decreasing φ_{det}, as realized by applying trajectory **B**, the critical global equivalence ratio for achieving reliable detonation initiation is decreased by roughly 0.1. A larger fuel stratification (trajectory **E**) even leads to reliable DDT down to a global equivalence ratio of 0.7. This effect can be partially attributed to stronger leading shocks when increasing the fuel concentration in the pre-detonation chamber, as shown in Fig. 4.13. In addition, the increased equivalence ratio at the focal point φ_{sf} results in a larger reactivity of the fuel–oxidizer mixture, and thus, promotes detonation initiation. Comparing the obtained success rates for control trajectories **B**, **C**, and **D** reveals that a positive spatial gradient hinders reliable detonation initiation at globally lean conditions, which can also be explained by the observations for the pressure ratio across the leading shock (Fig. 4.13). For trajectories **C** and **E**, similar success rates are obtained due to comparable values of Π_{L}.

Although the data indicate that the pressure ratio across the leading shock is the main driving parameter for ensuring reliable detonation initiation, the reactivity of the mixture at the focal

point also φ_{sf} contributes to the success rate. In order to quantify this effect, the pressure ratio across the leading shock is plotted in Fig. 4.15 against the local equivalence ratio at the focal point. In Fig. 4.15 a, the cycle-averaged pressure ratio is shown for all applied trajectories. The bars again represent the standard deviation of the cycle-to-cycle variation. The shown data emphasize the findings from above, that a negative spatial gradient in the fuel concentration along the pre-detonation chamber induces an increase in Π_L. The graphs of trajectories **A**, **B**, and **E**, which result in a constant equivalence ratio throughout the pre-detonation, collapse almost perfectly to a single line.

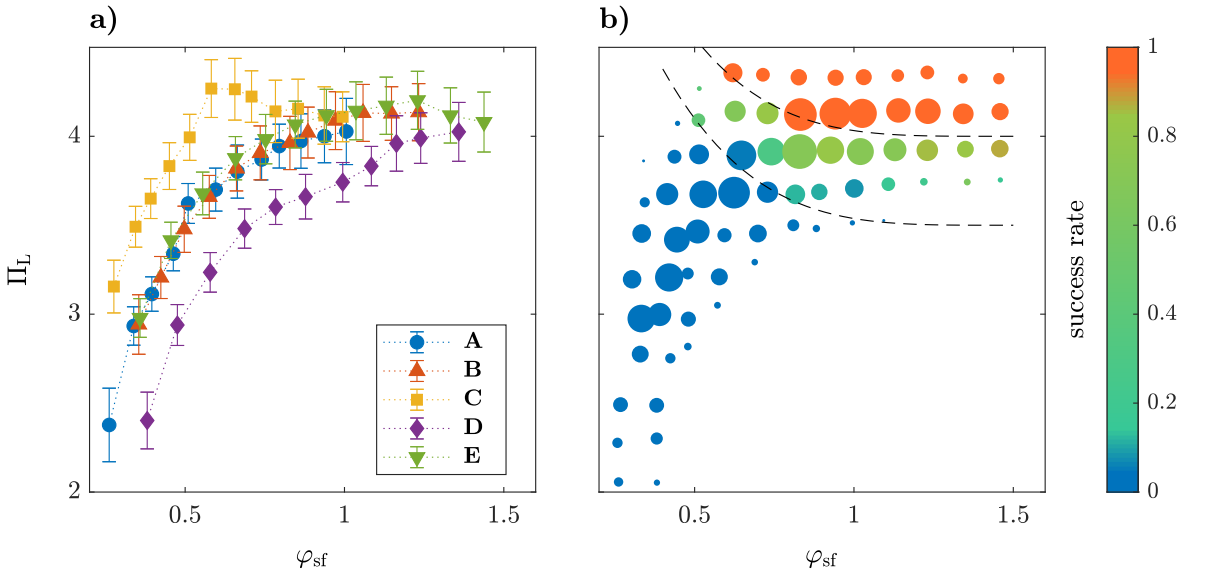

Figure 4.15: Pressure ratio across the leading shock ΠL as a function of the local equivalence ratio in the shock-focusing device φ_{sf}. The obtained data are shown for (a) the investigated injection trajectories individually and (b) with respect to the resulting success rate of detonation initiation by shock focusing.

The data shown in Fig. 4.15 b are deduced from considering all combustion cycles without differentiation between the applied control trajectories. The range of obtained values for the local equivalence ratio at the focal point and the pressure ratio are split into 15 segments, each. The data points represent the average values of all measurement data that fall in the respective segments. The color represents the success rate, while the size is a measure for the number of considered measurement cycles. It can well be seen that the pressure ratio across the leading shock is the main parameter for the determination of the success rate. Reliable successful detonations at a given value of φ_{sf} are only observed, when Π_L exceeds a certain threshold, as indicated by the upper dashed line. When decreasing φ_{sf} to lean conditions in the shock-focusing device, the required pressure ratio increases significantly indicating that detonation initiation by shock focusing under lean conditions at the focal point is extremely challenging. The presented results reveal that the reliable operation of a PDC with a shock-focusing device can be achieved when the formation of a strong leading shock and a reasonably high local equivalence ratio at the focal point are ensured simultaneously. As demonstrated by the conducted experiments with five different control trajectories, fuel stratification allows for reliable PDC operation down to a global equivalence ratio of 0.7, while $\varphi_{glob} > 0.85$ is required for constant fuel distributions along

the combustor.

4.3.4 Pollutant Emission and Combustion Efficiency

In order to evaluate the effects of both globally lean PDC operation and fuel stratification on the emission of pollutants and the combustion efficiency, the exhaust gas was analyzed in cooperation with Niclas Garan and Neda Djordjevic. Although the experimental results of NO_x concentration and remaining hydrogen in the exhaust gases have been published in [153] they contribute to the present discussion and are therefore included in this thesis. The concentration of NO_x in the exhaust gas was measured for each applied firing pattern and global equivalence ratio during the operation of the single-tube PDC at 5 Hz for 100 cycles. This measurement duration allowed the measured concentration to converge to a steady-state value. The average NO_x concentration of four repeating runs are shown in Fig. 4.16 as a function of the global equivalence ratio φ_{glob}. The measured concentration of NO_x is corrected to a reference oxygen volume fraction of 15 %. For a global equivalence ratio between 0.5 and 0.85, the measured NO_x concentration partly exceeded the maximum resolvable value of 3000 ppm. Therefore, no data could be obtained for these measurements, which leads to partly discontinuous lines.

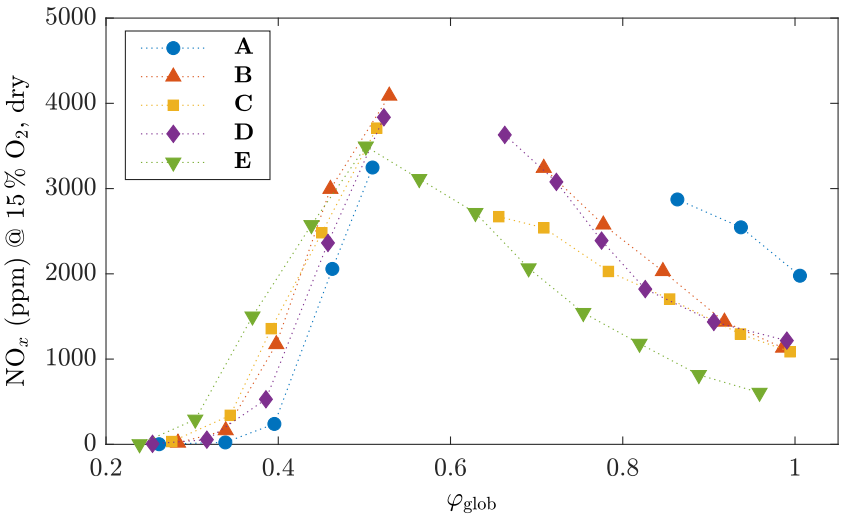

Figure 4.16: Oxygen corrected NO_x as a function of the global equivalence ratio for the investigated injection profiles (adapted from [153])

The displayed measurement results reveal a significant impact of the injection trajectory on the formation of NO_x. For a given global equivalence ratio with $\varphi_{globa} > 0.6$, the application of fuel stratification leads to a reduced NO_x concentration. By decreasing the fuel concentration in the detonation section and increasing the equivalence ratio in the pre-detonation chamber, regions of large NO_x production are avoided, which ultimately results in a lower overall NO_x concentration in the exhaust. The largest reduction of emissions was achieved by applying injection trajectory **E** that employs the greatest amount of stratification. A variation of the gradient in fuel concentration along the pre-detonation chamber was observed to only have a minor effect on the formation of NO_x.

When applying fuel stratification, partly rich mixture conditions are expected in the pre-

detonation chamber in order to maintain reliable detonation initiation. Therefore, the amount of unburnt hydrogen should be considered to evaluate the PDC performance. The average measured concentration of H_2 in the exhaust is shown in Fig. 4.17 for the five applied injection trajectories with respect to the global equivalence ratio.

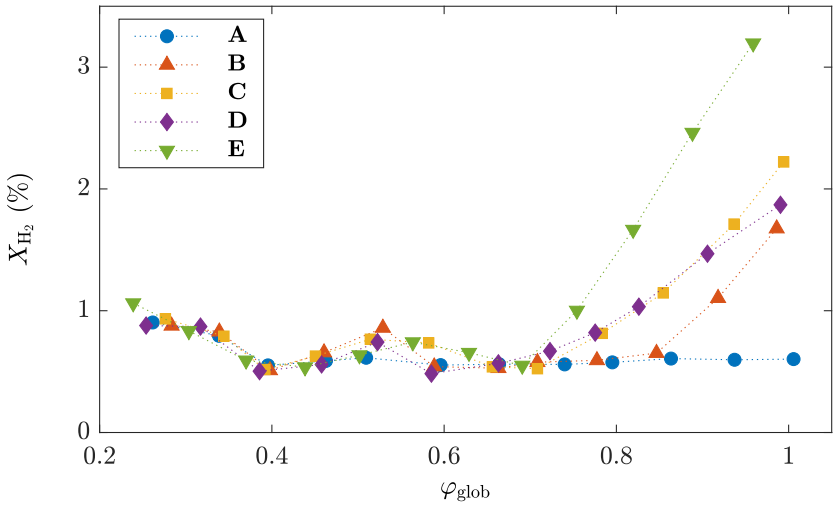

Figure 4.17: Exhaust H_2 as a function of the global equivalence ratio for investigated injection trajectories (adapted from [153])

For a constant fuel injection (trajectory **A**), nearly complete conversion of hydrogen is ensured for all conducted measurements. When applying fuel stratification, a significant increase in the H_2 concentration can be observed for rich conditions in the pre-detonation chamber. The rate of this increase over φ_{glob} is proportional to the difference between φ_{pre} and φ_{det} and is therefore the highest for trajectory **E**. The graphs of trajectories **C** and **D** nearly overlap over the entire measurement range. Slightly lower values are obtained for trajectory **B**, since the maximum fuel concentration in the pre-detonation chamber is reduced in comparison to trajectories **C** and **D**.

Combining the presented results for success rate of detonation initiation and unburnt H_2, suitable operating conditions can be found for trajectory **B** at $\varphi_{glob} \approx 0.8$ and for trajectories **C** and **E** at $\varphi_{glob} \approx 0.7$. In addition, all three parameter combinations induce a significant reduction in NO_x emission compared to the operation with a constant injected fuel flow rate, while trajectory **E** allows for the largest attenuation. When operating the PDC with pure air as oxidizer, as intended when integrating the combustor in a gas turbine, the huge kinetic impact of oxygen on the formation of NO_x decreases drastically, which is expected to result in significantly reduced pollutant emissions. Fuel stratification may then allow for a further reduction while ensuring reliable detonation initiation.

4.4 Concluding Remarks

The experimental studies presented in this chapter demonstrated the feasibility of PDC operation at gas turbine relevant conditions. In particular, the conducted investigations allow for assessing the performance of detonation initiation by shock focusing. Although the results suppose that the operation at elevated temperature and pressure conditions support the onset of a detonation

at the focal point, PDC operation at these conditions is not facilitated in general. In particular, the formation of a leading shock is hindered for certain conditions.

When increasing the initial pressure for a given Reynolds number, the pressure ratio across the leading shock is reduced based on two effects. First, the elevated initial pressure results in a decreased flame speed. Second, the turbulent fluctuations in the flow velocity are reduced. This ultimately results in smaller pressure waves being generated due to the interaction of the propagating flame front with the turbulent flow. For the operation of a PDC with hydrogen–air mixtures, it is therefore expected that the application of elevated pressure conditions hinders reliable DDT for a given Reynolds number of the flow. To assure successful detonation initiation, either the Reynolds number may be increased (e.g. by an increase in the mass flow rate) or the formation of a strong leading shock should be enhanced (e.g. by the means of additional obstacles in the pre-detonation chamber or turbulence generators). The operation of a PDC with lean hydrogen–oxygen–air mixtures is challenging since a reduced mixture reactivity hinders the formation of a strong leading shock. In this chapter, it was demonstrated that this drawback can be overcome by the application of fuel stratification. The results revealed that the strongest leading shocks were observed for a negative spatial gradient of the fuel concentration along the tube axis in the pre-detonation chamber with stoichiometric conditions close to the ignition spark. Hence, large pressure ratios can be achieved even for globally lean mixtures, which allows for reliable DDT operation at these conditions.

Despite the challenges in generating a strong leading shock, the process of detonation initiation by shock focusing is generally supported by elevated temperature and pressure conditions due to the increased mixture reactivity. Although PDC operation with the shock-focusing device could not be investigated directly at increased temperature conditions, the observed decrease in the detonation cell width for stoichiometric hydrogen–air mixtures at elevated temperature conditions indicates a significant increase in mixture reactivity. In addition, the examination of the success rate of detonation initiation by shock focusing at varying initial pressure conditions allowed for the determination of the required pressure ratio Π_{L} for reliable operation. It was found that increasing initial pressure conditions allow for the successful initiation of a detonation even for weaker leading shocks. When the oxygen enrichment is decreased, this effect is reduced. Nevertheless, it is expected that detonation initiation by shock focusing is facilitated by elevated pressure conditions for hydrogen–air mixtures compared to the operation at atmospheric pressure conditions. The evaluation of experiments with stratified fuel concentration revealed that the required pressure ratio across the leading shock to achieve reliable DDT depends on the equivalence ratio at the focal point φ_{sf}. For $\varphi_{\mathrm{sf}} > 0.8$, this critical pressure ratio was found to be nearly independent of the local equivalence ratio. For lean mixture conditions, however, the required value of Π_{L} increases drastically. Hence, a reasonably large equivalence ratio should be assured at the focal point in order to promote detonation initiation by shock focusing at globally lean conditions.

Chapter 5

Pressure Oscillations at Interfaces to Turbomachinery Components

Integrating a PDC into a conventional gas turbine poses several challenges. As discussed in the previous chapter, increased pressure and temperature with respect to atmospheric conditions affect the process of DDT, which has to be considered in the combustor design and the choice of operation parameters. Beside these aspects, the cyclic PDC process evokes fluctuating pressure conditions upstream and downstream of the combustor, which negatively influence the efficiency [114, 154] and the mechanical stress [118] of turbomachinery components. In this chapter, pressure fluctuations in the oxidizer supply are quantified and the influence of the cross section area of the oxidizer inlet is analyzed. Subsequently, acoustic pressure fluctuations in an annular plenum downstream of the multi-tube PDC are examined. By this, the boundary conditions for potentially attached turbomachinery components are characterized for the investigated PDC setup. Furthermore, possible paths towards reduced fluctuation amplitudes are proposed and evaluated experimentally. The results of this study have been partly published in [155]. The experiments, which are presented in this chapter, were all carried out on the multi-tube PDC that was introduced in Sec. 2.2. As sketched in Fig. 2.9, each PDC tube was equipped with a series of five orifice plates to achieve repeatable DDT within a reasonable run-up distance for the operation with hydrogen–air mixtures at atmospheric temperature and pressure conditions. The conducted investigations focused on the impact of variations in the operating conditions and in the geometry of the combustor inlet or the plenum outlet on pressure fluctuations upstream and downstream of the combustor. As a consequence of the observed differences in the operation characteristics for both considered DDT geometries, as presented in Sec. 3.3, the choice of the DDT geometry is expected to slightly influence the quantitative results from the studies presented in this chapter. Nevertheless, the qualitative findings and the deduced recommendations for favorable operation modes are assumed to be independent of the DDT process. Therefore, it was chosen to avoid additional efforts in terms of oxygen enrichment of the oxidizer, which would have been required for the operation with the shock-focusing device.

In a first step, conditions for stable operation of the multi-tube PDC were derived from

measurements with global equivalence ratios in the range of $0.75 < \varphi_{\mathrm{glob}} < 1.3$. As discussed in Sec. 2.2.2, the firing pattern was observed to affect the fuel supply pressure during the injection period. The recorded fluctuations in p_{fuel} are expected to result in a non-constant fuel mass flow rate during the injection period, and thus, in a non-uniform distribution of fuel concentration along the combustion tube. Since the process of DDT is highly sensitive to the reactivity of the flammable mixture, the success rate of detonation initiation, which is plotted as a function of the global equivalence ratio in Fig. 5.1, depends on the applied firing pattern. The data points represent the average success rate of all six PDC tubes, which were operated for 20 cycles each with a firing frequency of $f_{\mathrm{tube}} = 16.7\,\mathrm{Hz}$. Thus, the success rate was determined for a total number of 120 combustion events for each measurement. A continuous flow of air with $\dot{m}_{\mathrm{air}} = 720\,\mathrm{kg/h}$ was maintained, which was equally distributed to the six combustion tubes by a manifold upstream of the air plena.

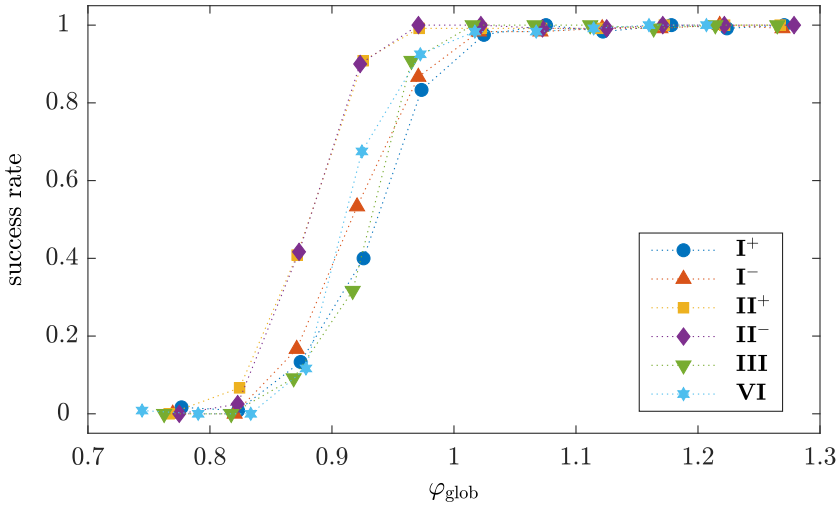

Figure 5.1: Success rate of detonation initiation as a function of the global equivalence ratio φ_{glob} for all investigated firing patterns

For very lean mixtures ($\varphi_{\mathrm{glob}} < 0.8$), no successful detonation initiation was observed for any firing pattern. When increasing the fuel concentration, successful DDT was achieved more frequently until reliable detonation initiation was obtained for rich mixtures ($\varphi_{\mathrm{glob}} > 1$). Comparing the graphs for the different firing patterns reveals that applying patterns **II**$^+$ and **II**$^-$ allows for reliable detonation initiation at slightly leaner conditions than for the other patterns. According to the findings from Sec. 2.2.2, this can be explained by the increased local fuel concentration in the range of $0.2 < x/L_{\mathrm{tube}} < 0.5$, which coincides with the expected position of DDT. Hence, the onset of the detonation is supported by a locally increased reactivity of the mixture allowing for reliable operation at lower global equivalence ratios. For all other investigated firing patterns, a nearly constant distribution in fuel concentration was obtained along the PDC tube. As a consequence the success rate with respect to the global equivalence ratio is similar for firing patterns **I**, **III**, and **VI**. For a global equivalence ratio of $\varphi_{\mathrm{glob}} = 1$, the data reveal reliable detonation initiation for all firing patterns. Thus, the operation of the multi-tube PDC with a stoichiometric hydrogen–air mixture was chosen for the experimental investigations on pressure fluctuations in the annular plenum downstream of the combustor

outlet, which are presented in Sec. 5.2. For the examination of upstream propagating pressure waves, the entire range of equivalence ratios was applied. The results of this study are discussed in the following section.

5.1 Pressure Fluctuations Upstream of a Multi-tube PDC

A systematic evaluation of the correlation between the pressure fluctuations in the oxidizer supply and the inlet geometry of the PDC tubes was realized in the scope of this thesis by conducting measurements with two different cross section areas of the air supply, i.e. $27.9\,\mathrm{mm}^2$ and $37\,\mathrm{mm}^2$), respectively. This allowed for evaluating the effect of the pressure drop of the oxidizer flow across the combustor inlet on the measured pressure amplitudes. As discussed above, pure air was used as oxidizer, which was suitable for achieving reliable detonation initiation inside the DDT section with a series of five orifice plates. In the following, pressure fluctuations in the air supply are analyzed in the air plena of the multi-tube PDC (Fig. 2.9) for all six firing patterns, which have been introduced in Fig. 2.10: $\mathbf{I}^+$, $\mathbf{I}^-$, $\mathbf{II}^+$, $\mathbf{II}^-$, **III**, and **VI**. A constant cycle duration of 60 ms for each tube was chosen, implying a firing frequency of 16.7 Hz. The injection period was set to 30 ms, which represents half of the cycle duration, and thus, a duty cycle of the fuel valves of $g_{\mathrm{inj}} = 0.5$. The measurements were conducted at ambient pressure and temperature conditions. All applied measurement parameters are summarized in Tab. 5.1.

Pressure fluctuations were measured in the air plenum of tube 1 by a piezoresistive transducer (Kulite EWCTV-312). To examine the effect of the ignition event in a single combustion tube on the pressure fluctuations in the air plena, each PDC tube was operated individually for

Configuration	
test facility	multi-tube PDC
injection geometry	choked nozzles in air supply and mixing tubes
DDT geometry	orifice plates
number of orifice plates	5
Constant parameters	
firing frequency	$f_{\mathrm{tube}} = 16.7\,\mathrm{Hz}$
injection duration	$t_{\mathrm{inj}} = \frac{1}{2}\,t_{\mathrm{cycle}} = 30\,\mathrm{ms}$
initial temperature	$T_0 = 300\,\mathrm{K}$
initial pressure	$p_0 = 1\,\mathrm{bar}$
oxidizer	air ($X_{\mathrm{O_2,ox}} = 0.21$)
Variable parameters	
firing pattern	single-tube operation, $\mathbf{I}^+$, $\mathbf{I}^-$, $\mathbf{II}^+$, $\mathbf{II}^-$, **III**, **VI**
cross section area of the choked nozzles in the air supply	$A_{\mathrm{air}} = [27.9\,\mathrm{mm}^2, 37\,\mathrm{mm}^2]$
equivalence ratio	$0.75 < \varphi < 1.3$

Table 5.1: Parameters for investigations on the pressure fluctuations in the air supply

20 cycles. The obtained cycle-averaged pressure fluctuations p'_{air} for the exclusive operation of PDC tubes 1 to 6 are shown in Fig. 5.2 a for $A_{\mathrm{air}} = 27.9\,\mathrm{mm}^2$. All signals show an increase in pressure subsequent to the ignition event triggered at $t = 34\,\mathrm{ms}$. The largest amplitude of approximately 0.6 bar was observed for the operation of tube 1. Subsequent to the first pressure peak, harmonic pressure oscillations are visible, which fade until being excited by the combustion event of the next cycle. This pressure history can be explained by acoustic waves oscillating in the oxidizer supply. For the operation of tube 2, the maximum amplitude of the measured pressure fluctuations is considerably smaller and appears 0.7 ms later than during the operation of tube 1. This time delay can be attributed to the additional propagation time of the pressure wave generated by the combustion event due to the increased distance between the location of the sensor and the position of the firing PDC tube. A similar pressure history can be observed for the operation of tube 6 due to the symmetric arrangement of the PDC tubes. Analogue statements can be used to explain the pressure signals when tubes 3 or 5 are fired. The longest delay between the ignition trigger and the detection of a pressure increase in the air plenum of tube 1 is observed for the firing of tube 4, where an additional time delay of 2.1 ms is deduced compared to the signal for the operation of tube 1.

The measured pressure histories, shown in Fig. 5.2 b, represent the pressure fluctuations during multi-tube operation. The measurement data are complemented by the superpositions of the pressure fluctuations for single-tube operation, which were calculated by

$$p'_{\mathrm{air,sup}}(t) = \sum_{k=1}^{6} p'_{\mathrm{air},k}(t - t_{\mathrm{ign},k}), \tag{5.1}$$

where $p'_{\mathrm{air},k}$ denotes the pressure fluctuations that were measured during the single-tube operation of tube k. The ignition time of each tube for the applied firing pattern with respect to the ignition of tube 1 is represented by $t_{\mathrm{ign},k}$ and can be derived from Fig. 2.10 by applying the cycle duration of $t_{\mathrm{cycle}} = 60\,\mathrm{ms}$.

The reconstructed signals agree remarkably well with the measured signals for all firing patterns, as illustrated by the congruence of both pressure histories in Fig. 5.2 b. Two conclusions can be drawn from this observation. Firstly, there exists no significant interaction between the individual PDC tubes during the multi-tube operation as the upstream propagating pressure waves from a given combustion tube are obviously not affected by the operation mode (single-tube or multi-tube) or the applied firing pattern. Secondly, the observed pressure fluctuations can be attributed to linear acoustics, which indicates that no shock waves travel upstream into the air supply. This is clearly a consequence of the small cross section area of the oxidizer supply. However, as the induced pressure loss for the used geometry exceeds acceptable values to achieve an overall gain in total pressure across the combustor, this cross section area must be increased for realistic PDC applications. Nevertheless, the experimental setup, which was considered in the scope of this thesis, allowed for the systematic examination of pressure fluctuations in the oxidizer supply with respect to the cross section area and the operating conditions. Furthermore, the elaborated methodology for reconstructing the pressure signal in the air plena for multi-tube operation allows for assessing the pressure fluctuations upstream of the combustor for an arbitrary firing pattern.

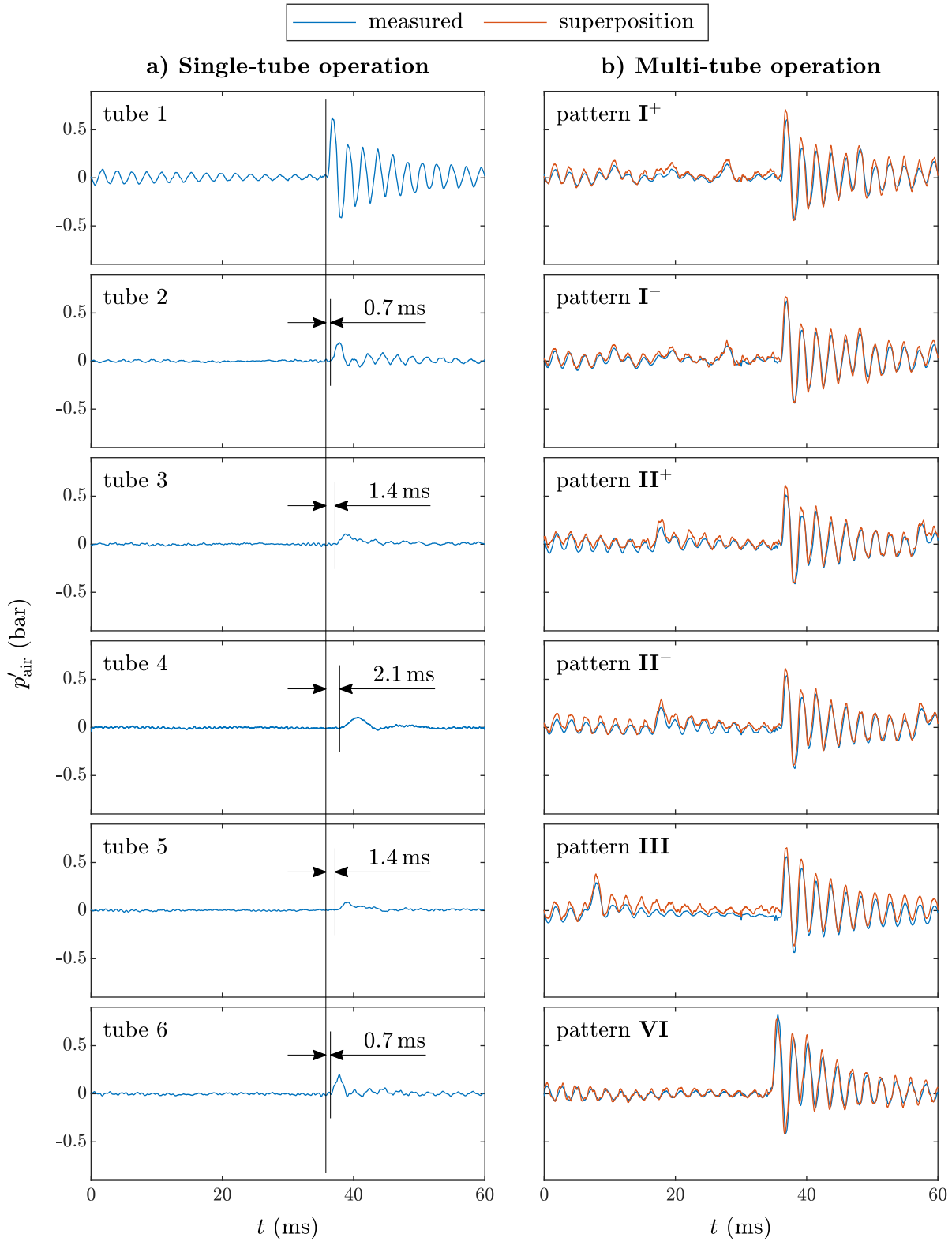

Figure 5.2: Pressure fluctuations in the air supply p'_{air} during (a) single-tube operation and (b) multi-tube operation. The measured data from multi-tube experiments are complemented by reconstructed signals from the superposition of data from single-tube operation.

To quantitatively examine the observed amplitudes in the pressure fluctuations, the cycle-averaged maximum amplitude in $p'_{\mathrm{air,max}}$ and the RMS value of the recorded pressure history $p'_{\mathrm{air,RMS}}$ are determined. The deduced values are plotted in Fig. 5.3 as a function of the global equivalence ratio φ_{glob} for all investigated firing patterns. In addition, data from experiments with an increased cross section area of the air supply of $A_{\mathrm{air}} = 37\,\mathrm{mm}^2$ are visualized.

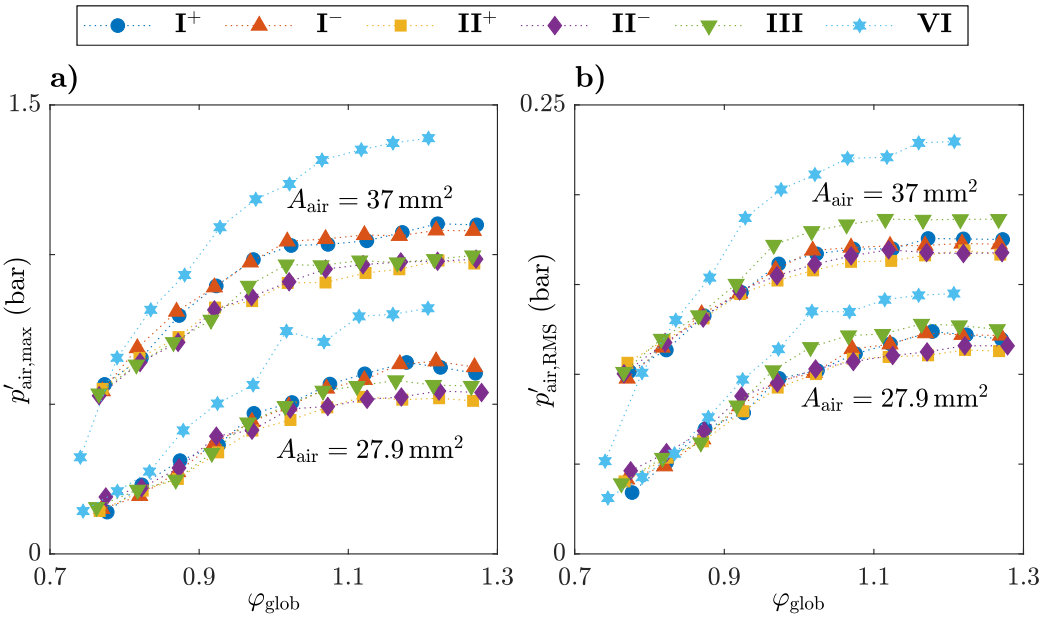

Figure 5.3: (a) Maximum amplitude and (b) RMS value of pressure fluctuations in the air plenum of tube 1 as a function of the global equivalence ratio for all investigated firing patterns and two different cross section areas of the choked nozzles in the air supply

The graphs clearly indicate that the observed pressure fluctuations in the air plenum are significantly affected by both the cross section area of the choked nozzles and the equivalence ratio. For $A_{\mathrm{air}} = 27.9\,\mathrm{mm}^2$, an increase in the equivalence ratio leads to a nearly linear increase in the maximum pressure amplitude up to slightly rich mixtures ($\varphi_{\mathrm{glob}} < 1.1$), as shown in Fig. 5.3 a. The increase in fuel concentration leads to a higher heat release rate, and thus, to stronger pressure wave generated in the combustor. Simultaneously, the RMS value increases. For larger equivalence ratios, the influence of φ_{glob} diminishes, as the gradients in $p'_{\mathrm{air,max}}$ and $p'_{\mathrm{air,RMS}}$ over φ_{glob} vanishes. When comparing the measured data for the different firing patterns, the smallest values were observed for pattern **II**. This can be explained by the reduced fuel concentration close to the ignition spark for this firing pattern due to the observed fluctuations in the fuel supply pressure, which eventually resulted in a smaller amplitudes in the shock waves propagating upstream in the air supply. The application of firing patterns **I** and **III** resulted in slightly increased values of $p'_{\mathrm{air,max}}$ for $\varphi_{\mathrm{glob}} > 1.1$. The data shown in Fig. 5.3 reveal maximum pressure fluctuations for firing pattern **VI**, which denotes the simultaneous firing of all six PDC tubes. This discrepancy to the results from the operation with the other firing patterns is especially pronounced for $\varphi_{\mathrm{glob}} > 1$, which matches the conditions for reliable detonation initiation, as shown in Fig. 5.1. These findings agree well with the observations from other experimental studies [127], and thus, underline the unsuitability of this firing pattern for the

operation of a multi-tube PDC.

Increasing the cross section area of the choked nozzles in each PDC tube to $A_{\mathrm{air}} = 37\,\mathrm{mm}^2$ resulted in a significant increase in the maximum pressure amplitude $p'_{\mathrm{air,max}}$ for all values of φ_{glob} and all firing patterns. Analogous, the increase in A_{air} also led to higher values of $p'_{\mathrm{air,RMS}}$. Thus, both the maximum pressure amplitude and the RMS value of the pressure fluctuations are positively correlated to the cross section area of the air supply. In addition, the affects of the firing pattern and the global equivalence ratio on the measured pressure fluctuations is similar for both investigated cross section areas of the air supply. The following statements can be deduced from the quantitative comparison of the measured data from experiments with differing cross section area of the air supply. Firstly, the increase of 33 % in A_{air} resulted in a rise of $p'_{\mathrm{air,RMS}}$ of similar extent for large global equivalence ratios. For smaller values of φ_{glob}, the absolute increase in the RMS value is maintained, resulting in a larger relative increase for these conditions. Secondly, the maximum pressure amplitude is almost doubled for the applied increase in cross section area for large equivalence ratios. As for the RMS value, the absolute increase in $p'_{\mathrm{air,max}}$ is constant for all applied values of φ_{glob}.

In conclusion, the pressure fluctuations in the air supply are mainly dependent on the global equivalence ratio and the cross section area. The applied firing pattern only has a minor influence, which results from spatial inhomogeneities in the fuel concentration along the combustion tube for some configurations. For firing pattern **VI**, however, considerably larger pressure fluctuations are obtained, compared to the other firing patterns, which can be explained by reduced expansion opportunities of the upstream propagating pressure waves into the neighboring air plena. For globally lean mixture conditions, the maximum pressure amplitude and the RMS value of pressure fluctuations in the air plenum increase almost linearly with increasing fuel concentration. For larger equivalence ratios, the pressure fluctuations converge to a maximum value. Increasing the cross section area of the air supply, which is required to achieve the efficient operation of a PDC-driven gas turbine, has a drastic impact on pressure waves traveling upstream. However, operation at lean mixture conditions is expected to be suitable for reducing the pressure fluctuations in order to achieve acceptable values for the operation of an upstream attached compressor. Moreover, identifying the best firing pattern to minimize pressure fluctuations upstream of the combustor is an important challenge in order to ensure safe operation of the hybrid compressor–PDC system. The results, which were presented in this section, suggest that best conditions can be found for the simultaneous firing of two opposed PDC tubes. However, the operation with a sequential firing pattern or the alternate firing of three simultaneously operated tubes resulted in only marginally increased pressure amplitudes, respectively.

5.2 Pressure Fluctuations Downstream of a Multi-tube PDC

Although considerable pressure fluctuations were observed upstream of PDCs, most published studies on the interaction with turbomachinery components focused on the effect of pressure waves on the turbine performance [115, 116, 117]. When the propagating detonation waves reach the combustor exit, strong shock waves are emitted [156], which largely affect the flow conditions at the turbine inlet. As discussed in Sec. 1.3.2, reducing these fluctuations is crucial to achieve efficient turbine operation. Rezay Haghdoost et al. [74] reported a significant reduction of the

shock amplitude by the integration of an annular plenum downstream of the multi-tube PDC. Measurements in the scope of this thesis, however, revealed that the operation of the multi-tube PDC evoked additional acoustic pressure oscillations in the annular plenum, which are evaluated in this section. The cycle-averaged pressure fluctuations $p'_{55}(t)$ at the outer wall of the annular plenum are shown in Fig. 5.4. The shown pressure history was recorded by sensor P_{55}, which was installed downstream of PDC tube 5. The naming convention of the combustion tubes is given in Fig. 2.10. For the considered measurement, the multi-tube PDC was operated with firing pattern $\mathbf{I}^+$ and a firing frequency of $f_{\text{tube}} = 16.7\,\text{Hz}$, while providing a stoichiometric hydrogen–air mixture at a continuous air mass flow rate of 900 kg/h. In this measurement, the tubes were fired sequentially with a time delay of 10 ms between two combustion events, starting with tube 1 at $t = 0\,\text{ms}$.

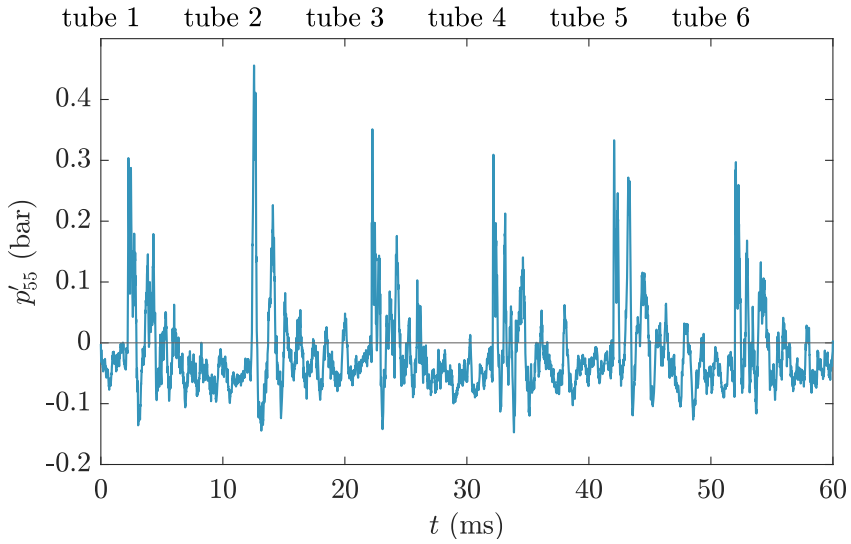

Figure 5.4: Cycle-averaged signal of pressure fluctuations p' in the annular plenum downstream of tube 5 (sensor P_{55}) for firing pattern $\mathbf{I}^+$. The labels above the figure indicate the ignition times of the PDC tubes.

The propagating shocks from the combustor exit are visible as sharp peaks in the pressure history. The largest pressure amplitude of roughly 0.45 bar is observed subsequent to the firing of tube 2. When firing the other PDC tubes, pressure peaks of approximately 0.3 bar are recorded. As discussed in Sec. 1.3.2, these peaks have been observed by other research groups [74, 121, 122]. Results of their investigations suggest a potential for substantial reduction of the peak amplitude by proper adjustment of the firing pattern, the firing frequency and the integration of a plenum between the combustor exit and the turbine inlet. However, the recorded pressure history shown in Fig. 5.4 reveal pressure fluctuations with significant amplitude for the entire operation duration, which cannot be attributed completely to propagating shock waves exiting the PDC tubes. Since conventional turbines are designed for steady-state inflow conditions, the observed fluctuations are expected to have a considerable impact on the performance of turbine operation. The aim of the conducted investigations is to shed some light on the excitation of these pressure oscillations in the plenum and how they are affected by operation parameters of the multi-tube PDC. For this, measured pressure signals at the outer plenum wall are examined by azimuthal frequency

decomposition, which allows for accounting the observed oscillations to their respective azimuthal mode number. In addition, acoustic eigenmodes and eigenfrequencies of the annular plenum are calculated numerically and compared to measurement results. Finally, a measure for the acoustic energy is determined and evaluated with respect to the firing pattern, firing frequency, and the blockage ratio of the plenum outlet.

5.2.1 Measurement Procedure

The measurements were conducted on the multi-tube PDC test rig, introduced in Sec. 2.2. The annular plenum with an axial length of $L = 0.5\,\mathrm{m}$ was instrumented with 13 piezoelectric pressure sensors, allowing for measuring pressure fluctuations at the outer wall at various axial and circumferential positions. A sketch of the test facility including the sensor positions is given in Fig. 5.5. In the following, the plotted cylindrical coordinate system will be used with $x = 0$ at the plenum inlet plane. The azimuthal position of PDC tube j is given by θ_j with $\theta_5 = 0$.

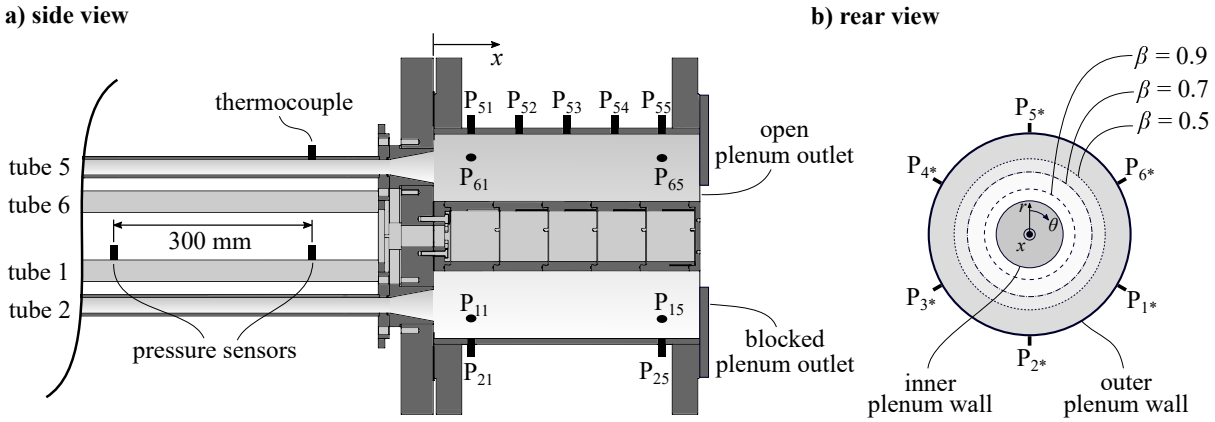

Figure 5.5: Sketch of the measurement setup for investigations on pressure fluctuations in the annular plenum downstream of the multi-tube PDC. (a) The axial position of the installed sensors are depicted in a side view of a cross section of the downstream part of the test rig. (b) The azimuthal sensor positions and an illustration of the applied outlet blockages is given by a rear view perspective of the annular plenum.

Two pressure sensors in PDC tube 1 with an axial distance of 300 mm allowed for the detection of the propagating detonation waves. The time-averaged gas temperature upstream of the combustor outlet was deduced from the signal of a sheathed thermocouple in tube 5. Downstream of each PDC tube, two pressure sensors were flush mounted to the plenum outer wall at $x/L = 0.14$ and $x/L = 0.86$, respectively. At the azimuthal position of tube 5, three additional sensors were installed for equidistant evaluation of pressure fluctuations at $\theta = 0$. Blockage plates with varying inner diameter were applied to the plenum outlet to allow for a modification of the acoustic boundary conditions. As illustrated in Fig. 5.5 b, this resulted in four blockage ratios: 0, 0.5, 0.7, and 0.9. Pressure fluctuations in the plenum were recorded for the operation with firing patterns $\mathbf{I}^+$, $\mathbf{II}^+$, **III**, and **VI**. For all conducted measurements, air was used as oxidizer at a continuous mass flow rate of 900 kg/h, which was equally distributed to the six PDC tubes through a manifold upstream of the air plena. This increased mass flow rate in comparison to the measurements of pressure fluctuations upstream of the PDC (Sec. 5.1) was chosen to allow

for experiments at elevated firing frequencies due to a smaller required injection duration. As the amount of injected fuel is expected to have a considerable impact on the amplitude of pressure fluctuations in the annular plenum, it was varied by means of two operation parameters. On the one hand, two different equivalence ratios, i.e. $\varphi = 0.8$ and $\varphi = 1$, were applied by adjusting the fuel supply pressure during the injection period. This procedure resulted in a Reynolds number of the injected mixture flow of $7.37 \cdot 10^4$ and $7.44 \cdot 10^4$ for lean and stoichiometric mixture compositions, respectively. On the other hand, the injection duration was varied to realize the operation with two different fill fractions ξ of the PDC tubes, which represents the fraction of the combustor length that is filled with a fuel–air mixture. The firing frequency f_{tube} was varied from 11.1 Hz to 33.3 Hz, which induced a duty cycle of the fuel injection valves between 0.23 and 0.7. A summary of all measurement settings is given in Tab. 5.2.

Configuration	
test facility	multi-tube PDC
injection geometry	choked nozzles in air supply and mixing tubes
DDT geometry	orifice plates
number of orifice plates	5
Constant parameters	
initial temperature	$T_0 = 300\,\mathrm{K}$
initial pressure	$p_0 = 1\,\mathrm{bar}$
oxidizer	air ($X_{\mathrm{O_2,ox}} = 0.21$)
Variable parameters	
firing frequency	$11.1\,\mathrm{Hz} < f_{\mathrm{tube}} < 33.3\,\mathrm{Hz}$
fill fraction	$\xi = [0.8, 1]$
global equivalence ratio	$\varphi = [0.8, 1]$
firing pattern	**I$^+$**, **II$^+$**, **III**, **VI**
plenum outlet blockage ratio	$\beta = [0, 0.5, 0.7, 0.9]$

Table 5.2: Parameters for investigations on pressure fluctuations in the annular plenum downstream of the multi-tube PDC

5.2.2 Determination of Suitable Injection Durations

In order to find adequate injection durations to achieve the desired fill fractions of 0.8 and 1, the propagation velocity of the shock front in PDC tube 1 normalized by the respective CJ velocity was examined for all investigated firing patterns. The cycle-averaged results are visualized in Fig. 5.6 with respect to the injection duration t_{inj} for both applied equivalence ratios. For all firing patterns and both values of φ, the velocity u_{det} monotonically increases with increasing injection duration. For the largest applied value ($t_{\mathrm{inj}} = 21\,\mathrm{ms}$), the measured propagation velocity of the shock front nearly matches the CJ velocity. Thus, propagating detonations are observed for these conditions. The decrease in the measured velocity when reducing t_{inj}, however, does not indicate a reduction in the DDT success rate, but can rather be explained by a smaller

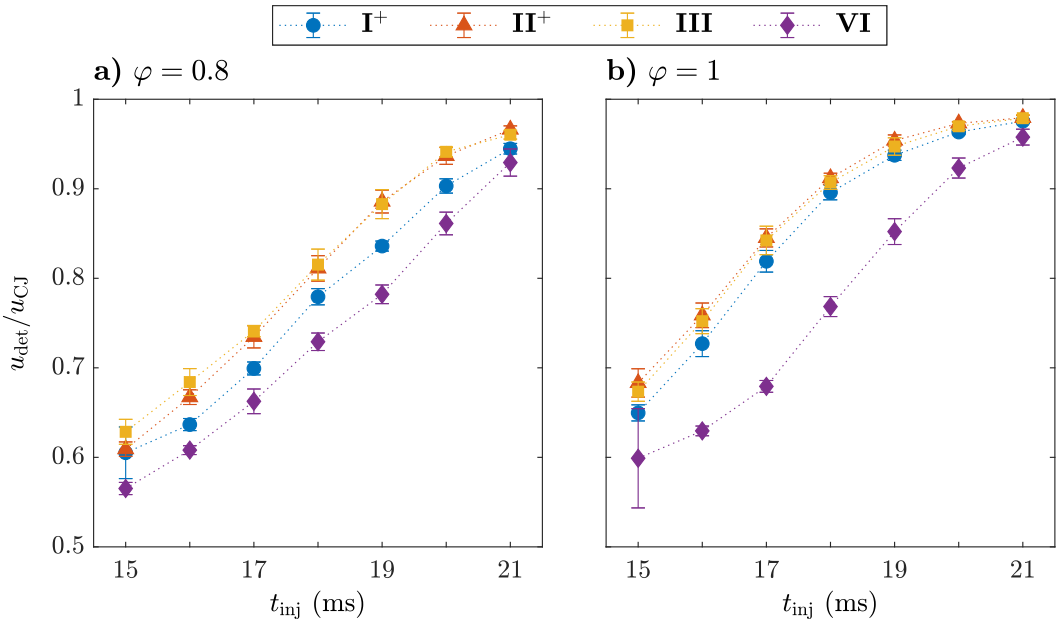

Figure 5.6: Shock velocity normalized by the respective CJ velocity as a function of the injection period t_{inj} for (a) $\varphi = 0.8$ and (b) $\varphi = 1$

fill fraction ξ of the PDC tube. When a propagating detonation, which was initiated in the DDT section, reaches the end of the injected fuel–air package, a shock with gradually decreasing strength propagates further downstream into the previously injected air buffer. Hence, the propagation velocity obtained from the time-of-flight between the two pressure sensors in PDC tube 1 decreases when reducing the injection duration. The small standard deviations of the cycle-to-cycle variation, that is represented by the bars, indicate repeatable propagation velocities of the shock front in the PDC tube. As this value is closely linked to the fill fraction of the PDC tube, the measurement results suggest a reproducible mixture injection for all applied conditions. Taking a closer look at the results reveals that the firing pattern also has an impact on the measured shock velocity. The smallest CJ fraction was observed for pattern **VI**. For patterns **II**$^+$ and **III**, the highest propagation velocity was detected. As discussed in Sec. 2.2.2, the simultaneous firing of all PDC tubes resulted in a reduced global equivalence ratio. This induces a slightly lower flow velocity, and thus, a reduced length of the tube to be filled with flammable mixture than for the other firing patterns. Therefore, the obtained values of $u_{\mathrm{det}}/u_{\mathrm{CJ}}$ in Fig. 5.6 are the lowest for firing pattern **VI**. However, an injection duration of $t_{\mathrm{inj}} = 21\,\mathrm{ms}$ resulted in $u_{\mathrm{det}}/u_{\mathrm{CJ}} > 0.9$ for all applied firing patterns and both equivalence ratios, which indicates an almost completely filled PDC tube. Therefore, $t_{\mathrm{inj}} = 21\,\mathrm{ms}$ is considered as reference case in this study. Increasing the injection duration above 21 ms was avoided for safety reasons in order to ensure that no flammable mixture could accumulate in the plenum. Based on these considerations, the fill fraction is defined by

$$\xi = \frac{t_{\mathrm{inj}}}{21\,\mathrm{ms}}. \tag{5.2}$$

The evaluation of pressure fluctuations in the annular plenum was conducted for two different injection durations, i.e. 17 and 21 ms, which induced fill fractions of 0.8 and 1.

5.2.3 Prediction of Acoustic Eigenmodes in the Annular Plenum

Numerical solutions of the acoustic Helmholtz equation were calculated based on the considerations presented in Sec. 2.4. The results of these calculations are used in the following section to support the interpretation of the measured pressure fluctuations in the annular plenum. In particular, the measurement data are subdivided with respect to the shapes and frequencies of the acoustic eigenmodes. The predicted mode shapes $\Psi_{l,m}$ are illustrated in Fig. 5.7 for axial mode numbers $l \in [0, 1, 2]$ and azimuthal mode numbers $m \in [0, 1, 2, 3]$ for two different blockage ratios ($\beta = 0.9$ and $\beta = 0.5$). The geometries of the plenum with these two outlet blockages are visualized in Fig. 5.7 a and Fig. 5.7 f, respectively. A smaller blockage ratio results from an increase in the inner diameter of the installed blockage plate, as visualized in Fig. 5.5 b. The spatial distributions of the absolute value of $\Psi_{l,m}$ are shown below in Fig. 5.7 b – e ($\beta = 0.9$) and Fig. 5.7 g – j ($\beta = 0.9$). Red colored areas indicate high amplitudes of pressure oscillations, while pressure nodes are visualized by blue color. The blue circular area at the front plane, which can be observed in all eigenmodes, represents the open outlet of the plenum, were a sound soft acoustic boundary condition was applied for the numerical calculations. In addition, the calculated eigenfrequencies $f_{l,m}$ are given for all considered axial and azimuthal mode numbers.

It can well be seen that the axial mode number l determines the number of pressure nodes along the axial dimension x at the outer plenum wall for $\theta = 0$. Along the circumference, the number of pressure nodes is twice the value of the azimuthal mode number m (only half are visible in Fig. 5.7). As expected, an increased open outlet area results in a larger area with $p' = 0$ at the outlet plane of the plenum. Besides, a smaller blockage ratio evokes a decreased wave length of $\Psi_{l,m}$ along the tube axis at the outer wall, which leads to an increase in the associated eigenfrequencies $f_{l,m}$ for given values of l and m.

5.2.4 Evaluation of Acoustic Pressure Oscillations

As a periodic signal with a period equal to the cycle duration $t_{\mathrm{cycle}} = 1/f_{\mathrm{tube}}$, the pressure fluctuations p' in the plenum can be written as a superposition of harmonically oscillating signals. In addition, the spatially distributed pressure sensors allow for a decomposition of p' in azimuthal modes. Combining spatial and temporal decomposition, as done by von Saldern et al. [157], allows for expressing the pressure signal at a given axial position as a function of the azimuthal position θ and time t through

$$p'(\theta, t) = \Re\left(\sum_{m=-\infty}^{\infty} \int_{-\infty}^{\infty} \hat{p}_m(\omega)\, e^{i(\omega t - m\theta)} \mathrm{d}\omega\right), \tag{5.3}$$

where m is the azimuthal mode order and ω the angular frequency. As the azimuthal mode shapes have to fulfill periodic boundary conditions, only integer values of m are relevant. In contrast, ω may be any real number. The spectra $\hat{p}_m(f)$ with $\omega = 2\pi f$ represent the amplitude of acoustic pressure oscillations as a function of the oscillation frequency for the respective azimuthal mode number m.

The values of $\hat{p}$ are calculated from the recorded pressure signals by two sequentially performed discrete Fourier transforms (FTs), first in azimuthal direction and then in time. Based on

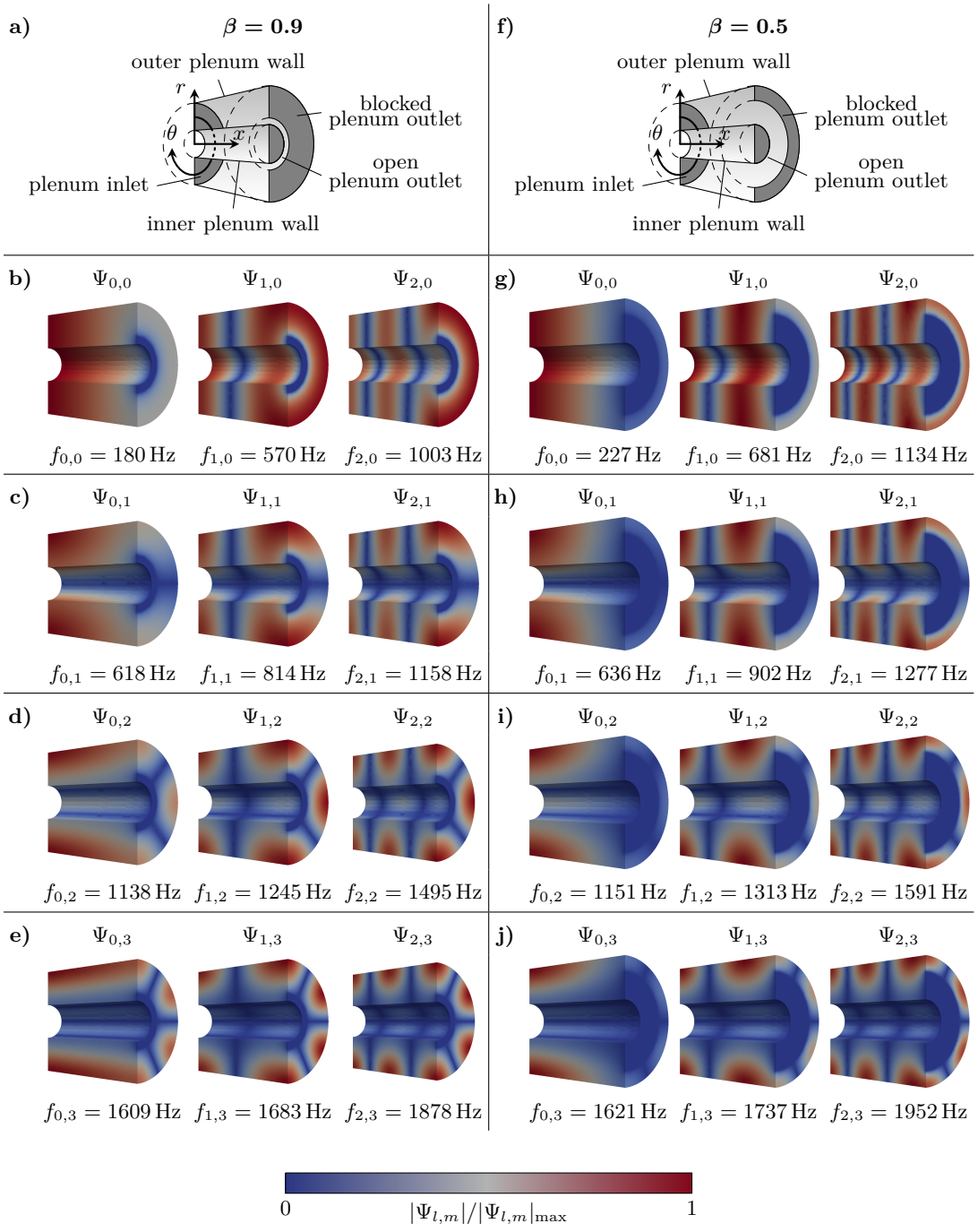

Figure 5.7: Predicted acoustic eigenmodes $\Psi_{l,m}$ and respective eigenfrequencies $f_{l,m}$ for blockage ratios (a–e) $\beta = 0.9$ and (f–j) $\beta = 0.5$. Pressure nodes are visualized by blue color, while red areas represent high amplitudes in pressure oscillation.

the sampling rate of $f_\mathrm{s} = 1\,\mathrm{MHz}$ and the known firing frequency, the obtained spectra cover oscillation frequencies up to a maximum of $f_\mathrm{s}/2 = 500\,\mathrm{kHz}$ with a resolution of $\mathrm{d}f = f_\mathrm{s}/N_\mathrm{s}$, with the total number of samples N_s. As a number of 20 combustion cycles was recorded for each measurement, $N_\mathrm{s} = 20 f_\mathrm{s}/f_\mathrm{tube}$ holds. Thus, the resolution of the spectra can be determined as $\mathrm{d}f = f_\mathrm{tube}/20$. Similar considerations can be performed for the spatial resolution in azimuthal direction. In this work, pressure sensors were installed at six azimuthal positions θ_j downstream of the six circumferentially arranged PDC tubes. For the normalized azimuthal coordinate $\theta/2\pi$ a resolution of $\mathrm{d}m = 1$ and a maximum resolved mode number of 3 are deduced. This allows for the calculation of $\hat{p}_m$ with $m \in [-2, -1, 0, +1, +2, 3]$.

Analogue to the predicted eigenmodes, shown in Fig. 5.7, $m = 0$ denotes acoustic modes with constant amplitude along the circumference. For $m \neq 0$, the obtained spectra consider pressure oscillations with $2|m|$ pressure nodes in azimuthal direction. The decomposition in azimuthal modes allow for the definition of spinning and standing modes. When a spinning mode is established, the pressure nodes move in azimuthal direction with the angular frequency ω. A positive value of m denotes a spinning mode in positive azimuthal direction with respect to θ, while an opposite rotation direction is indicated by $m < 0$. The occurrence of two spinning modes with azimuthal order $+/-m$ and equal amplitudes result in a standing oscillation pattern, which is defined by constant positions of the pressure nodes over time. Due to the number of installed sensors, acoustic modes with $|m| > 3$ cannot be resolved and are captured by spectra with lower azimuthal mode number due to aliasing. However, only acoustic modes with $|m| \leq 3$ are expected as a result of the symmetry of the can-annular configuration of PDC multitube and annular plenum. Moreover, only insignificant amplitudes in the spectra $\hat{p}_m(f)$ were obtained in the range of frequencies that correspond to the predicted eigenfrequencies for larger absolute values of m. Thus, the number of installed pressure sensors along the circumference of the annular plenum is sufficient to allow for the examination of acoustic modes.

The spectra obtained by azimuthal frequency decomposition are discussed in the following for a reference case, that is defined by the operation of the multi-tube PDC with firing pattern $\mathbf{I}^+$, a firing frequency of $f_\mathrm{tube} = 16.7\,\mathrm{Hz}$, an injection duration of $t_\mathrm{inj} = 21\,\mathrm{ms}$, and an equivalence ratio of $\varphi = 1$. Analogous to the predicted acoustic modes (Fig. 5.7), the spectra $\hat{p}_m$ are shown in Fig. 5.8 for blockage ratios of 0.9 (a–f) and 0.5 (g–l), respectively. The plotted data represent the power spectral density (PSD) of $\hat{p}_m$ as a function of the oscillation frequency f. The values of the PSD are calculated by

$$\mathrm{PSD}_m(f) = \frac{1}{t_\mathrm{meas} f_\mathrm{s}^2} |\hat{p}_m^2(f)| \tag{5.4}$$

with the measurement duration $t_\mathrm{meas} = 20/f_\mathrm{tube}$ and the sampling frequency $f_\mathrm{s} = 1\,\mathrm{MHz}$. This presentation of the spectra obtained by azimuthal frequency decomposition was chosen in order to illustrate the distribution of energy, which is contained by pressure oscillations, with respect to the oscillation frequency. To allow for comparison of the peaks in the obtained spectra with the numerical results in Fig. 5.7, the predicted eigenfrequencies $f_{l,m}$ are visualized above each spectrum. As the examination of pressure fluctuations in the annular plenum in the scope of this thesis focus on acoustic oscillations, the obtained spectra are evaluated for frequencies with

$f > f_0$. The smallest considered frequency is defined as

$$f_0 = f_{\text{eff}} + \frac{1}{2} f_{\text{tube}}. \tag{5.5}$$

By this, pressure fluctuations due to the shock waves, which are periodically emitted from the PDC tubes, are ignored while the amplitudes in PSD_m due to acoustic pressure oscillations remain unchanged. A comparison of the integral values of the spectra with and without neglecting frequencies smaller than f_0 revealed, that acoustic pressure oscillations with $f > f_0$ contain up to 50 % of the total energy of pressure fluctuations in the annular plenum, which emphasizes the relevance of this topic.

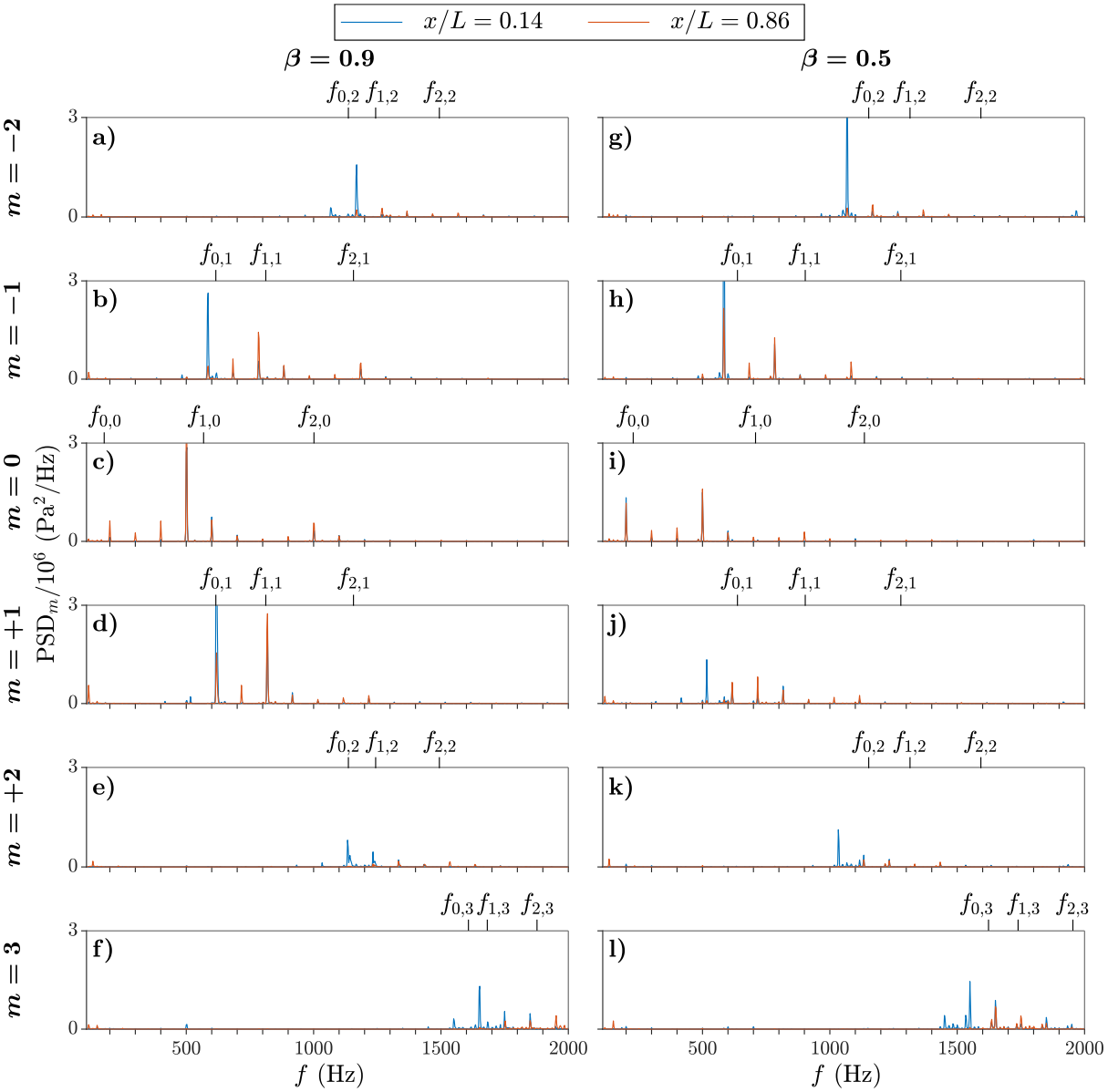

Figure 5.8: PSD of spectra $\hat{p}_m$ obtained by azimuthal frequency decomposition for firing pattern $\mathbf{I}^+$ and $f_{\text{tube}} = 16.7\,\text{Hz}$ at two axial positions for (a–f) $\beta = 0.9$ and (g–l) $\beta = 0.5$. The predicted acoustic eigenfrequencies $f_{l,m}$ are marked above each spectrum.

All presented spectra show multiple peaks. Thus, the operation of the multi-tube PDC leads to the excitation of multiple acoustic modes in the annular plenum. For a blockage ratio of $\beta = 0.9$ and an azimuthal mode number of $m = 0$ (Fig. 5.8 c), peaks are observed at multiples of the effective firing frequency ($f_{\mathrm{peak}} = k f_{\mathrm{eff}}$ with $k \in \mathbb{N}$). The largest amplitude is visible at 500 Hz, which is close to the predicted eigenfrequency $f_{1,0}$. Additionally, large peaks are visible for 200 and 1000 Hz, which are close to the values of $f_{0,0}$ and $f_{2,0}$, respectively. For $m = +1$ (Fig. 5.8 d), peaks are visible at frequencies of 616.7 and 816.7 Hz. Analogous to the findings for $m = 0$, these frequencies are located close to the predicted predicted eigenfrequencies $f_{l,1}$. For $m = -1$ (Fig. 5.8 b), the largest amplitudes are found at 583.3 and 783.3 Hz. The correlation between the firing frequency and the peaks in $\hat{p}_m$ for $\beta = 0.9$ can also be used to explain the peaks for $m = \pm 2$ and $m = 3$. In conclusion, all dominant peak frequencies are closely linked to the frequencies of the predicted acoustic eigenmodes of the annular plenum. Nevertheless, the observed peak frequencies f_{peak} in the PSDs do not exactly match the eigenfrequencies. Rather, the values of f_{peak} are defined by the effective firing frequency and the applied firing pattern by

$$f_{\mathrm{peak}} = \left(k + \frac{m}{N}\right) f_{\mathrm{eff}}, \; k \in \mathbb{N} \tag{5.6}$$

with the total number of PDC tubes N. This results in spinning modes where the azimuthal position of pressure maxima match the location of the firing PDC tubes, which results in an excitation of the respective mode by the pressure pulse exiting the combustor. In particular, for firing pattern $\mathbf{I}^{+}$ and $m = +1$, peak frequencies are obtained for $f_{\mathrm{peak}} = (k + 1/6) f_{\mathrm{eff}}$. When considering a spinning mode with maxima in the azimuthal pressure distribution at $\theta = 0$ (and a minimum at $\theta = 2\pi$) for $t = 0$, the azimuthal position of the maximum matches the position of PDC tube 1 that fires at this time. In the time period until the firing of tube 2, the mode rotates by an angle of $\Delta\theta = (k + 1/6)2\pi$, which results in the congruence of the pressure maximum and PDC tube 2. Therefore, acoustic modes with f matching one of the peak frequencies from Eq. 5.6 are potentially amplified, while modes with other oscillation frequencies are suppressed. This mechanism eventually leads to the distinct peaks at f_{peak}, shown in the PSDs in Fig. 5.8. The amplitude of the peaks are clearly affected by the distance to the nearest acoustic eigenfrequency. Large amplitudes are observed, when the difference between f_{peak} and the nearest value of $f_{l,m}$ is small. For oscillation frequencies far off the predicted eigenfrequencies, only insignificant pressure amplitudes are obtained. Nevertheless, other parameters might as well impact the peak amplitude, e.g. the axial distribution of the respective mode shape $\Psi_{l,m}$ and damping mechanisms due to the interaction of the modes with the mean flow field and the applied acoustic boundary conditions.

When the blockage ratio is decreased to $\beta = 0.5$ (Fig. 5.8 g–l), the peaks in PSD_m still follow the regularity from Eq. 5.6. Similar to the findings for $\beta = 0.9$, a clear correlation between the predicted eigenfrequencies $f_{l,m}$ and the amplitude of the peaks can be seen. However, the congruence of the peaks in $\hat{p}_m$ and the predicted eigenfrequencies is slightly reduced. This increased deviation may be due to a mismatch of the actual temperature inside the plenum and the assumed constant temperature of $T = 550$ K. In addition, the reduced outlet blockage increases the area of the open plenum outlet, and thus, promotes the effect of a potentially incorrect boundary conditions in the calculations ($p' = 0$), when compared to the actual conditions

in the experiments. Nevertheless, the distinct peaks in the spectra obtained from azimuthal frequency decomposition indicate that numerous acoustic modes are excited by PDC operation for both evaluated blockage ratios.

To further investigate the correlation between the measured pressure oscillations and the acoustic eigenmodes, the oscillation amplitudes of the measured pressure fluctuations are evaluated at various axial position and compared against the predicted mode shapes. For this, the recorded pressure signals downstream of PDC tube 5 are Fourier transformed. The amplitudes of the obtained spectra at various frequencies are plotted against the axial position of the sensors in Fig. 5.9. The chosen frequencies correspond to the peaks in the spectra of $\hat{p}_m$ for $m = [-1, 0, +1]$. For these values of m, several distinct peaks are visible in the spectra shown in Fig. 5.8. For higher absolute values of m, less dominant peaks are observed, which indicates that acoustic modes with large values of both mode numbers (l and m) do not contribute significantly to pressure fluctuations in the plenum. The following evaluation of the axial distribution of pressure oscillation amplitudes is therefore limited to $l \leq 2$ and $|m| \leq 1$. The data points are accomplished by the spatial distribution of the absolute value of the predicted eigenmodes $\Psi_{l,m}$ at $\theta = 0$ and $r = r_o$ with respect to the axial position x normalized by the total length of the plenum L. Both data sets are normalized by their respective maximum values.

The first longitudinal mode ($l = 0$) is examined in Fig. 5.9 a for a blockage ratio of 0.9. The frequencies 200, 583.3, and 616.7 Hz were chosen based on the peaks close to the predicted eigenfrequencies $f_{0,m}$ in the PSDs for $m = 0$, -1, and $+1$, respectively. The obtained amplitudes of pressure oscillations decrease monotonically from the inlet to the outlet of plenum for all three frequencies. Hence, the data clearly suggest that the observed pressure oscillations in the plenum are linked to the shape of the predicted eigenmodes. However, the measured amplitudes do not perfectly match the predictions. In particular, the amplitude of the 200 Hz oscillations at $x/L = 0.14$ is considerably smaller than expected. This data point deviates from the monotonic decrease in amplitude over x, which is observed for all other points. This is most likely a result of the measured pressure oscillation at this frequency to be composed of two elements. On the one hand, the pressure oscillations at the plenum wall occur due to the excitation of the acoustic eigenmode $\Psi_{0,0}$. On the other hand, considerable pressure amplitudes most likely emerge from higher harmonic oscillations of the effective firing frequency of $f_{\text{eff}} = 100$ Hz. The effective firing frequency describes the succession of pressure waves entering the plenum. However, as the multi-tube PDC was operated with firing pattern $\mathbf{I}^+$, the pressure amplitude due the shock waves alternate, as shown in Fig. 5.4. In particular, this statement holds close to the plenum inlet. As the shock waves propagate in both axial and circumferential direction, the differences in the shock amplitudes diminish towards the plenum outlet. As a consequence, the amplitude of 200 Hz oscillations at $x/L = 0.14$ deviates from the predicted mode shape $\Psi_{0,0}$. In Fig. 5.9 b, the axial distribution of pressure oscillation amplitudes were examined at 500, 783.3, and 816.7 Hz. At these frequencies, local maxima in PSD_m were observed close to the predicted eigenfrequencies $f_{1,m}$. The axial distributions of the absolute value of both $\Psi_{1,0}$ and $\Psi_{1,1}$ contain a pressure node at $x/L \approx 0.4$ and two maxima in pressure amplitude close to the inlet and exit of the plenum, respectively. Overall, the measurement data qualitatively agree well with the predictions. Nevertheless, minor deviations between the data series for the three chosen frequencies are visible. This may indicate slight deviations in the mode shapes between experiments and numerical

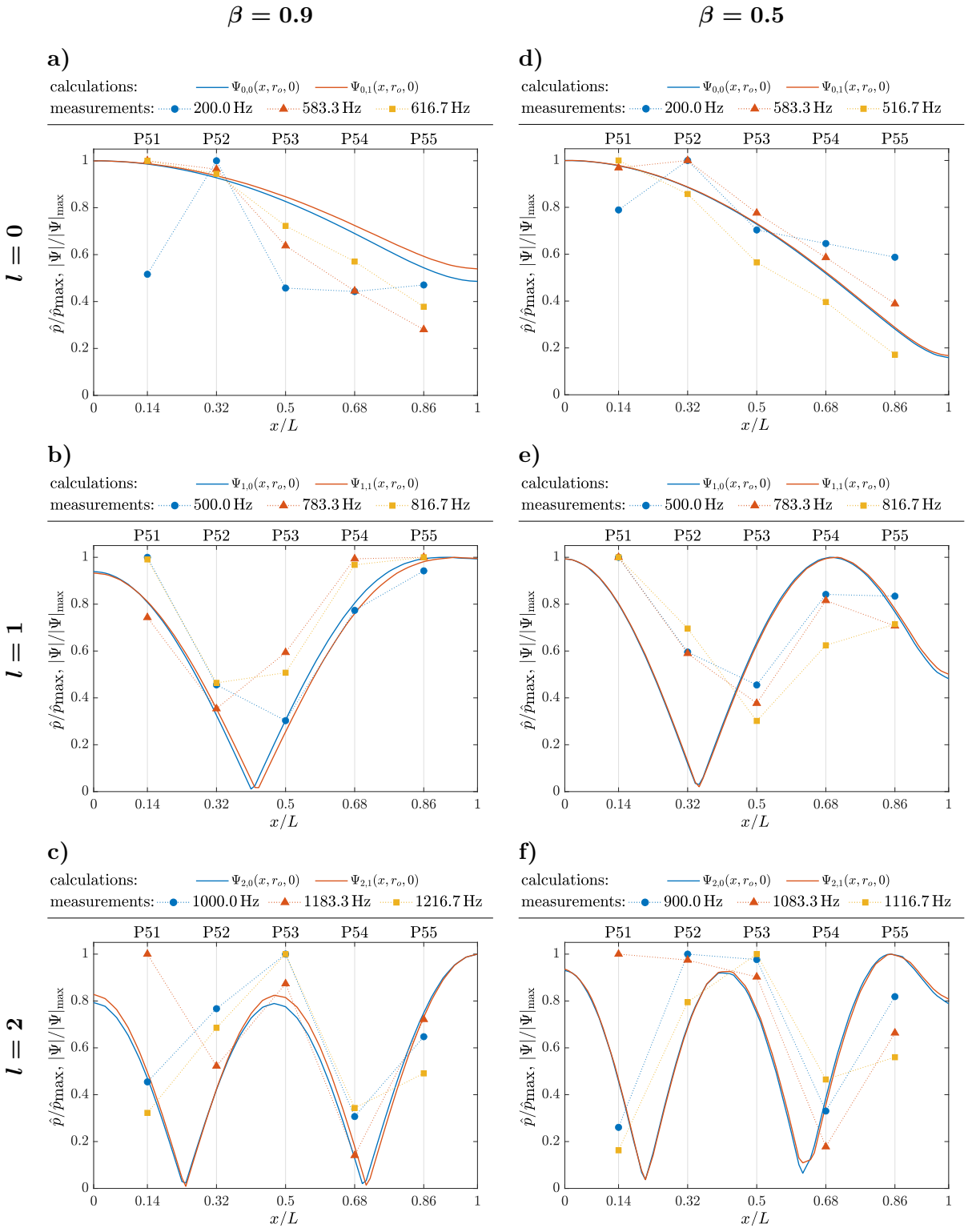

Figure 5.9: Shape of predicted eigenmodes compared against amplitudes of pressure oscillations at different axial locations.

predictions, which can be explained by small differences in the considered oscillation frequencies. However, the qualitatively good congruence of the measurement data with the axial distributions of $\Psi_{1,m}$ support the conclusion that the pressure oscillations at 500, 783.3, and 816.7 Hz represent excited acoustic modes with one pressure node along the plenum axis. The axial distributions of the eigenmodes for $l = 2$ are plotted in Fig. 5.9 c. The FTs of the pressure signals of sensors P_{5*} downstream of tube 5 were evaluated at 1000, 1183.3, and 1216.7 Hz. Analogous to the findings for $l = 0$ and $l = 1$, the amplitudes of the measured pressure oscillations qualitatively match the predicted mode shape. However, for $f = 1183.3$ Hz, which was chosen due to the observed peak in PSD_{-1} near $f_{2,1}$ (Fig. 5.8 b), the amplitude at $x/L = 0.14$ significantly exceeds the expected value. For all other data points, the measured amplitudes follow the predictions.

When the blockage ratio at the plenum outlet is reduced to $\beta = 0.5$, the shapes of the predicted eigenmodes slightly change. The most obvious effect is a reduction in the pressure amplitude at the plenum outer wall for $x/L = 1$ due to a modified acoustic boundary condition at the plenum outlet. Qualitatively, the previous findings for $\beta = 0.9$ can be adapted to the axial distribution of measured pressure amplitudes shown in Fig. 5.9 d–f for a blockage ratio of 0.5. In particular, the measured amplitudes at $x/L = 0.14$ that do not follow the predicted mode shapes (200 Hz for $l = 0$ and 1183.3 Hz/1083.3 Hz for $l = 2$) are equal for both examined blockage ratio. These deviations are most likely caused by local deviations of the excited mode shapes from the predicted distribution of $\Psi_{l,m}$. However, the restricted number of measurements positions are not sufficient for a detailed examination of these discrepancies. Nevertheless, the conducted evaluation revealed a strong link between the observed axial pressure distribution and the acoustic eigenmodes of the annular plenum. This supports the presumption that acoustic eigenmodes were excited by PDC operation, resulting in considerable pressure oscillations in the plenum throughout the entire cycle duration, as shown in Fig 5.4.

In the following, a quantitative comparison of the acoustic pressure oscillations in the annular plenum is presented for differing operating conditions, which involves variations of the firing frequency, the firing pattern, the injection period, the equivalence ratio, and the blockage of the plenum outlet. The goal of this examination is to find the best operation parameters to reduce acoustic pressure oscillations. For this, two quantities are determined: the integral energy of acoustic pressure oscillations and the number of excited modes. In particular, large pressure amplitudes are expected, when a single acoustic mode contains high energy. In contrast, when the same amount of energy is distributed over a large number of mode shapes, only small amplitudes are expected. First, the applied evaluation methods are introduced and the effect of a variation in the outlet blockage is discussed. Second, results from experiments with different firing patterns are examined. Lastly, the impact of variations in the injection duration and the equivalence ratio, respectively, on pressure oscillations in the plenum is evaluated. As the quantification of pressure fluctuations at the plenum outlet is of particular interest, the following examinations are conducted for the pressure signals of sensors P_{*5} at $x/L = 0.86$.

Plenum Outlet Blockage

The integral value of the cumulative PSD obtained from azimuthal frequency decomposition represents a measure for the acoustic energy of pressure oscillations in the annular plenum [158]. The cumulative PSD is calculated as the sum of the spectra for all investigated azimuthal mode

numbers according to

$$\mathrm{PSD}_{\mathrm{cum}}(f) = \sum_{m=-2}^{3} \mathrm{PSD}_m(f). \tag{5.7}$$

To account for the amount of injected fuel per combustion cycle, the integral value is normalized by the fill fraction $\xi = t_{\mathrm{inj}}/21\,\mathrm{ms}$ and the equivalence ratio φ. Since the PSDs revealed no significant peaks above 4 kHz only frequencies below this value are considered. The integral energy e can then be defined as

$$e = \frac{1}{\xi\varphi} \int_{f_0}^{f_0+4\,\mathrm{kHz}} \mathrm{PSD}_{\mathrm{cum}}(f)\,\mathrm{d}f. \tag{5.8}$$

Although the value of e quantifies the integral energy of pressure oscillations in the plenum, it does not give information on the distribution of this energy over different modes. To get further insights into the number of excited acoustic modes, the spectrum of $\mathrm{PSD}_{\mathrm{cum}}$ is evaluated at the peak frequencies f_{peak}, which are defined in Eq. 5.6. These peak amplitudes are shown in Fig. 5.10 for the reference case (firing pattern $\mathbf{I}^{+}$, $\beta = 0.9$, $t_{\mathrm{inj}} = 21\,\mathrm{ms}$, $\varphi = 1$, $f_{\mathrm{tube}} = 16.7\,\mathrm{Hz}$). It can clearly be seen that the majority of the integral energy is concentrated in only a few modes. The distributions of the peak amplitudes look qualitatively similar for the other operating conditions (not shown). Four regimes can be identified in the series of sorted peak amplitudes (Fig. 5.10 a). A small number of modes are associated to large amplitudes. For the reference case, a large peak at 500 Hz in the spectrum $\hat{p}_0$ (Fig. 5.8 c) is observed. These dominant modes are followed by several considerably large amplitudes, which represent the excited acoustic modes that correspond to the predicted eigenmodes of the plenum, as shown in Fig. 5.8. Then a series of small-amplitude pressure oscillations is visible, which correspond to amplitudes at peak frequencies that are well off the eigenfrequencies $f_{l,m}$. Lastly, a large number of negligible values

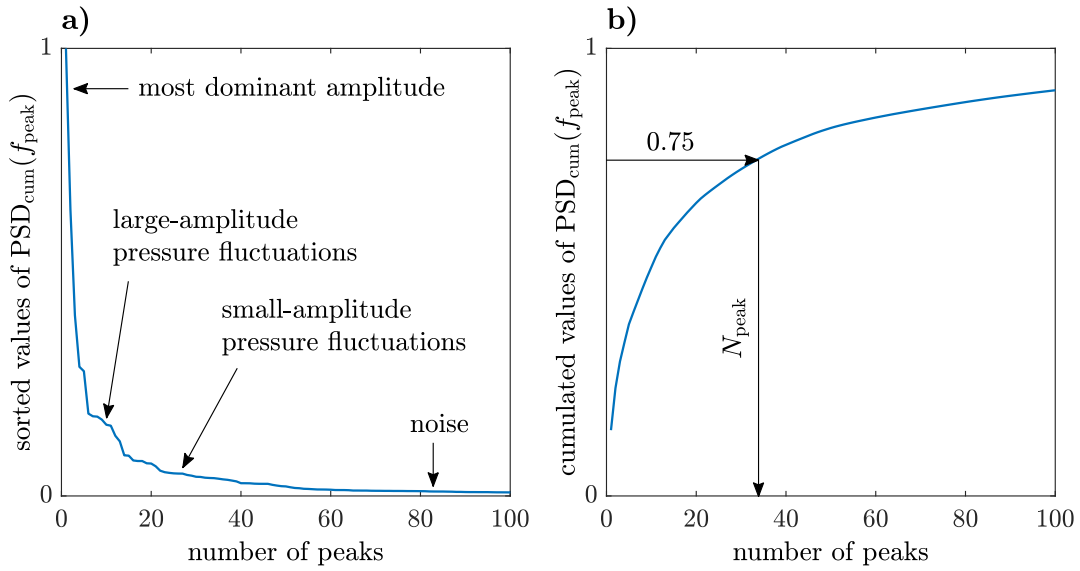

Figure 5.10: Distribution of the integral energy over the peak frequencies: (a) sorted values of normalized peak amplitudes and (b) cumulative sum of the sorted values

represent measurement noise. As the obtained distributions of peak amplitudes were found to be qualitatively similar for all operating conditions, a quantitative comparison was performed on the basis of a scalar parameter that represents the number of modes N_{peak}, which contain 75 % of the total integral energy. The methodology for calculating N_{peak} is visualized in Fig. 5.10 b.

The two obtained scalar parameters e and N_{peak} are plotted in Fig. 5.11 with respect to the firing frequency for measurements with firing pattern $\mathbf{I}^{+}$. For all visualized measurement results, a constant injection duration of $t_{\mathrm{inj}} = 21\,\mathrm{ms}$ and an equivalence ratio of $\varphi = 1$ were applied. The integral energy is normalized by the value for the reference case.

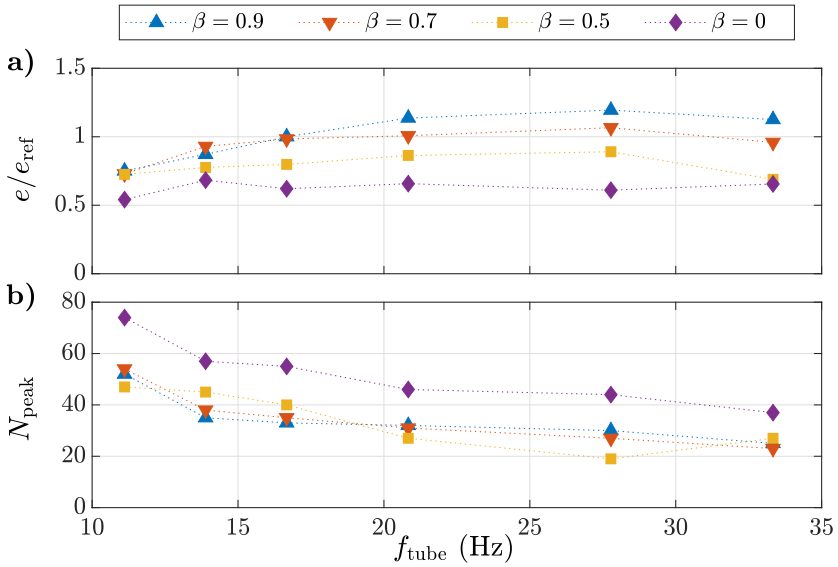

Figure 5.11: (a) Normalized integral energy e and (b) number of dominant modes N_{peak} with respect to the firing frequency f_{tube} when applying firing pattern $\mathbf{I}^{+}$ for various values of the blockage ratio β at the plenum outlet

The obtained normalized integral energy, shown in Fig. 5.11 a, is dependent on both the firing frequency and the blockage ratio. When increasing f_{tube}, the integral energy first increases and then converges to a value that depends on the plenum outlet blockage. This can be explained a larger fraction of the energy that is contained in the shock wave exiting the PDC to be reflected at the plenum outlet plane when a larger value of β is applied. Thus, a larger amount of energy is contained inside the plenum, leading to larger amplitudes of acoustic pressure oscillations. The data shown in Fig. 5.11 b reveal that increasing the firing frequency leads to a reduction of the number of excited acoustic modes. This gradual decrease is a consequence of the reduced number of peak frequencies in the fixed range from f_0 to $f_0 + 4\,\mathrm{kHz}$. According to Eq. 5.6, the difference between two neighboring values of f_{peak} is given by the effective firing frequency, which is proportional to f_{tube}. Thus, the number of excited modes is reduced when increasing the firing frequency of the PDC tubes, ultimately resulting in a reduced value of N_{peak}. For all investigated blockage ratios with $\beta > 0$, the number of excited acoustic modes is nearly independent of β. However, removing the plenum outlet blockage results in an increased value of N_{peak} for all investigated firing frequencies. These results suggest that the largest pressure fluctuations are obtained for $\beta = 0.9$, as a maximum value of e and a small number of excited mode shapes were

observed when applying this outlet blockage. Further, an increasing firing frequency appears to have a negative effect on the value of N_{peak}. However, the condensed presentation by the two scalar values does not allow for analyzing the underlaying mechanisms that cause the observed variation in the number of excited acoustic modes.

To gain more knowledge about the distribution of the energy over the different azimuthal modes and how this distribution is affected by the operating conditions, a more detailed examination of the peak amplitudes is conducted in the following for the individual azimuthal mode numbers. This allows for quantifying the energy of pressure oscillations for a given azimuthal mode number. For this, a condensed version of the PSD_m is introduced as a function of the non-dimensional frequency ζ. An overview of the methodology for the calculation of this spectra $\hat{q}_m$ is given in Fig. 5.12 for the reference case and $m = 0$.

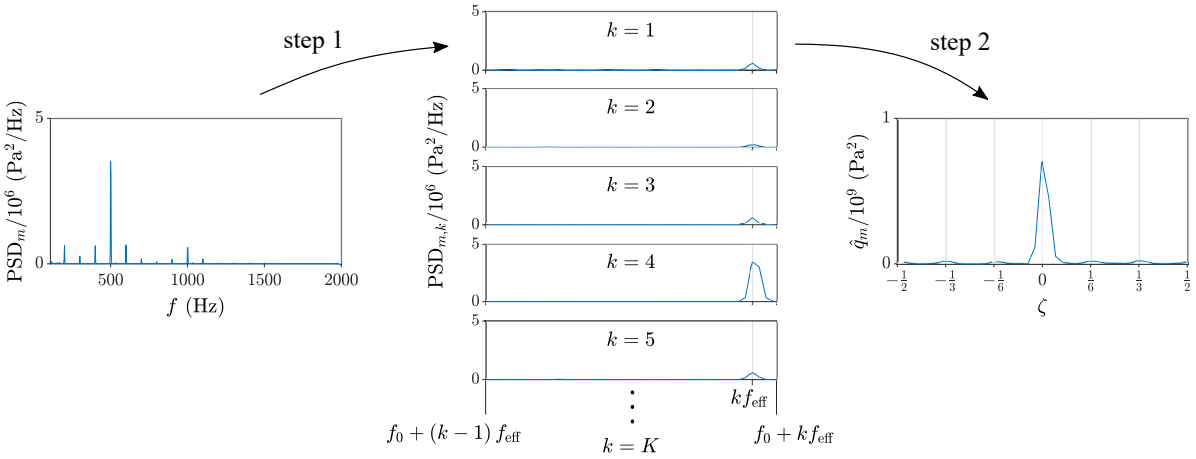

Figure 5.12: Schematic of the applied methodology for the determination of the cumulative PSD $\hat{q}_m\,(\zeta)$ from PSD_m

In the first step, the data of PSD_m is split into segments with an individual length of f_{eff}. A number of K segments is considered with K denoting the largest integer value with $K f_{\mathrm{eff}} \leq 4\,\mathrm{kHz}$. As for the previous examinations, frequencies smaller than $f_0 = f_{\mathrm{eff}} + \frac{1}{2} f_{\mathrm{tube}}$ are neglected to allow for the exclusive evaluation of acoustic pressure oscillations. In the second step, the values of $\hat{q}_m\,(\zeta)$ are calculated from the segments $\mathrm{PSD}_{m,k}$ by

$$\hat{q}_m\,(\zeta) = f_{\mathrm{eff}} \sum_{k=1}^{K} \mathrm{PSD}_{m,k}\,(f) \tag{5.9}$$

with the non-dimensional frequency $\zeta = f/f_{\mathrm{eff}} - k$. Lastly, the values of ζ are corrected to fit the range of $[-0.5, 0.5]$. This definition of the condensed spectra $\hat{q}_m$ ensures the preservation of the integral energy:

$$\int_{-0.5}^{0.5} \hat{q}_m\,(\zeta)\,\mathrm{d}\zeta = \int_{f_0}^{f_0 + K f_{\mathrm{eff}}} \mathrm{PSD}_m\,(f)\,\mathrm{d}f. \tag{5.10}$$

As indicated by the obtained spectrum shown in Fig. 5.12, the spectra of $\hat{q}_m$ contain one distinct

peak each at ζ_{peak}, which is given by

$$\zeta_{\text{peak}} = \frac{m}{N}. \tag{5.11}$$

For all other values of ζ, only negligible amplitudes in $\hat{q}_m$ are received. The distribution of the peak amplitudes $\hat{q}_{m,\text{peak}}$ over the azimuthal mode number m is shown in Fig. 5.13 for the six applied firing frequencies and the four blockage ratios. It should be noted that the first and the last value of each data set is equal, since the conducted azimuthal frequency decomposition does not allow to distinguish between $m = -3$ and $m = +3$. In addition, all values are normalized by the value of $\hat{q}_{0,\text{peak}}$ for the reference case. When applying a blockage ratio of $\beta = 0.9$ (Fig. 5.13 a), the maximum amplitude is observed for $m = 0$ for most investigated firing frequencies. In average slightly smaller amplitudes are obtained for $m = \pm 1$. For larger absolute values of m, only small values of $\hat{q}_{m,\text{peak}}$ are visible. This agrees with the observation in Fig. 5.8, where

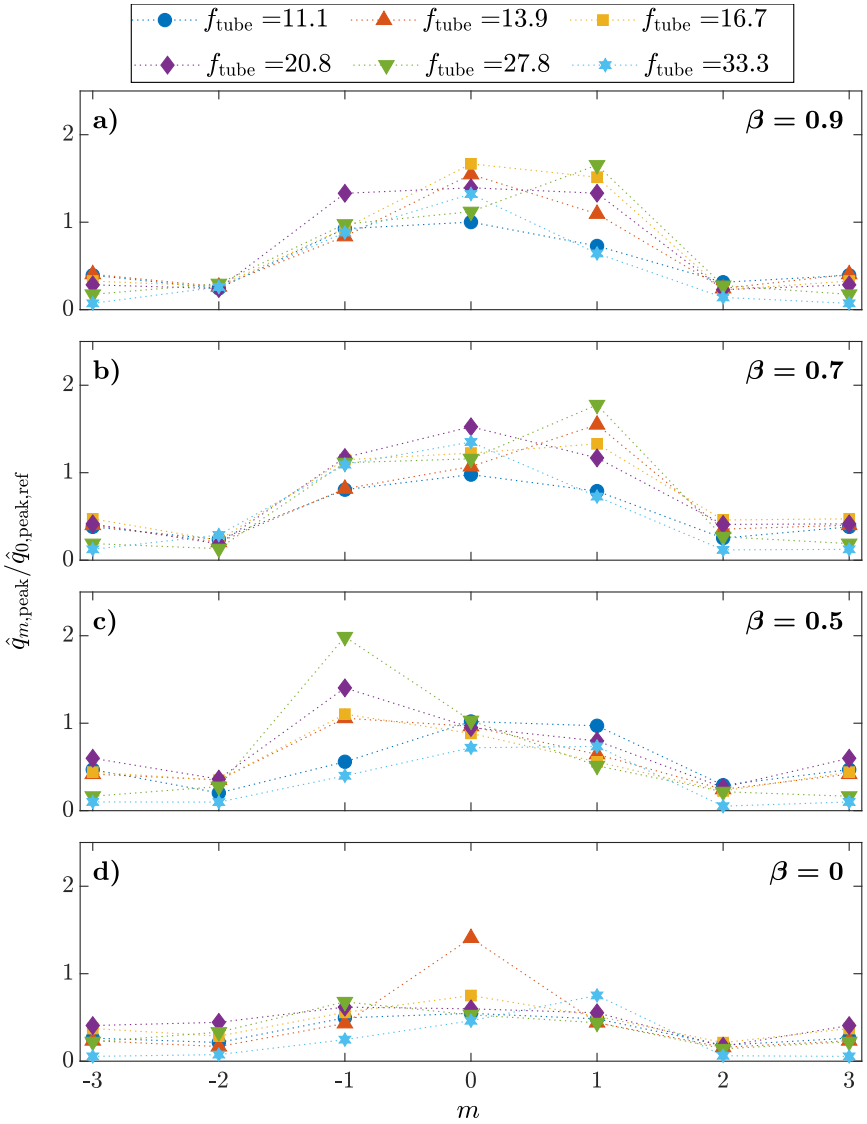

Figure 5.13: Peaks of the cumulative PSD with respect to the azimuthal mode number m when applying firing pattern $\mathbf{I}^+$ for various values of the plenum outlet blockage ratio β normalized by the peak value of $\hat{q}_0$ for the reference case

only small peaks were observed for these azimuthal mode numbers at $x/L = 0.86$. Comparable values of $\hat{q}_{m,\mathrm{peak}}$ are obtained for $m = \pm 1$ and ± 2, respectively, indicating that acoustic modes of both rotation directions are excited equivalently. The variations in the specific values of $\hat{q}_{m,\mathrm{peak}}$ for the different investigated firing frequencies are most likely due to a variation in the difference between the acoustic eigenfrequencies and the peak frequencies f_{peak}. As a result, the distribution of the energy on the various acoustic modes is changed leading to a variation in the peak amplitudes of $\hat{q}_m$. A reduction of the blockage ratio to $\beta = 0.7$ (Fig. 5.13 b) leads to maximum values of $\hat{q}_{m,\mathrm{peak}}$ at $m = 1$ for firing frequencies of 13.9, 16.7, and 27.8 Hz. The operation of the multi-tube PDC with these settings causes the values of f_{peak} to be close to the acoustic eigenfrequencies $f_{l,1}$, which promotes the excitation of positively spinning acoustic modes with two pressure nodes along the circumference. When further decreasing the blockage ratio to $\beta = 0.5$ (Fig. 5.13 c), a similar effect evokes the amplification of pressure oscillations with $m = -1$ for $13.9\,\mathrm{Hz} \leq f_{\mathrm{tube}} \leq 27.8\,\mathrm{Hz}$. Removing the plenum outlet blockage (Fig. 5.13 d) results in a considerable increase in the amplitude of pressure oscillations with $m = 0$ for $f_{\mathrm{tube}} = 13.9\,\mathrm{Hz}$. For this configuration, a dominant acoustic oscillation with $m = 0$ at $f = 166.7\,\mathrm{Hz}$ was observed, resulting in a clear local maximum in $\hat{q}_{m,\mathrm{peak}}$ for this azimuthal mode number. Overall, the decrease of the plenum outlet blockage leads to a broader distribution of the acoustic energy on azimuthal mode shapes. In addition, the number of peak amplitudes with $\hat{q}_{m,\mathrm{peak}} > \hat{q}_{0,\mathrm{peak,ref}}$ decreases when reducing the value of β.

Firing Pattern

In this section, the effect of the applied firing pattern when operating the multi-tube PDC on acoustic pressure oscillations in an attached annular plenum is discussed. The normalized integral energy and the number of dominant modes is shown in Fig. 5.14 for the four investigated

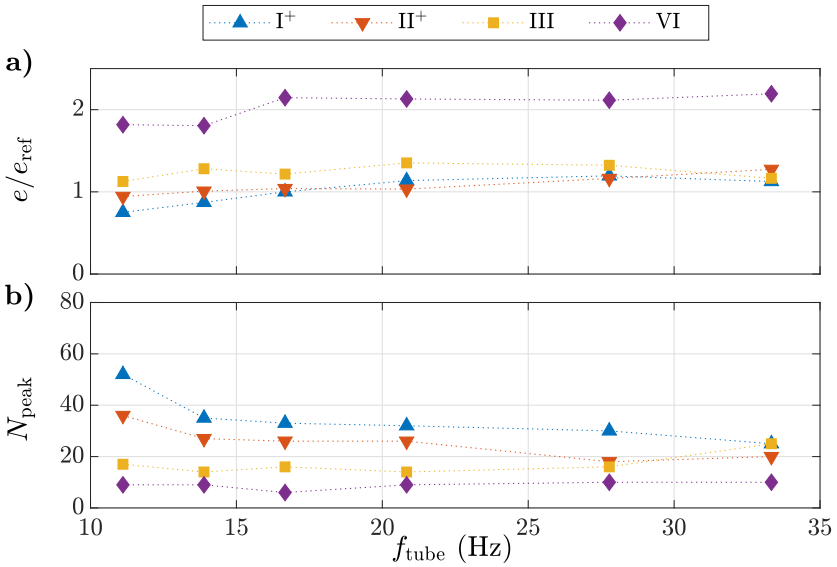

Figure 5.14: (a) Normalized integral energy e and (b) number of dominant modes N_{peak} with respect to the firing frequency f_{tube} for $\beta = 0.9$ and firing patterns **I**$^+$, **II**$^+$, **III**, and **VI**

firing patterns with respect to the firing frequency of a single combustion tube. The presented data is obtained from measurements with $\beta = 0.9$, $t_{\mathrm{inj}} = 21\,\mathrm{ms}$, and $\varphi = 1$. For small firing frequencies, e increases for an increasing number of simultaneously firing tubes ($\mathbf{I}^{+} \rightarrow \mathbf{VI}$). At higher frequencies, however, this effect can not be observed for the patterns $\mathbf{I}^{+}$, $\mathbf{II}^{+}$, and **III**. When all tubes are operated simultaneously (pattern **VI**), the largest integral energy is obtained across the whole considered frequency range. The number of excited modes, which contain 75 % of the integral energy, decreases with increasing number of simultaneously firing tubes, while the sensitivity of N_{peak} on the pattern diminishes with increasing firing frequency. These observations reveal that the operation with firing pattern **VI** results in the largest pressure oscillations. In addition, this energy is concentrated in a small number of modes. In contrast, the integral energy of acoustic pressure oscillations is reduced for sequential firing of the PDC tubes. Simultaneously, the energy is distributed to a larger number of mode shapes for firing pattern $\mathbf{I}^{+}$.

Analogous to the previous discussion on the effect of the outlet blockage β, the distribution

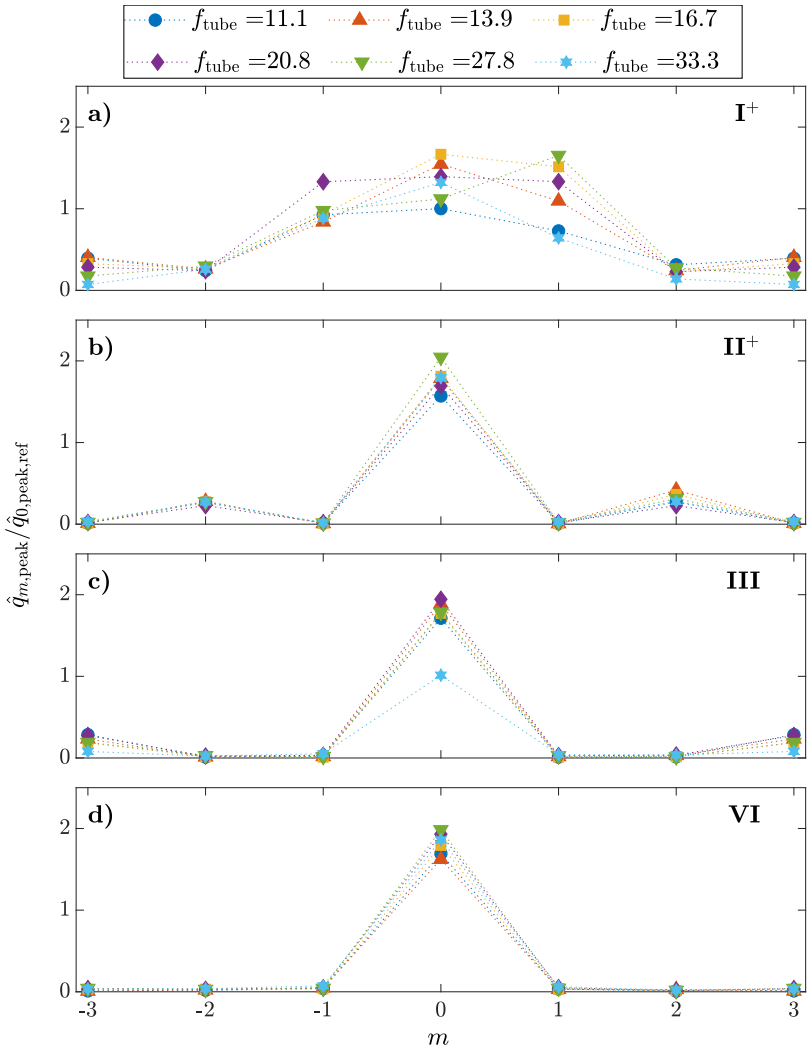

Figure 5.15: Peaks of the cumulative PSD with respect to the azimuthal mode number m for $\beta = 0.9$ and firing patterns $\mathbf{I}^{+}$, $\mathbf{II}^{+}$, **III**, and **VI** normalized by the peak value of $\hat{q}_0$ for the reference case

of the energy on the acoustic modes with differing azimuthal mode number is evaluated in the following. The peak frequencies of the cumulative PSD $\hat{q}_m(\zeta)$ with respect to the azimuthal mode number m are shown in Fig. 5.15 for all the investigated firing patterns. It can be well seen, that the firing frequency has no significant impact on the values of $\hat{q}_{m,\mathrm{peak}}$ for firing patterns **II**$^+$, **III**, and **VI**. However, significant variation in the amplitudes are visible for $-1 \leq m \leq +1$ in 5.15 a. It should be noted that the data in this plot are equal to the graphs in Fig. 5.13 a. Nevertheless, it was chosen to include the data here in order to allow for the direct comparison of the distributions of $\hat{q}_{m,\mathrm{peak}}$ for all applied firing patterns. For the application of firing pattern **II**$^+$, acoustic oscillations are only observed for $m = -2$, 0, and $+2$. This corresponds to the degree of rotational symmetry of the firing pattern that only promotes the amplification of acoustic modes with two opposing maxima at a given time. Similar arguments hold for the operation with pattern **III**, where peaks in $\hat{q}_{m,\mathrm{peak}}$ for $m = 0$ and $m = 3$ are obtained. When pattern **VI** is applied, only acoustic modes with homogeneous pressure along the circumference ($m = 0$) are observed. Thus, the decreasing number of acoustic modes with increasing number of simultaneously operated PDC tubes (Fig. 5.14 b) can be explained by a smaller number of excited modes with different azimuthal mode numbers.

Injection Duration and Equivalence Ratio

By changing the injection duration or the equivalence ratio, the amount of injected fuel is modified causing a variation in the amount of energy, released during the combustion event. It is thus expected that the integral energy is larger for elevated values of the injection duration and the equivalence ratio. Due to this, both parameters were used to normalize the integral energy e, as introduced in Eq. 5.8. The normalized integral energy and the number of dominant

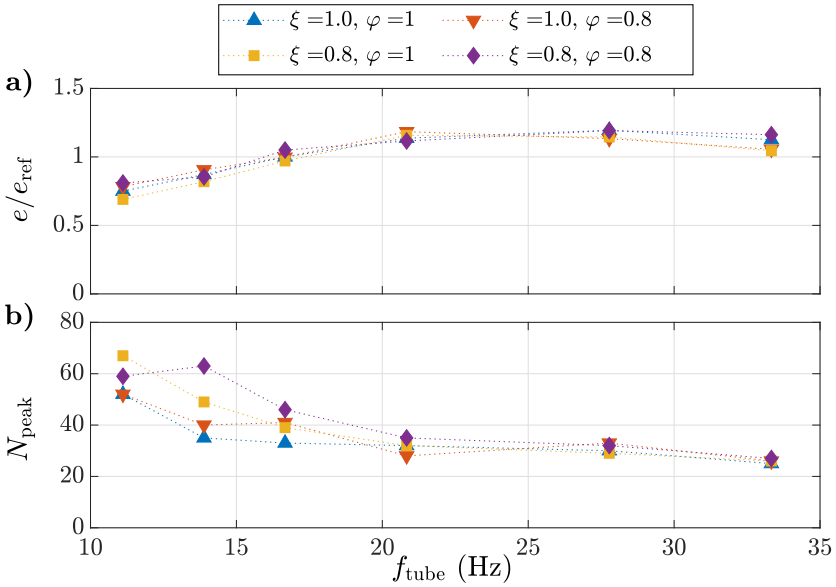

Figure 5.16: (a) Normalized integral energy e and (b) number of dominant modes N_{peak} with respect to the firing frequency f_{tube} for $\beta = 0.9$ and firing pattern **I**$^+$. The fuel consumption is modified by variations in the injection duration t_{inj} and the equivalence ratio φ.

modes are plotted in Fig. 5.16 with respect to the firing frequency. The data reveal that both the normalized integral energy and the number of excited acoustic modes, are mostly independent of the amount of injected fuel that is linearly correlated to the product of ξ and φ. Thus, the integral energy of pressure oscillations in the annular plenum are proportional to the injection duration and the equivalence ratio. The distribution of the energy over the excited acoustic modes is not affected significantly. Only for small firing frequencies, a larger number of dominant modes is obtained when operating the PDC with a larger fill fraction ξ. The results therefore suggest that lean operation of the PDC with only partially filled combustion tubes is favorable in order to achieve a broad distribution of the energy over the excited acoustic modes. This ultimately results in small amplitudes in pressure fluctuations at the plenum outlet.

5.3 Concluding Remarks

As reported by other research groups, significant pressure fluctuations were observed upstream and downstream the multi-tube PDC, which is one of the main drawbacks on the way to realize efficient gas turbine operation with an integrated PDC. The experimental investigations, presented in this chapter, contribute to gain profound knowledge on the sources of pressure fluctuations at the interfaces to turbomachinery components and how there are affected by variations in the operating conditions of the PDC. Furthermore, the conducted systematic studies allowed for the identification of favorable operating conditions to reduce the pressure amplitudes.

Measurements of the pressure in the oxidizer supply with various firing patterns revealed that the amplitudes of upstream propagating pressure fluctuations are mainly affected by the global equivalence ratio and the cross section area of the air supply. In addition, the largest pressure fluctuations in the oxidizer supply were observed for simultaneous firing of all six PDC tubes. For all other firing patterns, comparable pressure amplitudes were recorded. However, a choked air inlet, as it was used in the scope of this thesis, is not suitable for gas turbine application as the generated pressure loss across the combustor inlet would hinder the efficient operation of the PDC. The conducted parametric study revealed that an increase in the cross section area of the air supply was found to result in considerably larger pressure fluctuations upstream of the combustor. Therefore, operation with lean fuel–oxidizer mixture is suggested to minimize both the maximum pressure amplitude and the RMS value of pressure fluctuations at the compressor outlet. By this, the unavoidable increase in the pressure amplitudes due to an increased cross section area of the oxidizer supply could be attenuated.

The integration of an annular plenum, as suggested by Rezay Haghdoost et al. [74], can contribute to the reduction of the amplitudes of shock waves exiting the PDC tubes. Pressure histories at the outer wall of the annular plenum, however, revealed significant pressure fluctuations throughout the entire operation duration, which are expected to have a negative impact on the mechanical stress and the efficiency of a potentially attached turbine. In the scope of this thesis, signal processing by azimuthal and frequency decomposition allowed to ascribe these pressure oscillations to a variety of acoustic modes, which were excited by the firing of the PDC tubes. These mode shapes were found to correspond to the acoustic eigenmodes of the plenum, which were predicted by the numerical solution of the acoustic Helmholtz equation. The dominant oscillation frequencies were closely linked to the effective firing frequency, the

firing pattern, and the azimuthal mode number of the respective mode shape. In particular, the amplitude of the corresponding pressure oscillations were dependent on the distance to the nearest acoustic eigenfrequency of the annular plenum. The evaluation of the integral energy of pressure oscillations, which was examined by the means of the integral value of the PSD obtained from azimuthal and frequency decomposition, revealed that simultaneous firing of all six PDC tubes resulted in the largest pressure fluctuations. Most promising results were found for sequential firing, which led to a comparably small integral energy of acoustic pressure oscillations and a large number of excited modes. By this, the energy is distributed, resulting in small amplitudes in pressure oscillations.

Chapter 6

Conclusions and Outlook

Although pulse detonation combustors (PDCs) have been investigated extensively in the past decades and their development status is more advanced than for other pressure gain combustion (PGC) concepts, there are still remaining challenges to face before PDCs can demonstrate their potential in increasing the thermal efficiency of gas turbines. The goal of this thesis was to tackle several challenging aspects of PDC operation by means of experimental investigations to provide a step towards the integration of a PDC into a gas turbine. First, the required operating conditions to ensure reliable deflagration-to-detonation transition (DDT) were determined for two different geometries: a shock-focusing device and a series of orifice plates. In addition, the feasibility of the two concepts for PDC application in a gas turbine was analyzed. Subsequently, the operation of a single-tube PDC at elevated temperature and pressure conditions was examined, which allowed for predicting the operating regime of the combustor at boundary conditions comparable to a micro gas turbine ($T_0 = 400\,\mathrm{K}$ and $p_0 = 3\,\mathrm{bar}$). Furthermore, fuel stratification was studied and identified as promising strategy to allow for reliable detonation initiation in globally fuel-lean mixtures. Lastly, the pressure fluctuations upstream and downstream of a multi-tube PDC were quantified and favorable operation parameters were proposed to reduce the effect of the periodic combustion process on attached turbomachinery components.

The integration of a shock-focusing device have been proposed recently [107] as an attractive alternative to conventional DDT geometries, such as a series of orifice plates. In this work, the process of detonation initiation at the focal point was investigated in detail by high-speed imaging to expand the knowledge on the underlaying physical processes. The combined examination of the recorded frames from two perspectives confirmed the onset of a detonation at the focal point, which was located at the tube axis close to the smallest cross section area of the converging–diverging geometry. The initially overdriven detonation spherically propagated away from the focal point. While axially propagating parts developed to a CJ detonation, radially propagating parts were reflected at the tube walls and formed a shock structure, which was found to be similar to the cellular pattern of a planar detonation wave. Examinations of the leading shock over a range of Reynolds numbers and two different mixture reactivities revealed a nearly linear increase of the pressure ratio across the leading shock with increasing Reynolds number. This trend was explained by a simultaneous increase in turbulent velocity fluctuations, which promoted flame

acceleration and contributed to the generation of larger pressure waves that accumulated in front of the deflagration and form a stronger leading shock. Reliable detonation initiation by shock focusing was observed when the pressure ratio across the leading shock exceeded a certain threshold. For these conditions, the induced pressure and temperature conditions at the focal point triggered the onset of a detonation, while the induced amplitudes for the focusing of weaker shocks was not sufficient. An increase in the mixture reactivity was found to promote both the formation of the leading shock and the detonation initiation, which allowed for achieving repeatable DDT for considerably reduced Reynolds numbers. In order to assess the feasibility of the shock-focusing device for PDC application, these findings were compared to the results from experiments with a series of orifice plates. This examination revealed that the required volume of the DDT section to ensure repeatable detonation initiation was smaller when using a series of orifice plates. In addition, the application of the shock-focusing device resulted in a slightly decreased pressure drop across the combustor, as well as a more deterministic operation represented by a reduced cycle-to-cycle variation. Moreover, the evaluation of the pressure history at the combustor inlet revealed a smaller integral value throughout the combustion event when the shock-focusing device was installed, which is expected to result in a reduced backflow of hot exhaust gases. However, the usage of oxygen-enriched air as oxidizer was required to achieve elevated mixture reactivities that allowed for the reliable detonation initiation by shock focusing at atmospheric temperature and pressure conditions. Nevertheless, the results suggest shock focusing to be a suitable concept for PDC application, as the integration into a gas turbine induces elevated pressure and temperature conditions, which is expected to result in an increased mixture reactivity, making oxygen enrichment dispensable.

In order to examine the operating regime of the PDC at gas turbine relevant conditions, experiments were conducted with pre-heated air as oxidizer and an outlet blockage, respectively. When increasing the initial mixture temperature, a considerable decrease in the detonation cell width of stoichiometric hydrogen–air mixtures was observed, which confirmed the suggested increase in mixture reactivity. Therefore, detonation initiation by shock focusing is expected to be supported by an increased mixture temperature. Similar results were acquired from measurements at elevated pressure conditions, where a smaller pressure ratio across the leading shock was found to be sufficient for the reliable onset of a detonation. Nevertheless, the experimental results revealed that the generation of a strong leading shock at constant mass flow rates is challenging. Fuel stratification was proposed and experimentally confirmed as a promising strategy to enable reliable PDC operation at globally lean mixture conditions and simultaneously allowing for a significant reduction in NO_x production. By changing the number of open fuel valves throughout the injection period, a spatially stratified equivalence ratio along the combustion tube was achieved and validated by optical fuel concentration measurements. The pressure ratio across the leading shock mainly depended on the local equivalence ratio near the ignition spark. A maximum shock strength was obtained when providing stoichiometric mixture conditions in the pre-detonation chamber. Additional amplification of the leading shock was observed when a negative spatial gradient in fuel concentration between the combustor inlet and the shock-focusing device was applied with a local equivalence ratio of 1 close to the ignition spark. By applying this injection trajectory, reliable detonation initiation was observed down to an equivalence ratio of 0.65. For constant fuel distributions a larger value of 0.85 was needed. The detailed

examination of the success rate for the investigated range of global equivalence ratios and five injection trajectories revealed that both, the pressure ratio across the leading shock and the local equivalence ratio in the shock-focusing device impacted the probability of successful detonation initiation. The results indicate that the minimum required pressure ratio for reliable detonation initiation by shock focusing was nearly independent of the local equivalence ratio at the focal point for fuel-rich mixtures. For decreasing equivalence ratios below stoichiometric conditions, a gradual increase in the required pressure ratio was observed. In addition, the conducted analysis of the exhaust gas composition demonstrated a considerable decrease in NO_x emission when fuel stratification was applied. Thus the injection of a stratified fuel–oxidizer mixture allows for stable PDC operation at globally lean conditions and a significant reduction of pollutant emission.

When integrating the PDC into a gas turbine, achieving reasonably small pressure amplitudes upstream and downstream of the combustor is vital. Measurements of the pressure fluctuations in the oxidizer supply of a multi-tube PDC demonstrated that the maximum amplitudes mainly depend on the pressure drop across the combustor inlet and the equivalence ratio of the injected mixture. As the pressure loss needs to be further reduced for gas turbine applications, fuel-lean operation should be favored to prevent large pressure amplitudes at the compressor outlet. Regarding pressure fluctuations at the combustor outlet, previous investigations by Rezay Haghdoost et al. [74] revealed that integrating a plenum between PDC and turbine allows for a considerable reduction of the maximum pressure amplitudes at the turbine inlet. In the scope of this thesis, however, recorded pressure histories contained significant pressure oscillations in the annular plenum, which could be explained by the excitation of acoustic modes. As these acoustic oscillations considerably contributed to the measured pressure fluctuations at the plenum outlet, a systematic investigation on the influence of operation parameters and the plenum outlet blockage was conducted. The frequency and amplitudes of the various mode shapes were found to depend on the acoustic boundary conditions at the plenum outlet and the operation parameters of the PDC, e.g. the firing pattern and the firing frequency. Examining the energy of pressure oscillations and the number of dominant mode shapes suggested best conditions for sequential firing and small firing frequencies. In addition, the results demonstrated that the amplitudes of individual mode shapes are very sensitive to the acoustic eigenfrequencies of the annular plenum, which depend on both the geometry and the speed of sound. For a practical gas turbine application, a closed-loop control algorithm may therefore be needed in a practical application to adjust the PDC operation based on the measured pressure fluctuations in the plenum.

In the scope of this thesis, several experimental investigations were conducted, which were designed to increase the knowledge on the physical processes in PDCs and on the generation of pressure fluctuations at the interfaces to potentially attached turbomachinery components. By this, guidelines for both a suitable PDC design and the identification of required operating conditions were identified, which allow for the stable and efficient operation of PDCs at gas turbine relevant conditions. In addition, favorable operation modes were proposed to reduce pressure fluctuations upstream and downstream of the combustor due to the periodic nature of the PDC process. Further, all experimental investigations were conducted with hydrogen as fuel and were tailored for the operation at characteristic temperature and pressure conditions of a micro gas turbine in order to contribute to the ongoing research aiming for climate-neutral energy production by highly efficient gas turbines in decentralized applications.

Bibliography

[1] P. J. Crutzen, "The influence of nitrogen oxides on the atmospheric ozone content," *Quarterly Journal of the Royal Meteorological Society*, vol. 96, no. 408, pp. 320–325, 1970.

[2] B. Gaston, J. M. Drazen, J. Loscalzo, and J. S. Stamler, "The biology of nitrogen oxides in the airways." *American journal of respiratory and critical care medicine*, vol. 149, no. 2, pp. 538–551, 1994.

[3] P. Capros, A. De Vita, N. Tasios, P. Siskos, M. Kannavou, A. Petropoulos, S. Evangelopoulou, M. Zampara, D. Papadopoulos, C. Nakos *et al.*, "Eu reference scenario 2016 – energy, transport and ghg emissions. trends to 2050." 2016.

[4] R. Pavri and G. D. Moore, "Gas turbine emissions and control," *Atlanta: GE Energy Services*, 2001.

[5] I. Gökalp and E. Lebas, "Alternative fuels for industrial gas turbines (AFTUR)," *Applied Thermal Engineering*, vol. 24, no. 11-12, pp. 1655–1663, 2004.

[6] S. Verhelst and T. Wallner, "Hydrogen-fueled internal combustion engines," *Progress in Energy and Combustion Science*, vol. 35, no. 6, pp. 490–527, 2009.

[7] C. Koroneos, A. Dompros, and G. Roumbas, "Hydrogen production via biomass gasification – a life cycle assessment approach," *Chemical Engineering and Processing: Process Intensification*, vol. 47, no. 8, pp. 1261–1268, 2008.

[8] M. M. Rashid, M. K. Al Mesfer, H. Naseem, and M. Danish, "Hydrogen production by water electrolysis: a review of alkaline water electrolysis, pem water electrolysis and high temperature water electrolysis," *Int. J. Eng. Adv. Technol*, vol. 4, no. 3, pp. 2249–8958, 2015.

[9] D. Haeseldonckx and W. D'haeseleer, "The use of the natural-gas pipeline infrastructure for hydrogen transport in a changing market structure," *International Journal of Hydrogen Energy*, vol. 32, no. 10-11, pp. 1381–1386, 2007.

[10] M. W. Melaina, O. Antonia, and M. Penev, "Blending hydrogen into natural gas pipeline networks. a review of key issues," National Renewable Energy Laboratory, Tech. Rep., 2013.

[11] T. Boushaki, Y. Dhué, L. Selle, B. Ferret, and T. Poinsot, "Effects of hydrogen and steam addition on laminar burning velocity of methane–air premixed flame: experimental and numerical analysis," *International journal of hydrogen energy*, vol. 37, no. 11, pp. 9412–9422, 2012.

[12] M. Ilbas, İ. Yılmaz, and Y. Kaplan, "Investigations of hydrogen and hydrogen–hydrocarbon composite fuel combustion and nox emission characteristics in a model combustor," *International Journal of Hydrogen Energy*, vol. 30, no. 10, pp. 1139–1147, 2005.

[13] N. Djordjevic, N. Hanraths, J. Gray, P. Berndt, and J. Moeck, "Numerical study on the reduction of nox emissions from pulse detonation combustion," *Journal of Engineering for Gas Turbines and Power*, vol. 140, no. 4, 2018.

[14] A. Witkowski, A. Rusin, M. Majkut, and K. Stolecka, "Comprehensive analysis of hydrogen compression and pipeline transportation from thermodynamics and safety aspects," *Energy*, vol. 141, pp. 2508–2518, 2017.

[15] P. Stathopoulos, "Comprehensive thermodynamic analysis of the humphrey cycle for gas turbines with pressure gain combustion," *Energies*, vol. 11, no. 12, p. 3521, 2018.

[16] N. Neumann and D. Peitsch, "Potentials for pressure gain combustion in advanced gas turbine cycles," *Applied Sciences*, vol. 9, no. 16, p. 3211, 2019.

[17] W. J. Bräunling, *Flugzeugtriebwerke: Grundlagen, Aero-Thermodynamik, ideale und reale Kreisprozesse, Thermische Turbomaschinen, Komponenten, Emissionen und Systeme*. Springer-Verlag, 2015.

[18] W. H. Heiser and D. T. Pratt, "Thermodynamic cycle analysis of pulse detonation engines," *Journal of Propulsion and Power*, vol. 18, no. 1, pp. 68–76, 2002.

[19] S. J. Jacobs, "The energy of detonation," Naval Ordnance Lab White Oak MD, Tech. Rep., 1956.

[20] W. Fickett and W. C. Davis, *Detonation: theory and experiment*. Courier Corporation, 2000.

[21] J. A. T. Gray, J. Vinkeloe, J. Moeck, C. O. Paschereit, P. Stathopoulos, P. Berndt, and R. Klein, "Thermodynamic evaluation of pulse detonation combustion for gas turbine power cycles," in *ASME Turbo Expo 2016: Turbomachinery Technical Conference and Exposition*. American Society of Mechanical Engineers Digital Collection, 2016.

[22] M. Staats and W. Nitsche, "Active control of the corner separation on a highly loaded compressor cascade with periodic nonsteady boundary conditions by means of fluidic actuators," *Journal of Turbomachinery*, vol. 138, no. 3, 2016.

[23] D. Topalovic, S. Wolff, A. Heinrich, D. Peitsch, and R. King, "Minimization of pressure fluctuations in an axial turbine stage under periodic inflow conditions," in *AIAA Propulsion and Energy 2019 Forum*, 2019, p. 4213.

[24] C. D. Porter, "Valveless-gas-turbine combustors with pressure gain," in *Turbo Expo: Power for Land, Sea, and Air*, vol. 79979. American Society of Mechanical Engineers, 1958, p. V001T01A011.

[25] D. Paxson and K. Dougherty, "Ejector enhanced pulsejet based pressure gain combustors: an old idea with a new twist," in *41st AIAA/ASME/SAE/ASEE Joint Propulsion Conference & Exhibit*, 2005, p. 4216.

[26] J. Keller, T. Bramlette, J. E. Dec, and C. Westbrook, "Pulse combustion: the importance of characteristic times," *Combustion and Flame*, vol. 75, no. 1, pp. 33–44, 1989.

[27] P. Litke, F. Schauer, D. Paxson, R. Bradley, and J. Hoke, "Assessment of the performance of a pulsejet and comparison with a pulsed-detonation engine," in *43rd AIAA Aerospace Sciences Meeting and Exhibit*, 2005, p. 228.

[28] A. Naples, J. Hoke, J. Karnesky, and F. Schauer, "Flowfield characterization of a rotating detonation engine," in *51st AIAA aerospace sciences meeting including the new horizons forum and aerospace exposition*, 2013, p. 278.

[29] S. Zhou, H. Ma, Y. Ma, C. Zhou, D. Liu, and S. Li, "Experimental study on a rotating detonation combustor with an axial-flow turbine," *Acta Astronautica*, vol. 151, pp. 7–14, 2018.

[30] D. Schwer and K. Kailasanath, "Numerical investigation of rotating detonation engines," in *46th AIAA/ASME/SAE/ASEE joint propulsion conference & exhibit*, 2010, p. 6880.

[31] F. A. Bykovskii, S. A. Zhdan, and E. F. Vedernikov, "Continuous spin detonations," *Journal of propulsion and power*, vol. 22, no. 6, pp. 1204–1216, 2006.

[32] S. W. Theuerkauf, "Heat exchanger design and testing for a 6-inch rotating detonation engine," Master's thesis, Air Force Institute of Technology, 2013.

[33] A. Naples, J. Hoke, R. T. Battelle, M. Wagner, and F. R. Schauer, "RDE implementation into an open-loop T63 gas turbine engine," in *55th AIAA Aerospace Sciences Meeting*, 2017, p. 1747.

[34] R. Blümner, "Operating mode dynamics in rotating detonation combustors," Ph.D. dissertation, Technische Universität Berlin, 2020.

[35] A. S. George, R. Driscoll, V. Anand, and E. Gutmark, "On the existence and multiplicity of rotating detonations," *Proceedings of the Combustion Institute*, vol. 36, no. 2, pp. 2691–2698, 2017.

[36] R. Bluemner, M. D. Bohon, C. O. Paschereit, and E. J. Gutmark, "Single and counter-rotating wave modes in an rdc," in *2018 AIAA Aerospace Sciences Meeting*, 2018, p. 1608.

[37] V. Anand, A. S. George, R. Driscoll, and E. Gutmark, "Longitudinal pulsed detonation instability in a rotating detonation combustor," *Experimental Thermal and Fluid Science*, vol. 77, pp. 212–225, 2016.

[38] B. C. Bobusch, P. Berndt, C. O. Paschereit, and R. Klein, "Shockless explosion combustion: An innovative way of efficient constant volume combustion in gas turbines," *Combustion Science and Technology*, vol. 186, no. 10-11, pp. 1680–1689, 2014.

[39] F. C. Yücel, F. E. Habicht, M. Bohon, and C. O. Paschereit, "Autoignition in stratified mixtures for pressure gain combustion," *Proceedings of the Combustion Institute*, 2020.

[40] F. C. Yücel, F. E. Habicht, A. Jaeschke, F. Lückoff, K. Oberleithner, and C. O. Paschereit, "Investigation of the fuel distribution in a shockless explosion combustor," *Journal of Engineering for Gas Turbines and Power*, 2020.

[41] T. G. Reichel, J.-S. Schäpel, B. C. Bobusch, R. Klein, R. King, and C. O. Oliver Paschereit, "Shockless explosion combustion: experimental investigation of a new approximate constant volume combustion process," *Journal of Engineering for Gas Turbines and Power*, vol. 139, no. 2, 2017.

[42] J. H. Lee, *The detonation phenomenon*, 2008.

[43] F. A. Williams, *Combustion theory*. CRC Press, 2018.

[44] D. L. Chapman, "Vi. on the rate of explosion in gases," *The London, Edinburgh, and Dublin Philosophical Magazine and Journal of Science*, vol. 47, no. 284, pp. 90–104, 1899.

[45] E. Jouguet, "On the propagation of chemical reactions in gases," *J. de mathematiques Pures et Appliquees*, vol. 1, no. 347-425, p. 2, 1905.

[46] Y. B. Zel'dovich, "On the theory of detonation propagation in gaseous systems," *Zh. Eksp. Teor. Fiz*, vol. 10, no. 5, pp. 542–568, 1940.

[47] J. von Neuman, "Theory of detonation waves," Institute for Advanced Study Princeton NJ, Tech. Rep., 1942.

[48] W. Döring, "Über den Detonationsvorgang in Gasen," *Annalen der Physik*, vol. 435, no. 6-7, pp. 421–436, 1943.

[49] E. Wintenberger and J. Shepherd, "Model for the performance of airbreathing pulse-detonation engines," *Journal of Propulsion and Power*, vol. 22, no. 3, pp. 593–603, 2006.

[50] D. D. Joshi and F. K. Lu, "Unsteady thrust measurement for pulse detonation engines," *Journal of Propulsion and Power*, vol. 32, no. 1, pp. 225–236, 2016.

[51] J. Kasahara, M. Hirano, A. Matsuo, Y. Daimon, and T. Endo, "Thrust measurement of a multicycle partially filled pulse detonation rocket engine," *Journal of Propulsion and Power*, vol. 25, no. 6, pp. 1281–1290, 2009.

[52] D. R. White, "Turbulent structure of gaseous detonation," *The Physics of Fluids*, vol. 4, no. 4, pp. 465–480, 1961.

[53] Y. N. Denisov and Y. K. Troshin, "On the mechanism of detonative combustion," in *Symposium (International) on Combustion*, vol. 8, no. 1. Elsevier, 1961, pp. 600–610.

[54] B. Voitsekhovskii, V. V. Mitrofanov, and M. Topchiyan, "Structure of the detonation front in gases (survey)," *Combustion, Explosion and Shock Waves*, vol. 5, no. 3, pp. 267–273, 1969.

[55] R. Soloukhin, "Multiheaded structure of gaseous detonation," *Combustion and Flame*, vol. 10, no. 1, pp. 51–58, 1966.

[56] R. A. Strehlow and A. J. Crooker, "The structure of marginal detonation waves," *Acta Astronautica*, vol. 1, no. 3-4, pp. 303–315, 1974.

[57] R. Takai, K. Yoneda, and T. Hikita, "Study of detonation wave structure," in *Symposium (International) on Combustion*, vol. 15, no. 1. Elsevier, 1975, pp. 69–78.

[58] F. Pintgen, C. Eckett, J. Austin, and J. Shepherd, "Direct observations of reaction zone structure in propagating detonations," *Combustion and Flame*, vol. 133, no. 3, pp. 211–229, 2003.

[59] V. Mitrofanov and R. Soloukhin, "The diffraction of multifront detonation waves," in *Proceedings of the USSR Academy of Sciences*, vol. 159, no. 5, 1964, pp. 1003–1006.

[60] J. H. S. Lee, "Initiation of gaseous detonation," *Annual Review of Physical Chemistry*, vol. 28, no. 1, pp. 75–104, 1977.

[61] J. H. S. Lee, "Dynamic parameters of gaseous detonations," *Annual review of fluid mechanics*, vol. 16, no. 1, pp. 311–336, 1984.

[62] C. Campbell and D. W. Woodhead, "The ignition of gases by an explosion-wave. part i. carbon monoxide and hydrogen mixtures," *Journal of the Chemical Society (Resumed)*, vol. 129, pp. 3010–3021, 1926.

[63] A. J. Mooradian and W. Gordon, "Gaseous detonation. i. initiation of detonation," *The Journal of Chemical Physics*, vol. 19, no. 9, pp. 1166–1172, 1951.

[64] J. A. Fay, "A mechanical theory of spinning detonation," *The journal of chemical physics*, vol. 20, no. 6, pp. 942–950, 1952.

[65] R. E. Duff, "Investigation of spinning detonation and detonation stability," *The physics of fluids*, vol. 4, no. 11, pp. 1427–1433, 1961.

[66] G. L. Schott, "Observations of the structure of spinning detonation," *The Physics of Fluids*, vol. 8, no. 5, pp. 850–865, 1965.

[67] J. Shepherd, I. Moen, S. Murray, and P. Thibault, "Analyses of the cellular structure of detonations," in *Symposium (International) on Combustion*, vol. 21, no. 1. Elsevier, 1988, pp. 1649–1658.

[68] J. J. Lee, D. Garinis, D. Frost, J. H. S. Lee, and R. Knystautas, "Two-dimensional autocorrelation function analysis of smoked foil patterns," *Shock Waves*, vol. 5, no. 3, pp. 169–174, 1995.

[69] M. Kaneshige and J. E. Shepherd, "Detonation database," 1997.

[70] H. D. Ng, Y. Ju, and J. H. S. Lee, "Assessment of detonation hazards in high-pressure hydrogen storage from chemical sensitivity analysis," *International Journal of Hydrogen Energy*, vol. 32, no. 1, pp. 93–99, 2007.

[71] J. A. T. Gray, "Reduction in the run-up distance for the deflagration-to-detonation transition and applications to pulse detonation combustion," Ph.D. dissertation, Berlin, Technische Universität Berlin, 2018.

[72] G. Ciccarelli, T. Ginsberg, and J. Boccio, "Detonation cell size measurements in high-temperature hydrogen-air-steam mixtures at the bnl high-temperature combustion facility," Nuclear Regulatory Commission, Tech. Rep., 1997.

[73] D. W. Stamps and S. R. Tieszen, "The influence of initial pressure and temperature on hydrogen-air-diluent detonations," *Combustion and Flame*, vol. 83, no. 3-4, pp. 353–364, 1991.

[74] M. Rezay Haghdoost, B. S. Thethy, D. Edgington-Mitchell, F. E. Habicht, J. Vinkeloe, N. Djordjevic, C. O. Paschereit, and K. Oberleithner, "Mitigation of pressure fluctuations from an array of pulse detonation combustors," *Journal of Engineering for Gas Turbines and Power*, 2020.

[75] S. W. Rienstra and A. Hirschberg, "An introduction to acoustics," *Eindhoven University of Technology*, vol. 18, p. 19, 2004.

[76] J. P. Moeck, M. Paul, and C. O. Paschereit, "Thermoacoustic instabilities in an annular rijke tube," in *Turbo Expo: Power for Land, Sea, and Air*, vol. 43970, 2010, pp. 1219–1232.

[77] J.-F. Parmentier, P. Salas, P. Wolf, G. Staffelbach, F. Nicoud, and T. Poinsot, "A simple analytical model to study and control azimuthal instabilities in annular combustion chambers," *Combustion and Flame*, vol. 159, no. 7, pp. 2374–2387, 2012.

[78] M. Bauerheim, J.-F. Parmentier, P. Salas, F. Nicoud, and T. Poinsot, "An analytical model for azimuthal thermoacoustic modes in an annular chamber fed by an annular plenum," *Combustion and Flame*, vol. 161, no. 5, pp. 1374–1389, 2014.

[79] G. Walz, W. Krebs, S. Hoffmann, and H. Judith, "Detailed analysis of the acoustic mode shapes of an annular combustion chamber," *J. Eng. Gas Turbines Power*, vol. 124, no. 1, pp. 3–9, 2002.

[80] S. M. Camporeale, B. Fortunato, and G. Campa, "A finite element method for three-dimensional analysis of thermo-acoustic combustion instability," *Journal of Engineering for Gas Turbines and Power*, vol. 133, no. 1, 2011.

[81] G. A. Mensah, G. Campa, and J. P. Moeck, "Efficient computation of thermoacoustic modes in industrial annular combustion chambers based on bloch-wave theory," *Journal of Engineering for Gas Turbines and Power*, vol. 138, no. 8, 2016.

[82] G. Roy, S. Frolov, A. Borisov, and D. Netzer, "Pulse detonation propulsion: challenges, current status, and future perspective," *Progress in Energy and Combustion Science*, vol. 30, no. 6, pp. 545–672, 2004.

[83] G. Ciccarelli and S. Dorofeev, "Flame acceleration and transition to detonation in ducts," *Progress in energy and combustion science*, vol. 34, no. 4, pp. 499–550, 2008.

[84] D. M. Valiev, V. Bychkov, V. Akkerman, and L.-E. Eriksson, "Different stages of flame acceleration from slow burning to Chapman-Jouguet deflagration," *Physical Review E*, vol. 80, no. 3, p. 036317, 2009.

[85] J. H. S. Lee, R. Knystautas, and A. Freiman, "High speed turbulent deflagrations and transition to detonation in h2–air mixtures," *Combustion and Flame*, vol. 56(2), pp. 227–239, 1984.

[86] J. Chao and J. H. S. Lee, "The propagation mechanism of high speed turbulent deflagrations," *Shock Waves*, vol. 12, no. 4, pp. 277–289, 2003.

[87] A. K. Oppenheim, A. J. Laderman, and P. A. Urtiew, "The onset of retonation," *Combustion and Flame*, vol. 6, pp. 193–197, 1962.

[88] P. A. Urtiew and A. K. Oppenheim, "Experimental observations of the transition to detonation in an explosive gas," *Proceedings of the Royal Society of London. Series A. Mathematical and Physical Sciences*, vol. 295, no. 1440, pp. 13–28, 1966.

[89] Y. B. Zel'dovich, "Regime classification of an exothermic reaction with nonuniform initial conditions," *Combustion and Flame*, vol. 39, no. 2, pp. 211–214, 1980.

[90] J. H. Lee, R. Knystautas, and N. Yoshikawa, "Photochemical initiation of gaseous detonations," in *Gasdynamics of Explosions and Reactive Systems*. Elsevier, 1980, pp. 971–982.

[91] K. I. Shchelkin, "Rapid combustion and spin detonation in gases," Moscow, Voenizdat, 1949.

[92] T. New, P. Panicker, F. Lu, and H. Tsai, "Experimental investigations on ddt enhancements by Schelkin spirals in a PDE," *44th AIAA Aerospace Sciences Meeting and Exhibit*, p. 552, 2006.

[93] M. Silvestrini, B. Genova, G. Parisi, and F. L. Trujillo, "Flame acceleration and ddt run-up distance for smooth and obstacles filled tubes," *Journal of Loss Prevention in the Process Industries*, vol. 21, no. 5, pp. 555–562, 2008.

[94] J. H. S. Lee, R. Knystautas, and C. K. Chan, "Turbulent flame propagation in obstacle-filled tubes," in *Symposium (International) on Combustion*, vol. 20, no. 1. Elsevier, 1985, pp. 1663–1672.

[95] C. M. Guirao, R. Knystautas, and J. H. S. Lee, "A summary of hydrogen-air detonation experiments," Nuclear Regulatory Commission, Washington, DC (USA). Div. of Systems Research, Tech. Rep., 1989.

[96] G. Ciccarelli and S. Dorofeev, "Flame acceleration and transition to detonation in ducts," *Progress in energy and combustion science*, vol. 34, no. 4, pp. 499–550, 2008.

[97] H. Ma, Z. Xia, W. Gao, C. Zhuo, and D. Wang, "Numerical simulation of the deflagration-to-detonation transition of iso-octane vapor in an obstacle-filled tube," *International Journal of Spray and Combustion Dynamics*, vol. 10, no. 3, pp. 244–259, 2018.

[98] D. Paxson, F. Schauer, and D. Hopper, "Performance impact of deflagration to detonation transition enhancing obstacles," *47th AIAA Aerospace Sciences Meeting including The New Horizons Forum and Aerospace Exposition*, p. 502, 2009.

[99] C. Cathey, F. Wang, T. Tang, A. Kuthi, M. Gundersen, J. Sinibaldi, C. Brophy, E. Barbour, R. Hanson, J. Hoke *et al.*, "Transient plasma ignition for delay reduction in pulse detonation engines," *45th AIAA Aerospace Sciences Meeting and Exhibit*, p. 443, 2007.

[100] A. Starikovskiy, N. Aleksandrov, and A. Rakitin, "Plasma-assisted ignition and deflagration-to-detonation transition," *Philosophical Transactions of the Royal Society A: Mathematical, Physical and Engineering Sciences*, vol. 370, no. 1960, pp. 740–773, 2012.

[101] S. Zhou, W. Nie, X. Che, Q. Chen, and Z. Zhang, "Influence of equivalence ratio on plasma assisted detonation initiation by alternating current dielectric barrier discharge under rich burn condition," *Aerospace Science and Technology*, vol. 69, pp. 504–512, 2017.

[102] J. A. T. Gray and D. A. Lacoste, "Enhancement of the transition to detonation of a turbulent hydrogen–air flame by nanosecond repetitively pulsed plasma discharges," *Combustion and Flame*, vol. 199, pp. 258–266, 2019.

[103] S. Murray, F. Zhang, and K. Gerrard, "The influence of driver power and receptor confinement on pre-detonators for pulse detonation engines," *Proceedings of the 18th interna4 tional colloquium on the dynamics of explosions and reactive systems, Seattle, Washington*, 2001.

[104] S. M. Frolov and V. S. Aksenov, "Initiation of gas detonation in a tube with a shaped obstacle," *Doklady Physical Chemistry*, vol. 427, no. 1, pp. 129–132, 2009.

[105] S. Frolov, V. Aksenov, and A. Skripnik, "Detonation initiation in a natural gas-air mixture in a tube with a focusing nozzle," *Doklady Physical Chemistry*, vol. 436, no. 1, pp. 10–14, 2011.

[106] I. V. Semenov, P. S. Utkin, V. V. Markov, S. M. Frolov, and V. S. Aksenov, "Numerical and experimental investigation of detonation initiation in profiled tubes," *Combustion science and technology*, vol. 182, no. 11-12, pp. 1735–1746, 2010.

[107] J. A. T. Gray, M. Lemke, J. Reiss, C. O. Paschereit, J. Sesterhenn, and J. P. Moeck, "A compact shock-focusing geometry for detonation initiation: Experiments and adjoint-based variational data assimilation," *Combustion and Flame*, vol. 183, pp. 144–156, 2017.

[108] S. Bengoechea, J. A. T. Gray, J. Reiss, J. P. Moeck, C. O. Paschereit, and J. Sesterhenn, "Detonation initiation in pipes with a single obstacle for mixtures of hydrogen and oxygen-enriched air," *Combustion and Flame*, vol. 198, pp. 290–304, 2018.

[109] S. Bengoechea, J. Reiss, M. Lemke, and J. Sesterhenn, "Numerical investigation of shock waves as detonation initiator," in *27th International Colloquium on the Dynamics of Explosions and Reactive Systems*, 2019.

[110] A. Glaser, N. Caldwell, and E. Gutmark, "Performance measurements of a pulse detonation combustor array integrated with an axial flow turbine," in *44th AIAA aerospace sciences meeting and exhibit*, 2006, p. 1232.

[111] A. Glaser, N. Caldwell, and E. Gutmark, "Performance of an axial flow turbine driven by multiple pulse detonation combustors," in *45th AIAA Aerospace Sciences Meeting and Exhibit*, 2007, p. 1244.

[112] A. Rasheed, A. H. Furman, and A. J. Dean, "Experimental investigations of the performance of a multitube pulse detonation turbine system," *Journal of Propulsion and Power*, vol. 27, no. 3, pp. 586–596, 2011.

[113] K. Rouser, P. King, F. Schauer, R. Sondergaard, and J. Hoke, "Unsteady performance of a turbine driven by a pulse detonation engine," in *48th AIAA Aerospace Sciences Meeting Including the New Horizons Forum and Aerospace Exposition*, 2010, p. 1116.

[114] K. Rouser, P. King, F. Schauer, R. Sondergaard, and J. Hoke, "Experimental performance evaluation of a turbine driven by pulsed detonations," in *51st AIAA aerospace sciences meeting including the new horizons forum and aerospace exposition*, 2013, p. 1212.

[115] F. Schauer, R. Bradley, and J. Hoke, "Interaction of a pulsed detonation engine with a turbine," Air Force Research Lab Wright-Patterson AFB OH Propulsion Directorate, Tech. Rep., 2003.

[116] A. J. Dean, A. Rasheed, V. Tangirala, and P. F. Pinard, "Operation and noise transmission of an axial turbine driven by a pulse detonation combustor," in *Turbo Expo: Power for Land, Sea, and Air*, vol. 47306, 2005, pp. 1275–1284.

[117] A. Rasheed, A. Furman, and A. Dean, "Wave attenuation and interactions in a pulsed detonation combustor-turbine hybrid system," in *44th AIAA aerospace sciences meeting and exhibit*, 2006, p. 1235.

[118] A. Heinrich, M. Herbig, D. Peitsch, D. Topalovic, and R. King, "A testrig to evaluate turbine performance and operational strategies under pulsating inflow conditions," in *AIAA Propulsion and Energy 2019 Forum*, 2019, p. 4039.

[119] K. P. Rouser, P. I. King, F. R. Schauer, R. Sondergaard, J. L. Hoke, and L. P. Goss, "Time-resolved flow properties in a turbine driven by pulsed detonations," *Journal of Propulsion and Power*, vol. 30, no. 6, pp. 1528–1536, 2014.

[120] N. Caldwell, R. Brunet, E. Gutmark, and B. Drouin, "Experimental analysis of a hybrid pulse detonation combustor/gas turbine engine," in *46th AIAA Aerospace Sciences Meeting and Exhibit*, 2008, p. 121.

[121] A. Rasheed, A. H. Furman, and A. J. Dean, "Pressure measurements and attenuation in a hybrid multitube pulse detonation turbine system," *Journal of Propulsion and Power*, vol. 25, no. 1, pp. 148–161, 2009.

[122] H. Qiu, C. Xiong, and L. Zheng, "Experimental investigation of an air-breathing pulse detonation turbine prototype engine," *Applied Thermal Engineering*, vol. 104, pp. 596–602, 2016.

[123] M. Rezay Haghdoost, D. M. Edgington-Mitchell, C. O. Paschereit, and K. Oberleithner, "High-speed schlieren and particle image velocimetry of the exhaust flow of a pulse detonation combustor," *AIAA Journal*, vol. 58, no. 8, pp. 3527–3543, 2020. [Online]. Available: https://arc.aiaa.org/doi/abs/10.2514/1.J058540

[124] J. Hoke, R. Bradley, J. Stutrud, and F. Schauer, "Integration of a pulsed detonation engine with an ejector pump and with a turbo-charger as methods to self-aspirate," in *40th AIAA Aerospace Sciences Meeting & Exhibit*, 2002, p. 615.

[125] J. Lu, L. Zheng, Z. Wang, L. Wang, and C. Yan, "Experimental investigation on interactions between a two-phase multi-tube pulse detonation combustor and a centrifugal compressor," *Applied Thermal Engineering*, vol. 113, pp. 426–434, 2017.

[126] K. Matsuoka, M. Esumi, K. B. Ikeguchi, J. Kasahara, A. Matsuo, and I. Funaki, "Optical and thrust measurement of a pulse detonation combustor with a coaxial rotary valve," *Combustion and flame*, vol. 159, no. 3, pp. 1321–1338, 2012.

[127] Z. Wang, J. Lu, J. Huang, C. Peng, and L. Zheng, "Experimental investigation on the operating characteristics in a multi-tube two-phase valveless air-breathing pulse detonation engine," *Applied thermal engineering*, vol. 73, no. 1, pp. 23–31, 2014.

[128] A. International, "Standard guide for designing systems for oxygen service," *American Society for Testing and Materials*, 2012.

[129] F. Russo and N. T. Basse, "Scaling of turbulence intensity for low-speed flow in smooth pipes," *Flow Measurement and Instrumentation*, vol. 52, pp. 101–114, 2016.

[130] G. Ciccarelli, C. T. Johansen, and M. Parravani, "The role of shock–flame interactions on flame acceleration in an obstacle laden channel," *Combustion and Flame*, vol. 157, no. 11, pp. 2125–2136, 2010.

[131] F. E. Habicht, F. C. Yücel, J. A. T. Gray, and C. O. Paschereit, "Detonation initiation by shock focusing at elevated pressure conditions in a pulse detonation combustor," *International Journal of Spray and Combustion Dynamics*, vol. 12, p. 1756827720921718, 2020.

[132] M. Cooper, S. Jackson, and J. E. Shepherd, "Effect of deflagration-to-detonation transition on pulse detonation engine impulse," California Institute of Technology, Tech. Rep., 2000.

[133] H. Li, S. D. Wehe, and K. R. McManus, "Real-time equivalence ratio measurements in gas turbine combustors with a near-infrared diode laser sensor," *Proceedings of the combustion institute*, vol. 33, no. 1, pp. 717–724, 2011.

[134] R. Bluemner, C. O. Paschereit, and K. Oberleithner, "Generation and transport of equivalence ratio fluctuations in an acoustically forced swirl burner," *Combustion and Flame*, vol. 209, pp. 99–116, 2019.

[135] F. Pintgen and J. Shepherd, "Simultaneous soot foil and plif imaging of propagating detonations," in *Extended abstract for 19th International Colloquium on the Dynamics of Explosions and Reactive Systems, Hakone, Japan*, vol. 27, 2003.

[136] J. M. Austin, "The role of instability in gaseous detonation," Ph.D. dissertation, California Institute of Technology Pasadena, 2003.

[137] K. Inaba, A. Matsuo, K. Tanaka, A. K. W. Lam, F. Pintgen, E. Winterberger, and J. E. Shepherd, "Soot track generation by mach reflection over a wedge," in *Japanese Symp. Shock Waves, Ibarki, Japan, March 14*, vol. 16. Citeseer, 2002.

[138] J. Hébral and J. Shepherd, *Detonation Cell Size Measurement*, California Institute of Technology, 2000.

[139] G. A. Mensah and J. P. Moeck, "Limit cycles of spinning thermoacoustic modes in annular combustors: A bloch-wave and adjoint-perturbation approach," in *ASME Turbo Expo 2017: Turbomachinery Technical Conference and Exposition*. American Society of Mechanical Engineers Digital Collection, 2017.

[140] C. Qi and Z. Chen, "Effects of temperature perturbation on direct detonation initiation," *Proceedings of the Combustion Institute*, vol. 36, no. 2, pp. 2743–2751, 2017.

[141] M. Kellenberger and G. Ciccarelli, "Advancements on the propagation mechanism of a detonation wave in an obstructed channel," *Combustion and Flame*, vol. 191, pp. 195–209, 2018.

[142] L. Dittmar and P. Stathopoulos, "Numerical analysis of the stability and operation of an axial compressor connected to an array of pulsed detonation combustors," in *ASME Turbo Expo 2020: Turbomachinery Technical Conference and Exposition*. American Society of Mechanical Engineers Digital Collection, 2020.

[143] F. E. Völzke, F. C. Yücel, J. A. T. Gray, N. Hanraths, C. O. Paschereit, and J. P. Moeck, "The Influence of the Initial Temperature on DDT Characteristics in a Valveless PDC," in *Active Flow and Combustion Control 2018*. Springer, 2019, pp. 185–196.

[144] C. Guirao, R. Knystautas, J. Lee, W. Benedick, and M. Berman, "Hydrogen–air detonations," Sandia National Labs., Tech. Rep., 1982.

[145] S. B. Dorofeev, V. P. Sidorov, M. S. Kuznetsov, I. D. Matsukov, and V. I. Alekseev, "Effect of scale on the onset of detonations," *Shock Waves*, vol. 10, no. 2, pp. 137–149, 2000.

[146] F. N. Egolfopoulos, P. Cho, and C. K. Law, "Laminar flame speeds of methane-air mixtures under reduced and elevated pressures," *Combustion and flame*, vol. 76, no. 3-4, pp. 375–391, 1989.

[147] W. Lowry, J. de Vries, M. Krejci, E. Petersen, Z. Serinyel, W. Metcalfe, H. Curran, and G. Bourque, "Laminar flame speed measurements and modeling of pure alkanes and alkane blends at elevated pressures," *Journal of Engineering for Gas Turbines and Power*, vol. 133, no. 9, 2011.

[148] M. C. Krejci, O. Mathieu, A. J. Vissotski, S. Ravi, T. G. Sikes, E. L. Petersen, A. Kérmonès, W. Metcalfe, and H. J. Curran, "Laminar flame speed and ignition delay time data for the kinetic modeling of hydrogen and syngas fuel blends," *Journal of Engineering for Gas Turbines and Power*, vol. 135, no. 2, 2013.

[149] C. M. Brophy and R. K. Hanson, "Fuel distribution effects on pulse detonation engine operation and performance," *Journal of Propulsion and Power*, vol. 22, no. 6, pp. 1155–1161, 2006.

[150] S. Yungster, K. Radhakrishnan, and K. Breisacher, "Computational study of nox formation in hydrogen-fuelled pulse detonation engines," *Combustion Theory and Modelling*, vol. 10, no. 6, pp. 981–1002, 2006.

[151] F. Schauer, R. Bradley, V. Katta, and J. Hoke, "Emissions in a pulsed detonation engine," in *47th AIAA Aerospace sciences meeting including the new horizons forum and aerospace exposition*, 2009, p. 505.

[152] N. Hanraths, F. Tolkmitt, P. Berndt, and N. Djordjevic, "Numerical study on nox reduction in pulse detonation combustion by using steam injection decoupled from detonation development," *Journal of Engineering for Gas Turbines and Power*, vol. 140, no. 12, 2018.

[153] F. E. Habicht, F. C. Yücel, N. Hanraths, N. Djordjevic, and C. O. Paschereit, "Lean operation of a pulse detonation combustor by fuel stratification," *Journal of Engineering for Gas Turbines and Power*, vol. 143, no. 5, p. 051009, 2021.

[154] M. Asli, P. Stathopoulos, and C. O. Paschereit, "Investigation of stationary vanes aerodynamic performance under different rdc exhaust," 2020.

[155] F. E. Habicht, F. C. Yücel, M. Rezay Haghdoost, K. Oberleithner, and C. O. Paschereit, "Acoustic modes in a plenum downstream of a multi-tube pulse detonation combustor," *AIAA Journal*, 2021, (accepted).

[156] M. Rezay Haghdoost, D. Edgington-Mitchell, M. Nadolski, R. Klein, and K. Oberleithner, "Dynamic evolution of a transient supersonic trailing jet induced by a strong incident shock wave," *Physical Review Fluids*, vol. 5, no. 7, p. 073401, 2020.

[157] J. G. R. von Saldern, J. P. Moeck, and A. Orchini, "Nonlinear interaction between clustered unstable thermoacoustic modes in can-annular combustors," *Proceedings of the Combustion Institute*, vol. 38, no. 4, pp. 6145–6153, 2021.

[158] M. Shou and L. Leu, "Energy of power spectral density function and wavelet analysis of absolute pressure fluctuation measurements in fluidized beds," *Chemical Engineering Research and Design*, vol. 83, no. 5, pp. 478–491, 2005.